

**Faculty of Science and Engineering**

**WA School of Mines: Minerals, Energy and Chemical Engineering**

**Synthesis and Characterization of Biomass and Clay Mineral Based  
Adsorbents for the Removal of Cationic Dye and Metal Ion from  
Wastewater by Adsorption**

**Sara A Dawood**

**This thesis is presented for the Degree of  
Doctor of Philosophy  
of  
Curtin University**


**April 2018**

## Declaration

To the best of my knowledge and belief this thesis contains no material previously published by any other person except where due acknowledgment has been made.

This thesis contains no material which has been accepted for the award of any other degree or diploma in any university.

Signature..........

Date.../2018..

## **I dedicate this thesis**

*In loving memory of my late mother (Layla).*

*To my father (Abdul-Aziz) who always calls me (Marie Curie).*

*To my lovely husband (Mostafa).*

*To my beautiful daughter (Lana).*

## List of publications

### Book chapter

- **Dawood, S.**, T. Gupta, and T. K. Sen. 2017. "Adsorptive Removal of Methylene Blue (MB) Dye at Kaolin Clay-Water Interface: Kinetics, Isotherm Modelling and Process Design." In Clay Minerals: Properties, Occurrence and Uses Sen, T. K., 209-236 New York, USA: Nova Publishers Inc.

### Journal articles

- **Dawood, S.**, Sen, T.K. and Phan, C. (2018) "Performance and dynamic modelling of biochar and kaolin packed bed adsorption column for aqueous phase methylene blue dye removal". Environmental Technology, 2018: p. 1-11.
- **Dawood, S.**, Sen, T.K. and Phan, C. (2017) "Synthesis and characterization of slow pyrolysis pine cone bio-char in the removal of organic and inorganic pollutants from aqueous solution by adsorption: Kinetic, equilibrium, mechanism and thermodynamic". Bioresource Technology 246, 76-81.
- **Dawood, S.**, Sen, T.K. and phan, C. (2016) "Adsorption removal of Methylene Blue (MB) dye from aqueous solution by bio-char prepared from Eucalyptus sheathiana bark: kinetic, equilibrium, mechanism, thermodynamic and process design". Desalination and Water Treatment 57(59), 28964-28980.
- **Dawood, S.** and Sen, T. (2014) "Review on Dye Removal from Its Aqueous Solution into Alternative Cost Effective and Non-Conventional Adsorbents". J Chem Proc Engg (1), 1-7.

### Conference articles

- Sen, T.K., Afroze, S. and **Dawood, S.** (2017) "Aqueous phase dye removal by low cost alternative adsorbents". In 10<sup>th</sup> World Congress of Chemical Engineering, 1-5 October 2017, Barcelona, Spain.

- **Dawood, S.**, Sen, T.K. and phan, C. (2016). “Removal of Cationic and Anionic Dyes from Their Aqueous Solution into Cost Effective pine cone Bio-char Adsorbent by Adsorption”. In EMN Meeting on Bioenergy, 4-7 April 2016, Phuket, Thailand.

## Other publications

- Sen, T.K., Nnie, T. and **Dawood, S.** (2018) “Equilibrium, kinetics and thermodynamics of aqueous phase methylene blue (MB) dye adsorption onto mixture of eucalyptus bark biomass and kaolin clay minerals". Research on Chemical Intermediates. (Under Review).
- Shak, A., **Dawood, S.** and Sen, T.K. (2017) "Performance and dynamic modelling of mixed biomass-kaolin packed bed adsorption column for the removal of aqueous phase methylene blue (MB) dye". Desalination and Water Treatment 82, 67-80.
- **Dawood, S.**, Sen, T.K. and Phan, C. (2014) "Synthesis and characterisation of novel-activated carbon from waste biomass pine cone and its application in the removal of Congo red dye from aqueous solution by adsorption". Water, Air, and Soil Pollution 225(1).
- **Dawood, S.** and Sen, T.K. (2012) "Removal of anionic dye Congo red from aqueous solution by raw pine and acid-treated pine cone powder as adsorbent: Equilibrium, thermodynamic, kinetics, mechanism and process design". Water Research 46 (6), 1933-1946.
- Bashir, M., **Dawood, S.**, Yagub, M. and Sen, K.T. (2015) “Adsorptive Removal of Congo red Dye from Its Aqueous Solution by Pine Tree Leaves: Kinetics, Equilibrium and Thermodynamics”. In international Conference on Civil Engineering and Environmental Engineering., February 2015, Tokyo, Japan.
- **Dawood, S.**, T. Sen, and C. Phan. 2013. "Effect of phosphoric acid and temperature profile on pine cone based activated carbon production and its effectiveness in the removal of Congo red dye by adsorption." In International Congress on Engineering and Information, Aug 28, 2013, Macau, China: ICEAI.

# TABLE OF CONTENT

Acknowledgements.....	i
List of Figures.....	ii
List of Tables .....	vii
Nomenclature.....	x
Abstract.....	xii

## CHAPTER: 1 INTRODUCTION

1. 1 Background.....	1
1. 2 Research Significance .....	5
1. 3 Research Aim and Objectives.....	5
1.3.1 Specific Research Objectives .....	6
1. 4 Thesis Organisation.....	7
1. 5 References .....	10

## CHAPTER: 2 LITERATURE REVIEW

2.1 Introduction .....	14
2.2 Dye sources, structure and their classifications.....	14
2.3 Toxicity effects of dyes .....	20
2.4 Heavy metal ions, sources and their classification .....	22
2.5 Heavy Metals Potential Hazards.....	23
2.6 Treatment technologies for wastewater laden with heavy metal ions and dyes.....	25
2.6.1 Chemical Methods .....	28
2.6.2 Biological Methods.....	30
2.6.3 Physicochemical methods .....	33
2.7 Adsorption .....	35
2.7.1 Effect of physico-chemical process parameters on adsorption .....	36
2.7.1.1 Effect of solution pH on adsorption.....	36
2.7.1.2 Effect of adsorbent dose on adsorption.....	41
2.7.1.3 Effect of solution temperature on adsorption .....	45
2.7.1.4 Effect of initial adsorbate concentration and contact time on adsorption.....	48
2.7.1.5 Effect of ionic strength.....	52
2.7.2 Role of adsorbent characteristics on the adsorption process.....	57

2.7.2.1	Raw agricultural solid wastes in the removal of organic and inorganic pollutants .....	57
2.7.2.2	Modified agricultural solid wastes adsorbents .....	60
2.7.2.3	Agricultural solid wastes based bio-char and activated carbon adsorbents .....	63
2.7.2.4	Inorganic adsorbents in the removal of dyes and heavy metals .....	69
2.8	Batch Adsorption Kinetic Study .....	73
2.8.1	Langergren Pseudo-first-order and Pseudo-second-order kinetic models .....	73
2.8.2	Intra-particles-diffusion model and mechanism of adsorption.....	74
2.9	Batch Adsorption Isotherm.....	76
2.9.1	Freundlich adsorption isotherm model .....	76
2.9.2	Langmuir isotherm.....	77
2.10	Thermodynamic study.....	80
2.11	Column adsorption study on the removal of organic dye .....	82
2.11.1	Theory of breakthrough curve (BTC) and mass transfer zone (MTZ) .....	84
2.11.2	Packed-bed column kinetics models.....	87
2.11.2.1	Thomas Model .....	87
2.11.2.2	Yoon-Nelson Model.....	88
2.11.2.3	BDST Model.....	89
2.11.2.4	Clark Model .....	90
2.12	Summary .....	91
2.13	References .....	92

### **CHAPTER 3: MATERIALS, CHARACTERISATION AND EXPERIMENTAL METHODS**

3.1	Introduction.....	122
3.2	Adsorbents.....	122
3.2.1	Pine cone, eucalyptus bark (EB) and kaolin clay collection .....	122
3.2.2	Synthesis of slow pyrolysis EB and pine cone bio-chars.....	123
3.3	Adsorbates and other chemicals .....	124
3.3.1	Methylene Blue (MB) Dye.....	124
3.3.2	Nickel metal ions (Ni <sup>2+</sup> ) .....	126

3.3.3	Other chemicals .....	127
3.4	Adsorbents characterizations .....	128
3.4.1	CHNS Analysis.....	128
3.4.2	Fourier-Transform Infrared (FT-IR) .....	131
3.4.3	Scanning Electron Microscope (SEM) and Energy Dispersive X-ray Spectroscopy (EDS).....	136
3.4.4	X-Ray Diffraction spectrum (XRD) .....	140
3.4.5	Brunauere–Emmett–Teller (BET) Surface Area and Malvern particle sizer ..	142
3.4.6	Point of zero charge (pH <sub>zpc</sub> ) .....	145
3.4.7	Bulk density and yield percentage .....	147
3.5	Batch Adsorption Experiments.....	148
3.6	Isotherm Experiment .....	150
3.7	Desorption Process.....	150
3.8	Packed-Bed Column Adsorption Design and Experimental Procedure.....	151
3.9	Summary .....	153
3.10	References.....	154

**CHAPTER 4: ADSORPTIVE REMOVAL OF METHYLENE BLUE DYE FROM AQUEOUS SOLUTION BY EUCALYPTUS BARK BIO-CHAR: KINETICS, ISOTHERM, THERMODYNAMIC AND PROCESS DESIGN STUDY.**

4.1	Introduction .....	158
4.2	Results and discussion.....	159
4.2.1	Effect of initial solution pH on MB dye adsorption.....	159
4.2.2	Effect of EB bio-char dosage on MB dye adsorption.....	161
4.2.3	Effect of contact time and initial MB dye concentration.....	163
4.2.4	Effect of solution temperature and thermodynamics studies.....	165
4.2.5	Effect of monovalent and divalent presence of salts on adsorption.....	168
4.3	Applications of Adsorption Kinetic Models.....	170
4.3.1	Application of pseudo-first-order adsorption kinetic model.....	170
4.3.2	Application of pseudo-second-order kinetic model.....	173
4.3.3	Intra-particles-diffusion model and mechanisms of adsorption.....	176



4.4	Adsorption Equilibrium Isotherm Models.....	180
4.5	Design of Single Stage Batch Adsorber from Isotherm Data.....	184
4.6	Desorption Study.....	186
4.7	Conclusion.....	188
4.8	References.....	189

**CHAPTER 5: REMOVAL OF ORGANIC MB DYE AND INORGANIC NI (II) IONS FROM AQUEOUS SOLUTION BY PINE CONE BIOCHAR ADSORBENT**

5.1	Introduction.....	195
5.2	Results and discussion.....	196
5.2.1	Effect of initial solution pH on MB dye and Ni (II) ions adsorption.....	196
5.2.2	Effect of pine cone bio-char dosage on adsorption process.....	198
5.2.3	Effect of contact time and initial adsorbate concentration .....	200
5.2.4	Effect of solution temperature and thermodynamics studies.....	203
5.3	Applications of Adsorption Kinetic Models.....	206
5.3.1	Pseudo first order adsorption kinetics model.....	207
5.3.2	Application of pseudo-second order kinetic model.....	212
5.3.3	Intra Particles Diffusion Model and Mechanisms of Adsorption .....	218
5.4	Application of Adsorption Equilibrium Models .....	224
5.5	Design of Single Stage Batch Adsorber from Isotherm Data.....	229
5.6	Conclusion.....	232
5.7	References.....	233

**CHAPTER 6 ADSORPTIVE REMOVAL OF METHYLENE BLUE (MB) DYE AT KAOLIN CLAY-WATER INTERFACE: KINETIC, ISOTHERM MODELLING AND PROCESS DESIGN.**

6.1	Introduction.....	240
-----	-------------------	-----

6.2	Results and Discussion.....	241
6.2.1	Effect of Kaolin dosage on MB dye adsorption.....	241
6.2.2	Effect of initial solution pH on MB dye adsorption.....	243
6.2.3	Effect of initial MB dye concentration and contact time on adsorption.....	245
6.2.4	Effect of solution temperature and thermodynamics studies.....	247
6.3	Adsorption kinetic and mechanism of adsorption.....	249
6.3.1	Pseudo- first -order kinetic model.....	249
6.3.2	Pseudo-second -order kinetic model.....	252
6.3.3	Intra-particle-diffusion model.....	255
6.4	Adsorption Equilibrium Isotherm.....	258
6.5	Single Stage Batch Adsorption Design.....	262
6.6	Conclusion.....	264
6.7	References.....	265

**CHAPTER 7 PERFORMANCE AND DYNAMIC MODELLING OF PINE CONE BASED BIOCHAR AND KAOLIN PACKED BED ADSORPTION COLUMN IN THE REMOVAL OF METHYLENE BLUE (MB) DYE FROM ITS AQUEOUS PHASE.**

7.1	Introduction.....	270
7.2	Results and Discussion .....	271
7.2.1	Effect of adsorbents bed height on BTC.....	271
7.2.2	Effect of initial MB dye concentration on BTC.....	273
7.2.3	Effect of inlet MB dye flow rate .....	275
7.2.4	Dynamic modelling of pine cone biochar and kaolin packed bed adsorption column.....	277
7.2.4.1	Application of Thomas dynamic model.....	277
7.2.4.2	Application of Yoon-Nelson dynamic Model.....	280
7.2.4.3	Application of Bed Depth Service Time (BDST) model.....	282
7.2.4.4	Application of Clark model.....	283
7.3	Conclusion .....	286
7.4	References.....	288

**CHAPTER 8: CONCLUSION AND RECOMMENDATIONS**

8.1 Conclusion.....290

8.2 Recommendations and Future Research Direction.....294

Appendix A.....296

Appendix B.....310

Appendix C .....319

Appendix D.....331

## ACKNOWLEDGEMENTS

First of all, I would like to express my greatest appreciation to the almighty ALLAH for given me the blessings and encouragement to complete my study.

It gives me a great pleasure to express my gratitude to my supervisor A/P. Tushar K Sen for his enormous support and valuable guidance. I truly believe that without his continuous support and supervision, it was impossible for me to complete the project successfully on time. I would like to thank my co-supervisor Dr. Chi Phan for his support and encouragement during my study. Also, I would like to extend my thanks to the thesis chairperson Prof. Shaomin Liu.

Sincere thanks go to the technical staff members of chemical engineering laboratory, Araya Abera, Melina Miralles, Andrew Chan, Xiao Hua and Yu Long for their supports during my experiments. Special thank goes to Lemlem Solemon for her administration support.

I cannot find words to express my gratitude to my lovely family members and sincere friends Dr. Sharmeen Afroze, Dr. Rajinder AttarSingh and Edda Babic for their encouragement and support through my study. Finally, I will forever be thankful and grateful to my husband Mostafa, my sister Dunia and my niece Tamara for their unconditional love, care and support.

## LIST OF FIGURES

<b>Figure 1.1:</b> Schematic diagram of the current research activities.....	9
<b>Figure 2.1:</b> Various separation methods used in the removal of organic and inorganic pollutants from wastewater. ....	25
<b>Figure 2.2:</b> Solid-Liquid Adsorption separation process- Adapted from (Slejko 1985).....	35
<b>Figure 2.3:</b> Effect of solution pH in the removal of Reactive red 141 dye by raw pecan nutshell and its biochar (Zazycki et al. 2018). ....	38
<b>Figure 2.4:</b> The effect of adsorbent dose on MB dye adsorption by mango leaf. Initial dye concentration=100 mg/L and volume= 200ml (Uddin et al. 2017).....	42
<b>Figure 2.5:</b> Effect of temperature in the removal of Cd (II) ions by orange peel , initial ion concentration= 189 mg/L and pH =7 (Tran et al. 2016).....	46
<b>Figure 2.6:</b> The effect of initial Diazonium blue dye on percentage dye removal and adsorption capacity by modified sugarcane bagasse (Said et al. 2017).....	49
<b>Figure 2.7:</b> The effect of contact time on the adsorption capacity of Ni (II) ions by almond shell biochar. Adsorbent dose = 7 g/L, solution pH =7 and T = 40 °C. (Kılıç et al. 2013).....	50
<b>Figure 2.8:</b> Effect of NaCl concentration on the adsorption % of MB onto Kaolin and Zeolite where the other parameters kept constant (Rida et al. 2013a) .....	54
<b>Figure 2.9:</b> Methods used in the production of biomass based activated carbon, char and charcoal.....	65
<b>Figure 2.10:</b> Various types of inorganic clays and minerals.....	70
<b>Figure 2.11:</b> Typical Breakthrough Curve (BTC) (Dutta 2007) .....	85
<b>Figure 3.1:</b> a) Raw eucalyptus bark, b) raw pine cone and c) kaolin clay powder.....	123
<b>Figure 3.2:</b> Schematic diagram of the production of EB bio-char.....	124
<b>Figure 3.3:</b> a) MB dye of 1000 mg/L, b) SP-8001 UV/VIS Spectrophotometer.....	125
<b>Figure 3.4:</b> The calibration curve for various MB dye concentration.....	125
<b>Figure 3.5:</b> a) Nickel ions stock solution of 1000 mg/L, b) Atomic Absorption Spectrometer AAS 7000.....	126
<b>Figure 3.6:</b> Calibration curve for various nickel (Ni <sup>2+</sup> ) ions concentration.....	127
<b>Figure 3.7:</b> CHNS Analysis by PerkinElmer (CHNS-O analyser 2400).....	129
<b>Figure 3.8:</b> FTIR of EB biochar and EB biochar after MB dye adsorption.....	133
<b>Figure 3.9:</b> FTIR of pine cone bio-char, pine cone biochar-MB dye and pine cone biochar- Ni (II) adsorption.....	134

<b>Figure 3.10:</b> FTIR of kaolin clay before and after MB dye adsorption.....	<b>135</b>
<b>Figure 3.11:</b> a) SEM of EB bio-char before adsorption (2000x), b) SEM of EB bio-char after MB dye adsorption(2000x),c) EDS of EB bio-char.....	<b>137</b>
<b>Figure 3.12</b> a) SEM of pine cone bio-char before adsorption (2000x), b) SEM of pine cone bio-char after MB dye adsorption (2000x),c) EDS of pine cone bio-char.....	<b>138</b>
<b>Figure 3.13:</b> a) SEM of kaolin clay before adsorption (2000x), b) SEM of kaolin after MB dye adsorption (10000x),c) EDS of kaolin clay.....	<b>139</b>
<b>Figure 3.14:</b> XRD analysis of (a) EB biochar, (b) pine cone biochar and (c) kaolin clay.....	<b>141</b>
<b>Figure 3.15:</b> Malvern particle sizer analysis (a) EB based biochar, (b) pine cone based biochar and (c) kaolin clay.....	<b>144</b>
<b>Figure 3.16:</b> The point of zero charge pH pzc, a) EB bio-char, b) pine cone bio-char and c) kaolin. Mass of Adsorbent 10 mg, Volume of 0.1M KNO <sub>3</sub> Solution 50 ml, Temp 30 °C ,Shaker Speed 130 rpm and time =24 hrs.....	<b>146</b>
<b>Figure 3.17:</b> Thermo line scientific Orbital Shaker Incubator.....	<b>149</b>
<b>Figure 3.18:</b> Schematic diagram of packed pine cone biochar and kaolin bed column.....	<b>152</b>
<b>Figure 4.1:</b> Effect of initial solution pH on the adsorption of MB dye on EB bio-char. (a) amount of dye adsorbed $q_t$ (m/g) at time $t$ , (b) percentage dye removal at time $t$ and (c) amount of dye adsorbed $q_e$ (m/g) and dye removal at equilibrium. Adsorbent dose=20 mg, V= 50 ml, Initial dye Concentration =20 mg/L, T= 35 °C and rotating Speed= 130 rpm.....	<b>160</b>
<b>Figure 4.2:</b> Effect of adsorbent dose on MB dye adsorption. (a) Amount of dye adsorbed $q_t$ (m/g) at time $t$ , (b) percentage dye removal at time $t$ and (c) amount of dye adsorbed $q_e$ (m/g) and dye removal at equilibrium. Solution pH= 11.3, V= 50 ml, Initial dye Concentration =20 mg/L, T= 35 °C and rotating Speed= 130 rpm.....	<b>162</b>
<b>Figure 4.3:</b> Effect of MB dye concentration and contact time on MB dye adsorption by EB bio-char. (a) amount of dye adsorbed $q_t$ (m/g) at time $t$ , (b) percentage dye removal at time $t$ and (c) amount of dye adsorbed $q_e$ (m/g) and dye removal at equilibrium. Adsorbent dose=20 mg, V= 50 ml, solution pH=11.3, T= 35 °C and rotating Speed= 130 rpm.....	<b>164</b>
<b>Figure 4.4:</b> Effect of solution temperature on MB dye adsorption capacity $q_e$ (m/g) and percentage dye removal. Solution pH=11.3, V= 50 ml, Initial dye Concentration =20 mg/L, adsorbent dose= 20 mg and rotating Speed= 130 rpm.....	<b>166</b>
<b>Figure 4.5:</b> Plot of Van't Hoff equation for MB dye- EB bio-char adsorption.....	<b>167</b>
<b>Figure 4.6:</b> Effect of NaCl and CaCl <sub>2</sub> salts on MB dye adsorption, a) Amount of dye adsorbed $q_e$ (mg/g), b) Percentage Dye removal. Adsorbent dose=20 mg, initial dye concentration= 20 mg/L, V= 50 ml, solution pH=11.3, T= 35 °C and rotating Speed= 130 rpm.....	<b>169</b>
<b>Figure 4.7:</b> Pseudo-first-order kinetic model fitting for MB dye adsorption by EB bio-char at various a) adsorbent dosage, b) solution temperature, c) initial MB concentration, d) solution pH, e) initial NaCl concentration and f) initial CaCl <sub>2</sub> concentration.....	<b>172</b>

<b>Figure 4.8:</b> Pseudo-second-order kinetic model fitting for MB dye adsorption by EB bio-char at various a) initial MB concentration, b) adsorbent dosage, c) solution pH, d) solution temperature, e) initial NaCl concentration, and f) initial CaCl <sub>2</sub> concentration.....	<b>175</b>
<b>Figure 4.9:</b> Intra-particle-diffusion model fitting for the adsorption of MB dye by EB bio-char at various a) initial MB concentration, b) adsorbent dosage, c) solution temperature, d) solution pH, e) initial NaCl concentration, and f) initial CaCl <sub>2</sub> concentration.....	<b>179</b>
<b>Figure 4.10:</b> Langmuir isotherm plots. a) Langmuir (I) , b) Langmuir (II) , pH solution =11.3, V =50 ml, adsorbent dose=20mg, T =35 °C, rotating Speed = 130 rpm and t =210 min.....	<b>181</b>
Figure 4.11: Freundlich isotherm plot for MB dye on EB bio-char, pH solution =11.3, V =50 ml, adsorbent dose=20mg, T =35 °C, rotating Speed =130 rpm at t=210 min.....	<b>182</b>
<b>Figure 4.12:</b> Design of single stage batch adsorber - Adsorbent mass (m) against volume of solution treated (L).....	<b>185</b>
<b>Figure 4.13:</b> Batch desorption study of MB dye from EB bio-char by various solution pH and acetone solvent.....	<b>187</b>
<b>Figure 5.1:</b> Effect of initial solution pH into MB dye and Ni (II) ions adsorption. pine cone bio-char dose= 20 mg, V= 50 ml, adsorbate concentration = 20 mg/L, T= 35 °C, rotating Speed 130 rpm and time=120 mins.....	<b>198</b>
<b>Figure 5.2:</b> Effect of adsorbent dose into MB dye and Ni (II) ions adsorption. Amount of adsorbate=20 mg/L, V= 50 ml, solution pH (MB= 11.3) (Ni (II)=9.4), T= 35 °C, rotating Speed 130 rpm and time =120 min.....	<b>200</b>
<b>Figure 5.3:</b> Effect of initial adsorbate concentration and contact time onto pine cone bio-char adsorption a) Amount of MB dye adsorbed $q_t$ (mg/g) vs contact time, b) ) Amount of Ni (II) ions adsorbed $q_t$ (mg/g) vs contact time, c) Amount adsorbate adsorbed $q_t$ (mg/g) and percentage removal at t= 120 min. Where V= 50 ml, solution pH (MB= 11.3 and Ni (II)= 9.4), adsorbent dose = 20 mg, T= 35 °C and rotating Speed 130 rpm.....	<b>202</b>
<b>Figure 5.4:</b> Effect of solution temperature of MB and Ni (II) ions adsorption onto pine cone biochar: pH solution = 11.3 for MB, 9.4 for Ni (II), V=50 ml, Initial dose=20mg, initial adsorbate concentration =20 mg/L, rotating speed= 130 rpm at time=120 min.....	<b>204</b>
<b>Figure 5.5:</b> Plot of Van't Hoff equation for MB dye and Ni (II) ions adsorption onto pine cone bio-char adsorption.....	<b>205</b>
<b>Figure 5.6:</b> Fitted pseudo-first-order kinetic model for the adsorption of MB dye onto pine cone bio-char at a) initial MB concentration, b) adsorbent dosage c) solution pH and d) solution temperature.....	<b>210</b>
<b>Figure 5.7:</b> Fitted pseudo-first-order kinetic model for the adsorption of Ni (II) ions onto pine cone bio-char at a) initial MB concentration, b) adsorbent dosage c) solution pH and d) solution temperature.....	<b>211</b>
<b>Figure 5.8:</b> Fitted pseudo-second-order kinetic model for the adsorption of MB dye onto EB bio-char at various a) initial MB concentration, b) adsorbent dosage, c) solution pH, d) solution temperature.....	<b>216</b>
<b>Figure 5.9:</b> Fitted pseudo-second-order kinetic model for the adsorption of Ni (II) ions onto EB bio-char at various, a) adsorbent dosage, b) initial Ni concentration c) solution pH, d) solution temperature.....	<b>217</b>

<b>Figure 5.10:</b> Intra particle diffusion model for the adsorption of MB dye onto pine cone bio-char at various a) adsorbent dosage, b) initial MB concentration, c) solution pH, d) solution temperature.....	<b>222</b>
<b>Figure 5.11:</b> Intra particle diffusion model for the adsorption of Ni (II) onto pine cone bio-char at various a) adsorbent dosage, b) initial MB concentration, c) solution pH, d) solution temperature.....	<b>223</b>
<b>Figure 5.12:</b> a) Langmuir plot for MB dye , b) Langmuir plot for Ni (II), pH solution (MB=11.3,Ni= 9.4) Volume =50 ml, Initial dose=20mg, temperature =35 °C, Shaker Speed 130 rpm at time=180 min.....	<b>225</b>
<b>Figure 5.13:</b> Freundlich isotherm model for MB dye and Ni (II) onto pine cone bio-char, pH solution (MB=11.3,Ni= 9.4) Volume =50 ml, Initial dose=20mg, temperature =35 °C, Shaker Speed 130 rpm at time=180 min.....	<b>227</b>
<b>Figure 5.14:</b> Design of single stage batch adsorber for a) MB dye, b) Ni (II) ions, Adsorbent mass (m) against volume of solution treated (L).....	<b>231</b>
<b>Figure 6.1:</b> Effect of kaolin dose on MB dye adsorption. a) Amount of MB dye adsorbed, b) percentage dye removal c) Amount of dye adsorbed and dye removal at time=125 min. Where V= 50 ml, solution pH 11.3, MB = 20 mg/L, T= 35 °C and Shaker Speed 130 rpm.....	<b>242</b>
<b>Figure 6.2:</b> Effect of solution pH MB dye adsorption. a) Amount of MB dye adsorbed, b) Amount of dye adsorbed and dye removal at time=125 min. Where V= 50 ml, kaolin dose=20 mg, MB concentration= 20 mg/L, T= 35 °C and Shaker Speed 130 rpm.....	<b>244</b>
<b>Figure 6.3:</b> Effect of initial MB dye concentration and contact time on adsorption. a) Amount of MB dye adsorbed, b) percentage dye removal c) Amount of dye adsorbed and dye removal at time=125 min. Where V= 50 ml, solution pH 11.3, kaolin dose= 20 mg, T= 35 °C and Shaker Speed 130 rpm.....	<b>246</b>
<b>Figure 6.4:</b> Effect of solution temperature on Kaolin adsorption of MB dye: MB conc=20 mg/L, adsorbent dose= 20 mg, MB volume 50 ml, solution pH=11.3, Shaker Speed 130 rpm and time=125 min.....	<b>247</b>
<b>Figure 6.5:</b> Plot of Van't Hoff equation for MB dye- kaolin adsorption.....	<b>248</b>
<b>Figure 6.6:</b> Fitted pseudo-first-order kinetic parameters for the adsorption of MB dye onto kaolin at various a) initial MB concentration, b) kaolin dosage, c) solution pH and d) solution temperature.....	<b>251</b>
<b>Figure 6.7:</b> Pseudo-second-order kinetic model for the adsorption of MB dye onto kaolin at various a) initial MB concentration, b) kaolin dosage, c) solution pH and d) solution temperature.....	<b>254</b>
<b>Figure 6.8:</b> Intra particle diffusion model for the adsorption of MB dye onto kaolin at various a) initial MB dye concentration, b) adsorbent dosage, c) solution pH and d) solution temperature.....	<b>257</b>
<b>Figure 6.9:</b> Freundlich isotherm model for MB dye onto kaolin, pH solution =11.3, Volume =50 ml, Initial dose=20mg, temperature =35 °C, Shaker Speed 130 rpm at time=150 min.....	<b>259</b>
<b>Figure 6.10:</b> a) Langmuir (I) plot, b) Langmuir (II) plot, pH solution =11.3, Volume =50 ml, Initial dose=20mg, temperature =35 °C, Shaker Speed 130 rpm at time=150 min.....	<b>260</b>
<b>Figure 6.11:</b> Design of single stage batch adsorber- Adsorbent mass (m) against volume of solution treated (L).....	<b>263</b>



<b>Figure 7.1:</b> The breakthrough curves (BTC) for MB dye adsorption at various column bed heights where initial MB dye concentration =100 mg/L, flow rate= 15 ml/min, solution pH 6.9, and solution temperature =25 ±1 °C .....	<b>271</b>
<b>Figure 7.2:</b> The breakthrough curves (BTC) for MB dye adsorption at various initial MB dye concentration where bed height= 5 cm, flow rate= 15 ml/min, solution pH 6.9, and solution temperature =25°C.....	<b>273</b>
<b>Figure 7.3:</b> The breakthrough curves (BTC) for MB dye adsorption at various flow rate where initial MB dye =100 mg/L, bed height =5 cm, solution pH 6.9, and solution temperature =25 °C .....	<b>275</b>
<b>Figure 7.4:</b> Thomas Kinetic Plots for adsorption of MB dye under various effect (a) Effect of Bed Height, (b) Effect of Flow Rate, (c) Effect of Initial MB Concentration, (Temperature 25±1°C and solution pH of 6.9).....	<b>279</b>
<b>Figure 7.5:</b> Yoon-Nelson kinetics plots for the adsorption of MB dye on pine cone biochar and kaolin clay under various effect (a) Effect of Bed Height, (b) Effect of Flow Rate ,(c) Effect of Initial MB Concentration, (Temperature 25±1°C and solution pH =6.9).....	<b>281</b>
<b>Figure 7.6:</b> BDST kinetic plot for the adsorption of MB dye on pine cone biochar and kaolin at initial dye concentration of 100 mg/L and flow rate of 15 ml/min.....	<b>283</b>
<b>Figure 7.7:</b> Clark plots for the adsorption of MB dye on pine cone biochar and kaolin clay under various effect (a) Effect of Bed Height, (b) Effect of Flow Rate ,(c) Effect of Initial MB Concentration, (Temperature 25±1°C and solution pH =6.9).....	<b>285</b>

## LIST OF TABLES

<b>Table 2.1:</b> Dye’s classification and their chemical structure (Hernández-Montoya et al. 2013, Yagub et al. 2014a) .....	<b>15</b>
<b>Table 2.2:</b> The common dyes used in textile industry (Samanta and Konar 2011, Shahid et al. 2013, Velho et al. 2017).....	<b>17</b>
<b>Table 2.3:</b> The toxicity effects for various dyes used in textile industry (de Campos Ventura-Camargo and Marin-Morales 2013, Leyh et al. 2003, Padhi 2012) .....	<b>21</b>
<b>Table 2.4:</b> Heavy metals classification according to Lewis acid classification theory (Chantawong et al. 2003, Da Silva and Williams 2001).....	<b>22</b>
<b>Table 2.5:</b> The common heavy metals and their beneficial to the human health, recommended daily intake and toxicity effect of these metals upon exposure to high dose over prolonged period of time. (Al-Dhabi 2013, Fu and Wang 2011, Goldhaber 2003, Roohani et al. 2013) .....	<b>23</b>
<b>Table 2.6:</b> The advantages and limitations of various separation techniques used in the removal of dyes and heavy metal ions (Carmen and Daniela 2012, Dawood and Sen 2014, Ghosh et al. 2016, Yagub et al. 2014a) .....	<b>26</b>
<b>Table 2.7:</b> Bacteria and Fungi strains commonly used in dye biodegradation and heavy metals removal from wastewater.....	<b>31</b>
<b>Table 2.8:</b> Removal of dyes and heavy metal ions by adsorbents at various initial solution pH.....	<b>39</b>
<b>Table 2.9:</b> The effect of adsorbent dosage of various adsorbents on the adsorption capacity and percentage removal of dyes and heavy metals .....	<b>43</b>
<b>Table 2.10:</b> The effect of solution temperature in the removal of dyes and heavy metals ions using various adsorbents .....	<b>46</b>
<b>Table 2.11:</b> The removal of dyes and heavy metals ions under various initial dyes and heavy metal ions concentration.....	<b>50</b>
<b>Table 2.12:</b> The effect of ionic strength on the percentage dye and heavy metal ions removal onto various adsorbents .....	<b>54</b>
<b>Table 2.13:</b> The maximum adsorption capacity in the removal dyes and heavy metals by raw agricultural by-product waste adsorbents .....	<b>58</b>
<b>Table 2.14:</b> The maximum adsorption capacity in the removal dyes and heavy metals by modified agricultural biomass adsorbents .....	<b>61</b>
<b>Table 2.15:</b> The maximum adsorption capacity $q_m$ (mg/g) of various biomass based bio-char, charcoal and activated carbon (AC) in the removal of dyes and heavy metal ions.....	<b>66</b>
<b>Table 2.16:</b> The maximum adsorption capacity $q_m$ (mg/g) of various inorganic clay adsorbents in the removal of dyes and heavy metals.....	<b>71</b>
<b>Table 2.17:</b> Langmuir (I) and (II) isotherm model equations.....	<b>77</b>

<b>Table 2.18:</b> Adsorption process feasibility at various ( $R_L$ ) values (Kaur et al. 2013) .....	<b>78</b>
<b>Table 2.19:</b> The applicability of various isotherm models for dyes and heavy metal ions removal by various adsorbents. ....	<b>78</b>
<b>Table 2.20:</b> The removal of dyes and heavy metal ions in a fixed bed column under various operational conditions.....	<b>82</b>
<b>Table 3.1:</b> Element comparative analysis of various char, charcoal and activated carbon. ....	<b>129</b>
<b>Table 3.2:</b> BET surface area for the synthesized bio-char, kaolin and other published biochar .....	<b>143</b>
<b>Table 3.3:</b> Bulk density and percentage yield for EB bio-char, pine cone bio-char and kaolin.....	<b>148</b>
<b>Table 4.1:</b> Thermodynamics parameters for MB dye adsorption onto EB bio-char at various solution temperature.....	<b>167</b>
<b>Table 4.2:</b> Fitted pseudo-first-order kinetic parameters under various process conditions in the removal of MB dye by EB biochar.....	<b>171</b>
<b>Table 4.3:</b> Fitted pseudo-second-order kinetic parameters at various process conditions in the removal of MB dye by EB biochar.....	<b>174</b>
<b>Table 4.4:</b> Fitted intra-particle-diffusion model parameters under different process conditions in the removal of MB dye by EB biochar.....	<b>178</b>
<b>Table 4.5:</b> Calculated values for Freundlich and Langmuir isotherm models.....	<b>183</b>
<b>Table 4.6:</b> Comparison of adsorption capacities of various adsorbents in the removal of MB dye.....	<b>183</b>
<b>Table 5.1:</b> Thermodynamics parameters for MB dye and Ni (II) ions adsorption onto pine cone bio-char at various temperature .....	<b>206</b>
<b>Table 5.2:</b> Fitted pseudo-first-order kinetic model parameters for MB dye adsorption onto pine cone bio-char.....	<b>208</b>
<b>Table 5.3:</b> Fitted pseudo-first-order kinetic model parameters for Ni (II) ions adsorption onto pine cone bio-char.....	<b>209</b>
<b>Table 5.4:</b> Fitted pseudo-second-order kinetic model parameters for MB dye adsorption onto pine cone bio-char.....	<b>214</b>
<b>Table 5.5:</b> Fitted pseudo-second-order kinetic model parameters for Ni (II) ions adsorption onto pine cone bio-char.....	<b>215</b>
<b>Table 5.6:</b> Intra particle diffusion model parameters for MB dye adsorption onto pine cone bio-char.....	<b>220</b>
<b>Table 5.7:</b> Intra particle diffusion model parameters for Ni (II) ions adsorption onto pine cone bio-char .....	<b>221</b>

<b>Table 5.8:</b> Calculated values for Freundlich and Langmuir isotherm models.....	<b>228</b>
<b>Table 5.9:</b> Comparison of adsorption capacities in the removal of MB dye and Ni (II) ions by various adsorbents.....	<b>228</b>
<b>Table 6.1:</b> The thermodynamic properties of MB dye adsorption onto Kaolin clay .....	<b>249</b>
<b>Table 6.2:</b> Fitted pseudo –first- order kinetic model parameters for MB dye adsorption by kaolin clay .....	<b>250</b>
<b>Table 6.3:</b> Fitted pseudo-second-order kinetic model calculated parameters for MB dye adsorption onto kaolin clay.....	<b>253</b>
<b>Table 6.4:</b> Intra particle diffusion model parameters for MB dye adsorption on kaolin.....	<b>256</b>
<b>Table 6.5:</b> Calculated values for Freundlich and Langmuir isotherm models.....	<b>261</b>
<b>Table 6.6:</b> Comparison of adsorption capacities of various adsorbents in the removal of MB dye ...	<b>261</b>
<b>Table 7.1:</b> Breakthrough curves (BTCs) parameters for various bed height containing pine cone biochar and kaolin adsorbents in the removal of MB dye in a fixed bed column.....	<b>272</b>
<b>Table 7.2:</b> Breakthrough curves (BTCs) parameters for various initial MB dye concentration in a fixed bed column.....	<b>274</b>
<b>Table 7.3:</b> Breakthrough curves (BTCs) parameters for various inlet MB dye flow rate in a fixed bed column .....	<b>276</b>
<b>Table 7.4:</b> Kinetic parameters of Thomas Model under various experimental conditions (Bed Height (cm) , Flow Rate (mL/min) and Initial MB Concentration (mg/L)).....	<b>278</b>
<b>Table 7.5:</b> Yoon-Nelson calculated parameters under various experimental process conditions (Bed Heig (cm), Flow Rate (mL/min) and Initial MB Concentration (mg/L)) .....	<b>282</b>
<b>Table 7.6:</b> Clark model parameters in the adsorption of MB dye on cone biochar and kaolin .....	<b>284</b>

## NOMENCLATURE

$C_0$	Initial dye concentration, (mg/L)
$C_t$	Initial dye concentration at time t, (mg/L)
$D_p$	Diffusion coefficient, (cm <sup>2</sup> /sec)
$\Delta G^0$	Gibbs free energy change, (kJ/mole)
$\Delta H^0$	Enthalpy change, (kJ/mole)
$\Delta S^0$	Entropy change, (J/k mole)
$K_f$	Pseudo-first-order rate constant (min <sup>-1</sup> )
$K_s$	Pseudo-second-order rate constant, (mg/g.min)
$K_F$	Freundlich adsorption constant, (L/g)
$K_{id}$	Intra-particle rate constant [(mg/g) min <sup>0.5</sup> ]
$m$	Amount of adsorbent added in g
$n$	Freundlich constant
$q_e$	Amount of adsorbate per gram of adsorbent at equilibrium, (mg/g)
$q_t$	Amount of adsorbate per gram of adsorbent at any time, t
$q_{max}$	Maximum adsorption capacity (mg/g)
$R^2$	Linear regression coefficient
$R_L$	Separation factor
$A$	Cross sectional area of bed in column (cm <sup>2</sup> )
$A_1$	Used bed area (cm <sup>2</sup> )
$A_2$	Unused bed area (cm <sup>2</sup> )
$C_t$	Outlet pollutant concentration (mg/L)

$C_o$	Inlet pollutant concentration (mg/L)
$H$	Height of bed in column (cm)
$H_B$	Used bed length up to break point (cm)
$H_T$	Bed height of column (cm)
$H_{UNB}$	Unused bed length (cm)
$K_o$	Rate constant in BDST model (L/mg min)
$K_T$	Thomas rate constant (mL/mg min)
$K_{YN}$	Yoon and Nelson rate constant ( $\text{min}^{-1}$ )
$MTZ$	Mass transfer zone (cm)
$m_{total}$	Total amount of methylene blue dye sent to column (g)
$N_o$	Adsorption capacity (mg/L)
$Q$	Volumetric flow rate (mL/min)
$q_{total}$	Total adsorbed methylene blue dye quantity (g)
$q_o$	Equilibrium adsorbate uptake (mg/g)
$t_t$	Total time (min)
$t_{total}$	Total flow time (min)
$t_b$	Usable capacity of bed up to the breakthrough point time (min)
$t_u$	Time equivalent to usable capacity (min)
$U$	Influent linear velocity (cm/min)
$V$	Effluent volume (ml)
$V_{eff}$	Total effluent volume (mL)
$\tau$	Time required for 50 % adsorbate breakthrough (min)

## ABSTRACT

Water pollution occurs when potential pollutants from various industrial activities are directly and indirectly discharged into water bodies without adequate treatment. These pollutants may be organic and inorganic contaminations such as dyes and heavy metal ions. Several wastewater treatment technologies have been used in the removal of these organic and inorganic contaminants. Among these, adsorption separation process is considered to be an effective and widely used technique in wastewater and water treatment. Commercial activated carbon (CAC) originally produced from coal is widely used as an effective adsorbent for water and wastewater treatment containing heavy metal ions and dyes. However due to its high cost, non-renewable production source and difficulties associated with its regeneration, a great research interest in the production of low-cost and an effective alternative adsorbent to commercial activated carbon such as biomass and biomass based biochar has grown rapidly in the last few decades.

In this research study, we have selected pine cone (*Pinus. Radiate*) and eucalyptus bark (EB) (*Sheathiana*) agricultural solid wastes as precursors for the synthesis of biochar by slow pyrolysis method. These agricultural solid wastes are available in large quantities in Australia with little or no economic value and present a disposal problem. Therefore, the utilization of these solid waste biomass as effective adsorbents give sustainable solution for water and wastewater treatment as well as effective biomass solid wastes management. Also, various researchers reported the use of inorganic clay minerals adsorbents such as kaolin, zeolite, bentonite etc. as low-cost and effective adsorbents for the removal of dyes and heavy metals ions. Therefore, to increase the feasibility of our adsorption system, we also have selected kaolin clay as another adsorbent in the removal of organic MB dye pollutants.

The synthesized biomass based biochar and kaolin clay were characterized by CHN-O analysis and energy dispersive spectroscopy (EDS) to determine the elements composition. Fourier-transform infrared spectroscopy (FTIR) was used to determine the presence of various functional groups which are responsible for adsorption. Scanning Electron Microscope (SEM) and X-Ray diffraction spectrum (XRD) were used to examine the surface morphology and the presence of minerals in the adsorbents. Textural adsorbents characteristics such as BET surface area, pore size, specific surface area, particle size, bulk density and Point of zero charge ( $\text{pH}_{\text{zpc}}$ ) were also determined.

EDS analysis of EB biochar indicates the presence of carbon, oxygen and calcium while carbon, oxygen and a trace of sodium were presented in pine cone biochar. These results were supported by CHN-O analysis as the amount of carbon was calculated as 75.1% for pine cone biochar and 60.0% for EB biochar. Aluminium, silicon, oxygen and titanium were the main components presented in kaolin clay. FTIR analysis of the synthesized biochar indicated the presence of aromatic C=C stretching, C-H bending and O-H bend from carboxylic acid group which are responsible for the adsorption of MB dye and Ni (II) ions. FTIR of kaolin clays suggested the presence of  $\nu$  (Si-O) planer stretching, O-H deformation and Si-O Stretching functional groups. BET surface area was calculated as 73 m<sup>2</sup>/g for EB biochar, 335 m<sup>2</sup>/g for pine cone biochar and 30.5 m<sup>2</sup>/g for kaolin clay. The bulk density of EB biochar, pine cone biochar and kaolin were calculated as 0.42, 0.54 and 0.67 g/cm<sup>3</sup> respectively. Further, the point of zero charge (pH<sub>zpc</sub>) was determined as 9.5 for EB biochar, 8.5 for pine cone biochar and 6.5 for kaolin.

In this research study, batch adsorption study was carried out to evaluate the effectiveness of synthesized biomass derived biochar and kaolin clay adsorbents in the removal of organic MB dye and inorganic Ni (II) ions from aqueous solution under various physico-chemical process parameters. These physico-chemical process parameters such as initial adsorbate concentration, solution pH, solution temperature, adsorbent dose and contact time have great influences on the adsorption capacity and mechanism of adsorption. It was found that the amount of MB dye adsorbed  $q_t$  (mg/g) by EB biochar increased with the increase of initial dye concentration, contact time, temperature and solution pH, but decreased with the increase of adsorbent dose and presence of salt. High linear regression coefficient values and low error values presented from Chi-square test indicated that the adsorption system follows pseudo-second-order kinetic model. Also, kinetic experiments clearly indicated that adsorption process was multi steps processes: a rapid adsorption of dye onto the adsorbent external surface followed by intra-particle diffusion into the interior of adsorbent which has also been confirmed by intra-particle-diffusion model. Equilibrium data were fitted into Langmuir and Freundlich isotherm models and were best presented by Langmuir (I) isotherm model with a maximum adsorption capacity  $q_m$  of 104.2 mg/g which is very comparative to CAC. Also, from thermodynamic analysis, it was observed that the adsorption system was an endothermic, spontaneous and physical in nature.



The feasibility of another pine cone based bio-char adsorbent in the removal of MB dye and Ni (II) ions from its aqueous solution were also explored here. It was found that the amount of adsorbates adsorbed  $q_t$  (mg/g) by pine cone biochar increased with the increase of initial adsorbate concentration, contact time, solution temperature and solution pH but decreased with the increase of adsorbent dose. High linear regression coefficient values and low error values presented from Chi-square test indicated that the adsorption system followed pseudo-second-order model. Also, kinetic experiments clearly indicated that adsorption process of MB dye and Ni (II) ions by pine cone biochar were multi steps processes: a rapid adsorption of dye onto the adsorbent external surface followed by intra-particle diffusion into the interior of adsorbent which has also been confirmed by intra-particle-diffusion model. Equilibrium data were fitted well in both Langmuir (I) and Freundlich isotherm models and the maximum adsorption capacity  $q_m$  was calculated as 106.4 mg/g for MB dye and 117.7 mg/g for Ni (II) ions which are comparative to available CAC. Also, it was observed from the thermodynamic study that the adsorption system was an endothermic, physical and spontaneous in nature for both adsorbate system.

Further, kaolin clay was selected as an inorganic adsorbent and its effectiveness in the removal of MB dye from its aqueous solution has been studied here. It was also observed that the amount of dye adsorbed  $q_t$  (mg/g) by kaolin increased with the increase of initial dye concentration, solution pH and temperature but decreased with the increase of adsorbent dose. High linear regression coefficient values and low error values obtained from Chi-square test indicated that the adsorption system follows pseudo-second-order kinetic model. Also, equilibrium data were fitted well into Langmuir (I) and Freundlich isotherm models and the maximum adsorption capacity  $q_m$  was calculated as 104.2 mg/g. Further, from the thermodynamic analysis, it was observed that the adsorption system was an endothermic, spontaneous and physical processes in nature.

The results obtained earlier in this study such as the maximum adsorption capacity, adsorption equilibrium isotherm, adsorption kinetic and mechanism of adsorption under optimum physico-chemical conditions were conducted by batch adsorption mode. These results cannot be scaled up and applied directly in a continuous real column operations because the contact time in a flow column is not adequate to reach equilibrium. Therefore, the feasibility of pine cone based biochar and kaolin adsorbents were investigated for the removal of MB dye in a packed bed continuous adsorption column.

Pine cone biochar and kaolin packed bed adsorbents have been chosen over EB biochar/kaolin because pine cone biochar adsorbent has a higher BET surface area of 335 m<sup>2</sup>/g and carbon content of 75.1% compared to EB biochar of 73 m<sup>2</sup>/g and 60% respectively. The column studies were conducted under various operation parameters such as bed height (3-7 cm), inlet flow rate (13-17 ml/min) and initial dye concentration (50-150 mg/L). Two separate layers of pine cone based biochar and kaolin clay were used as packed bed adsorbents in fixed bed column at volume ratio of 1:1. Experimental data were fitted to obtain the optimum column kinetic parameters using Thomas, Yoon-Nelson, Clark and Bed Depth Service Time (BDST) models. High linear regression coefficient values obtained indicated the suitability of these models. Thomas model indicated that the value of maximum solid phase concentration ( $q_o$ ) increased with increasing flow rate and initial MB dye concentration and decreased with the increase of bed height. Yoon-Nelson model showed that the time required for 50% adsorbate breakthrough ( $\tau$ ) were agreed with the experimental data ( $\tau_{50\% \text{ exp}}$ ) and Yoon-Nelson rate constant ( $K_{yn}$ ) value was decreased as the bed height increased and increased with the increase of flow rate and initial MB dye concentration. Also, from BDST model, the bed sorption capacity ( $N_o$ ) was calculated as 7636 mg/L assuming a constant initial dye concentration ( $C_o$ ) and linear velocity ( $v$ ). Clark model was applied and ( $r$ ) value was found to be decreased with the increase of bed height and flow rate and increased with the increase of initial MB dye concentration respectively.

In conclusion, the results obtained from the batch and continuous column adsorption studies showed that low-cost biomass derived biochar and kaolin were effective, feasible and comparative adsorbents to CAC in the removal of MB dye and inorganic Ni (II) ions from wastewater. Therefore, this present study determined that EB and pine cone biomass based biochar and kaolin clay mineral adsorbents may be used in the removal of organic and inorganic pollutants from water and wastewater.

# **CHAPTER 1**

## **INTRODUCTION**

## 1.1 Background

Clean water availability has been considered to be a major challenge over the last few decades with major impacts on our social and economic well-being. A geological survey from the United States indicated that almost 96.5% of earth's water is salt water and it is not suitable for human consumption without further treatment (Greenlee et al. 2009). Polar ice and underground water are currently among the main sources of fresh water with only 0.8% of it accessible for human and industry utilization. Research shows that the demand for water consumption doubles every 21 years worldwide due to the increase in population and industrial activities and the decrease in rainfall (Toor 2010). Fresh water from rivers, lakes, and aquifers used to meet the global consumption has increased rapidly in the last few decades. Due to anthropogenic water consumption, the annual runoff in many river basins decreased by more than 5% during 1971 to 2000 (Haddeland et al. 2014). According to Water Research Group, it is estimated that global industrial water requirements would increase from 800 billion m<sup>3</sup> to 1500 billion m<sup>3</sup> by 2030 and the industrial withdrawals which accounts for 16% of today's global demand is expected to increase by 22% in 2030 (Vajnhandl and Valh 2014). It has been estimated that by 2025, approximately 60% of the total world population would live in regions potentially experiencing moderate to extreme water resource unavailability (Kulshreshtha 1998). Anthropogenic water, a by-product from various industry activities such as textile finishing, paper, pharmaceutical, printing, carpet, plastic, food, cosmetic and heavy metal industries have high amounts of organic and inorganic pollutants that cause harmful effects to human and other living organisms (Dawood and Sen 2014). Textile effluents are discharged in the water streams and it contain high amounts of organic dyes and inorganic heavy metal ions pollutants. Natural and synthetic dyes are generally classified into cationic, anionic, reactive dyes, direct dyes, azo dyes, mordant dyes, vat dyes, disperse dyes and sulphur dyes (Mahmoud et al. 2012). There are more than 100,000 commercial dyes that are used in textile industry worldwide with a total annual production of 10,000 tonnes per year (Gómez et al. 2007, Gupta et al. 2013). Almost 10–25% of these dyes are released as effluents into water streams during the dyeing finishing process (Carmen and Daniela 2012). Synthetic dyes have complex

structure and are photo-chemically stable, thus their effects on the environment have been a matter of concern for public and governments at all levels (Quan et al. 2017).

Cationic dyes impose serious health hazards to the environment and human being and are known to cause skin and eye irritation, increase heart rates, vomiting upon digestion, coronary vasoconstriction, decreased cardiac output, renal and reproductive system dysfunction as well as damage to central nervous system (Leyh et al. 2003, Shakoor and Nasar 2016). Humans exposed to anionic and azo dyes as well as their by-products through the digestion process, skin and lungs can cause disturbance in blood formation and even DNA damage which may lead to the genesis of malignant tumors (Khan and Malik 2014). Dye effluents from industrial activities are generally not suitable for conventional biological wastewater treatment due to their synthetic origin, high solubility and complex molecular structures, thus decrease their ability to biodegrade.

Consequently, inorganic pollutants presented in wastewater such as heavy metals ions have become a series of public health concern. The heavy metal ions of copper, zinc, cobalt, magnesium, manganese, selenium, chromium, cadmium, lead, mercury, iron, nickel and others metals are not biodegradable and accumulate in nature (Demirbas 2009). Some heavy metal such as zinc, nickel, copper, iron, chromium, manganese and selenium are beneficial to the human health if taken at very low concentration. For example, nickel ions increase iron absorption in human body and help treating osteoporosis, however, the maximum recommendation for the daily dose is 0.4 mg/day only (Al-Dhabi 2013, Goldhaber 2003). But, other heavy metals ions such as mercury, lead and cadmium have no health benefits and may cause serious damage to the kidneys, liver, bones and central nervous system. According to UNICEF, 2–5 million people die as a result of water contamination related diseases every year (Cooley et al. 2014). The health benefits and toxicity effects of various heavy metals are summarized and presented in Table 2.4 of chapter 2.

Various separation technologies have been successfully used in the removal of organic dyes and inorganic heavy metal ions from wastewater such as adsorption, coagulation/flocculation, ion exchange, advanced oxidation technologies, ozonation, membrane filtration, precipitation, electrokinetic coagulation, photocatalyst, aerobic and anaerobic degradations (EI-Latif et al. 2010, Yagub et al. 2014). These separation methods are classified into three categories,

namely, physio-chemical; chemical; and biological separation method. Each method has its own advantage and limitation in terms of efficiency, cost, design and operational conditions.

Among the various separation techniques, adsorption process is a physiochemical separation method and is widely used in the removal of organic and inorganic wastewater contaminations due to its high adsorption capacity, low initial cost, simple design and ease of operation as well as insensitivity to toxic substances (Afroze et al. 2016, Dawood et al. 2014). Adsorption separation process involves the transfer of adsorbate ions, atoms or molecules from the bulk aqueous phase to the surface of the adsorbent. The adsorption capacity depends on the nature of adsorbate such as molecular weight, molecular structure, molecular size, polarity and solution concentration, adsorbent-adsorbate interaction and adsorbent surface properties such as particle size, surface area and surface charge and presence of various functional groups.

The adsorptive removal of organic dyes and inorganic heavy metal ions from their aqueous phases by commercial activated carbon (CAC) is very well established and successful technology. Commercial activated carbon is widely used due to its excellent adsorption capacity, mesoporous structure and large surface area. However, due to the high cost associated with its production and regeneration, researchers have been focusing upon the production of alternative adsorbents such as agricultural solid waste based charcoal, bio-char, biomass based activated carbon and clay minerals. The utilization of the large quantities of agriculture solid wastes as precursor in the synthesis of biomass based char and activated carbon poses double benefits with wastewater treatment and solid waste management. These agricultural solid wastes have no economical value and their disposal are encouraged (Yagub et al. 2014). Numerous research articles reported the use of biomass waste as a precursor in the production of biomass based charcoal, char, activated carbon and also mineral clays in the removal of organic dyes and inorganic heavy metal ions from wastewater. Liao et al., (Liao et al. 2012) reported the use of bamboo charcoal adsorbent in the removal of methylene blue and Acid orange 7 dyes. Zazycki et al., (Zazycki et al. 2018) reported the use of pecan nutshell biochar in the removal of reactive red 141 dye by adsorption. Zhou et al., (Zhou et al. 2017) reported the removal of Pb (II) ions from its aqueous solution onto banana peel biochar. Also, Dawood et al., (Dawood et al. 2014) reported the removal of Congo red dye onto pine cone based activated carbon. In addition, Shaban et al., studied the removal of methylene blue and Congo

red dyes onto bentonite and zeolite composite (Shaban et al. 2017) while Khan et al., studied the removal of Basic Fuchsin and Crystal violet dyes onto magnetic kaolin clay (Khan et al. 2015). Also, Aguayo-Villarreal et al., (Aguayo-Villarreal et al. 2017) reported the removal of Zn(II), Cd(II), Ni(II) and Cu(II) onto pecan nutshell activated carbon and Chai et al., evaluated the effectiveness of kaolin and bentonite clays in the removal of Al (III) ions (Chai et al. 2017). There is a review article where various research results in the removal of aqueous phase organic and inorganic by agricultural solid wastes, modified solid waste, biomass based activated carbon and clay minerals have been explored (De Gisi et al. 2016).

Pine cones (*P. radiata*) are native trees available in Australia. The ovulate cone is the well-known cone of the Pinus and other conifers. Large quantities of pine cones are collected annually as agricultural by-product throughout the world. These scale of this ovulate cone as cone biomass is a waste itself and can be used as an effective adsorbent. Each cone consists of an axis upon which is a borne, in a spiral fashion and the mature cone is composed of epidermal and sclerenchyma cells which contain cellulose, hemicelluloses, lignin, rosin and tannins in its cell walls (Dawood and Sen 2012, Pholosi et al. 2018). Also, eucalyptus tree (*sheathiana*) is another fast growing native tree which is available in Australia at no cost. Eucalyptus bark is considered a good source of lignin-cellulose carbonaceous material. Large quantities of pine cones and eucalyptus bark are collected annually as agricultural by-product throughout the world. In this research study, pine cones and eucalyptus barks biomasses have been selected as effective feedstocks in the production of slow pyrolysis bio-char adsorbents and its adsorptive effectiveness in the removal of aqueous phase MB dye and Ni (II) ions under various physio-chemical process parameters has been tested here. Further, to make the adsorption process more feasible, two layers of pine cone bio-char and kaolin clay have been used in the continuous dynamic fixed bed column adsorption study.

## **1.2 Research Significance**

In the last few decades, industrial activities from agricultural, textile, chemical, petroleum and mining processing have increased rapidly. These industries discharge significant amount of organic and inorganic contaminations into the water stream. Currently CAC is widely used to remove these pollutants from wastewater by adsorption process. However, due to its high cost and its origin from non-renewable source, an alternative adsorbent to commercial activated carbon is essential. In this research project, the use of pine cone and eucalyptus bark waste as precursors in the synthesis of bio-char will be investigated. These wastes are native trees which are available in Australia at no cost and their utilization is encouraged in terms of solid waste disposal management. Further, the synthesized bio-char can be used in various applications such as in oil and gas industry, catalyst, food and chemical industry, solvent recovery, air pollution control, waste water treatment and in hydrometallurgy for the recovery of gold and silver. However, in this project, we are evaluating the effectiveness of synthesized bio-char effectiveness as adsorbents in the removal of organic MB dye and inorganic Ni (II) ions from wastewater by adsorption process. This biomass based adsorbents can also be used for the removal of other organic and inorganic pollutants.

## **1.3 Research Aim and Objectives**

The overall objective of this research work is to synthesize a cost-effective, environmentally friendly and sustainable agricultural solid waste based bio-char adsorbent and evaluate its effectiveness in the removal of organic MB dye and inorganic Ni (II) from their aqueous solution by adsorption. Pine cone and eucalyptus bark have been used as precursor in the production of slow pyrolysis bio-char at various temperature. The nature of adsorption depends on the adsorbents origin, characterization, the mechanism of the adsorption behaviour under various process parameters has been explored in this study. The effectiveness of synthesized biomass biochar adsorbents have been justified by adsorption kinetics and isotherm adsorption mechanism study under various physico- chemical process conditions.



### 1.3.1 Specific Research Objectives

The specific objectives of this research study are:

- ❖ To collect pine cone and eucalyptus bark biomass solid wastes.
- ❖ To synthesize slow pyrolysis pine cone biochar and eucalyptus bark biochar under various temperature profiles and examine its characterisation using various analytical instruments such as Scanning Electron Microscopy (SEM), Electron Diffraction Spectrum (EDS), X-ray Diffractometer (XRD), Fourier Transform Infrared (FTIR), BET surface area, bulk density, percentage yield, CHN-O analyser and Malvern particle size analyser.
- ❖ To carry out batch adsorption kinetics and isotherm experiments in the removal of MB dye onto EB biochar adsorbent under various physico-chemical process conditions such as initial solution pH, adsorbent dose, initial dye concentration, contact time, solution temperature and ionic strength.
- ❖ To carry out batch adsorption kinetics and isotherm experiments in the removal of MB dye and Ni (II) ions onto pine cone biochar adsorbent under various physico-chemical process conditions such as initial solution pH, adsorbent dose, initial dye concentration, contact time and solution temperature.
- ❖ To carry out batch adsorption kinetics and isotherm experiments in the removal of MB dye onto kaolin clay adsorbent under various physico-chemical process conditions such as initial solution pH, adsorbent dose, initial dye concentration, contact time and solution temperature.
- ❖ To find the optimum process parameters and the identification of adsorption mechanism.
- ❖ To perform continuous fixed bed column operation containing two separate layers of pine cone biochar and kaolin clay at a volume ratio of 1:1 for the removal of MB dye by varying inlet flow rate, initial dye concentration and bed height thus determine the its feasibility in the industrial application.
- ❖ To establish several breakthrough plots and evaluate the applicability of various packed bed column kinetics models under various column experimental conditions.

## 1.4 Thesis Organisation

This thesis has been organized in eight chapters and covers all the detail aspects of this research study. A list of references is included at the end of each chapter. An overview of the thesis flow structure is summarized and presented in Figure 1.1.

Chapter 1 outlines a brief background of water sources, water pollutants and current methodologies used in the purification and treatment of wastewater containing organic dyes and inorganic heavy metal ions. It also describes the aim and the specific objectives of this research study as well as the organisation of this thesis.

Chapter 2 presents the detailed and up to date literature review on organic/ inorganic pollutants in wastewater, sources, toxicity effects and various treatment technologies for their removal. Also, it describes the latest and current state of art in development of cost effective and environmentally friendly adsorbents which are comparative to the high adsorption capacity commercial activated carbon in the removal of organic and inorganic pollutants. In addition, this chapter presents the theory of adsorption kinetics, isotherm adsorption and thermodynamics evaluation for batch and continuous column adsorption processes.

Chapter 3 outlines the adsorbents synthesis, research methodology and the physical and chemical characterizations of eucalyptus biochar, pine cone biochar and kaolin clay minerals.

Chapter 4 deals with the adsorptive removal of methylene blue dye from its aqueous solution by bio-char prepared from eucalyptus sheathiana bark biomass. It also provides the detailed experimental and data analysis results on the adsorption kinetics, equilibrium, thermodynamic, desorption and process design under various physio-chemical process parameters.

Chapter 5 evaluates the effectiveness of pine cone based biochar in the removal of organic cationic Methylene blue dye and inorganic Ni (II) ions from aqueous solution under various physio-

chemical process parameters by batch adsorption kinetics, isotherm, thermodynamic and process design studies. The data analysis and mechanism of adsorption also presented here.

Chapter 6 reports the removal of Methylene blue dye from aqueous solution by kaolin clay adsorbent. It also presents the experimental results and data analysis on the adsorption kinetic, equilibrium, thermodynamic, process design and mechanism of adsorption.

Chapter 7 presents the experimental results of fixed bed column operation using two layers of pine cone bio-char and kaolin clay at volume ration of 1:1 in the removal of Methylene blue dye. In this chapter, the nature breakthrough curves under various process conditions such as inlet dye flow rate, initial dye concentration and bed height were examined and the experimental results were fitted into various adsorption column kinetic models.

Chapter 8 gives an overview of the successful outcomes of this research project. Also, it explains the research gaps associated with this research and future research direction and recommendations.

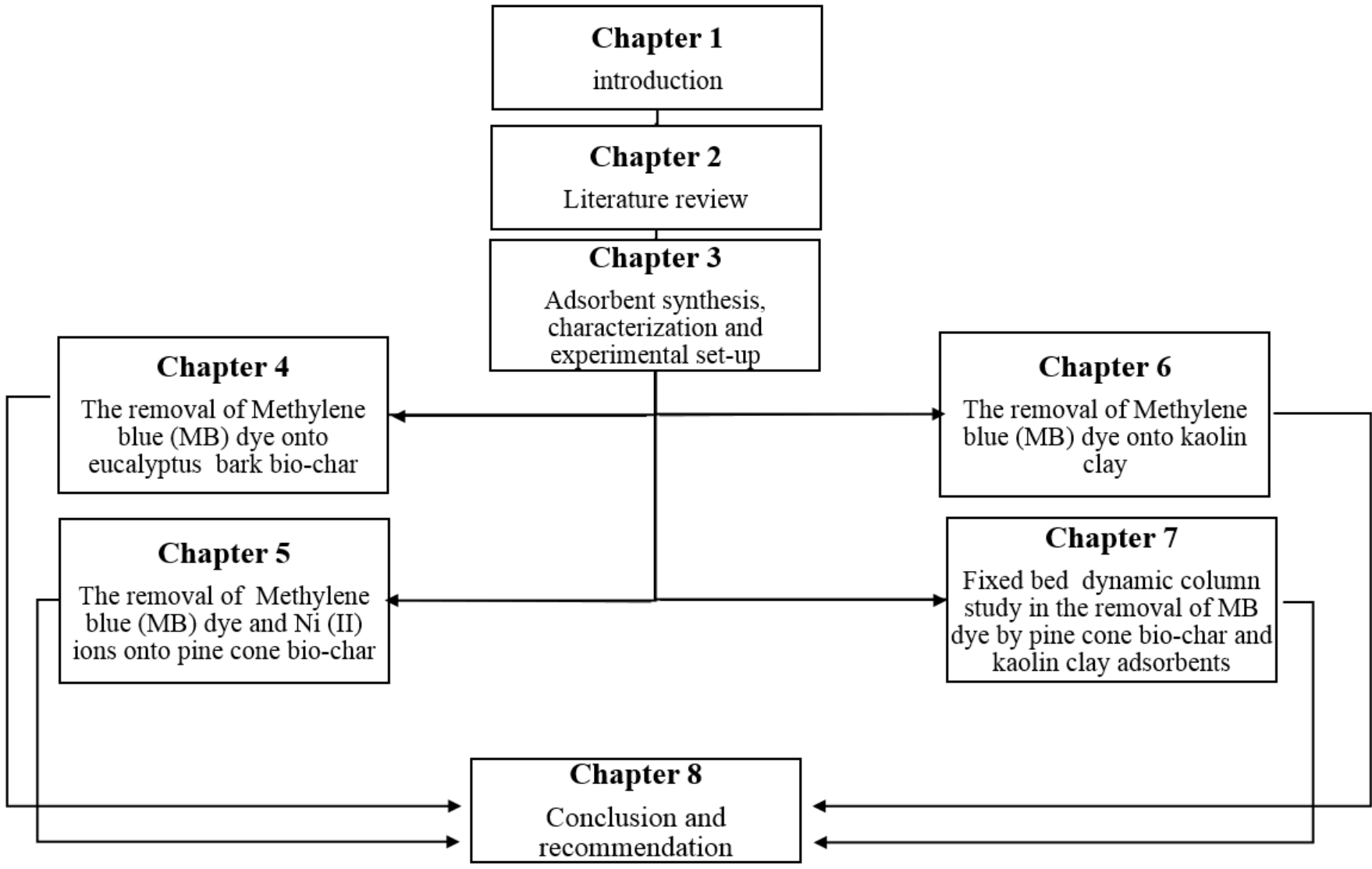


**Figure 1.1:** Schematic diagram of the current research activities.

## 1.5 References

- Afroze, S., Sen, T.K. and Ang, H.M. (2016) "Adsorption removal of zinc (II) from aqueous phase by raw and base modified Eucalyptus sheathiana bark: Kinetics, mechanism and equilibrium study". Process Safety and Environmental Protection **102**, 336-352.
- Aguayo-Villarreal, I.A., Bonilla-Petriciolet, A. and Muñiz-Valencia, R. (2017) "Preparation of activated carbons from pecan nutshell and their application in the antagonistic adsorption of heavy metal ions". Journal of Molecular Liquids **230**, 686-695.
- Al-Dhabi, N.A. (2013) "Heavy metal analysis in commercial Spirulina products for human consumption". Saudi Journal of Biological Sciences **20**(4), 383-388.
- Carmen, Z. and Daniela, S. (2012) "Textile Organic Dyes – Characteristics, Polluting Effects and Separation/Elimination Procedures from Industrial Effluents – A Critical Overview". Organic Pollutants Ten Years After the Stockholm Convention - Environmental and Analytical Update T.Puzyn and Mostrag-Szlichtyng, A. (eds), IntechOpen.
- Chai, W., Huang, Y., Han, G., Liu, J., Yang, S. and Cao, Y. (2017) "An Enhanced Study on Adsorption of Al(III) onto Bentonite and Kaolin: Kinetics, Isotherms, and Mechanisms". Mineral Processing and Extractive Metallurgy Review **38**(2), 106-115.
- Cooley, H., Ajami, N., Ha, M.-L., Srinivasan, V., Morrison, J., Donnelly, K. and Christian-Smith, J. (2014) "Global Water Governance in the Twenty-First Century". The World's Water: The Biennial Report on Freshwater Resources Gleick, P.H. (ed), pp. 1-18, Island Press/Center for Resource Economics, Washington, DC.
- Dawood, S. and Sen, T. (2014) "Review on Dye Removal from Its Aqueous Solution into Alternative Cost Effective and Non-Conventional Adsorbents". J Chem Proc Engg **1**(1), 1-7.
- Dawood, S. and Sen, T.K. (2012) "Removal of anionic dye Congo red from aqueous solution by raw pine and acid-treated pine cone powder as adsorbent: Equilibrium, thermodynamic, kinetics, mechanism and process design". Water Research **46**(6), 1933-1946.

Dawood, S., Sen, T.K. and Phan, C. (2014) "Synthesis and characterisation of novel-activated carbon from waste biomass pine cone and its application in the removal of congo red dye from aqueous solution by adsorption". Water, Air, and Soil Pollution **225**(1).

De Gisi, S., Lofrano, G., Grassi, M. and Notarnicola, M. (2016) "Characteristics and adsorption capacities of low-cost sorbents for wastewater treatment: A review". Sustainable Materials and Technologies **9**, 10-40.

Demirbas, A. (2009) "Agricultural based activated carbons for the removal of dyes from aqueous solutions: A review". Journal of Hazardous Materials **167**(1–3), 1-9.

EI-Latif, M.M.A., Ibrahim, A.M. and EI-Kady, M.F. (2010) " Adsorption equilibrium, kinetics and thermodynamics of methylene blue from aqueous solutions using biopolymer oak sawdust composite". J. Am. Sci. **6**(6), 267-283.

Goldhaber, S.B. (2003) "Trace element risk assessment: essentiality vs. toxicity". Regulatory Toxicology and Pharmacology **38**(2), 232-242.

Gómez, V., Larrechi, M.S. and Callao, M.P. (2007) "Kinetic and adsorption study of acid dye removal using activated carbon". Chemosphere **69**(7), 1151-1158.

Greenlee, L.F., Lawler, D.F., Freeman, B.D., Marrot, B. and Moulin, P. (2009) "Reverse osmosis desalination: Water sources, technology, and today's challenges". Water Research **43**(9), 2317-2348.

Gupta, V.K., Kumar, R., Nayak, A., Saleh, T.A. and Barakat, M.A. (2013) "Adsorptive removal of dyes from aqueous solution onto carbon nanotubes: A review". Advances in Colloid and Interface Science **193–194**(0), 24-34.

Haddeland, I., Heinke, J., Biemans, H., Eisner, S., Flörke, M., Hanasaki, N., Konzmann, M., Ludwig, F., Masaki, Y. and Schewe, J. (2014) "Global water resources affected by human interventions and climate change". Proceedings of the National Academy of Sciences **111**(9), 3251-3256.

Khan, S. and Malik, A. (2014) "Environmental and Health Effects of Textile Industry Wastewater". Environmental Deterioration and Human Health: Natural and anthropogenic

determinants Malik, A., Grohmann, E. and Akhtar, R. (eds), pp. 55-71, Springer Netherlands, Dordrecht.

Khan, T.A., Khan, E.A. and Shahjahan (2015) "Removal of basic dyes from aqueous solution by adsorption onto binary iron-manganese oxide coated kaolinite: Non-linear isotherm and kinetics modeling". Applied Clay Science **107**(Supplement C), 70-77.

Kulshreshtha, S.N. (1998) "A global outlook for water resources to the year 2025". Water Resources Management **12**(3), 167-184.

Leyh, R.G., Kofidis, T., Struber, M., Fischer, S., Knobloch, K., Wachsmann, B., Hagl, C., Simon, A.R. and Haverich, A. (2003) "Methylene blue: the drug of choice for catecholamine-refractory vasoplegia after cardiopulmonary bypass?". J Thorac Cardiovasc Surg **125**(6), 1426-1431.

Liao, P., Malik Ismael, Z., Zhang, W., Yuan, S., Tong, M., Wang, K. and Bao, J. (2012) "Adsorption of dyes from aqueous solutions by microwave modified bamboo charcoal". Chemical Engineering Journal **195–196**, 339-346.

Mahmoud, D.K., Salleh, M.A.M., Karim, W.A.W.A., Idris, A. and Abidin, Z.Z. (2012) "Batch adsorption of basic dye using acid treated kenaf fibre char: Equilibrium, kinetic and thermodynamic studies". Chemical Engineering Journal **181–182**(0), 449-457.

Pholosi, A., Naidoo, E.B. and Ofomaja, A.E. (2018) "Removal of Ni(II) and Co(II) from Aqueous Solution Using Pine Cone: A Mechanism Study". Emerging Trends in Chemical Sciences Ramasami, P., Gupta Bhowon, M., Jhaumeer Laulloo, S. and Li Kam Wah, H. (eds), pp. 163-183, Springer International Publishing, Cham.

Quan, X., Luo, D., Wu, J., Li, R., Cheng, W. and Ge, s. (2017) "Ozonation of acid red 18 wastewater using O<sub>3</sub>/Ca(OH)<sub>2</sub> system in a micro bubble gas-liquid reactor". Journal of Environmental Chemical Engineering **5**(1), 283-291.

Shaban, M., Abukhadra, M.R., Shahien, M. and Ibrahim, S.S. (2017) "Novel bentonite/zeolite-NaP composite efficiently removes methylene blue and Congo red dyes". Environmental Chemistry Letters, 1-6.

Shakoor, S. and Nasar, A. (2016) "Removal of methylene blue dye from artificially contaminated water using citrus limetta peel waste as a very low cost adsorbent". Journal of the Taiwan Institute of Chemical Engineers **66**, 154-163.

Toor, M.K. (2010) Enhancing adsorption capacity of Bentonite for dye removal: Physiochemical modification and characterization University of Adelaide.

Vajnhandl, S. and Valh, J.V. (2014) "The status of water reuse in European textile sector". Journal of Environmental Management **141**(Supplement C), 29-35.

Yagub, M.T., Sen, T.K., Afroze, S. and Ang, H.M. (2014) "Dye and its removal from aqueous solution by adsorption: A review". Advances in Colloid and Interface Science **209**(0), 172-184.

Zazycki, M.A., Godinho, M., Perondi, D., Foletto, E.L., Collazzo, G.C. and Dotto, G.L. (2018) "New biochar from pecan nutshells as an alternative adsorbent for removing reactive red 141 from aqueous solutions". Journal of Cleaner Production **171**(Supplement C), 57-65.

Zhou, N., Chen, H., Xi, J., Yao, D., Zhou, Z., Tian, Y. and Lu, X. (2017) "Biochars with excellent Pb(II) adsorption property produced from fresh and dehydrated banana peels via hydrothermal carbonization". Bioresource Technology **232**, 204-210.

*Every reasonable effort has been made to acknowledge the owners of copyright material.*

*I would be pleased to hear from any copyright owner who has been omitted or incorrectly acknowledged.*



# **CHAPTER TWO**

## **LITERATURE REVIEW**

## **2.1 Introduction**

In the last few decades, industrial activities from agricultural, textile, chemical, petroleum and mining processing have been increased rapidly. These industries discharge significant amount of organic and inorganic contaminations into water stream. This chapter provides extensive literature information about inorganic heavy metals ions and organic dyes, their classification, toxicity and applications. Further, this chapter presents the latest state of art in the treatment technology used in the removal and degradation of organic contaminations such as dyes and heavy metal ions from wastewater and water treatments. Various separation techniques such as physiochemical, chemical and biological techniques have been discussed here in details. Also, this chapter highlights wide range of adsorbents used in the removal of these pollutants such as agricultural solid waste, modified biomass waste, biomass based char, charcoal, biomass based activated carbon and other inorganic adsorbents such as kaolin clay and siliceous materials. Further adsorptive kinetics and isotherm studies under various process parameters such as solution pH, initial adsorbate concentration, adsorbent dose, contact time, temperature and salt presence have been critically analysed here. Column adsorption study through the use of fixed bed column has been analysed along with the common column kinetics models such as Thomas model, Yoon-Nelson model, Clark constants and Bed Depth Service Time.

## **2.2 Dye sources, structure and their classifications**

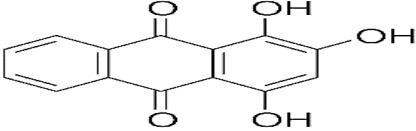
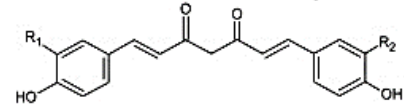
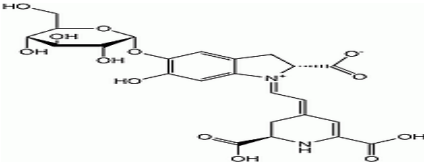
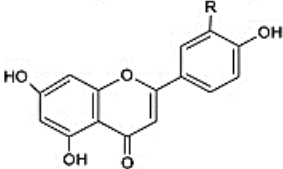
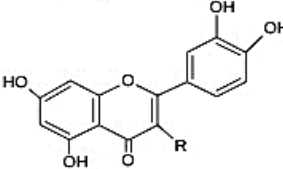
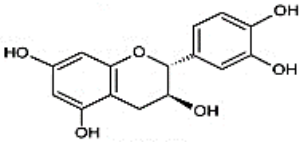
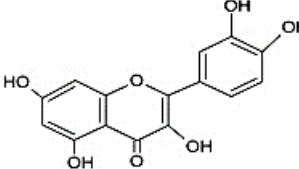
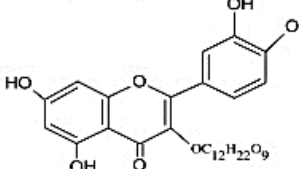
Dyes have been used as colour agents in textile, leather, paper, plastic, rubber, painting, cosmetic, food and pharmaceutical industries for centuries. The majority of natural dyes are extracted from plants and mineral sources (Shahid et al. 2013). Upon the introduction of industrial revolution, the industrial activities were increased dramatically and thus natural dyes production did not meet the industrial demand. Aniline purple was the first synthesised dye produced by W. H. Perkin back in 1856. Since then, synthetic dyes production have been increased significantly. Synthetic dyes can be classified into acid dyes, reactive dyes, basic dyes, azo dyes, direct dyes, vat dyes and disperse dyes (Yagub et al. 2014a). Dye's classification and their chemical structure are presented in Table 2.1.

**Table 2.1:** Dye's classification and their chemical structure (Hernández-Montoya et al. 2013, Yagub et al. 2014a).

<b>Class</b>	<b>Examples of dyes</b>	<b>Chemical structure type</b>
<b>Acid</b>	congo red ,methyl (orange and red) acid (blue, black, violet, yellow)	Anthraquinone, xanthene, azo (including, nitroso, premetallised), nitro, and triphenylmethane.
<b>Direct</b>	martius yellow, direct (black, orange blue, violet, red)	Phthalocyanine, azo, oxazine, and stilbene.
<b>Reactive</b>	reactive (red, blue, yellow, black ) remazol (blue, yellow, red)	Anthraquinone, formazan, phthalocyanine, azo, oxazine and basic.
<b>Disperse</b>	disperse (blue, red ,orange, yellow, brown )	Benzodifuranone, azo, anthraquinone, nitro, and styryl.
<b>Vat</b>	indigo,, benzanthrone vat (blue and green)	Indigoids and anthraquinone.
<b>Cationic</b>	methylene blue, basic (red, brown, blue), brilliant green, crystal violet and aniline yellow	Hemicyanine, azo, cyanine, diazahemicyanine, azine diphenylmethane, xanthene, oxazine, triarylmethane, acridine and anthraquinone.

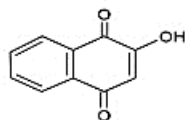
Chromophores and auxochromes are the main components presented in dye's molecules. Chromophores functional groups such as carbonyl, amide, carboxylic acid, acetylenic, ester, nitro and olefin are responsible for the production of colours while auxochromes enhance the dye binding towards the object (Dawood and Sen 2014, Salleh et al. 2011). Auxochromes can be classified as acidic (-COOH, -OH, -SO<sub>3</sub>H) or basic (NHR, -NR<sub>2</sub>, -NH<sub>2</sub>). Synthetic dyes are able to absorb light in the visible spectrum (400-700 nm) and they are highly visible in water even at very low concentration. Dye effluents resulted from industrial activities are generally not suitable for conventional biological wastewater treatment due to their synthetic origin, high solubility and complex molecular structures, thus decrease their ability to biodegrade. Generally, the dyes that are used in the textile industry are basic dyes, acid dyes, reactive dyes, direct dyes, azo dyes, mordant dyes, vat dyes, disperse dyes and sulphur dyes (Mahmoud et al. 2012). All dyes are water soluble except disperse dyes and vat dyes and they contain traces of metals such as copper, zinc, lead, chromium and cobalt in their aqueous solution. Synthetic dyes are generally classified into cationic dye, anionic dyes and non-ionic dyes based on the dye's particle charge in its aqueous solution. Cationic dyes is also known as basic dyes due to the presence of positive ions in the molecule's structure. Cationic dye interacts with the negative group presented on the fibre's molecules thus colour can be attached firmly to the fibre. Anionic dyes contain acidic, direct and reactive dyes. Anionic dyes have negative ions presence in their aqueous solution. Synthetic dyes exhibit characteristic differences in chemical bond structure such as azo, anthraquinone, triphenylmethane, phthalocyanine, formazin and oxazine. However they posse common features such as water solubility and ionic substituents (Hunger et al. 2000). Reactive dyes contain reactive functional groups such as vinyl sulfone, chlorotriazine, trichloropyrimidine, and difluorochloropyrimidine that can undergo addition or substitution chemical reactions with the -OH, -SH, and -NH<sub>2</sub> groups present in textile fibers during the dyeing process (Demirbas 2009, Labanda et al. 2009). Azo dyes represent almost 60% of all the reactive dyes used in the textile industry followed by anthraquinone and phthalocyanine classes (Wu et al. 2008). Dye bearing effluents from various industries are characterized by its high colour, organic content and hazardous as well. It is reported that more than 100,000 dyes are available commercially with an annual production of more than 7x10<sup>5</sup> tonnes per year (Gupta et al. 2013). It is also estimated that the total dye consumption in textile industry worldwide is more than 10,000 tonnes per year and almost 10–25% of these dyes are released as effluents into water streams during the dyeing finishing process (Bilińska et al. 2016, Pang and Abdullah 2013). The most common natural and synthetic dyes used in textile industry are presented in Table.2.2 along with their scientific names and chemical structures

**Table 2.2:** The common dyes used in textile industry (Samanta and Konar 2011, Shahid et al. 2013, Velho et al. 2017).

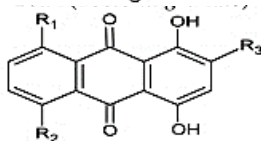
Dyes	Scientific names	Chemical structure
Indian madder	<i>purpurin</i>	
Turmeric	<i>Curcuma Longa</i>	
Beetroot	<i>Betalain</i>	
Weld	<i>Reseda Luteola</i>	
Eucalyptus	<i>Eucalyptus globules</i>	
Cutch	<i>Acacia Catechu</i>	
Onion	<i>Alium cepa</i>	
Flos sophorae	<i>Sophora japonica</i>	

---

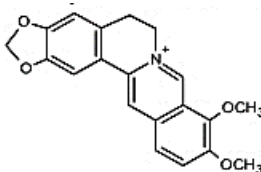
Henna *Lawsonia inermis*



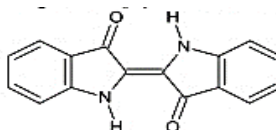
Teak *Tectona grandis*



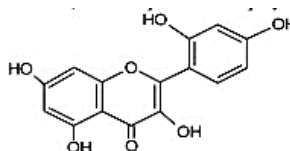
Berberberry *Berberis aristata*



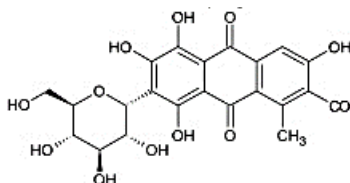
Indigo *Indigofera tinctoria*



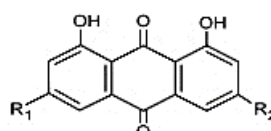
Jackfruit *Artocarpus heterophyllus*



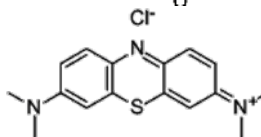
Cochineal *Dacylopius Coccus*



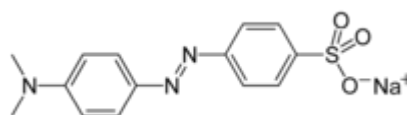
Indian Rhubarb *Rheum emodi*



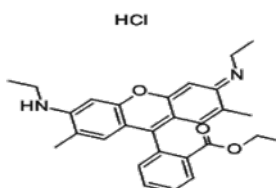
Methylene blue *methylthioninium chloride*



Methyl orange *Sodium 4-[4-(dimethylamino)phenyl]diazenebenzene-1-sulfonate*

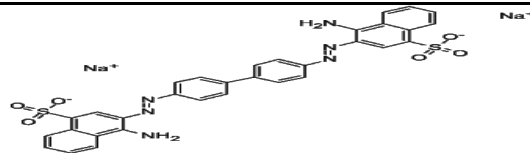


Basic red 1 *Rhodamine 6G molbdosilicate*

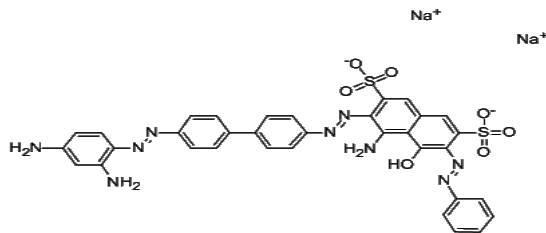


---

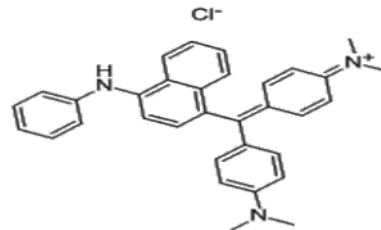
Congo red      *Lithium hydroxide 1H2O*



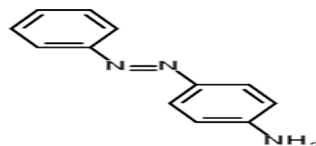
Direct black 38      *Chlorazol black E*



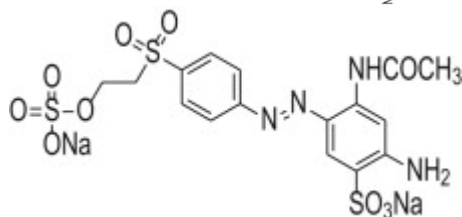
Basic blue 26      *Tertrophen Blue*



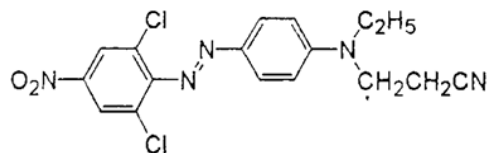
Aniline yellow      *4-(Phenyldiazenyl)aniline*



Remazol  
golden yellow      *Reactive Orange 107*



Disperse orange  
37      *3-[4-(2,6-Dichloro-4-nitrophenylazo)-N-ethylanilino]propionitrile*



## 2.3 Toxicity effects of dyes

Dyes are generally toxic therefore their discharge into water bodies can cause significant damages to the environment and human health. Synthetic dyes have complex structure and are photo-chemically stable, thus their effects on the environment have been a matter of concern for public and environmentalist (Quan et al. 2017). Dyes are highly visible in water even at very low concentration and therefore their discharge into the water body can reduce light penetration through the water and disturb the photosynthetic activity of aquatic organism's life. Basic dyes are water soluble and they are highly visible in water even at very low concentration. Cationic dyes such as malachite green, aniline yellow, butter yellow, basic red, basic black, turquoise reactive, neutrichrome red and methylene blue are mainly used in textile and paper industries. Basic dye bearing effluents are toxic and can cause allergic dermatitis, skin irritation, mutations and even cancer (Eren 2009). Also, cationic dyes can cause increased in heart rate, shock, vomiting, coronary vasoconstriction, decreased cardiac output, renal blood flow and mesenteric blood flow (Leyh et al. 2003, Mahmoud et al. 2012, Shakoor and Nasar 2016).

It is reported that more than 2000 structurally different azo dyes are currently in use and up to 130 azo dyes can form carcinogenic aromatic amines during anaerobic degradation process (Khan and Malik 2014, Yaneva and Georgieva 2012). Human expose to anionic and azo dyes and their by-products through the digestion, skin and lungs can cause disturbance in blood formation and even DNA damage which may lead to the genesis of malignant tumors (Khan and Malik 2014). Further, the use of direct dyes is limited and it is generally used to colour the cellulosic and protein fibres through hydrogen bonds and Van der Waals force (Chakraborty 2014). Some of direct dyes such as direct blue 6, direct brown 95 and direct black 38 can be metabolized to benzidine which is carcinogenic to humans. Table 2.3 presents the toxicity effects for the common dyes used in textile industry.



**Table 2.3:** The toxicity effects for various dyes used in textile industry (de Campos Ventura-Camargo and Marin-Morales 2013, Leyh et al. 2003, Padhi 2012).

<b>Dye</b>	<b>Toxicity effects</b>
Methylene blue	Palpitation, vomiting, decreased cardiac output, eye and skin irritations.
Crystal violet	Eye damage, nausea, vomiting, dermal irritation, carcinogen and promoting tumor growth in some species of fish.
Congo red	Eye and skin irritation, vomiting, nausea, respiratory tract irritation, reduce fertility and carcinogenic upon prolonged exposure.
Direct blue 6	Known to be human carcinogens.
Direct black 38	Eye irritation and damage, cause bladder cancer upon prolonged exposure and effect the reproductive system.
Methyl orange	Cause skin and eye irritation. May cause gastrointestinal tract irritation with nausea, vomiting, and diarrhea.
brilliant green	Severe eye damage, skin burn, diarrhea and abdominal pain.
Basic red 1	Serious eye damage and very toxic to aquatic life.
Basic blue 26	Eye, skin and respiratory tract irritations.
Vat blue VD043	Eye, skin and respiratory tract irritations.
Disperse red 17	Skin irritation, mutagenicity and reproduction system toxicity.
Disperse orange 25	Asthma like symptoms and may cause bladder cancer.

## 2.4 Heavy metal ions, sources and their classification

The heavy metal ions of copper, zinc, cobalt, magnesium, manganese, selenium, chromium cadmium, lead, mercury, iron, nickel and others metals are not biodegradable and accumulate in nature. Generally heavy metal ions have atomic weights between 63.5 and 200.6 and a specific gravity greater than 5.0 (Fu and Wang 2011). Heavy metals also known as trace elements due to their presence in a very low concentration (ppm and ppb) are presented in nature in the earth's crust. Natural phenomena such as weathering and volcanic eruptions have been reported to contribute to heavy metal pollution. Also, the presence of these heavy metal ions can occur through metal corrosion, atmospheric deposition, soil erosion of metal ions and sediment re-suspension. However large amount of these heavy metal ions are accumulated and presented in the wastewater due to anthropogenic activities such as fertilizer, mineral processing, textile, mining, smelting operations, industrial production, domestic and agricultural use of metals and metal-containing compounds (Tchounwou et al. 2012). According to the periodic table, heavy metals can be divided into s-block, p-block, d-block (transition) and f-block (inner- transition). Further, heavy metals can be classified into soft, hard and intermediate metals as per Lewis acid theory (Da Silva and Williams 2001). Metals of large particle size, high polarizability and low oxidation state is called soft metals while hard metals is defined for smaller particle size with low polarizability and high oxidation state (Chantawong et al. 2003). Intermediate metals have zero oxidation state. The classification of heavy metal ions are presented in Table 2.4.

**Table 2.4:** Heavy metals classification according to Lewis acid classification theory (Chantawong et al. 2003, Da Silva and Williams 2001).

<b>Metal classification</b>	<b>Class A (Hard metals)</b>	<b>Class B (Soft metals)</b>	<b>Borderline (Intermediate metals)</b>
<b>Examples</b>	Li, Be, Na, Mg, Al, K, Ca, Sc, Fe(III), Sr ,Y, Zr, Cs, Ba, La, Hf, Fr, Ra, Ac, Th	Cu (I), Pd, Ag, Cd, Ir, Pt, Au, Hg, Ti, Pb(II)	V, Cr, Fe(II), Co, Ni, Cu(II), Zn, Rh, Pb(IV), Sn

## 2.5 Heavy Metals Potential Hazards

Heavy metals pollution presented in the wastewater and water streams has a potential and serious risks to the living organisms and the environment. Many heavy metals are toxic such as zinc, copper, nickel, mercury, lead, cadmium, selenium, cobalt and chromium and known to cause serious health issues upon prolonged period of exposure. However, some of trace elements are essential for human health and other living organisms. Exposure to high dose of these metals over a prolonged period of time have adverse effects on human health according to the U.S. Environmental Protection Agency, and the International Agency for Research on Cancer (Tchounwou et al. 2012). Table 2.5 lists the common heavy metals and their beneficial to the human health. Also, Table 2.5 includes all toxicity effect of these metals upon prolonged exposure to high dose of these elements.

**Table 2.5:** The common heavy metals and their beneficial to the human health, recommended daily intake and toxicity effect of these metals upon exposure to high dose over prolonged period of time. (Al-Dhabi 2013, Fu and Wang 2011, Goldhaber 2003, Roohani et al. 2013).

<b>Trace elements</b>	<b>Health beneficial</b>	<b>RDI</b>	<b>Toxicity effects</b>
<b>Zinc</b>	Essential for immunity system, cell growth, wound healing and breakdown of carbohydrates.	15 mg/day	Stomach cramps, skin Irritations, vomiting, nausea and anaemia
<b>Copper</b>	Maintain normal nervous and reproductive systems	2.0 mg/day	Vomiting, cramps, convulsions, or even death
<b>Nickel</b>	Increases iron absorption and treat osteoporosis.	0.4 mg/day	Lung and kidney problems, skin dermatitis, pulmonary Fibrosis and gastrointestinal distress.

<b>Mercury</b>	N/A	0.01 mg/day	Cause damage to the central nervous system, impairment of pulmonary and kidney function, chest pain and dyspnoea.
<b>Cadmium</b>	N/A	N/A	Bone disease, kidney and liver dysfunction.
<b>Lead</b>	N/A	0.002 mg/day	Cause damage to central nervous system, kidney, liver and reproductive system, basic cellular processes and brain functions.
<b>Chromium</b>	maintaining normal glucose metabolism	0.12 mg/day	Skin irritation and lung cancer.
<b>Iron</b>	Maintain healthy haemoglobin and myoglobin production.	18 mg/day	Vomiting, cardiovascular, blood, central nervous systems, kidney, and liver damage.
<b>Manganese</b>	Prevent Osteoporosis and arthritis. Maintain cognitive function, lung and respiratory healthy system.	2 mg/day	Psychologic and neurologic disorder.
<b>Selenium</b>	Regulate thyroid hormone metabolism and redox status of vitamin C	0.07 mg/day	Hair and nail loss, gastrointestinal problems, skin rash and nervous system dysfunction.

## 2.6 Treatment technologies for wastewater laden with heavy metal ions and dyes

Wastewater effluents contain organic synthetic dyes and inorganic heavy metal ions which are potential hazardous to the environment, human and other living organism. These pollutants are purged from multiple sources such as textile, cosmetic, paper, fertilizer, mineral processing, textile, and mining, smelting operations, heavy and fine chemicals industrial production and pharmaceuticals (Dawood and Sen 2014, Kara et al. 2017). It is estimated that 10-25% of textile dyes are lost during the dyeing process, and 2-20% are directly discharged as effluents into the environment (Carmen and Daniela 2012). Various physical, chemical and biological methods are used to treat these aqueous phase pollutants (Sen et al. 2012). Fig.2.1 presented the various technologies used in water and wastewater treatment. However, these separation techniques have their own limitations in terms of design, operation method and cost. The advantages and limitations of these techniques in the removal of organic dyes and inorganic heavy metals have been presented in Table 2.6.

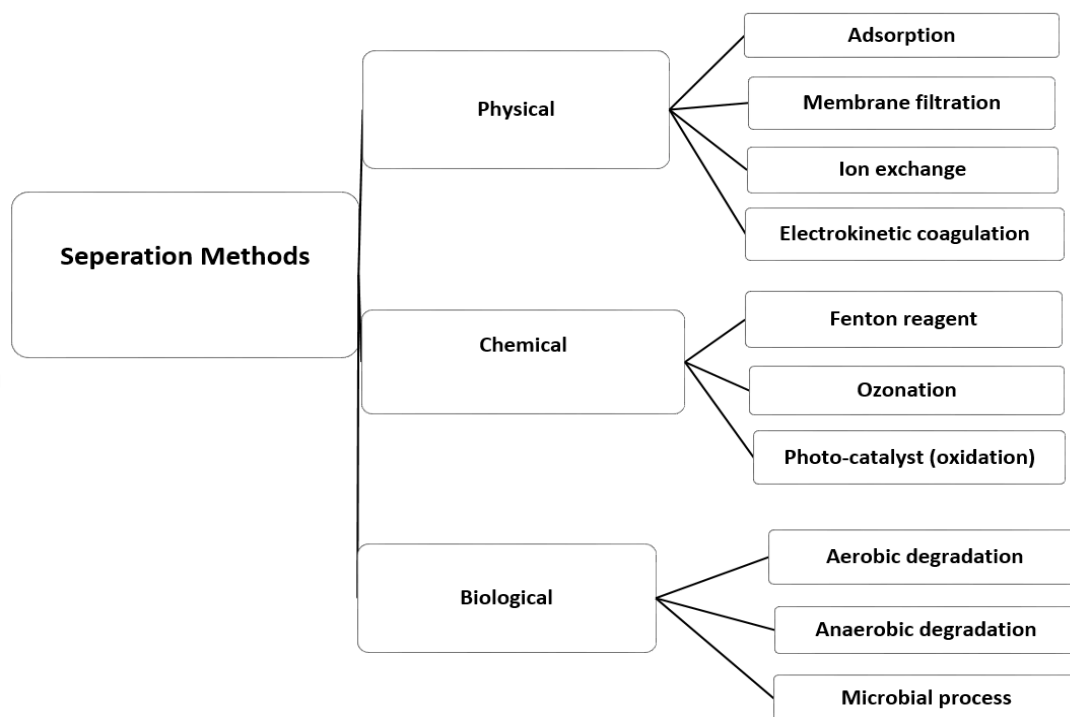


**Figure 2.1:** Various separation methods used in the removal of organic and inorganic pollutants from wastewater.

**Table 2.6:** The advantages and limitations of various separation techniques used in the removal of dyes and heavy metal ions (Carmen and Daniela 2012, Dawood and Sen 2014, Ghosh et al. 2016, Yagub et al. 2014a).

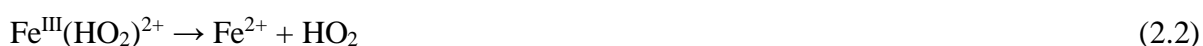
<b>Separation Technique</b>	<b>Advantages</b>	<b>Limitations</b>
<b>Physical</b>		
Adsorption	Good adsorption capacity for wide variety of dyes and heavy metal ions.	High cost of adsorbents and intensive regeneration process.
Ion exchange	Low loss of adsorbents during regeneration.	Not effective for all dyes.
Membrane filtration	Effective for all dyes and heavy metal ions. Able to recovery and reuse of chemicals and water.	Suitable for treating low effluent volume and produce high concentrated sludge.
Electrokinetic coagulation	Economically feasible.	High sludge production.
<b>Chemical</b>		
Fenton reagent	Effective process. No energy need to activate hydrogen peroxide.	Sludge production and costly.
Ozonation	Applied in gaseous state with no alteration to volume.	Half-life is very short (20 min). Not applicable for dispersed dyes.
Photo-catalyst	Good removal of heavy metal ions and dyes and by-products are non-toxic.	Long duration time and suitable for small amount of coloured compounds.

Photochemical	No sludge production.	Formation of by-products. Requires large amount of dissolved oxygen.
Electrochemical oxidation	Rapid process for most dyes and some metal ions and by-products are non-hazardous.	Expensive process.
Chemical precipitation	Low capital cost and simple operation process.	Sludge generation. Extra operational cost for sludge removal.
<b>Biological</b>		
Aerobic degradation	Efficient in the removal of heavy metal ions and all types of dyes	Sludge production and an expensive process.
Anaerobic degradation	By-products such as methane gas can be used as an energy source. Effective for wide range of dyes.	Slow process requires long acclimatization time of the microorganism. Production of toxic by-product
Microbial process	Good removal efficiency for heavy metal ions and dyes with low volume and concentration.	Culture maintenance is costly. Not suitable for industrial application because it cannot handle large effluent volume.

### 2.6.1 Chemical Methods

Chemical separation methods such as photochemical, photocatalyst, electrochemical, chemical precipitation, redox mediator and advanced oxidation technologies (AOTs) are widely used in the removal of organic and inorganic pollutants from wastewater. The effectiveness of advanced oxidation technologies (AOTs) are based on the generation of oxidizing reagent ( $\bullet\text{OH}$ ) radicals as they attack the Chromophores leading to the production of organic peroxide radicals and finally convert to  $\text{CO}_2$ ,  $\text{H}_2\text{O}$  and inorganic salts (Antoniadis et al. 2010). Chemical oxidation is very effective but the efficiency strongly influenced by the type of oxidant (Forgacs et al. 2004). ATOs include the use of oxidants such as chloride, ozone, Fenton and Fenton-like reagents and chlorine dioxide.

**Fenton's reagent** is also known as hydrogen peroxide and it is more effective if applied at low pH aqueous solution. Iron ions such as  $\text{Fe}^{+2}$  and  $\text{Fe}^{+3}$  are the most common reagents used in Fenton activation where Fenton's reagent is cheap and easy to handle compared to other reagents. The decomposition of Fenton-like reagent is presented in the following equations (Jiang et al. 2013).



The iron (III) reacts with hydrogen peroxide to form iron (III) peroxy complex. The complex is decomposed to produce iron (II) then it reacts with hydrogen peroxide to yield the oxidant, hydroxyl radicals. This process has its own limitations as these reagents are toxic and may cause more harm to the treatment system used for the post treatment (Arslan-Alaton et al. 2008). Also, the hazards associated with the disposal of large amount of sludge limits the use of this process in industrial scale. The removal of organic and inorganic pollutants by Fenton and Fenton-like reagents are reported such as the removal of Direct Red (Babaei et al. 2017), Direct Blue (Ertugay and Acar 2017), Reactive Red, Acid Blue and Direct Blue (Forgacs et al. 2004), Acid Orange and Reactive Blue (Arslan-Alaton et al. 2008), Reactive Black 5, Reactive Orange 16 and Reactive Blue 2 (Su et al. 2011). Fenton and Fenton like also have been reported in the removal of trace element such as nickel (Fu et al. 2009) and zinc (Mikhailov et al. 2017).



**Ozonation** is one of the AOTs used in the removal of various pollutants from wastewater effluents. Ozonation works when Ozone ( $O_3$ ) attacks the nitrogen conjugated double bonds which are often associated with colours. Also, Ozonation reactions can be categorized into direct reaction and indirect reaction based on solution pH (Gao et al. 2012, Turhan et al. 2012). The decomposition rate of ozone is affected by solution pH and initial solute concentration as higher pH solution tends to decompose rapidly to yield the hydroxyl radical while at lower pH solution, ozone can directly react with organic substrates as an electrophile (Turhan et al. 2012). Ozonation is widely used in the removal of organic wastewater and selected inorganic waste. Reactive Red 135 (Sharma et al. 2013), Reactive Black 5 (Venkatesh et al. 2017) and cobalt-Nickel (Flett 2004) have been removed by ozonation process. However, the half-life of ozone is very short and it requires a high voltage to run a continuous ozonation process thus increases the capital cost and limits its uses in the industrial scale (Robinson et al. 2001).

**Photocatalyst** is a process used in the removal of organic and inorganic contaminations simultaneously from wastewater effluents. Photocatalyst works by the production of positively oxidative radicals which cause the decomposition of organic and inorganic contaminations in wastewater. Band gap can be described as a region between the valence band and the conduction band of the semiconductor. Photon energy equal or higher than the band gap energy is required to excite the electrons from the valence band to the conduction band thus electrons leave holes with positively charged ions ( $H^+$ ) in the valence band. The electrons at the conduction band react with the oxygen molecules to form strong oxidative radicals that also cause the decomposition of organic and inorganic contaminations in wastewater (Cao et al. 2011). Photocatalyst has feasible applications in wastewater treatment as it can operate at ambient temperature and pressure with complete mineralization thus reduce total operating cost. Photocatalyst operates at ambient operation conditions such as temperature and pressure with complete mineralization and shorter detention time therefore reduce total operating cost. Photocatalyst, such as titanium dioxide ( $TiO_2$ ), zinc oxide ( $ZnO$ ), iron (III) oxide ( $Fe_2O_3$ ), zirconia ( $ZrO_2$ ), vanadium (V) oxide ( $V_2O_5$ ), niobium pentoxide ( $Nb_2O_5$ ) and tungsten trioxide ( $WO_3$ ) have been successfully used in the removal of various organic and inorganic contaminations (Lee et al. 2016a). Various photocatalysts have been reported in the removal of dyes and heavy metals ions from wastewater such as Methyl Orange dye (Cao et al. 2011, Fan et al. 2012), Rhodamine B, Methyl Orange and methylene Blue dyes (Li et al. 2016a), Brilliant Green and Methylene Blue dyes (Ragupathy et al. 2015), Cadmium and lead (Priyadharsan et al. 2017) and Chromium, cobalt and lead (Harraz et al. 2013).

**Electrochemical** (EC) oxidation is a successful method in the removal of most types of dyes and some metal ions. The high cost associated with the energy use and the formation of by-product are the main drawbacks of this technique (Woissetschläger et al. 2013). This reaction involves an electric charges moving between the electrodes and an electrolyte (dye or heavy metal in its aqueous solution). Electrochemical oxidation of pollutants can take place through direct anodic oxidation, where the pollutants are destroyed at the anode surface or through indirect oxidation, where a mediator ( $\text{HClO}$ ,  $\text{O}_3$ ,  $\text{H}_2\text{S}_2\text{O}_8$ , etc.) is electrochemically generated to carry out the oxidation (Vasudevan and Oturan 2014). EC oxidation process has been used in the removal of Novacron Yellow and Remazol Red dyes (Araújo et al. 2014), Acid Blue 29, Acid Red 97, Reactive Red 2 and Reactive Blue4 dyes (Körbahti et al. 2011), Copper and nickel (Körbahti et al. 2011) and Chromium (Vasudevan et al. 2010).

### 2.6.2 Biological Methods

Biological treatment involves the use of microorganisms under aerobic or anaerobic conditions in order to degrade the organic contamination such as dyes and inorganic pollutant such as heavy metal ions from wastewater. Aerobic degradation process involves the presence of oxygen while anaerobic process is in the absence of oxygen. Biological treatment may also involves the use of combined aerobic and anaerobic methods. Further, microbial process is used in the removal of dyes and heavy metal ions from aqueous solutions through a microbial biomass such as fungi, bacteria, yeast, algal biomass and non-living biomass such as squid, crab shell, shrimps, etc.(Pang and Abdullah 2013).

**Aerobic Degradation** can be defined as the use of microorganisms such as bacteria, yeast, algae and fungi in the decolourization of dyes and heavy metal ions from their aqueous solution under aerobic conditions. Bacteria are able to culture and grow more quickly than fungi because they are able to metabolize chlorinated and other organic contaminants and use them as an energy source. Bacteria presented in the wastewater has either mono-oxygenase or di-oxygenase enzymes and they are used to catalyse the incorporation of oxygen from  $\text{O}_2$  into the aromatic ring of organic compounds such as azo dyes and reactive dyes (dos Santos et al. 2007, Khouni et al. 2012). Many researchers have investigated the use of bacteria in the removal of dyes and heavy metals from wastewater such as the removal of Blue Bezaktiv dye BB150 by lyophilised bacterial consortium (Khouni et al. 2012), Reactive Black 5 dye, Ni(II) and Cr(VI) by *Lysinibacillus* sp. bacteria CD-F (San Keskin et al. 2018), Congo red dye by consortium

SKB-II bacteria (Tony et al. 2009) ,Cd (II) and Cu (II) by *Bacillus thuringiensis* FQ1 and *Stenotropho monasmaltophilia* bacteria respectively (Liu et al. 2017a).

The use of fungi in the removal of dyes and heavy metal ions is more effective compared to bacteria and algae. The successful use of fungi have been reported such as the removal of azo dyes by *Candida tropicalis* (Tan et al. 2013), Lanaset Grey G dye by *Coriolopsis gallica*, *Bjerkandera adusta*, *Trametes versicolor* and *Trametes trogii* white-rot fungi (Daâssi et al. 2013) and acid red B by *Pichia sp TCL* (Qu et al. 2012), Zn(II), Cu(II), Cd(II), Cr(VI) and Ni(II) by *Beauveria bassiana* fungi (Gola et al. 2016), Cu(II) and Acid Blue 161 dye by *Aspergillus lentulus* fungi (Mishra and Malik 2014), Cr(VI) and Pigment Orange 34 by *Aspergillus terreus* fungi and *Rhizopus oryzae* fungi respectively (Mishra and Malik 2014). Fungi have high capacity of biodegradation of dyes as they are able to deplete complex organic compounds by producing extracellular ligninolytic enzymes including laccase, manganese peroxidase and lignin peroxidase (Tan et al. 2013). The use of bacteria and fungi for the complete decolourization and degradation of dyes and removal of heavy metals from wastewater have the advantages of low cost process compared to other methods and the ability to complete mineralization of dyes with nontoxic by-products (Dawkar et al. 2010). However, this process is not applicable for real wastewater treatment because it is a very slow process and due to the production of large amount of sludge. Bacteria and fungi strains commonly used in the removal of textile dyes and heavy metals are presented in Table 2.7.

**Table 2.7:** Bacteria and Fungi strains commonly used in dye biodegradation and heavy metals removal from wastewater.

Culture	Adsorbate	Removal (%)	References
<i>Lysinibacillus sp.</i> bacteria	Ni(II)	70	(San Keskin et al. 2018)
<i>CD-F</i>	Cr(VI)	58	
	Reactive Black 5	82	
<i>R. blasticus</i> , <i>R.</i> bacteria	R. Brilliant blue	80	(Talaiekhosani and Rezania 2017)

<i>Bacillus thuringiensis FQ1</i> bacteria	Cd (II)	95.1	(Liu et al. 2017a)
<i>Stenotropho monas- maltophilia</i> bacteria	Cu (II)	76.9	
<i>Beauveria bassiana</i> fungi	Cu(II)	74.1	(Gola et al. 2016)
	Ni(II)	75	
	Cd(II)	63.4	
	Zn(II)	67.8	
	Cr(II)	61.1	
<i>Aspergillus terreus</i> fungi	Cr (VI)	95.6	(Mishra and Malik 2014)
<i>Rhizopus oryzae</i> fungi P	Orange dye	100	
<i>Candida tropicalis</i> fungi	Acid orange II	91.1	(Tan et al. 2013)
	Reactive yellow	94.2	
<i>Aspergillus lentulus</i> fungi	Cu(II)	67.3	(Mishra and Malik 2014)
	Acid blue	98	
<i>P. chrysosporium</i> fungi	Coracryl violet	100	(Chander and Arora 2007)
<i>D. squalens</i> fungi	Coracryl pink	100	
<i>Aspergillus niger</i> fungi	Direct violet	92	(Abd El-Rahim et al. 2009)
<i>T. versicolor</i> fungi	Reactive red 4	94	(Junghanns et al. 2008)
<i>Consortium Lyophilised</i> bacteria	Blue Bezaktiv	62	(Khouni et al. 2012)
<i>Consortium SKB-II</i> bacteria	Congo red	90	(Tony et al. 2009)
<i>Consortium SKB-I</i> bacteria	Blue BCC	74	

**Anaerobic degradation** process occurs in the absence of oxygen. Anaerobic digestion process is able to decompose complex organic compounds so that they can be further treated either aerobically or by other dye removal methods (Balamurugan et al. 2011). Anaerobic degradation technologies have shown their efficiency in the treatment of wastewater effluent such as anaerobic membrane bioreactor, up-flow anaerobic sludge blanket, anaerobic sequencing batch reactor and moving bed biofilm reactor. Anaerobic sludge blanket is the widely used in the domestic and industrial wastewater treatment due to its high biomass concentration, microbial diversity, low cost, flexibility and ability to withstand various range of pH and temperature (Shi et al. 2017). Anaerobic process is usually carried out as a first step followed by aerobic process as it increases dye's biodegradability by partially hydrolysing organic pollutants with complex structure into simpler compounds. Anaerobic process is particularly suitable for the degradation of azo dyes as the highly electrophilic azo bonds undergo reductive cleavage and produce colourless aromatic amines which are easier to be degraded in the aerobic process (Deng et al. 2016). Dyes and heavy metals reduction under anaerobic conditions have been reported such as removal of Acid orange 7 (Deng et al. 2016), Pb(II) and Cu(II) (Liu et al. 2017b), Methyl orange and Naphthol green B (Cao et al. 2013), Ni(II) and Cd(II) (Inyang et al. 2012), Reactive red (Balamurugan et al. 2011) and Pb(II) (Inyang et al. 2011). The limitations of this process include the need for further treatment under aerobic conditions and production of toxic methane gas and hydrogen sulphide by-products. Thus a combination of anaerobic and aerobic process is recommended for the biodegradation of textile azo dyes.

### 2.6.3 Physicochemical methods

**Ion exchange** resins contains insoluble solids which are able to absorb positively or negatively charged ions from aqueous electrolyte solutions and releases other ions of equivalent amount into the aqueous solution spontaneously (Haddad 2005). Ion-exchange membranes have been used successfully in the removal and controlling of wastewater pollution due to lower capital cost, smaller space requirement and low loss of adsorbent during regeneration (Labanda et al. 2009). The cost effectiveness, rapid kinetics and high removal efficiency in the recovery of heavy metals depend on the ion selectivity, ion-exchange binding capacity, and the resin surface area (Chitpong and Husson 2017). However, ion exchange membranes are not suitable for all types of dyes. The removal of toxic dyes and heavy metals from wastewater by ion exchange resins have been successfully reported such as removal of Cu(II), Cd(II), Co(II) and Pb(II) ions (Kołodzyńska et al. 2017a), Cd(II), Ni(II) and Ca(II) (Chitpong and Husson 2017),

cationic Rhodamine B dye and Pb (II) (Saruchi and Kumar 2016), anionic Orange-G dye (Labanda et al. 2009) and cationic Methyl violet dye (Wu et al. 2008).

**Membrane Filtration** is used to separate ions from solution. Some undesirable particles may pass into the filtrate solution depend on the pore size and thickness of the filter membrane. Microfiltration, ultrafiltration (UF), nanofiltration (NF), reverse osmosis (RO) are used in the removal of wastewater effluents due to the availability of membranes with higher flux and lower process cost (Nandi et al. 2008). Polymeric and ceramic membranes are commonly used due to their high mechanical, thermal and chemical stability. However, some polymeric membrane have a low hydrophobic nature, thus limit their applications in membrane separation techniques. Therefore, to increase their hydrophilicity, an addition of inorganic fillers into the membrane such as zeolite has been reported (Yurekli et al. 2017). Various membrane filtration have been reported in the removal of toxic dyes and heavy metals from wastewater such as Pb(II) and Ni(II) ions (Yurekli et al. 2017), Reactive black 5 (Alventosa-deLara et al. 2014), Methylene blue (Cheng et al. 2012) and cotton dye effluent (Avlonitis et al. 2008). Filtration separation techniques are applicable for all types of dyes. However, it is only suitable for effluents with low volume. Further, chemical auxiliaries such as suspended particles, salts and other organic matter tend to accumulate within a thin boundary layer adjacent to the membrane surface, causing concentration polarization (Alventosa-deLara et al. 2014). This increases the osmotic pressure near the membrane–solution interface, which decreases the driving force and thus the permeation of solvent.

**Electrokinetic coagulation (EC)** is an economically feasible method used in the wastewater treatment. It involves the use of direct current source between metal electrodes immersed in water effluent which cause the dissolution of metal plates into wastewater (Aoudj et al. 2010). Usually aluminium and iron electrodes are used. The metal ions form coagulated for particulates flocculating which cause metal hydroxides to precipitate thus adsorb the dissolved organic and inorganic contaminants. The use of electrokinetic coagulation is more favourable than conventional coagulation as it requires less chemicals, ability to remove hydrophobic and hydrophilic colloids and its ease to adapt other existing treatments (Matilainen et al. 2010). EC separation process has been reported in the removal of acid Black 194 (Vidal et al. 2016), direct red 81 (Aoudj et al. 2010), reactive blue 140 (Phalakornkule et al. 2010), disperse red (Merzouk et al. 2011), Zn(II) and Ni (II) (Bratskaya et al. 2009) by various researcher. The disadvantages

associated with this process are the need for further treatment by flocculation and filtration and high amount of sludge produced.

## 2.7 Adsorption

Adsorption separation process involves the transfer of adsorbate ions, atoms or molecules from the bulk aqueous phase to the surface of the adsorbent creating a thin film as shown in Fig 2.2. The adsorbate can be in gas, liquid or dissolved solute phases. The adsorption process depends on the type of bond occurs between the adsorbate molecules and the adsorbent surface. Physical adsorption occurs due to weak physical forces such as Van der Waals, hydrophobicity, hydrogen bond, polarity, static interaction, dipole –dipole interaction and  $\pi$ -  $\pi$  interaction therefore in most cases it is reversible process. Chemical adsorption which is also known as chemisorption or Langmuir adsorption occurs if the adsorbate is chemically bound to the adsorbent surface through the formation of ionic or covalent bonds and thus it is irreversible (Yagub et al. 2014a). The adsorption capacity depends on the nature of adsorbate such as molecular weight, molecular structure, molecular size, polarity and solution concentration and adsorbent-adsorbate interaction. It is also depends on the surface properties of adsorbent such as particle size, surface area, surface charge etc. Also, various process parameters such as solution pH, initial adsorbate concentration, adsorbent dose, ionic strength, contact time and temperature may affect the total adsorption capacity.

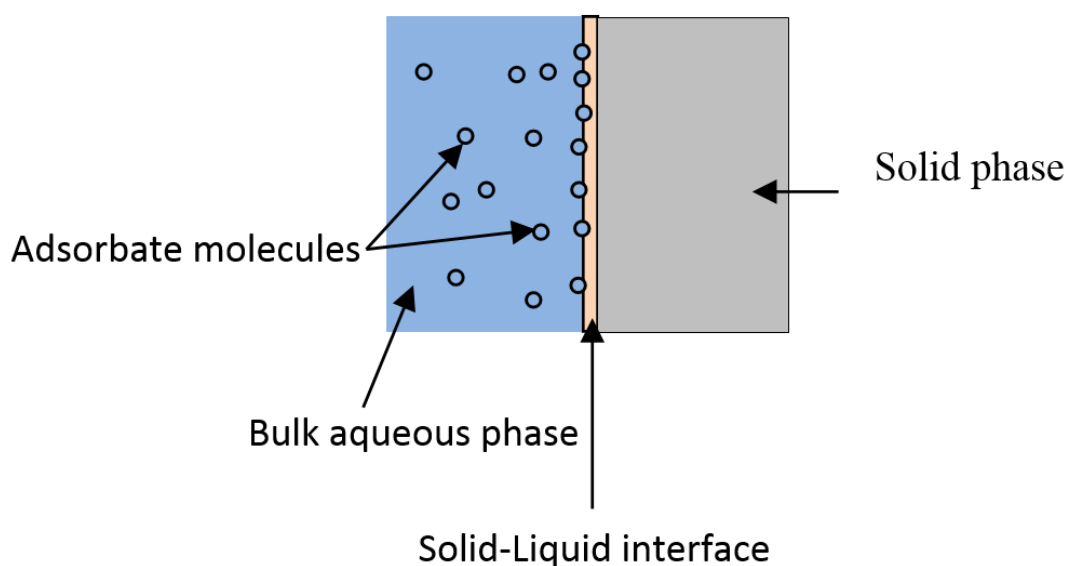


**Figure 2.2:** Solid-Liquid Adsorption separation process- Adapted from (Slejko 1985).

Adsorption separation process is widely used in the removal of various organic and inorganic pollutants from wastewater due to its simple design, ease of operation, cost effective and insensitive to toxic substances (Afroze et al. 2016c, EI-Latif et al. 2010). Various adsorbents are used in the removal of contaminants from wastewater, however commercial activated carbon is widely used (Ribas et al. 2014, Uğurlu et al. 2008) due to its excellent adsorption capacity, large surface area and hydrophobicity (Sreńscek-Nazzal et al. 2016). But due to the high cost associated with CAC production and difficulties in the adsorbent regeneration process, recent trend of research is to find alternative cost effective and nonconventional potential adsorbents. In this research direction, various alternative adsorbents such as raw and modified agricultural solid wastes (Afroze et al. 2016c, Deniz and Karaman 2011, Senthil Kumar et al. 2014), clay minerals (Hernández-Montoya et al. 2013, Kara et al. 2017), biomass based activated carbon (Aboua et al. 2015, Aguayo-Villarreal et al. 2017) and biomass based char (Sewu et al. 2017b, Zhou et al. 2017) were successfully used in the removal of organic dyes and inorganic heavy metals from wastewater by adsorption. It is evident that waste materials from industry and agriculture sources, clays and mineral oxides are effective potential adsorbents alternatives to commercial activated carbon.

### **2.7.1 Effect of physico-chemical process parameters on adsorption**

Various physio-chemical factors affect the adsorption process and the maximum adsorption capacity of adsorbent towards organic dyes and inorganic heavy metals from wastewater. The effect of initial adsorbate concentration, solution pH, adsorbent dose, solution temperature, contact time, presence of ions and stirring speed are significantly influence the adsorption process which are discussed below. The study of these physio-chemical process parameters are important in order to optimize and develop the adsorption process in an industrial scale operation.

#### **2.7.1.1 Effect of solution pH on adsorption**

The effect of solution pH in the adsorption process is very significant. The change in solution pH is an important parameter for maximum solute adsorption due to change in adsorbent's surface characteristics and change in chemistry of adsorbate. The adsorption process depends heavily on the initial adsorbate solution pH and adsorbent surface point of zero charge ( $\text{pH}_{\text{pzc}}$ ). The point of zero charge ( $\text{pH}_{\text{pzc}}$ ) is used to determine the linear range of pH sensitivity thus define the electrokinetic properties of the adsorbent surface (Yagub et al. 2014a). Solid addition



method is used to identify adsorbent's ( $pH_{pzc}$ ) as described in section 3.4.6 of chapter 3. Cationic adsorbate adsorption is favored at  $pH > pH_{pzc}$ , due to presence of functional groups such as  $OH^-$ ,  $COO^-$  groups while anionic adsorbate adsorption is favored at  $pH < pH_{pzc}$  upon the presence of  $H^+$  ions (Salleh et al. 2011). The effects of solution pH on the removal of various organic and inorganic contaminations were determined by preparing a fixed amount of adsorbate-adsorbent mixture under various solution pH while other process parameters were kept constant such as solution temperature, initial adsorbate concentration, adsorbent dose, contact time and rotating speed (Afroze et al. 2016c, Dawood and Sen 2012b).

Kolodynska et al. (Kolodyńska et al. 2017b) studied the removal of Cu(II), Zn(II) and Cd(II) by commercial activated carbon (CAC) and found that the point of zero charge ( $pH_{pzc}$ ) for CAC was about 6.8 while the maximum adsorption capacity occurred at pH of 5. Therefore, the maximum adsorption capacity occurred at  $pH < pH_{pzc}$ . On the other hand, Afroze et al. (Afroze et al. 2016c) studied the adsorption of Methylene blue dye onto raw eucalyptus bark and found that the zero point of charge ( $pH_{PZC}$ ) for raw eucalyptus bark was about 5.0 and the maximum adsorption capacity of MB was reported at pH of 10, thus maximum adsorption capacity occurred at  $pH > pH_{pzc}$ . Sewu et al. (Sewu et al. 2017b) reported the maximum adsorption capacity for Crystal violet dye by Korean cabbage biochar and rice straw biochar occurred at solution pH of 11. The adsorption of Reactive red 141 dye on raw pecan nutshell and its biochar was observed at a solution pH of 2-8 and the maximum percentage dye removal occurred at solution pH of 2 (Zazycki et al. 2018) as shown in Fig.2.3. Table 2.8 presented the various reported results on the maximum adsorption capacity and percentage removal of dyes and heavy metals under various initial solution pH.

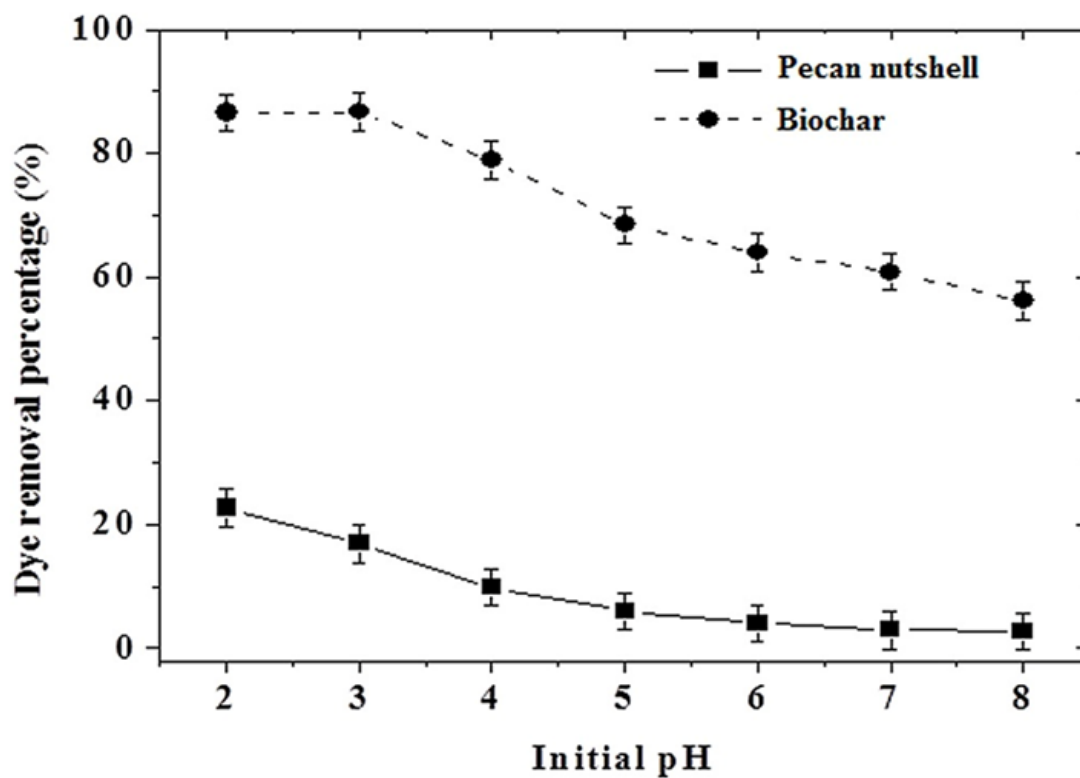


**Figure 2.3:** Effect of solution pH in the removal of Reactive red 141 dye by raw pecan nutshell and its biochar (Zazycki et al. 2018).

**Table 2.8:** Removal of dyes and heavy metal ions by adsorbents at various initial solution pH.

<b>Adsorbent</b>	<b>Adsorbate</b>	<b>pH range</b>	<b>Removal range</b>	<b>Reference</b>
Raw pecan nutshell	Reactive	2-8	85-60%	(Zazycki et al. 2018)
Pecan nutshell char	red 141		23-5%	
Korean cabbage biochar	Crystal violet	4-11	Increase	(Sewu et al. 2017b)
Bentonite	Al (III)	2-9	52- 96%	(Chai et al. 2017)
Kaolin			40- 95%	
Commercial activated carbon	Cu(II)	5	80.6%	(Kołodzyńska et al. 2017b)
Fe <sub>3</sub> O <sub>4</sub> /kaolin composite	Direct red	3-11	90-63%	(Magdy et al. 2017)
Mushroom biochar	Crystal violet	2-8	Increase	(Sewu et al. 2017a)
banana peel biochar	Pb (II)	4-7	70-90%	(Zhou et al. 2017)
Mango leaf	Methylene blue	2.5-10	10-40 mg/g	(Uddin et al. 2017)
Chitosan /carbon composite	Methylene blue	3-11	80-93 mg/g	(Marrakchi et al. 2017)
Chickpea shell	Acid blue 25	2-12	83-20%	(Krishna et al. 2017)
Black eyed biomass	Pb (II)	2-6	35-93%	(Guyo and Moyo 2017)

Tea leaf activated carbon	Orange G	2.5-11	198-85 mg/g	(Goswami and Phukan 2017)
Bamboo leaf	Methylene blue	2-12	8-84.7%	(Zhu et al. 2016)
Cucumis peel	Acid blue 113	2-11	97.7-75%	(Lee et al. 2016b)
Eucalyptus bark (EB) Base modified EB	Zn (II)	3-5.1	20-40% 40-69%	(Afroze et al. 2016b)
Eucalyptus bark	Methylene blue	2.5-10	58-89%	(Afroze et al. 2016c)
iron-manganese oxide /kaolin composite	Crystal violet	4-11	27-94.8%	(Khan et al. 2015)
Rapeseed oil cake activated carbon	Ni (II) Pb (II)	1-6 1-6	30-100 mg/g 25-110 mg/g	(Uçar et al. 2015)
Pine cone activated carbon	Congo red	2.6-8.2	77-7.6%	(Dawood et al. 2014)
Coal fly ash	Ni (II) Cu(II)	3-10	5-95% 2-98%	(Sočo and Kalembkiewicz 2013)
Zeolite	Methylene blue	5-12	99-77%	(Rida et al. 2013a)
Raw pine cone Acid modified pine cone	Congo red	3.6-11 3.6-7.5	5.8- 60.5% 16-79%	(Dawood and Sen 2012b)
Pine tree leaves	Methylene blue	2-9	20-80%	(Yagub et al. 2012)
kaolin	Zn(II)	3.4-8	6-62.5 mg/g	(Aries and Sen 2009)

### 2.7.1.2 Effect of adsorbent dose on adsorption

Adsorbent dosage is another important parameter for the determination of adsorbent quantity. The effect of adsorbent dosage on the removal of various organic and inorganic contaminations is determined by preparing a fixed amount of adsorbate concentration with various amount of adsorbent dose while other process parameters were kept constant such as solution temperature, solution pH and rotating speed until equilibrium time attained (Afroze et al. 2016c, Dawood and Sen 2012b).

In general, the adsorbate percentage removal is increasing with the increase of the adsorbent dosage while the amount of adsorbate adsorbed  $q_e$  (mg/g) is decreasing with the increases of the adsorbent dosage (Dawood and Sen 2014, Salleh et al. 2011). The increase in the percentage of dye and heavy metal removal with adsorbent dosages could be attributed to increase in the adsorbent surface areas thus the number of adsorbent active sites due to the increase in the adsorbent mass. However, the decrease in adsorption capacity  $q_e$  (mg/g) with increasing adsorbent dose is due to the split in the flux or the concentration gradient between solute concentration in the solution and the solute concentration in the surface of the adsorbent causing a decrease in equilibrium adsorption capacity (Sen et al. 2012). Kılıç et al. (Kılıç et al. 2013) studied the adsorption of Ni (II) and Co (II) onto almond shell biochar by increasing the adsorbent dose from 1-10 g/L and found the percentage Ni (II) and Co (II) ions removal increased from 10% to 38% and from 25% to 50% respectively while the amount of Ni (II) and Co (II) ions adsorbed  $q_e$  (mg/g) decreased from 10 mg/g to 3 mg/g and from 24 mg/g to 7 mg/g respectively.

However, few researchers reported a decrease in the percentage adsorbate removal with the increases of adsorbent dose (Senthil Kumar et al. 2014). Senthil Kumar et al., (Senthil Kumar et al. 2014) observed the percentage of methylene blue dye removal onto modified mango seed decreased from 99.8% to 79% upon the increases of adsorbent dose from 0.1 g to 1.2 g. Uddin et al., observed that the percentage removal of Methylene blue dye increased from 82% to 99% while the adsorption capacity decreased from 164 mg/g to 25 mg/g with an increase in the mango leaf adsorbent dose from 0.1 to 0.8 g respectively (Uddin et al. 2017) as shown in Fig.2.4. The effect of adsorbent dosage of various adsorbents on the adsorption capacity and percentage removal of dyes and heavy metals is compiled and presented in Table 2.9.

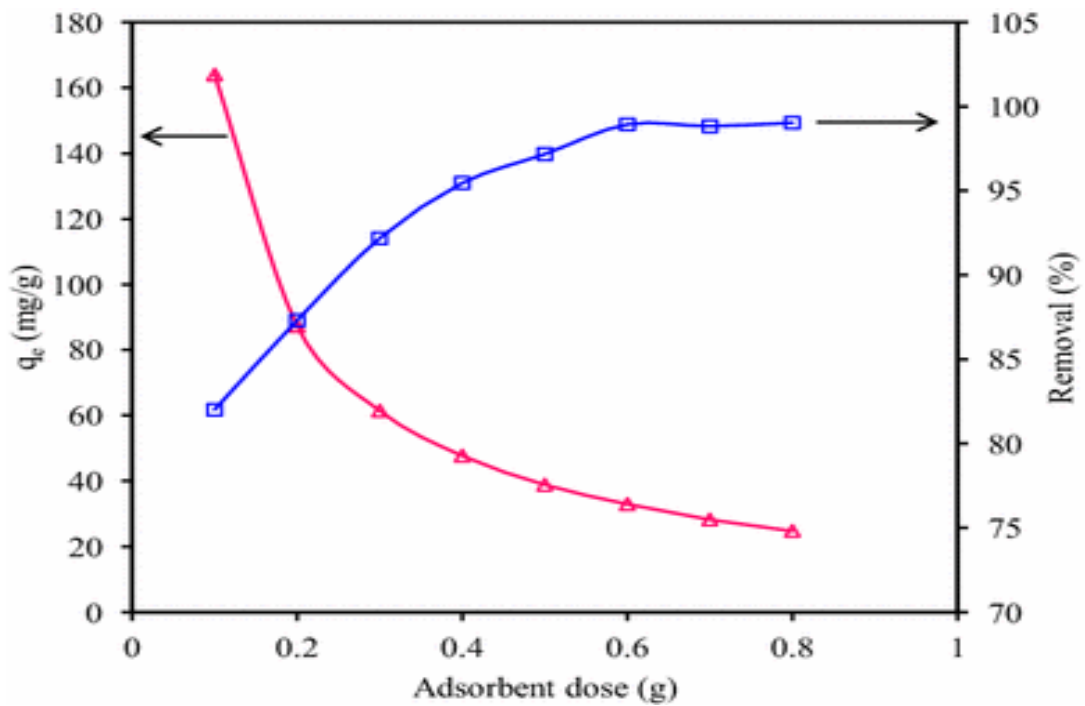


**Figure 2.4:** The effect of adsorbent dose on MB dye adsorption by mango leaf. Initial dye concentration=100 mg/L and volume= 200ml (Uddin et al. 2017).

**Table 2.9:** The effect of adsorbent dosage of various adsorbents on the adsorption capacity and percentage removal of dyes and heavy metals.

<b>Adsorbent</b>	<b>Adsorbate</b>	<b>Adsorbent dose range</b>	<b>Removal range</b>	<b>Reference</b>
banana peel biochar	Pb (II)	10-200 mg	200-19 mg/g	(Zhou et al. 2017)
Mango leaf	Methylene blue	0.1-0.8 g	60-98%	(Uddin et al. 2017)
Fe <sub>3</sub> O <sub>4</sub> / kaolin composite	Direct red 23	0.25-0.75 g	79-100%	(Magdy et al. 2017)
Base modified cedar biomass	Ni (II) Pb (II)	0.1-1.5 g	28-8% 88-23%	(Lago et al. 2017)
Chickpea shell	Acid blue 25	10-300 mg	1-55%	(Krishna et al. 2017)
Black eyed biomass	Pb (II)	0.2-1.6 g/L	77-96%	(Guyo and Moyo 2017)
Bamboo leaf	Methylene blue	0.05-0.3 g	37-93%	(Zhu et al. 2016)
Bentonite Kaolin	Al (III)	4-20 g/L	35-98% 12-90%	(Chai et al. 2017)
Cucumis peel	Acid blue 113	0-20 g/L	8-78%	(Lee et al. 2016b)
Eucalyptus bark (EB) Base modified EB	Zn (II)	10-30 mg	45-30% 70-55%	(Afroze et al. 2016b)
Eucalyptus bark	Methylene blue	10-30 mg	73-94%	(Afroze et al. 2016c)

Iron-manganese oxide /kaolin composite	Crystal violet Basic fuchsin	1-4 g/L 2-5 g/L	84-97% 41-94.5%	(Khan et al. 2015)
Tea waste AC	Eosin yellow	1-3 g/L	88-98%	(Borah et al. 2015)
Peanut husk	Indosol orange	0.05-0.3 g	41-8 mg/g	(Sadaf and Bhatti 2014)
Pine cone carbon	Congo red	10-30 mg	77-81%	(Dawood et al. 2014)
Modified mango seed	Methylene blue	0.1-1.2 g	69-98%	(Senthil Kumar et al. 2014)
Almond shell biochar	Ni (II) Co(II)	1-10 g/L	10-38% 26-50%	(Kılıç et al. 2013)
Zeolite Kaolin	Methylene blue	0.1-3 g/L	92-96% 92-94.5%	(Rida et al. 2013a)
Raw pine cone Acid modified pine cone	Congo red	10-30 mg 30 mg	13.5-19% 85%	(Dawood and Sen 2012b)
Pine tree leaves	Methylene blue	10-30 mg	95.5-98%	(Yagub et al. 2012)
Kaolin	Zn (II)	10-30 mg	29-10.7 mg/g	(Aries and Sen 2009)



### **2.7.1.3 Effect of solution temperature on adsorption**

The effect of temperature is an important process parameter for the adsorption process. The equilibrium capacity of any adsorption system changes with the changes of initial solution temperature. The effect of temperature changes on the removal of various organic and inorganic contaminations is determined by preparing a fixed amount of adsorbate-adsorbent mixture while other process parameters were kept constant such as adsorbent dose, initial adsorbate concentration, solution pH, contact time and rotating speed (Afroze et al. 2016c, Dawood and Sen 2012b).

Increasing the temperature of the adsorbate-adsorbent system leads to increase the adsorbate molecules rate diffusion into the external boundary layer and in the internal pores of the adsorbent particles due to the decrease in the viscosity of the solution (Hameed and Ahmad 2009). An endothermic reaction occurs if the adsorption capacity increase with the increases of solution temperature. This is due to the increases of the adsorbate's molecules mobility and kinetic energy resulting in a higher intra-particle diffusion rate and unequivocally attributable to chemisorption (Afroze et al. 2016c). On the other hand, if the adsorption capacity decreased with the increases of solution temperature, this indicates an exothermic reaction. An exothermic reaction results in the emission of heat as a form of energy into its surroundings during the adsorptive process, due to the decreases of adsorptive forces between the adsorbate molecules and the active site on the adsorbent surface (Tran et al. 2016).

Various researchers reported an endothermic reaction process with the increases of solution temperature such as the removal rhodamine B dye by tea leaf activated carbon (Goswami and Phukan 2017), Congo red dye by pine cone activated carbon (Dawood et al. 2014), Zn(II) and Ni (II) ions by metakaolin based geopolymer (Kara et al. 2017). Other research articles reported an exothermic reaction process with the increases of solution temperature such as reactive red 141 dye by pecan shell biochar (Zazycki et al. 2018), methylene blue dye by bamboo leaf (Zhu et al. 2016) and Cd (II) ions by orange peel (Tran et al. 2016) as shown in Fig. 2.5. The effect of temperature in the removal of dyes and heavy metals ions by various adsorbents is compiled and presented in Table.2.10.

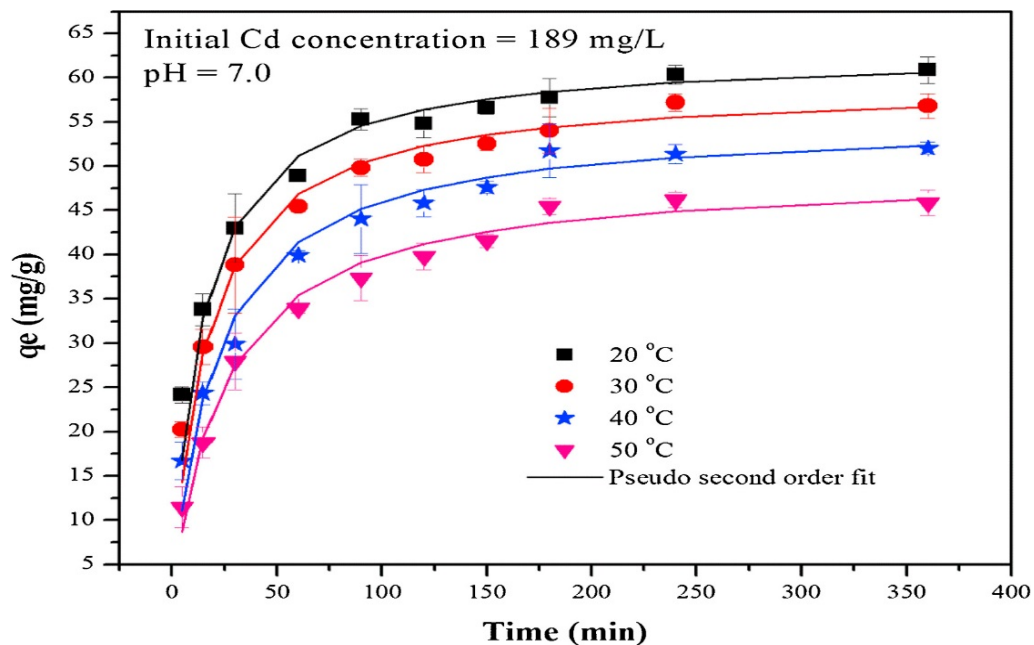


**Figure 2.5:** Effect of temperature in the removal of Cd (II) ions by orange peel , initial ion concentration= 189 mg/L and pH =7 (Tran et al. 2016).

**Table 2.10:** The effect of solution temperature in the removal of dyes and heavy metals ions using various adsorbents.

Adsorbent	Adsorbate	T(°C) range	Reaction type	Reference
Pecan nutshell char	Reactive red 141	20-80	Exothermic	(Zazycki et al. 2018)
Fe <sub>3</sub> O <sub>4</sub> / kaolin composite	Direct red 23	25-50	Endothermic	(Magdy et al. 2017)
Chitosan AC	Methylene blue	30-50	Endothermic	(Marrakchi et al. 2017)
Meta-kaolin	Zn(II) , Ni (II)	10-25	Endothermic	(Kara et al. 2017)

---

Chickpea shell	Acid blue 25	35-65	Exothermic	(Krishna et al. 2017)
Black eyed Biomass	Pb (II)	20-40	Endothermic	(Guyo and Moyo 2017)
Tea leaf AC	Orange G	30-50	Endothermic	(Goswami and Phukan 2017)
Bentonite Kaolin	Al (III)	25-50	Endothermic Exothermic	(Chai et al. 2017)
Bamboo leaf	Methylene blue	10-60	Exothermic	(Zhu et al. 2016)
Cucumis peel	Acid blue 113	30-50	Endothermic	(Lee et al. 2016b)
Eucalyptus bark	Zn (II)	30-60	Exothermic	(Afroze et al. 2016b)
Eucalyptus bark	Methylene blue	30-60	Endothermic	(Afroze et al. 2016c)
Wood char	Rhodamine B	25-60	Exothermic	(Maneerung et al. 2016)
Iron-manganese oxide /kaolin Composite	Crystal violet	30-40	Endothermic	(Khan et al. 2015)
Tea waste AC	Eosin yellow	30-50	Endothermic	(Borah et al. 2015)
Peanut husk	Indosol orange	30-50	Exothermic	(Sadaf and Bhatti 2014)
Pine cone AC	Congo red	25-55	Endothermic	(Dawood et al. 2014)
Almond shell char	Ni (II), Co (II)	20-40	Endothermic	(Kılıç et al. 2013)
Raw pine cone	Congo red	30-60	Endothermic	(Dawood and Sen 2012b)

---

---

Pine tree leaves	Methylene blue	30-60	Endothermic	(Yagub et al. 2012)
Kenaf fibre char	Methylene blue	30-50	Endothermic	(Mahmoud et al. 2012)
Pine tree leaves	Basic red 46	25-45	Endothermic	(Deniz and Karaman 2011)
Kaolin	Zn (II)	30-65	Exothermic	(Aries and Sen 2009)

---

#### 2.7.1.4 Effect of initial adsorbate concentration and contact time on adsorption

Understanding the effect of initial adsorbate concentration on adsorption process is essential for developing sorbent based wastewater technology. The effect of initial adsorbate on adsorption process depends heavily on the adsorbates concentration and the available active sites on the adsorbent surface. The effects of initial adsorbate concentration on the adsorption capacity and percentage adsorbate removal were determined by preparing a adsorbate-adsorbent solution under various initial adsorbate concentration while other process parameters were kept constant such as adsorbent dose, temperature, solution pH, contact time and rotating speed until equilibrium time attained (Afroze et al. 2016c, Dawood and Sen 2012b).

Increasing the initial adsorbate concentration leads to the decreases of percentage adsorbate removal and an increases in the amount of organic dye or inorganic heavy metal ions adsorbed per gram adsorbent. The initial adsorbate concentration provides a driving force to overcome the resistance to the mass transfer of the organic or inorganic adsorbate between the its aqueous phase and solid phase (Salleh et al. 2011). This increases in the adsorbate concentration tends to increase the adsorbate sorption at the initial stages however after initial adsorption stage, the adsorbate concentration gradient reduce and reach an equilibrium phase due to the accumulation of adsorbate molecules on the adsorbent available active sites (Uddin et al. 2017). The amount of adsorbate adsorbed per unit adsorbent mass  $q_t$  (mg/g) increases with the increase in initial dye and heavy metal ions concentration due to the decrease in resistance to the uptake of solute from bulk solution (Foo and Hameed 2011a, Purkait et al. 2007, Sen et al. 2011). Ding et al., reported (Ding et al. 2016) that the equilibrium adsorption  $q_e$  (mg/g) of Cd

(II), Cu (II), Zn (II) and Ni (II) by Hickory wood biochar and its base modified char increased with increasing initial metal ions concentration from 2- 100 mg/L respectively. Afroze et al., (Afroze et al. 2016c) studied the effect of initial methylene blue dye removal on raw eucalypts bark and reported that the percentage dye removal decreased from 85.9% to 38.8% with the increases of initial dye concentration from 20 to 70 mg/L, however, the amount of dye adsorbed  $q_t$  increased from 43 mg/g to 67.9 mg/g for the same dye concentration range. Said et al.,(Said et al. 2017) investigated the removal capacity of Diazonium blue dye by acid modified sugarcane bagasse and found that the percentage dye removal decreased from 66.4% to 28% while the adsorption capacity increased from 4.5 mg/g to 7 mg/g in the initial dye concentration of 50-250 mg/L as shown in Fig.2.6. Further, Kilic et al.,(Kılıç et al. 2013)reported that the adsorption capacity of Ni (II) ions (50-150 ppm) on almond shell biochar increased rapidly at initial time then slow down and reached an equilibrium at 240 mins as shown in Fig 2.7. The removal of dyes and heavy metals ions under various initial adsorbate concentration reported recently by many researchers are compiled and presented in Table 2.11.

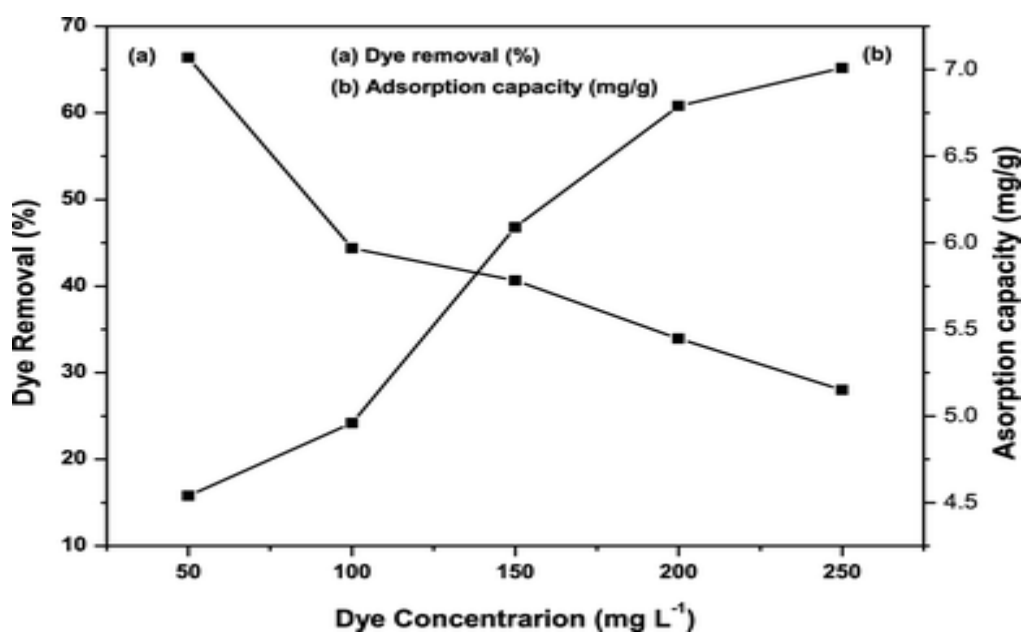


**Figure 2.6:** The effect of initial Diazonium blue dye on percentage dye removal and adsorption capacity by modified sugarcane bagasse. (Said et al. 2017).

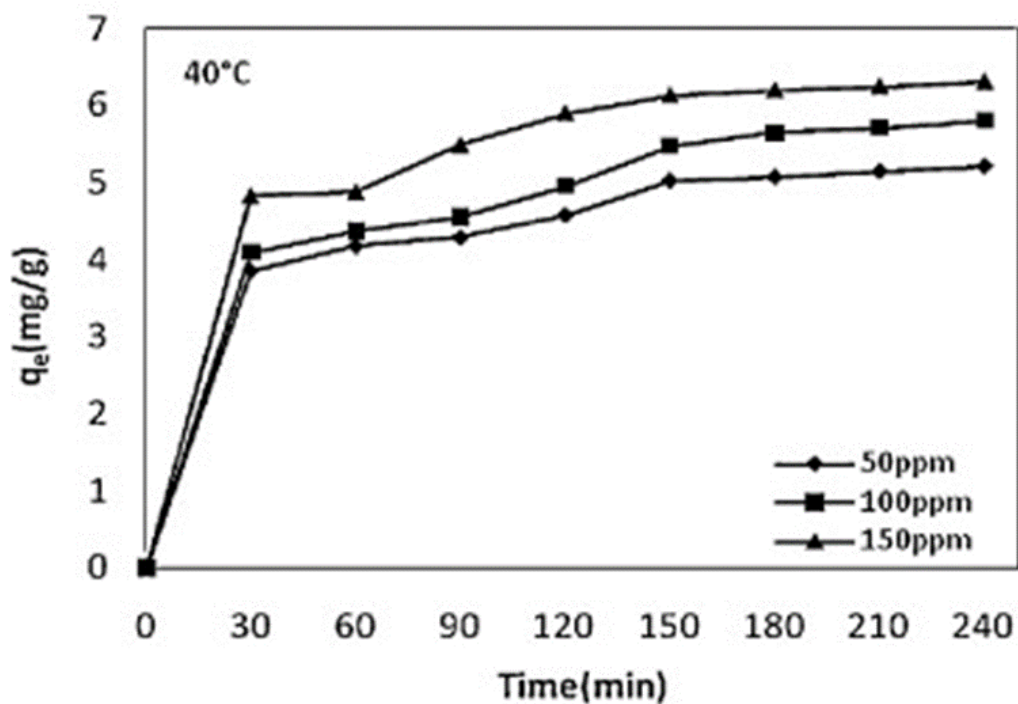


**Figure 2.7:** The effect of contact time on the adsorption capacity of Ni (II) ions by almond shell biochar. Adsorbent dose = 7 g/L, solution pH =7 and T = 40 °C. (Kılıç et al. 2013).

**Table 2.11:** The removal of dyes and heavy metals ions under various initial adsorbate concentration.

Adsorbent	Dyes and heavy metal ions	Initial Concentration Range (mg/L)	Adsorption amount and % removal range	Reference
Fe <sub>3</sub> O <sub>4</sub> /kaolin composite	Direct red 23	20-60	46- 93%	(Magdy et al. 2017)
Weed biochar	Methylene blue	50-400	27 -78 mg/g	(Güzel et al. 2017)
Acid modified Sugarcane bagasse	Diazonium blue	50-250	66- 28%	(Said et al. 2017)

Bentonite	Al (III)	10-80	1-8.5 mg/g	(Chai et al. 2017)
Banana peel biochar	Pb (II)	5-1000	7-270 mg/g	(Zhou et al. 2017)
Mango leaf	Methylene blue	100-250	79-172 mg/g	(Uddin et al. 2017)
Chitosan based AC	Methylene blue	25-400	27-129 mg/g	(Marrakchi et al. 2017)
Chickpea shell	Acid blue 25	25-100	2.1-7.7 mg/g	(Krishna et al. 2017)
Black eyed biomass	Pb (II)	10-80	95-65%	(Guyo and Moyo 2017)
Tea leaf AC	Orange G	200-800	58-99 mg/g	(Goswami and Phukan 2017)
Bamboo leaf	Methylene blue	50-250	23-52 mg/g 90-42%	(Zhu et al. 2016)
Cucumis peel	Acid blue 113	20-100	12.5-48 mg/g	(Lee et al. 2016b)
Hickory wood biochar	Pb (II)	2-100	1.5-17.8 mg/g	(Ding et al. 2016)
	Cu(II)		1.7- 15.6 mg/g	
Base modified eucalyptus bark	Zn (II)	20-70	35-60 mg/g 69-34%	(Afroze et al. 2016b)
Eucalyptus bark	Methylene blue	20-70	43-78 mg/g 86-39%	(Afroze et al. 2016c)
Kaolin/iron- manganese oxide Composite	Crystal violet	35-50	16-19 mg/g	(Khan et al. 2015)
Rapeseed cake AC	Ni (II)	50-500	40-115 mg/g	(Uçar et al. 2015)
	Pb (II)		45-122 mg/g	

Peanut husk	Indosol orange	10-200	10-79.5 mg/g	(Sadaf and Bhatti 2014)
Pine cone activated carbon	Congo red	20-60	77-216 mg/g 77-72%	(Dawood et al. 2014)
Zeolite	Methylene blue	4-37	3.4-33.5 mg/g	(Rida et al. 2013a)
Kaolin			3.3-30 mg/g	
Almond shell char	Ni (II)	50-150	4.6-5.5 mg/g	(Kılıç et al. 2013)
	Co (II)	100-200	8.6-9.8 mg/g	
Coal fly ash	Ni (II)	5-100	100-98%	(Sočo and Kalembkiewicz 2013)
	Cu (II)		96-97.6%	
Raw pine cone	Congo red	20-50	8.4-24 mg/g	(Dawood and Sen 2012b)
Kenaf fibre char	Methylene blue	50-200	10.6-17.8 mg/g	(Mahmoud et al. 2012)
Kaolin	Zn (II)	30-50	29-41 mg/g	(Aries and Sen 2009)

### 2.7.1.5 Effect of ionic strength

Industrial waste water and natural water contain significant amount of dissolved salts and hence the effect of salt on the adsorption process has to be considered. The presence of these salts in industrial effluents affects both electrostatic and non-electrostatic interactions between the adsorbent surface and adsorbate molecules hence affects the amount of adsorption. The presence of dissolved salts and its concentration depend on the water source and its quality. The effect of ionic strength on the adsorption capacity and percentage adsorbate removal was determined by preparing a fixed amount of adsorbate-adsorbent solution under various initial salt concentration while other process parameters were kept constant such as solution temperature, contact time, solution pH and rotating speed until equilibrium time attained (Afroze et al. 2016c, Stavropoulos et al. 2015).



Monovalent salt (NaCl), (KCl) and divalent salt (CaCl<sub>2</sub>) are generally used in the adsorbent-adsorbate solution to evaluate the effect of ionic presence on the amount of adsorption. The effect of ionic strength can be analysed using electric double layer model. Generally, the adsorbent surface has a net electrical charge which depends heavily on the solution pH thus the excess ions reside in a very thin layer at the solid surface (Stavropoulos et al. 2015). Ionic strength presented in the adsorbate solution influences on the hydrophobic and electrostatic interaction between adsorbate and surface functional adsorptive sites of the adsorbent (Peng et al. 2014). If the electrostatic forces between the adsorbent surface and adsorbate ions are present, an increase in ionic strength will decrease the adsorption capacity (Zhao et al. 2014a). However when the electrostatic attraction is repulsive, an increase in ionic strength will increase adsorption. The presence of external electrolyte, such as (Na<sup>+</sup>), (K<sup>+</sup>) and (Ca<sup>+2</sup>) have a limited effect on the binding efficiency between the adsorbent and the adsorbate and ions may compete with the adsorbate for binding sites on the adsorbent surface and hence reduce the adsorption capacity. Further, the molecular weight size, atomic radii and atomic charge of ions contribute significantly towards the efficiency of the adsorption process. Divalent ions have higher contribution to ionic strength and positive charge compared to monovalent ions and hence the effect of divalent ions on adsorption process is more serious than the monovalent ions (Afroze et al. 2016c) . Rida et al., (Rida et al. 2013b) studied the removal of Methylene blue dye onto kaolin and zeolite and found that the percentage dye removal decreases rapidly for both the adsorbents upon the increases of ionic salt concentration (0.1-0.g g/L) as shown in Fig.2.8. The effect of presence of ionic strength on adsorption removal of dyes and metal ions are compiled and presented in Table.2.12.

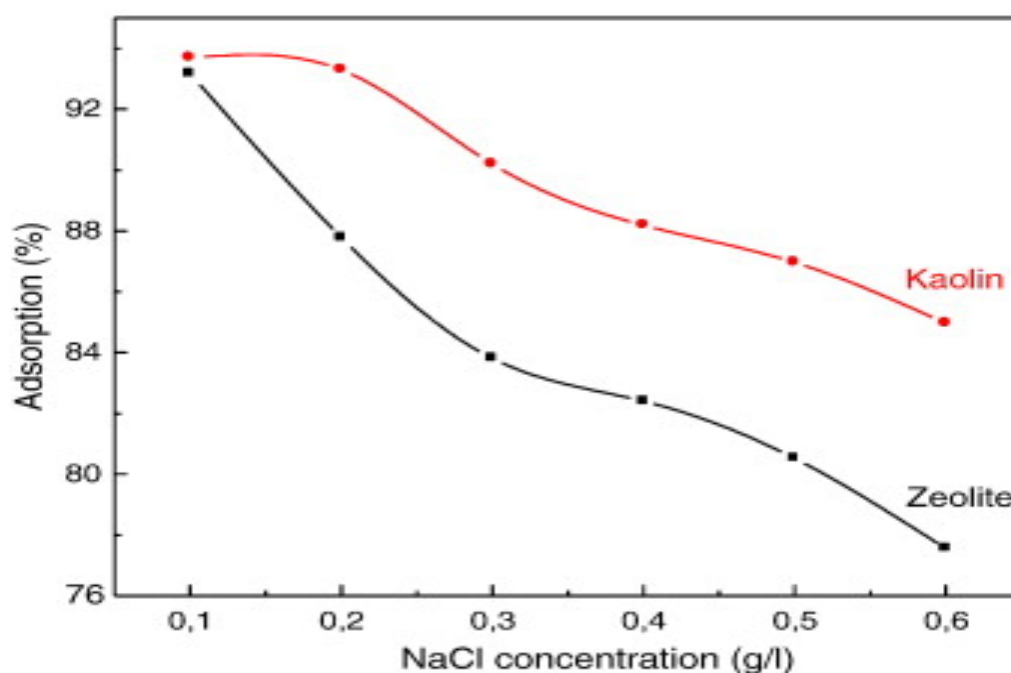


**Figure 2.8:** Effect of NaCl concentration on the adsorption % of MB onto Kaolin and Zeolite where the other parameters kept constant (Rida et al. 2013a).

**Table 2.12:** The effect of ionic strength on the percentage dye and heavy metal ions removal onto various adsorbents.

Adsorbent	Adsorbate	Initial salt concentration range (mg/L)	Percentage Removal (%)	Reference
Tea leaf AC	Orange G Rhodamine B	0.0-0.5 mol/L (NaCl)	85-110 mg/g 375-415mg/g	(Goswami and Phukan 2017)
SDS-Fe <sub>3</sub> O <sub>4</sub> nanoparticles	Cu (II) Ni (II) Zn (II)	0-10 % (W/V) (NaCl)	38-10 % 83- 32% 98- 38%	(Adeli et al. 2017)

Raw eucalyptus bark	Methylene blue	100-300 (NaCl)	59-70%	(Afroze et al. 2016c)
Bentonite/chitosan composite	Amido black 10B	0.0-0.5 mol/L (NaCl)	99- 89%	(Zhang et al. 2016)
Guar gum/silica nanocomposite	Reactive blue Congo red	0.0-1 M (NaCl)	60-48% 67- 53%	(Pal et al. 2015)
Based modified eucalyptus bark	Zn (II)	100-300 (NaCl)	31.4-27 mg/g	(Afroze et al. 2016b)
		100-300 (CaCl <sub>2</sub> )	30-26.6 mg/g	
		100-300 (FeCl <sub>3</sub> )	28-26 mg/g	
Commercial activated carbon Amberlite 747 resin	CN <sup>-</sup> Cu (II) Ni (II)	0.01-0.1 M (KNO <sub>3</sub> ) 100-1600 mmol/L(NaNO <sub>3</sub> )	Decrease 0.8-0.6 mmol/g 0.33-0.08 mmol/g	(Stavropoulos et al. 2015) (Zhu et al. 2015)
Modified breadnut peel	Malachite green	0.0-1.0 M	Decrease	(Chieng et al. 2015)
Raw pine cone	Methylene blue	50-200 mg/L (NaCl)	28.5-25mg/g	(Yagub et al. 2014b)
Base modified pine cone	Reactive black 5	0.01-1M (NaCl)	33-31 mg/g	
coconut shell based carbon			17-55 mg/g	(Kyzas et al. 2014)
Diatomite/nickel oxide composite	Basic red 46	0-0.01 M (Na <sub>2</sub> SO <sub>4</sub> )	90-81%	(Sheshdeh et al. 2014)
Peanut husk-CPB	Light green	(NaCl) (CaCl <sub>2</sub> ) 0.0-0.1 mol/L	128- 60 mg/g 130-50 mg/g	(Zhao et al. 2014a)

Mesoporous carbon	Methylene blue	0.2-1 mol/L (NaCl)	322-336mg/g	(Peng et al. 2014)
	Orange II		274-333mg/g	
Kaolin	Methylene blue	100-600 (NaCl)	94- 85%	(Rida et al. 2013b)
Zeolite			93-77%	
Modified sawdust	Methylene blue	0.01-0.1 mol/L (KCl)	83-65%	(Zou et al. 2013)
Modified bamboo charcoal	Acid Orange 7	0-1 M (NaNO <sub>3</sub> )	Increase	(Liao et al. 2012)
Sludge based activated carbon	Methylene blue	0.0-1.0 mol/L (NaCl)	Increase	(Li et al. 2011a)
	Reactive red 24			
Activated carbon	Reactive red 4	0-0.6 M (NaCl)	22-34%	(Al-Degs et al. 2008)
	Reactive yellow 2		50-55 %	
	Reactive blue 2		70-75 %	
Ulmas tree leaves	Pb (II)	0-0.15M (NaNO <sub>3</sub> )	98-88 %	(Sangi et al. 2008)
	Cu (II)		73- 47 %	
	Cd (II)		83- 64 5	

## **2.7.2 Role of adsorbent characteristics on the adsorption process**

The adsorbent characteristics such as specific surface area, BET surface area, particle size, pore volume, point of zero charge, bulk density and the presence of various functional groups on the adsorbent surface are greatly affecting the adsorbent-adsorbate interaction and thus the adsorption capacity (Dawood and Sen 2014, Yagub et al. 2014a). In general, the amount of adsorption is known to increase with the increases of specific surface area and BET surface area. The presence of various functional groups on the adsorbent surface are important for the adsorption process (De Gisi et al. 2016, Salleh et al. 2011). Commercial activated carbon (CAC) is mainly used as an adsorbent in the removal of wide variety of organic dyes and inorganic heavy metal ions due to its high surface area, high degree of surface reactivity and an excellent adsorption capacity. However, the high cost associated with its generation has encouraged researchers to find alternative low-cost and non-conventional adsorbents such as agricultural solid waste, modified agricultural solid waste, biomass based bio-char and activated carbon. Also, researchers have been studying the effectiveness of other inorganic adsorbents such as clay minerals in the removal of wide range of dyes and heavy metal ions.

### **2.7.2.1 Raw agricultural solid wastes in the removal of organic and inorganic pollutants.**

Agricultural solid wastes such as leaves, bark, fibres, seeds, fruit peels and sawdust have been successfully reported as potential adsorbents in the removal of dyes and heavy metals from wastewater. These wastes usually have high molecular weight due to the presence of lignin, cellulose and hemicelluloses components (Salleh et al. 2011). Cellulose is a renewable and biodegradable polymer which is insoluble in most solvents due to hydrogen bonding and crystallinity. These agricultural solid wastes are available in large quantities with little or no economic value and present a disposal problem. The utilization of these wastes as adsorbents help to provide low-cost and effective adsorbents as well as an implementation of an effective solid waste management. Various low-cost agriculture solid waste adsorbents have been reported in the removal of organic dyes and inorganic heavy metals from wastewater as tabulated in Table 2.13.

**Table 2.13:** The maximum adsorption capacity in the removal dyes and heavy metals by raw agricultural by-product waste adsorbents.

<b>Adsorbent</b>	<b>Adsorbate</b>	<b>Adsorption capacity <math>q_{\max}</math> (mg/g)</b>	<b>Reference</b>
Mango leaf	Methylene blue	156	(Uddin et al. 2017)
chickpea shell	Acid Blue25	29.4	(Krishna et al. 2017)
Orange sawdust	Methylene blue	39.7	(Azzaz et al. 2017)
Coco-peat	Malachite green	276.8	(Vijayaraghavan et al. 2016)
Bamboo leaves	Methylene blue	54.2	(Zhu et al. 2016)
Cucumis sativus peel	Acid blue 113	59.8	(Lee et al. 2016b)
Coco-peat	Crystal violet	119.2	(Vijayaraghavan et al. 2016)
Citrus limetta peel	Methylene blue	227.3	(Shakoor and Nasar 2016)
Eucalyptus bark	Methylene blue	204.1	(Afroze et al. 2016c)
Olive pomace	Basic green 4	41.7	(Koçer and Acemioğlu 2016)
Durian peel	Acid blue 25	26.6	(Dahri et al. 2016)
Conyzoides leaf	Methylene blue	192.4	(Ezechi et al. 2015)
Peanut husk	Indosol Orange	79.5	(Sadaf and Bhatti 2014)
Mango seed	Methylene blue	25.4	(Senthil Kumar et al. 2014)
Peanut hulls	Golden yellow	35.7	(Nawaz et al. 2014)
Coffee waste	Toluidine blue	142.5	(Lafi et al. 2014)
Pine cone leaf	Methylene blue	126.6	(Yagub et al. 2012)
Pine cone	Congo red	32.7	(Dawood and Sen 2012b)
Date Stones	Methylene blue	43.5	(Belala et al. 2011)
Sugar cane bagasse	Congo red	38	(Zhang et al. 2011b)
Palm shell	Reactive red 141	14.0	(Sreelatha et al. 2011)

---

	Reactive blue 21	24.7	
Papaya seed	Methylene blue	200	(Nasuha et al. 2011)
	Congo red	71	
Peanut hull	Reactive black 5	55.6	(Tanyildizi 2011)
Pine cone	Acid black 26	62.9	(Mahmoodi et al. 2011)
	Acid green 25	43.3	
	Acid blue 7	37.4	
Pine cone	Methylene blue	109.9	(Sen et al. 2011)
Pine tree leaves	Basic red 46	71.9	(Deniz and Karaman 2011)
Palm kernel fiber	Crystal violet	78.9	(El-Sayed and Owes 2011)
	Methylene blue	95.4	
Grapefruit peel	Crystal violet	254.2	(Saeed et al. 2010)
Organo-attapulgit	Congo red	189.4	(Chen and Zhao 2009)
Garlic peel	Methylene blue	142.9	(Hameed and Ahmad 2009)
Rice husk	Indigo Carmine	65.9	(Lakshmi et al. 2009)
Black eyed biomass	Pb (II)	32.9	(Guyo and Moyo 2017)
Nauclea-diderrichi seed	Cr (III)	483.8	(Omorie et al. 2016)
Eucalyptus bark	Zn (II)	131.6	(Afroze et al. 2016b)
Tomato leaf	Ni (II)	58.8	(Gutha et al. 2015)
Rapeseed waste	Zn (II)	13.9	(Paduraru et al. 2015)
Jackfruit leaf	Ni (II)	11.5	(Boruah et al. 2015)
Coconut tree sawdust	Cu (II)	3.9	(Putra et al. 2014)
	Pb (II)	25.0	
	Zn (II)	23.8	
Coir pith	Cr (VI)	165.0	(Suksabye and Thiravetyan 2012)

---

Orange peel	Ni (II)	9.8	(Feng et al. 2011)
	Cd (II)	63.4	
Rice husk	Cd (II)	73.9	(Akhtar et al. 2010)
Brown seaweed	Cd (II)	320.9	(Jha et al. 2008)

### 2.7.2.2 Modified agricultural solid wastes adsorbents

Modified agricultural solid waste have been used widely as an effective adsorbent in the removal of various contaminations from wastewater. Raw agricultural solid wastes contain cellulose as a main component however, natural cellulose shows lower adsorption capacity compared to modified cellulose in the removal of dyes and heavy metals from wastewater (Suhas et al. 2016). Raw biomass can be modified through the use of acids such as hydrochloric, phosphoric, sulphuric, nitric, citric acids etc. or alkaline solutions such as sodium hydroxide, potassium hydroxide, zinc chloride, calcium chloride, ammonia etc. or cross linked with other materials. Chemical treatments enhance the adsorption capacity by removing the natural fat, waxes and other soluble impurities on the adsorbent's surface thus increases the active functional group, external surface area and pore size on adsorbent's surface (Dawood and Sen 2012b). Afroze et al. reported the adsorption capacity of Zn (II) has been increased from 128 mg/g to 250 mg/g by raw and base modified eucalyptus bark adsorbents respectively (Afroze et al. 2016b). Further, the adsorption capacity of Congo red dye has been increased from 32.7 mg/g to 40.2 mg/g by the use of acid modified pine cone biomass compared to raw pine cone (Dawood and Sen 2012b). The maximum adsorption capacity  $q_m$  (mg/g) for modified agriculture solid waste adsorbents have been reported in the removal of organic dyes and inorganic heavy metals from wastewater as compiled and presented in Table 2.14.



**Table 2.14:** The maximum adsorption capacity in the removal dyes and heavy metals by modified agricultural biomass adsorbents.

<b>Modified adsorbent</b>	<b>Adsorbate</b>	<b>q<sub>max</sub> (mg/g)</b>	<b>Reference</b>
Orange sawdust (NaOH)	Methylene blue	78.7	(Azzaz et al. 2017)
sugarcane bagasse (Tatric)	Diazonium blue	9.1	(Said et al. 2017)
Sea grass (Iron oxide)	Bismarck brown	233.5	(Safarik et al. 2016)
	Safranin O	88.1	
Breadnut peel (NaOH)	Malachite green	353	(Chieng et al. 2015)
Rubber leaf (H <sub>3</sub> PO <sub>4</sub> )	Acid blue 25	28.1	(Khalid et al. 2015)
Pine cone (NaOH)	Methylene blue	142.3	(Yagub et al. 2014b)
Sugarcane bagasse (HCL)	Indosol	65.1	(Sadaf et al. 2014)
	Turquoise		
Mango seed (H <sub>2</sub> SO <sub>4</sub> )	Methylene blue	58.1	(Senthil Kumar et al. 2014)
Corn straw (Iron oxide)	Methylene blue	196.5	(Zhao et al. 2014b)
pine sawdust (Citric)	Methylene blue	111.5	(Zou et al. 2013)
Eucalyptus wood (NaOH)	Congo red	66.7	(Mane and Vijay Babu 2013)
Pine cone (HCL)	Congo red	40.2	(Dawood and Sen 2012b)
Papaya seed (carboxyl)	Methylene blue	250	(Nasuha et al. 2011)
	Congo red	58.8	
Kenaf fibres ( Citric)	Methylene blue	131.6	(Sajab et al. 2011)
Eucalyptus wood (NaOH)	Brilliant green	58.5	(Mane and Babu 2011)
Cedar waste (KOH)	Pb (II)	25.8	(Lago et al. 2017)
	Ni (II)	7.7	
	Zn (II)	7.7	

---

Moss biomass (TTP)	Pb (II)	70.6	(Okoli et al. 2016)
Rice straw (Amine)	Cr (VI)	15.82	(Wu et al. 2016)
	Ni (II)	4.0	
Eucalyptus bark (NaOH)	Zn (II)	250	(Afroze et al. 2016b)
Lyocell fibre (Xanthate)	Pb (II)	531.3	(Bediako et al. 2015)
	Cu (II)	123.1	
Okra (Succinylation)	Zn (II)	57.1	(Singha and Guleria 2015)
	Cd (II)	121.5	
Cashew shell (H <sub>2</sub> SO <sub>4</sub> )	Ni (II)	456.3	(Senthil Kumar et al. 2012)
	Cu (II)	406.6	
	Cd (II)	436.7	
Coir pith (Acrylic acid)	Cr (VI)	196.0	(Suksabye and Thiravetyan 2012)
Orange peel (copolymer)	Pb (II)	476.1	(Feng et al. 2011)
	Cd (II)	293.3	
	Ni (II)	162.6	
Wheat straw (Urea)	Cd (II)	39.2	(Farooq et al. 2011)

---

### 2.7.2.3 Agricultural solid wastes based bio-char and activated carbon adsorbents

Commercial activated carbon (CAC) is widely used as an effective adsorbent in the removal of variety of organic and inorganic pollutants dissolved in aqueous media or from gaseous environment. The effectiveness of this versatile adsorbent is due to its high surface area, microporous or mesoporous structure, excellent adsorption capacity and high degree of surface reactivity (Dawood et al. 2014). Activated carbon of pore size up to 2 nm is called a microporous material while mesoporous carbon has a pore size between 2 to 50 nm. Microporous carbon can be utilized for the adsorption of gases and vapors while mesoporous carbon is required to accelerate the kinetics of the adsorption process or for the adsorption of larger molecules such as organic dyes and heavy metal ions (Kyzas et al. 2014). However, the high cost and difficulties associated with the production and regeneration of commercial activated carbon have encouraged researchers to find alternative adsorbents. In the recent years, growing research interest is focusing on the production of activated carbon, char and charcoal from agricultural solid residual. The applications of agricultural solid wastes as a feed material in the production of charcoal and biochar offer several advantages as they are naturally available in large quantities, require less processing time, renewable source and have little or no commercial value (Ribas et al. 2014, Yagub et al. 2014a). Also, utilize these low cost by-products will valorise their economic value, help to reduce the cost of waste disposal and provide a potentially inexpensive alternative adsorbents to commercial activated carbons. Biomass waste can be utilized into the production of char, charcoal and activated carbon. The production of these valuable adsorbents depend on the production methods as presented in Fig.2.9.

Bio-char is a pyrogenic carbonaceous material produced through slow pyrolysis of biomass residue at a heating rate of up to 10°C/min and high temperature profile ( 350-800°C) in a limited oxygen presence while charcoal can be produced from animal or biomass compounds in the absence of oxygen (Hardy et al. 2017, Hu et al. 2015). Further, the production of bio-char and charcoal do not require the use of chemicals such as acids and bases thus they are considered to be more environmental friendly compared to biomass based activated carbon (Dawood et al. 2017b). Agricultural solid waste based char and charcoal have been used as effective adsorbents in the removal of organic dyes and inorganic heavy metals such as Crystal violet and Congo red by Korean cabbage bio-char (Sewu et al. 2017b), Methylene blue and

Acid orange by bamboo bio-char (Liao et al. 2012), mercury by coconut pith char (Johari et al. 2016) , nickel and cobalt by almond shell bio-char (Kılıç et al. 2013).

Biomass based activated carbon adsorbent is considered to be an excellent alternative to commercial activated carbon due to its low-cost, high surface area and high degree of surface reactivity. Biomass based activated carbon can be synthesized through chemical or physical activation process. Generally, chemical activation is favoured over physical activation as biomass carbonization and activation can be carried out at single step and at relatively lower temperature profile than physical activation (Fathy et al. 2012). Various chemical activation agents are used in the production of biomass activated carbon such as phosphoric acid, hydrochloric acid, nitric acid, citric acid, acetic acid, sulfonic acid, potassium carbonate, zinc chloride, ammonium hydroxide, potassium hydroxide and sodium hydroxide. However, alkali hydroxides and Zinc chloride are not preferred due to their corrosive natures and the harmful effects associated with the disposal (Gurten et al. 2012). Biomass based activated carbon production depend on various process parameter such as precursor properties, reagent used, impregnation ratio, activation time and temperature. Dawood et al., reported the use of phosphoric acid under various temperature range in the production of pine cone based activated carbon and its effectiveness in the removal of Congo red dye from its aqueous solution (Dawood et al. 2013, Dawood et al. 2014). Also, Aguayo-Villarreal et al., reported the use of chemical activation followed by a physical activation of CO<sub>2</sub> in the production of pecan nutshell based activated carbon in the removal of Zn (II), Cd(II), Ni (II) and Cu (II) metals (Aguayo-Villarreal et al. 2017). Further, hydrothermal carbonization of banana peel in the removal of Pb (II) is discussed by Zhou et al., (Zhou et al. 2017). Physical activation method is used to improve the porosity of biomass based activated carbon by exposing the carbonaceous material to carbon dioxide gas, air mixture or steam under higher temperature profile in compared to chemical activation. Generally, high surface area and high micropores ratio are produced from the physical activation due to the oxidation of partial carbon atoms by carbon dioxide gas and steam (Liu et al. 2013).

Furthermore, in the recent years, researchers have been focusing in the development and production of shaped controlled and highly stable magnetic carbon. It has promising applications in various industries such as biomedicine, magnetic catalyst bodies, wastewater treatment and quantitative magnetic force microscopy (Zhu and Diao 2011). The multifunctional nano carbon composites are considered as an excellent absorbent due to its

fast, convenient, and highly efficient pollutants removal from wastewater, which plays an important role in the purification or separation of natural water and industrial effluents (Zhang et al. 2011a). Several methods are used in the synthesis magnetic carbon nanocomposites such as filling process, template-based synthesis, chemical vapor deposition, hydrothermal/solvothermal method, pyrolysis procedure, sol–gel process, detonation induced reaction, self-assembly method. Pyrolysis method is widely used in the production of biomass based non-magnetic carbon adsorbent. The pyrolysis procedure is based on the exposure of a mixture to a high temperature containing the soluble metal salt (Ferric and ferrous salts) and a type of organic compounds which is high in carbon. A comprehensive collection of biomass based bio-char, charcoal, activate carbon, nano-magnetic biochar and carbon in the removal of dyes and heavy metals along with maximum adsorption capacity  $q_m$  (mg/g) is presented in Table 2.15.

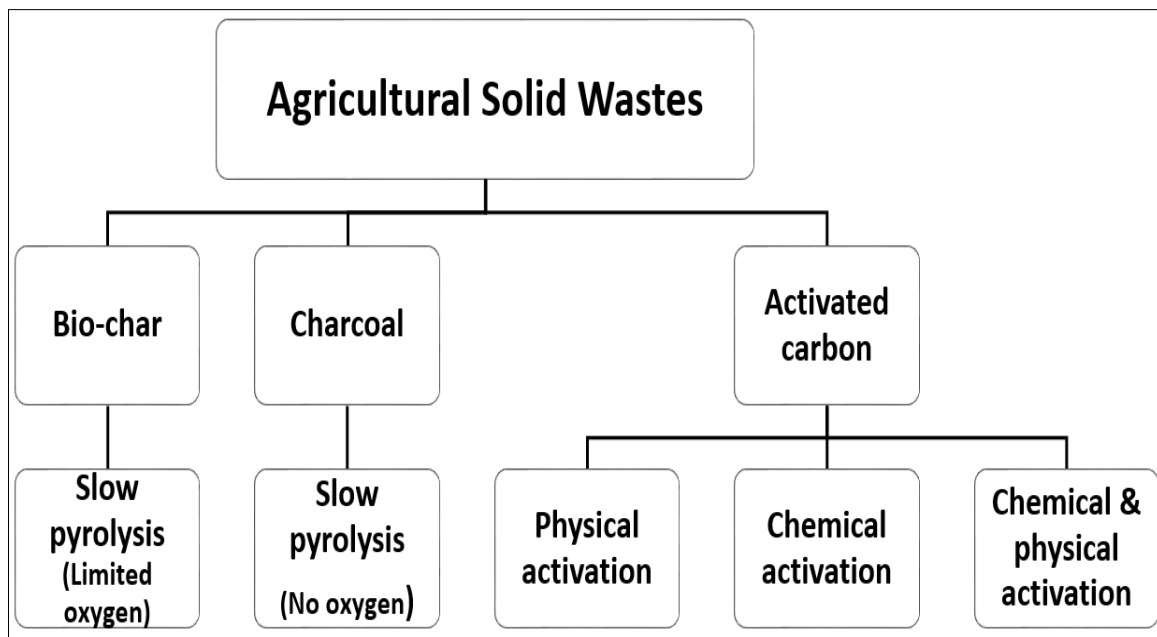


**Figure 2.9:** Methods used in the production of biomass based activated carbon, char and charcoal.

**Table 2.15:** The maximum adsorption capacity  $q_m$  (mg/g) of various biomass based bio-char, charcoal and activated carbon (AC) in the removal of dyes and heavy metal ions.

<b>Adsorbent</b>	<b>Adsorbate</b>	<b><math>q_{max}</math> (mg/g)</b>	<b>Reference</b>
Pecan nutshell biochar	Reactive red 141	130	(Zazycki et al. 2018)
Korean cabbage biochar	Crystal violet	1304	(Sewu et al. 2017b)
	Congo red	95.8	
Oxidized weed biochar	Methylene blue	161.3	(Güzel et al. 2017)
Catkins biochar	Methylene blue	534	(Liu et al. 2017c)
	Methyl orange	154	
	Congo red	350	
Rice straw biochar	Crystal violet	620.3	(Sewu et al. 2017b)
	Congo red	190.8	
Mushroom substrate char	Crystal violet	282.9	(Sewu et al. 2017a)
Kelp seaweed biochar	Crystal violet	610.1	(Sewu et al. 2017a)
Bamboo hydro-char	Congo red	33.7	(Li et al. 2016b)
Magnetic coconut shell based AC	Sunset yellow	22.3	(Cazetta et al. 2016)
Rice straw biochar	Brilliant green	111.1	(Saif Ur Rehman et al. 2016)
Algae biochar	Congo red	51.3	(Nautiyal et al. 2016)
Waste tea AC	Methylene blue	402	(Borah et al. 2015)
Macoře fruit shell AC	Methylene blue	10.6	(Aboua et al. 2015)
Cashew nut shell AC	Methylene blue	4.8	(Ragupathy et al. 2015)
	Brilliant green	5.0	
Magnetic waste hydrochar	Malachite green	476	(Zhu et al. 2014)

---

Magnetic coconut shell based activated carbon	Reactive black 5	58.7	(Kyzas et al. 2014)
Pine cone AC	Congo red	500	(Dawood et al. 2014)
Cocoa shell AC	Reactive violet 5	603.3	(Ribas et al. 2014)
Palm tree AC	Methylene blue	128	(AlOthman et al. 2014)
Charcoal Ash	Methylene blue	178	(Özbay et al. 2013)
Waste tea AC	Acid blue 29	596	(Auta and Hameed 2013b)
Myrtus communis AC	Congo red	19	(Ghaedi et al. 2012)
Kenaf fibre char	Methylene blue	22.7	(Mahmoud et al. 2012)
Pomegranate AC	Congo red	10	(Ghaedi et al. 2012)
Mesoporous carbon encapsulated with Fe <sub>3</sub> O <sub>4</sub>	Methylene blue	608	(Zhang et al. 2011a)
	Congo red	1657	
Rice husk AC	Methylene blue	442	(Foo and Hameed 2011b)
Rambutan peel AC	Malachite green	329	(Ahmad and Alrozi 2011)
Pomelo skin AC	Acid blue 15	444	(Foo and Hameed 2011a)
	Methylene blue	501	
Date stone AC	Methylene blue	316	(Foo and Hameed 2011c)
Bael shell AC	Congo red	98	(Ahmad and Kumar 2010)
Cattail AC	Neutral red	192	(Shi et al. 2010)
	Malachite green	196	
Olive stone AC	Remazol red B	9.0	(Uğurlu et al. 2008)
Rubber seed coat AC	Malachite green	227	(Hameed and Daud 2008)
Magnetic bamboo charcoal	As (III)	19.6	(Nomura et al. 2017)

---

---

Catkins biochar	U(VI)	71.9	(Liu et al. 2017c)
	Co (II)	110.2	
Celery stalk biochar	Pb (II)	304	(Zhang et al. 2017)
Magnetic watermelon peel carbon nanocomposites	As (III)	32.9	(Muneeb Ur Rahman Khattak et al. 2017)
	Cr (II)	21.1	
	Cu (II)	38.3	
	Pb (II)	29.8	
	Zn (II)	18.7	
Coconut pith biochar	Hg (II)	6.1	(Johari et al. 2016)
Sugarcane bagasse AC	Zn (II)	23.7	(Krishnan et al. 2016)
Sesame stalk biochar	Fe (III)	62.9	(Kırbıyık et al. 2016)
	Cd (III)	19.6	
Rapeseed oil cake AC	Ni (II)	133.3	(Uçar et al. 2015)
	Pb (II)	129.9	
Tomato waste AC	Co (II)	166.7	(Önal et al. 2014)
Almond shell biochar	Ni (II)	22.2	(Kılıç et al. 2013)
	Co (II)	28.1	
Buffalo weed biochar	Pb (II)	333.3	(Yakkala et al. 2013)
	Cd (II)	11.6	
Coal fly ash	Ni (II)	4.5	(Sočo and Kalembkiewicz 2013)
Pine cone activated carbon	Pb (II)	27.53	(Momčilović et al. 2011)
Sugarcane bagasse biochar	Pb (II)	81.9	(Inyang et al. 2011)

---



#### 2.7.2.4 Inorganic adsorbents in the removal of dyes and heavy metals

Clay minerals are abundantly available as the colloidal fraction in soils, sediments, rocks and water. Clay mineral is considered to be an effective adsorbent in the removal of organic and inorganic contaminations because of its large surface area, high ion exchange capacity. This is due to presence of Bronsted and Lewis acid in clays, layered structure, chemical and mechanical stability (Aries and Sen 2009). Clays are hydrous aluminium phyllosilicates which contain various exchangeable ions of  $\text{Ca}^{2+}$ ,  $\text{Mg}^{2+}$ ,  $\text{H}^+$ ,  $\text{K}^+$ ,  $\text{Na}^+$ ,  $\text{SO}_4^{2-}$ ,  $\text{PO}_4^{3-}$ ,  $\text{NO}_3^-$  and  $\text{Cl}^-$  on their surface. These ions can be exchanged with other cations and/or anions without affecting clay original structures (Dill 2016). The cation exchange is primarily due to weak bonds presented at the edges of the silica-alumina units, isomorphous substitution in clay structure or hydrogen bond presented in the interlayer space. Inorganic clay and other silica can be classified into kaolin-serpentine group (kaolinite, dickite, nacrite, halloysite, hisingerite, lizardite, antigorite, chrysotile, amesite, carlosturanite, greenalite), talc and pyrophyllite group (pyrophyllite, ferripyrophyllite), mica group (dioctahedral and trioctahedral), smectite group (montmorillonite, bentonite, beidellite, nontronite, saponite, hectorite, sauconite), chlorite group, 2:1 layer silicates involving a discontinuous octahedral sheet and a modulated tetrahedral sheet (kalifersite, palygorskite and sepiolite) and tectosilicate group as shown in Fig.2.10 (Brigatti et al. 2013, Yagub et al. 2014a).

Kaolin is non-metallic low cost natural clay, available worldwide in rocks as crystalline 1:1 layer clay structure. The phyllosilicates kaolinite-group minerals include kaolinite, dickite, nacrite and halloysite. Kaolin has a molecular formula of  $\text{Al}_2\text{Si}_2\text{O}_5(\text{OH})_4$  and characterized by a chemical composition of  $\text{SiO}_2$ : 42.14 mol%,  $\text{Al}_2\text{O}_3$ : 15.61 mol% and  $\text{H}_2\text{O}$ : 42.25 mol% (Dill 2016). Kaolinite exhibits low cation exchange capacity and low isomorphous substitution unlike other clays from smectite group due to strong hydrogen bond presented in the interlayer space. Therefore, cation exchange capacity occurs only on the external surface where  $(\text{SiOH}^{2+})$  species reacts with the anions presented in the aqueous solution. Kaolinite has a low cation exchange capacity of about 13.5 meq/100 g which is significantly lower than other 2:1 type clay minerals (up-to 100 meq/100g), however the anion exchange capacity of kaolinite is higher than its cation exchange capacity due to the replaceable  $(\text{OH})^-$  ions of the exposed alumina octahedral layer (Chai et al. 2017, Dill 2016). The hexagonal lattice structure of kaolin shows the centre of the hexagonal ring of oxygen atoms is at the silica tetrahedral layer while in the alumina octahedral layer, the hexagonal surface lattice ring of hydroxyls surrounded another

hydroxyl in the centre of the ring (Gupta 2011). Bentonite is a 2:1 layer structure and has a negative charges that arise due to the isomorphous substitution of  $Al^{3+}$  for  $Si^{4+}$  in the tetrahedral layer and  $Mg^{2+}$  for  $Al^{3+}$  in the octahedral layer. These charges are balanced by the presence of exchangeable cation ions such as  $Na^+$  and  $Ca^{2+}$ , in the lattice structure (Anirudhan and Ramachandran 2015). Further, Zeolite from tectosilicate group is microporous material where aluminosilicate material shaped in a cavity structure. There are various types of zeolites with different physio-chemical properties such as particle density, cation selectivity, molecular pore size, and strength due to various acid-basic properties, chemical composition and crystal structure (Busca 2017). Also, anion exchange capacity of various clays and silica materials can be enhanced using surfactants which change the surface charge from negative to positive or under acidic conditions when complexation occurs due to the amphoteric character of the clay crystal edges (Errais et al. 2012). Natural inorganic clays and aluminosilicates minerals have been used widely in the removal of both cationic dyes, anionic dyes and heavy metals from wastewater which are tabulated in Table 2.16.

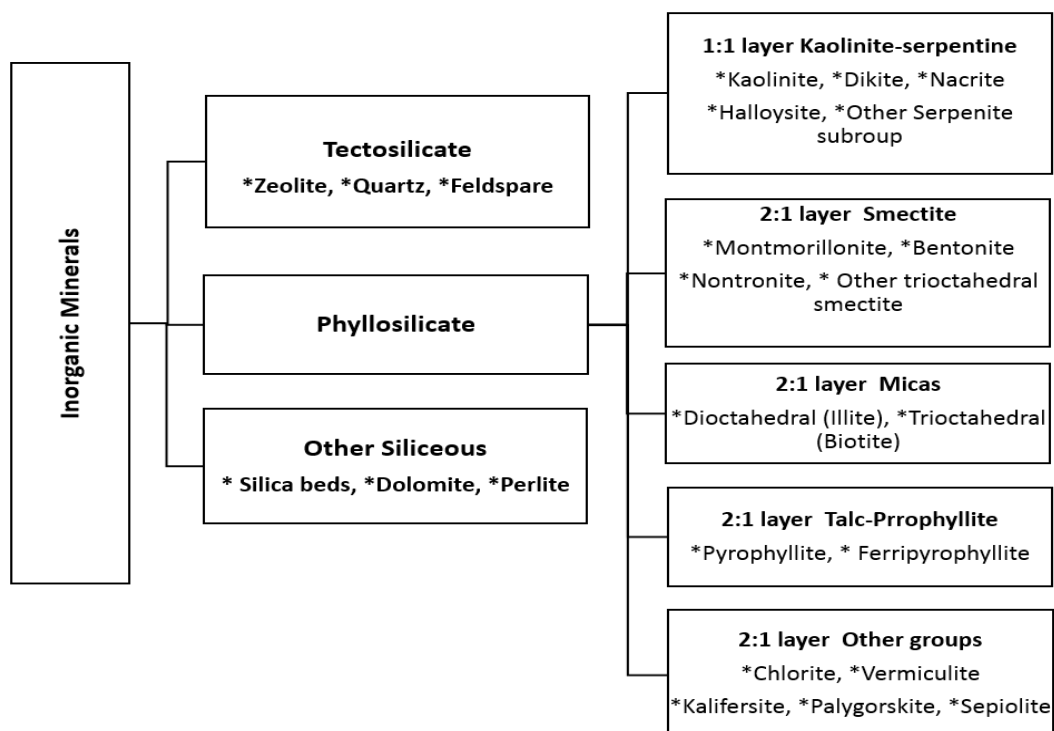


**Figure 2.10:** Various types of inorganic clays and minerals.

**Table 2.16:** The maximum adsorption capacity  $q_m$  (mg/g) of various inorganic clay adsorbents in the removal of dyes and heavy metals.

<b>Adsorbent</b>	<b>Adsorbate</b>	<b><math>q_m</math> (mg/g)</b>	<b>Reference</b>
bentonite/zeolite composite	Methylene blue	36.2	(Shaban et al. 2017)
	Congo red	46.3	
Kaolin ( Iron oxide)	Direct red 23	22.9	(Magdy et al. 2017)
Kaolin	Methylene blue	80.7	(Dawood et al. 2017a)
Acid modified zeolite	Methylene blue	2.1	(Hor et al. 2016)
Base modified zeolite		1.1	
Montmorillonite	Crystal violet	370.4	(Sarma et al. 2016)
Montmorillonite (H <sub>2</sub> SO <sub>4</sub> )		384.6	
Kaolinite (Fe,Mg Oxides)	Basic Fuchsin	10.4	(Khan et al. 2015)
	Crystal violet	20.6	
Natural clay	Reactive orange	30.3	(Abidi et al. 2015)
	Reactive red	54.6	
Clinoptilolite (Zeolite)	Basic blue 9	77.1	(Hernández-Montoya et al. 2013)
	Basic violet 3	70.7	
Erionite (Zeolite)	Basic blue 9	86.3	(Hernández-Montoya et al. 2013)
	Basic violet 3	83.8	
Kaolin	Methylene Blue	45	(Rida et al. 2013b)
Cold plasma kaolin	Methylene Blue	51.0	(Yavuz and Saka 2013)
Kaolin	Brilliant green	65.4	(Nandi et al. 2009)
	Crystal violet	47.2	
Montmorillonite clay	Methylene Blue	289.1	(Almeida et al. 2009)

---

Bentonite	Crystal violet	496	(Eren 2009)
Bentonite	Methylene Blue	151	(Hong et al. 2009)
Metkaolin (Geopolymer)	Zn (II)	74.5	(Kara et al. 2017)
	Ni (II)	42.6	
Bentonite	Al (III)	8.5	(Chai et al. 2017)
Kaolin		1.2	
Sepiolite	Hg (II)	54.7	(Vağzoğullar et al. 2015)
Modified Sepiolite (CTAB)	Hg (II)	104.1	(Vağzoğullar et al. 2015)
Kaolinite	Zn (II)	7.2	(Joh and Mbadcam 2015)
Metakaolinite		12.4	
Clinoptilolite (Zeolite)	Ni (II)	186.1	(Hernández-Montoya et al. 2013)
Erionite (Zeolite)	Cd (II)	9.6	
	Pb (II)	54.3	
Natural bentonite	Ni (II)	33	(Alandis et al. 2010)
	Fe (III)	69	
Kaolin	Zn (II)	250	(Aries and Sen 2009)

---

## 2.8 Batch Adsorption Kinetic Study

It is important to understand the adsorption kinetics, mechanism of adsorption and its transient behaviour by identifying the various process parameters and evaluate their influence on the batch adsorption process. The nature of the adsorption process such as solute uptake rate, rate control and residence time must be evaluated under various physio-chemical process control parameters such as adsorbent dose, initial adsorbate concentration, ionic strength, solution pH, and temperature profile and contact time. Lagergren Pseudo-first-order, Pseudo-second-order and Intra-particles-diffusion kinetic models were used to determine the most suitable and practical model in term of high adsorption capacity and fast adsorption rate. Chi-square ( $\chi^2$ ) is a statistic test and it was used to evaluate the accuracy and the applicability of kinetic models by determine the error between experimental ( $q_e$ ) and calculated ( $q_e$ ) as shown in equation (2.4).

$$\chi^2 = \frac{(q_{e \text{ exp}} - q_{e \text{ calc}})^2}{q_{e \text{ calc}}} \quad (2.4)$$

### 2.8.1 Lagergren Pseudo-first-order and Pseudo-second-order kinetic models

**Pseudo -first-order kinetic model** (Lagergren 1898) is used to analyse the kinetic behaviour of liquid–solid adsorptive system where the rate of the occupied adsorption sites are propositional to the number of unoccupied sites. The general form and linearized integral form of this model are shown as per equation (2.5) and (2.6) respectively.

$$\frac{dq_t}{dt} = k_f (q_e - q_t) \quad (2.5)$$

$$\text{Log } (q_e - q_t) = \text{log } q_e - \frac{k_f}{2.303} t \quad (2.6)$$

Where  $q_t$  (mg/g) is the amount of adsorbate adsorbed at time  $t$ ,  $q_e$  (mg/g) is the adsorption capacity at equilibrium.  $k_f$  ( $\text{min}^{-1}$ ) is the adsorption rate constant and  $t$  is the contact time (min). The rate constant  $k_f$  ( $\text{min}^{-1}$ ) and adsorption capacity at  $t$ ,  $q_e$  (mg/g) will be calculated from the slope and intercept of the linear plot of  $\text{log } (q_e - q_t)$  versus  $(t)$ . A straight line of  $\text{log } (q_e - q_t)$  versus  $(t)$  with high linear regression coefficient ( $R^2$ ) indicates the application of this model.

**Pseudo-second-order kinetic model** was described by (Ho and Mckay 2000) and the general and linearized integral forms of this model are given below respectively

$$\frac{dq_t}{dt} = k_s (q_e - q_t)^2 \quad (2.7)$$

$$\frac{t}{q_t} = \frac{1}{q_e} t + \frac{1}{k_s q_e^2} \quad (2.8)$$

where  $k_s$  (g/mg.min) is the pseudo second order rate constant,  $q_e$  (mg/g) is the adsorption capacity at equilibrium and which are obtained from slope and intercept of linear plot of  $t/q_t$  against  $(t)$ . A linear relationship between  $t/q_t$  against  $(t)$  and almost identical values between  $q_e$  and  $q_t$  indicate the applicability of this model. Also, the initial sorption rate  $h$  (mg/g-min) is calculated from equation (2.9) where  $t \rightarrow 0$ .

$$h = k_s q_e^2 \quad (2.9)$$

### 2.8.2 Intra-particles-diffusion model and mechanism of adsorption

Intra-particle diffusion model is developed by Weber and Morriss (Weber and Morriss 1963). It is used to identify the rate-controlling step in the adsorption process and the mechanism of adsorption. The mechanism of adsorption involves multiple steps: where the dye molecules migrant from the bulk solution phase to the surface of the adsorbent, diffuse through the boundary layer to the surface of sorbent and followed by intra-particle diffusion into the interior of the sorbent (Konicki et al. 2013). For most adsorption processes, the amount of dye adsorbed varies almost proportionately with  $t^{0.5}$  rather than with the contact time as expressed in equation (2.10)

$$q_t = K_{id} t^{0.5} + C \quad (2.10)$$

Where  $K_{id}$  (mg/g min<sup>0.5</sup>) is the intra-particle diffusion rate constant and it can be calculated from the slope of the linear equation (2.10) of the linear plot  $q_t$  against  $t^{0.5}$ . Also,  $C$  (mg/g) is a constant which indicates the thickness of the boundary layer.  $D_p$  (cm<sup>2</sup>/s) is the diffusion coefficient and it can be calculated from equation (2.11) where  $t^{0.5}$  is the half life time in sec and  $r_0$  is the particle radius in cm.

$$t^{0.5} = \frac{0.03r_0^2}{D_p} \quad (2.11)$$

The applicability of pseudo-first-order and pseudo-second-order models can be determined based on the high values of the linear regression coefficient ( $R^2$ ). Further, the best-fit of these models can be also determined if the amount of adsorption,  $q_e$  (mg/g) values obtained from the experimental data were very close to  $q_e$  (mg/g) theoretical values. In general, the kinetic adsorption data in the removal of various dyes and heavy metal ions is better presented by pseudo-second-order model.

Afroze et al. (Afroze et al. 2016c) studied the removal of methylene blue dye by raw eucalyptus bark and reported high values of the linear regression coefficient  $R^2 > 0.95$  for pseudo-second-order model. Kara et al., reported high values for the linear regression coefficient  $R^2 > 0.99$  for pseudo-second-order model in the removal of Ni (II) and Zn (II) by metakaolin based geopolymer (Kara et al. 2017). Also, Dawood et al. (Dawood et al. 2014) studied the removal of Congo red dye by pine cone based activated carbon and found that the values of linear regression coefficient  $R^2$  was 0.99 for pseudo-second-order model and 0.69 for pseudo-second-order model and thus indicates the applicability of pseudo-second-order model. The applicability of pseudo-second-order kinetic model was reported by many researchers in the removal of various dyes and heavy metal ions such as the removal of Pb (II) ions by banana peel biochar (Zhou et al. 2017), Methylene blue by weed biochar (Güzel et al. 2017), Congo red by raw pine cone (Dawood and Sen 2012b), Pb (II) and Ni (II) ions by rapeseed oil caked based activated carbon (Uçar et al. 2015). The applicability of pseudo-second-order kinetic model in a batch adsorption studies has been confirmed by many researchers and up to date literature information has been compiled by Yagub et al 2014 (Yagub et al. 2014a).

## 2.9 Batch Adsorption Isotherm

Adsorption isotherms explain how the adsorbate molecules distribute between the adsorbate concentration in solution (liquid phase) and the adsorbent (solid phase) at equilibrium during adsorption process (Tran et al. 2016). The amount of adsorbate adsorbed onto an adsorbent depended on the equilibrium concentrations of the adsorbate, solution pH, and temperature. Adsorption isotherm study is critical in understanding the mechanism of adsorption and to find the maximum adsorption capacity of adsorbent. Several adsorption isotherm models reported in the literatures such as Langmuir, Freundlich, Redlich–Peterson, Tempkin, and Toth isotherm models (Allen et al. 2004). However, Freundlich and Langmuir isotherm models are widely used in the adsorption process.

### 2.9.1 Freundlich adsorption isotherm model

Freundlich model was developed in 1906 (Freundlich 1906) and it is used to explain how adsorption takes place on heterogeneous solid surfaces which have unequal available sites with different energies of adsorption capacity (Yagub et al. 2014a) and hence multi steps adsorption take place. The linearized format of Freundlich isotherm model is shown as per equation (2.12)

$$\ln q_e = \frac{1}{n} \ln C_e + \ln k_f \quad (2.12)$$

Where  $q_e$  (mg/g) is the amount of adsorbate adsorbed at equilibrium time,  $C_e$  (mg/L) is equilibrium concentration of adsorbate in solution. The adsorption capacity of adsorbent,  $K_f$  (L/g) and Freundlich constant  $n$  can be calculated from slope and intercept of the linear plot of  $\ln(q_e)$  versus  $\ln(C_e)$ . Freundlich constant  $n$  is a measure of deviation from linearity of the adsorption and used to verify the types of adsorption. If  $n$  is equal to unity, the adsorption is considered to be linear. Further,  $n$  below unity indicates that adsorption is unfavourable whereas,  $n$  above unity is associated with a favourable adsorption and a physical process in nature (Dawood and Sen 2012b, Tran et al. 2017).



## 2.9.2 Langmuir isotherm

Langmuir isotherm model was developed in 1916 and based on assumptions that intermolecular forces decrease rapidly with distance thus predicts the existence of monolayer adsorption surface (Langmuir 1916). The active sites are usually fixed and proportional to their concentration therefore no further adsorption occurs after the equilibrium point. The linearized form of Langmuir (I) and Langmuir (II) isotherm models are shown in Table 2.17

**Table 2.17:** Langmuir (I) and (II) isotherm model equations.

Type	Equation	Plot parameters	Equation
I	$\frac{C_e}{q_e} = \frac{1}{K_L q_m} + \frac{C_e}{q_m}$	$\frac{C_e}{q_e}$ versus $C_e$	2.13
II	$\frac{1}{q_e} = \frac{1}{K_L q_m C_e} + \frac{1}{q_m}$	$\frac{1}{q_e}$ versus $\frac{1}{C_e}$	2.14

Where  $q_m$  (mg/g) is the maximum adsorption capacity and Langmuir constant related to the energy of adsorption  $K_L$  (L/mg) are calculated from the slope and intercept of the linearized forms of the plot parameters as shown above in Table 2.17. The separation factor ( $R_L$ ) from Langmuir model can be calculated as per equation (2.15)

$$R_L = \frac{1}{1 + (K_L C_o)} \quad (2.15)$$

The separation factor ( $R_L$ ) is a dimensionless unit used to investigate the feasibility of adsorption system (Kaur et al. 2013) as presented in Table 2.18 at various initial adsorbate concentration  $C_o$  (mg/L). Generally, the best isotherm model is chosen based on a high linear regression coefficient ( $R^2$ ) value. Table 2.19 presented the literature information on the applicability of isotherm models for different adsorbent systems.

**Table 2.18:** Adsorption process feasibility at various ( $R_L$ ) values (Kaur et al. 2013)

<b>Separation equilibrium factor (<math>R_L</math>)</b>	<b>Adsorption process feasibility</b>
$R_L > 1$	Unfavourable
$R_L = 1$	Linear
$0 < R_L < 1$	Favourable
$R_L = 1$	Irreversible

**Table 2.19:** The applicability of various isotherm models for dyes and heavy metal ions removal by various adsorbents.

<b>Adsorbent</b>	<b>Adsorbate</b>	<b>Isotherm model</b>	<b>Reference</b>
Pecan nutshell biochar	Reactive red 141	Freundlich	(Zazycki et al. 2018)
Mango leaf	Methylene blue	Langmuir	(Uddin et al. 2017)
Korean cabbage biochar	Crystal violet	Langmuir	(Sewu et al. 2017b)
Chitosan activated carbon	Methylene blue	Langmuir	(Marrakchi et al. 2017)
Magnetic kaolin	Direct Red 23	Langmuir	(Magdy et al. 2017)
Orange tree (Base)	Methylene blue	Langmuir	(Azzaz et al. 2017)
Bamboo leaf	Methylene blue	Langmuir	(Zhu et al. 2016)
Raw eucalyptus bark	Methylene blue	Langmuir	(Afroze et al. 2016c)
Algae biochar	Congo red	Freundlich	(Nautiyal et al. 2016)
Modified rubber leaf	Acid Blue 25	Langmuir	(Khalid et al. 2015)

---

Coconut husk carbon	Crystal violet	Freundlich	(Aljeboree et al. 2015)
Kaolin/iron-manganese oxide Composite	Basic fuchsin	Langmuir	(Khan et al. 2015)
Pine cone activated carbon	Congo red	Freundlich	(Dawood et al. 2014)
Pine leave	Methylene blue	Langmuir & Freundlich	(Yagub et al. 2012)
Pine cone	Congo red	Freundlich	(Dawood and Sen 2012b)
pomelo skin carbon	Methylene blue Acid blue 15	Langmuir	(Foo and Hameed 2011a)
Metakaolin geopolymer	Ni (II)	Langmuir & Freundlich	(Kara et al. 2017)
Banana peel biochar	Pb (II)	Langmuir	(Zhou et al. 2017)
Metakaolin geopolymer	Zn (II)	Langmuir	(Kara et al. 2017)
Raw eucalyptus bark	Zn (II)	Langmuir & Freundlich	(Afroze et al. 2016b)
Coconut pith biochar	Hg (II)	Freundlich	(Johari et al. 2016)
Sesame stalk biochar	Fe (III) Cr (III)	Langmuir	(Kırbıyık et al. 2016)
Tomato leaf	Ni (II)	Langmuir	(Gutha et al. 2015)
Tomato waste biochar	Co (II)	Freundlich	(Önal et al. 2014)
Almond shell biochar	Ni (II) Co (II)	Langmuir	(Kılıç et al. 2013)
Buffalo weed biochar	Cd (II) Pb (II)	Freundlich	(Yakkala et al. 2013)

---

Copolymerization- orange peel	Pb (II) Ni (II) Cd (II)	Langmuir	(Feng et al. 2011)
Sugarcane biochar	Pb (II)	Langmuir	(Inyang et al. 2011)
Kaolin	Zn (II)	Langmuir & Freundlich	(Aries and Sen 2009)

## 2.10 Thermodynamic study

Thermodynamic studies used to investigate the temperature effect on adsorption process. The determination of Gibb's free energy change ( $\Delta G^0$ ), enthalpy change ( $\Delta H^0$ ) and entropy change ( $\Delta S^0$ ) are the important parameters used to evaluate the process design feasibility such as the system spontaneity and the endothermic or exothermic nature of the adsorption process (Yaneva and Georgieva 2012). The Gibb's free energy change ( $\Delta G^0$ ), enthalpy change ( $\Delta H^0$ ) and entropy change ( $\Delta S^0$ ) are calculated by using equations (2.16) and (2.17) (Dawood and Sen 2012a, Sen et al. 2012).

$$\text{Log}\left(1000\left(\frac{q_e}{C_e}\right)\right) = \frac{\Delta S^0}{2.303 R} + \frac{-\Delta H^0}{2.303 RT} \quad (2.16)$$

$$\Delta G^0 = \Delta H^0 - T \Delta S^0 \quad (2.17)$$

Where  $q_e$  (mg/L) is the solid-phase concentration at equilibrium,  $C_e$  (mg/L) is equilibrium concentration in solution,  $T$  is the temperature in Kelvin ( $K$ ) and  $R$  is the gas constant (8.314 J/mol K). Based on Van't Hoff equation,  $(q_e/C_e)$  value must be a dimensionless therefore the equilibrium constant will be multiplying it by a factor of 1000 assuming the adsorbent solution density is equivalent to 1 (g/ml) (Dawood and Sen 2012a). The enthalpy change ( $\Delta H^0$ ) and entropy change ( $\Delta S^0$ ) values were calculated from the slope and intercept of the linear Van't Hoff plot of  $\text{Log}\left(1000\left(\frac{q_e}{C_e}\right)\right)$  versus  $(1/T)$ . Also, Gibb's free energy ( $\Delta G^0$ ) was calculated as per equation (2.17). The adsorption process is usually considered as a physical adsorption if the enthalpy change ( $\Delta H^0$ )  $< 84 \text{ kJ} \cdot \text{mol}^{-1}$  and as chemisorption adsorption process when

the enthalpy change lies between 84 and 420 kJ .mo<sup>-1</sup> (Ahmad and Kumar 2010, Yaneva and Georgieva 2012) . Also, the negative value of ( $\Delta H^0$ ) indicates an exothermic adsorption process where a positive value of ( $\Delta H^0$ ) indicates an endothermic adsorption process. The effect of solution temperature on the enthalpy change ( $\Delta H^0$ ) and the reaction type for various adsorbents was presented in Table 2.10 of section 2.7.1.3. The entropy change ( $\Delta S^0$ ) indicates the randomness at the solid/liquid interface. The Gibbs energy change ( $\Delta G^0$ ) plays a significant factor for determining the degree of spontaneity of the adsorption process. Higher negative value of ( $\Delta G^0$ ) indicates energetically favorable and spontaneous adsorption process in nature (Tran et al. 2016).

Dawood et al., (Dawood et al. 2014) studied the thermodynamic behaviour of Congo red dye removal by pine cone based activated carbon. The positive values of ( $\Delta H^0$ ) of 7.92 kJ/mole indicates an endothermic adsorption process and the negative values of Gibb's free energy change ( $\Delta G^0$ ) (-7.1, -7.6 and -8.6 kJ/mole at 30, 40 and 60 °C) suggested a spontaneous adsorption process. Also, Zazycki et al., (Zazycki et al. 2018) studied the removal of reactive red 141 dye by pecan nutshell biochar at various solution temperature of 25, 35, 45 and 55 °C. It was found that the negative values of Gibb's free energy change ( $\Delta G^0$ ) were decreasing from -20.1 to -16.6 kJ/mole with the increases of solution temperature from 25-55 °C respectively and thus indicates a spontaneous and favourable adsorption process. The negative ( $\Delta H^0$ ) value of -56.4 kJ/mole and ( $\Delta S^0$ ) value of -0.12 kJ/mole.K suggest an exothermic reaction process and randomness in the solid/liquid interface structure respectively.

Moreover, the thermodynamic properties in the removal of Al (III) ions by bentonite and kaolin clays were studied and reported by Chai et al (Chai et al. 2017). It was found that enthalpy change ( $\Delta H^0$ ) values were 32.9 kJ/mole for bentonite and -42.9 kJ/mole for kaolin therefore this indicates that the adsorption process was an endothermic for bentonite and an exothermic for kaolin. Also, the positive values of ( $\Delta G^0$ ) for bentonite and kaolin are indicating the adsorption of Al (III) ions on the two clays is non-spontaneous. Afroze et al., (Afroze et al. 2016b) reported negative values for enthalpy change ( $\Delta H^0$ ) and entropy change ( $\Delta S^0$ ) for all the temperatures in the removal of Zn (II) by base modified eucalyptus bark which suggest an exothermic adsorption process in nature and a decrease in the randomness at the solid solution interface structure of the adsorption process respectively.

## 2.11 Column adsorption study on the removal of organic dye

Batch experiments are useful to provide information about the effectiveness of adsorbent and to determine various operating parameters and their optimum value. However, the experimental data obtained from the batch study are not applicable in continuous operation where contact time is always less than equilibrium time. Therefore, continuous adsorption system is considered to be more accurate in term of finding the maximum adsorption capacity and adsorbent utilization in a continuous mode. Continuous adsorption system plays an important factor for determination of adsorbent's feasibility in a real industrial scale application. Fixed bed column is used to evaluate the operation and dynamic response of continues adsorption process. It is important to find the breakthrough curve shape and breakthrough time under various column operation conditions such as initial feedstock concentration, adsorbate flow rate and bed height. The removal of dyes and heavy metal ions in a fixed bed column under various operational parameters such as bed height, inlet flow rate and adsorbate concentration were presented in Table 2.20.

**Table 2.20:** The removal of dyes and heavy metal ions in a fixed bed column under various operational conditions.

Adsorbent/s	Adsorbate	Dye removal	Operational conditions	Reference
Tectona grandis leaves biochar	Ni (II)	27 mg/g	Bed height (1-3cm), flow rate (1-5 ml/min) and initial metal ions concentration (25-75 mg/L)	(Vilvanathan and Shanthakumar 2017)
	Co (II)	17.7 mg/g		
Kaolin/pine cone composite	Methylene blue	74 %	Bed height (3-7cm), flow rate (13-17 ml/min) and initial concentration (50-150 mg/L)	(Shak et al. 2017)
Eucalyptus bark	Methylene blue	48%	Bed height (10-15cm), flow rate (10-15 ml/min) and	(Afroze et al. 2016a)

			initial concentration (50-100 mg/L)	
Bone char	Cu (II)	51.8 mg/g	Bed height (2.5-7.5 cm), flow rate (4 and 6 ml/min) and initial concentration (100 and 200 mg/L)	(Hernández-Hernández et al. 2017)
	Zn (II)	41.1 mg/g		
Nut shell based activated carbon	Phenol	76.3 mg/g	Bed height (2-4cm), flow rate (5-15 ml/min) and initial concentration of 100 mg/L	(Kumar and Jena 2016)
	Methylene blue	126.1 mg/g		
Jujube shell	Congo red	80.5 mg/g	Bed height (2-6 cm), flow rate (2.8-6.4 ml/min) and initial concentration (100-300 mg/L)	(El Messaoudi et al. 2016)
Pine cone	Methylene blue			
Modified ball clay/chitosan	Methylene blue	142 mg/g	Bed height (2.5-4.5cm), flow rate (5-10 ml/min) and initial concentration (50-200 mg/L)	(Auta and Hameed 2014)
Allspice waste	Pb (II)	99%		
Modified corn stalk	Cr (VI)	93.8%	Bed height (1.4-2.9 cm), flow rate (5-15 ml/min) and initial concentration (100-300 mg/L)	(Chen et al. 2012)
Peanut husk	Indosol Orange	8.7 mg/g		
Bamboo based activated carbon	Reactive black 5	39.0 mg/g	Bed height (4-8cm), flow rate (10-30 ml/min) and	(Ahmad and Hameed 2010)

			initial concentration (50-200 mg/L)	
Chitosan/glass beads	Food dye yellow 5	75%	pH solution (3-6), flow rate of 5 ml/min) and initial concentration of 85 mg/L	(Vieira et al. 2014)
Acid modified clay	Methylene blue	76.7 mg/g	Bed height (2.5-4.5cm), flow rate (5-10 ml/min) and initial concentration (30-100 mg/L)	(Auta and Hameed 2013a)
Paper mill activated carbon	Reactive red 24	17.6 mg/g	Bed height (0.9-3.5cm), flow rate (3-7 ml/min) and initial concentration (50-200 mg/L)	(Li et al. 2011b)
Green coconut shell	Ni (II) Zn (II)	54.6 mg/g 17.1 mg/g	Bed height (5-18 cm), flow rate (2-6 ml/min) and initial metal ions concentration of 100mg/L	(Sousa et al. 2010)

### 2.11.1 Theory of breakthrough curve (BTC) and mass transfer zone (MTZ)

The theory of Breakthrough Curve (BTC) was used in analysing the adsorption performance of a packed-bed column. The shape of a BTC and its breakthrough time are important characteristics in evaluating the dynamic behaviour of an adsorption column (Baral et al. 2009). Maximum adsorption capacity takes place initially during a fixed bed column adsorption system. Over time, the mass transfer zone and the adsorption zone move along the bed to the outlet end till the outlet effluent concentration equals the inlet feedstock concentration. Thus, the prediction of a concentration-time profile based on the column effluent from BTC is required in designing a suitable and practical adsorption column. Adsorption performance is dependent on the inlet adsorbate flow rates, initial adsorbate concentration and bed depth. A typical BTC is usually expressed by a  $C_{\text{effluent}} (C_t)/C_{\text{influent}} (C_o)$  versus volume of effluent or service time plot for a given bed height as shown in Fig.2.11.



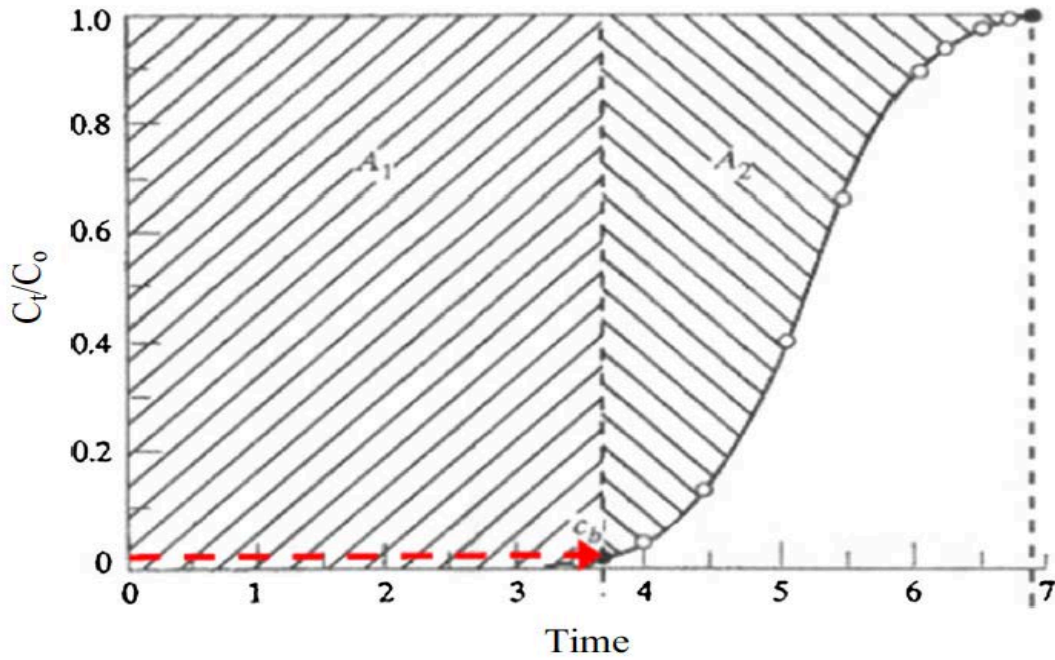


**Figure 2.11:** Typical Breakthrough Curve (BTC) (Dutta 2007).

The following parameters are calculated for column data analysis using various equations (2.18- 2.26) respectively (Afroze et al. 2016a, Cruz-Olivares et al. 2013, Yagub et al. 2015) . The time equivalent to total or stoichiometric capacity is calculated using the following equation

$$t_t = \int_{t=0}^{t=\infty} \left(1 - \frac{C_t}{C_o}\right) dt = A_1 + A_2 \quad (2.18)$$

Time equivalent to usable capacity is determined using Equation (2.19)

$$t_u = \int_{t=0}^{t=t_b} \left(1 - \frac{C_t}{C_o}\right) dt = A_1 \quad (2.19)$$

The usable capacity of bed up to the breakthrough time point  $t_b$  and  $A_2$  area calculation the height of unused bed.

$$t_u \approx t_b$$

Area under the curve as per equation (2.18) gives the total time value, while the area under the curve as per equation (2.19) gives usable capacity time. The area under the curve can be determined using graphical method or by numerical integration. The fraction of the total bed capacity or length utilized up to the break point is expressed as  $\frac{t_u}{t_t}$ . The height of the unused bed ( $H_{UNB}$ ) or Mass Transfer Zone (MTZ) is calculated using equation (2.20) and (2.21)

$$H_{UNB} = \left(1 - \frac{t_u}{t_t}\right) H_T = \left(1 - \frac{t_b}{t_t}\right) H_T \quad (2.20)$$

The used bed length up to the break point is calculated using equation (2.21)

$$MTZ = H_{UNB} \quad (2.21)$$

$$H_B = \left(\frac{t_b}{t_t}\right) H_T \quad (2.22)$$

The total effluent volume  $V_{eff}$  is estimated using equation (2.23)

$$V_{eff} = Q \cdot t_{total} \quad (2.23)$$

Where,  $Q$  = volumetric flow rate (mL/min),  $t_{total}$  = total flow time (min) and  $H_T$  = total bed height (cm). The BTC plot can be used to find the total quantity of adsorbate adsorbed. The total amount of dye and heavy metal ions adsorbed in milligrams for a given inlet concentration is determined using equation (2.24)

$$q_{total} = \frac{QA}{1000} = \left(\frac{QC_o}{1000}\right) \int_{t=0}^{t=t_{total}} \frac{C_t}{C_o} dt \quad (2.24)$$

The total amount of adsorbate pumped into the column  $m_{total}$  is calculated using equation (2.25) (Ataei-Germi and Nematollahzadeh 2016).

$$m_{total} = \frac{C_o Q t_{total}}{1000} \quad (2.25)$$

The total percentage for the removal of dye and heavy metal ions is calculated from the ratio of total quantity of adsorbate adsorbed  $q_{total}$  to the total amount pumped into the column  $m_{total}$  as shown in equation (2.26) (Ataei-Germi and Nematollahzadeh 2016).

$$\% \text{ Removal} = \frac{q_{total}}{m_{total}} \times 100 \quad (2.26)$$

## 2.11.2 Packed-bed column kinetics models

Kinetic modelling of fixed bed column is required to predict the dynamic behaviour of the bed in an industrial scale operation. Thomas model, Yoon-Nelson model, Clark constants and Bed Depth Service Time model are the commonly used kinetic models to analyse the column performance. These models are used to calculate the column kinetics parameters and the maximum adsorption capacity of the fixed bed column.

### 2.11.2.1 Thomas Model

Thomas model is developed in 1944 (Thomas 1944) and it is widely used to study the column performance and to predict the BTC. This model is based on the equation for conservation of mass in a flow system. It assumes plug flow behaviour in the bed and follows Langmuir kinetic of adsorption (Ghasemi et al. 2011, Han et al. 2008). Also, this model assumes a negligible axial dispersion in the column adsorption due to the fact that the rate driving force in the adsorption process follows the second-order reversible kinetics reaction (Han et al. 2008, Xu et al. 2013). Thomas model equation is presented as per equation (2.27) while the linearized form of the model is expressed in equation (2.28) (Vilvanathan and Shanthakumar 2017).

$$\frac{C}{C_o} = \frac{1}{1 + \exp\left[K_T \left(\frac{q_o m - C_o V}{Q}\right)\right]} \quad (2.27)$$

$$\ln\left(\frac{C_o}{C} - 1\right) = \left(\frac{K_T q_o m}{Q}\right) - \left(\frac{K_T C_o V}{Q}\right) \quad (2.28)$$

Where,  $K_T$  is Thomas Rate Constant (mL/mg min),  $q_o$  is equilibrium adsorbate uptake (mg/g),  $m$  is the amount of adsorbent in column (g),  $C_o$  is the inlet adsorbate Concentration (mg/L),  $C_t$  is the effluent adsorbate Concentration (mg/L),  $V$  is total volume (mL) and  $Q$  is the flow rate (ml/min). The kinetic coefficient  $K_T$  and  $q_o$  can be calculated from the slope and intercept of the linear plot  $\ln\left(\frac{C_o}{C_t}\right) - 1$  against  $t$  at a given flow rate.

### 2.11.2.2 Yoon-Nelson Model

The Yoon and Nelson model (Yoon and Nelson 1984) does not require any detailed data on the characteristics of adsorbate, the physical properties of the adsorbent bed and the type of adsorbent used, therefore it is less complicated compared to the other models. This model assumes that the rate of decrease in the probability of adsorption for each adsorbate molecule is proportional to the probability of adsorbate adsorption and the probability of adsorbate breakthrough on the adsorbent (Ahmad and Hameed 2010). The linearized form of the model is expressed as per equation (2.29).

$$\ln\left(\frac{C}{C_o - C}\right) = K_{YN}t - K_{YN}\tau \quad (2.29)$$

Where,  $K_{YN}$  is Yoon and Nelson rate constant ( $\text{min}^{-1}$ ),  $C_o$  is the inlet adsorbate Concentration (mg/L),  $C$  is the effluent adsorbate concentration (mg/L),  $t$  is the breakthrough time (min) and  $\tau$  is the time required for 50% adsorbate breakthrough (min). The values for  $K_{YN}$  and  $K_{YN}\tau$  is obtained from the slope and intercept of the linear plot  $\ln\left(\frac{C}{C_o - C}\right)$  against time ( $t$ ).

### 2.11.2.3 BDST Model

The BDST model is widely used in comparing the adsorption capacity in adsorption columns under different experimental conditions (Baral et al. 2009) . BDST model evaluate the efficiency of the column under constant operating conditions for achieving a desired breakthrough level (Sadaf and Bhatti 2014). This model presents a linear relationship between the column bed depth and the service time in terms of process concentration and adsorption parameters. Service time is the time required for an adsorbent to adsorb a specific amount of adsorbate from a solution before regeneration is needed. Further, this model assumes that intra-particle-diffusion and external mass transfer resistance forces are negligible and that the adsorption kinetic is controlled by a surface chemical reaction between the solute in the solution and the unused adsorbent (Afroze et al. 2016a). The BDST model physically measures the capacity of the bed at different breakthrough values and provides useful modelling equations for the changes of system parameters (Han et al. 2007). The experimental data can be fitted into this model as shown in equation (2.30) (Sadaf and Bhatti 2014).

$$t = \left( \frac{N_o H_T}{C_o u} \right) - \left( \frac{1}{K_o C_o} \right) \ln \left( \frac{C_o}{C_t} - 1 \right) \quad (2.30)$$

Where,  $C_o$  is the inlet solute concentration (mg/L),  $C_t$  is effluent concentration of solute in the liquid phase (mg/L),  $u$  is influent linear velocity (cm/min),  $N_o$  is the adsorption capacity (mg/L),  $K_o$  is the rate constant (L/mg min),  $t$  is time (min) and  $H_T$  is the bed height of column (cm). The value of  $N_o$  and  $K_o$  can be calculated from the slope and intercept of time (t) against bed height  $H_T$  linear plot. The BDST model can be further simplified into equation (2.31).

$$t = az + b \quad (2.31)$$

Where  $a = \frac{N_o}{C_o u}$  is the slope and  $b = - \left( \frac{1}{K_o C_o} \right) \ln \left( \frac{C_o}{C_t} - 1 \right)$  is the intercept.

#### 2.11.2.4 Clark Model

Clark model was developed by Clark in 1987(Clark et al. 1987). This model is based on the use of a mass-transfer concept in combination with the Freundlich isotherm. Clark model assumes that the shape of the mass transfer zone is constant and all the adsorbates are removed at the end of the column (Dhanasekaran et al. 2017). Clark model is expressed as per equation (2.32)

$$\left(\frac{C_0}{C_t}\right)^{n-1} - 1 = A e^{-rt} \quad (2.32)$$

Where,  $C_0$  is the initial adsorbate concentration (mg/L),  $C_t$  is the adsorbate concentration at time 't',  $n$  is the Freundlich constant parameter,  $A$  and  $r$  ( $\text{min}^{-1}$ ) are Clark constants. The linearized form of equation (2.33) can be expressed as shown below:

$$n \left[ \left(\frac{C_0}{C_t}\right)^{n-1} - 1 \right] = -rt + \ln A \quad (2.33)$$

The constants value are calculated from the plot of  $\ln \left[ \left(\frac{C_0}{C_t}\right)^{n-1} - 1 \right]$  vs.  $t$ .

## 2.12 Summary

Industrial effluents from various industrial activities discharge significant amount of dyes and heavy metal ions contaminations into the water stream. These contaminations pose a serious health hazards to living organisms. Therefore, this chapter presents the latest treatment technologies used in the removal of organic dyes and heavy metal ions from water and wastewater. Also, it provides extensive literature information about natural dyes, synthetic dyes, heavy metal ions, their classification, sources and toxicity effects. The effectiveness of various physio-chemical, chemical and biological separation techniques used in the removal of dyes and heavy metal ions have been evaluated here in term of their design simplicity, operation efficiency and total cost. Adsorption process is a physical method widely used in the separation of most organic and inorganic pollutants from their aqueous solution due to its high adsorption efficiency, ease of operation and low operation cost. Also, this chapter highlights a wide range of adsorbents used in the removal of these pollutants such as agricultural solid waste, modified biomass waste, biomass based bio-char, charcoal and activated carbon as well as other inorganic clay mineral materials. Commercial activated carbon is used widely as an adsorbent in the removal of dyes and heavy metals with great success due to its excellent adsorption capacity, large surface area and mesoporous structure. However, due to the high cost and difficulties associated with its regeneration, various researchers have explored alternative non-conventional and cost-effective adsorbents in the removal of dyes and heavy metal ions. Agricultural solid waste based biochar and activated carbon are considered interesting alternative to available commercial activated carbon. These natural waste materials are available locally in a large quantity and have little or no commercial value. This literature review provides an overview and up to date of current uses of biomass based biochar and carbon in the removal of organic dyes and inorganic heavy metal ions from wastewater. Also, the mechanism of adsorption and identification of various process parameters such as solution pH, initial adsorbate concentration, adsorbent dose, contact time, solution temperature and presence of ionic strength have been critically analysed here. Further, this review describe the continuous column adsorption study and the application of various column dynamic models such as Thomas, Yoon-Nelson, Clark constants and Bed Depth Service Time models.

## 2.13 References

Abd El-Rahim, W.M., El-Arady, O.A.M. and Mohammad, F.H.A. (2009) "The effect of pH on bioremediation potential for the removal of direct violet textile dye by *Aspergillus niger*". Desalination **249**(3), 1206-1211.

Abidi, N., Errais, E., Duplay, J., Berez, A., Jrad, A., Schäfer, G., Ghazi, M., Semhi, K. and Trabelsi-Ayadi, M. (2015) "Treatment of dye-containing effluent by natural clay". Journal of Cleaner Production **86**(Supplement C), 432-440.

Aboua, K.N., Yobouet, Y.A., Yao, K.B., Goné, D.L. and Trokourey, A. (2015) "Investigation of dye adsorption onto activated carbon from the shells of Macoré fruit". Journal of Environmental Management **156**, 10-14.

Adeli, M., Yamini, Y. and Faraji, M. (2017) "Removal of copper, nickel and zinc by sodium dodecyl sulphate coated magnetite nanoparticles from water and wastewater samples". Arabian Journal of Chemistry **10**, S514-S521.

Afroze, S., Sen, T.K. and Ang, H. (2016a) "Adsorption performance of continuous fixed bed column for the removal of methylene blue (MB) dye using *Eucalyptus sheathiana* bark biomass". Research on Chemical Intermediates **42**(3), 2343-2364.

Afroze, S., Sen, T.K. and Ang, H.M. (2016b) "Adsorption removal of zinc (II) from aqueous phase by raw and base modified *Eucalyptus sheathiana* bark: Kinetics, mechanism and equilibrium study". Process Safety and Environmental Protection **102**, 336-352.

Afroze, S., Sen, T.K., Ang, M. and Nishioka, H. (2016c) "Adsorption of methylene blue dye from aqueous solution by novel biomass *Eucalyptus sheathiana* bark: equilibrium, kinetics, thermodynamics and mechanism". Desalination and Water Treatment **57**(13), 5858-5878.

Aguayo-Villarreal, I.A., Bonilla-Petriciolet, A. and Muñoz-Valencia, R. (2017) "Preparation of activated carbons from pecan nutshell and their application in the antagonistic adsorption of heavy metal ions". Journal of Molecular Liquids **230**, 686-695.

Ahmad, A.A. and Hameed, B.H. (2010) "Fixed-bed adsorption of reactive azo dye onto granular activated carbon prepared from waste". Journal of Hazardous Materials **175**(1), 298-303.



Ahmad, M.A. and Alrozi, R. (2011) "Removal of malachite green dye from aqueous solution using rambutan peel-based activated carbon: Equilibrium, kinetic and thermodynamic studies". Chemical Engineering Journal **171**(2), 510-516.

Ahmad, R. and Kumar, R. (2010) "Adsorptive removal of congo red dye from aqueous solution using bael shell carbon". Applied Surface Science **257**(5), 1628-1633.

Akhtar, M., Iqbal, S., Kausar, A., Bhangar, M.I. and Shaheen, M.A. (2010) "An economically viable method for the removal of selected divalent metal ions from aqueous solutions using activated rice husk". Colloids and Surfaces B: Biointerfaces **75**(1), 149-155.

Al-Degs, Y.S., El-Barghouthi, M.I., El-Sheikh, A.H. and Walker, G.M. (2008) "Effect of solution pH, ionic strength, and temperature on adsorption behavior of reactive dyes on activated carbon". Dyes and Pigments **77**(1), 16-23.

Al-Dhabi, N.A. (2013) "Heavy metal analysis in commercial Spirulina products for human consumption". Saudi Journal of Biological Sciences **20**(4), 383-388.

Alandis, N., Aldayel, O., Mekhemer, W., Hefne, J. and Jokhab, H. (2010) "Thermodynamic and kinetic studies for the adsorption of Fe (III) and Ni (II) ions from aqueous solution using natural bentonite". Journal of dispersion science and technology **31**(11), 1526-1534.

Aljeboree, A.M., Alkaim, A.F. and Al-Dujaili, A.H. (2015) "Adsorption isotherm, kinetic modeling and thermodynamics of crystal violet dye on coconut husk-based activated carbon". Desalination and Water Treatment **53**(13), 3656-3667.

Allen, S.J., McKay, G. and Porter, J.F. (2004) "Adsorption isotherm models for basic dye adsorption by peat in single and binary component systems". Journal of Colloid and Interface Science **280**(2), 322-333.

Almeida, C.A.P., Debacher, N.A., Downs, A.J., Cottet, L. and Mello, C.A.D. (2009) "Removal of methylene blue from colored effluents by adsorption on montmorillonite clay". Journal of Colloid and Interface Science **332**(1), 46-53.

AlOthman, Z.A., Habila, M.A., Ali, R., Abdel Ghafar, A. and El-din Hassouna, M.S. (2014) "Valorization of two waste streams into activated carbon and studying its adsorption kinetics, equilibrium isotherms and thermodynamics for methylene blue removal". Arabian Journal of Chemistry **7**(6), 1148-1158.

Alventosa-deLara, E., Barredo-Damas, S., Zuriaga-Agustí, E., Alcaina-Miranda, M.I. and Iborra-Clar, M.I. (2014) "Ultrafiltration ceramic membrane performance during the treatment of model solutions containing dye and salt". Separation and Purification Technology **129**(0), 96-105.

Anirudhan, T.S. and Ramachandran, M. (2015) "Adsorptive removal of basic dyes from aqueous solutions by surfactant modified bentonite clay (organoclay): Kinetic and competitive adsorption isotherm". Process Safety and Environmental Protection **95**(Supplement C), 215-225.

Antoniadis, A., Takavakoglou, V., Zalidis, G., Darakas, E. and Poullos, I. (2010) "Municipal wastewater treatment by sequential combination of photocatalytic oxidation with constructed wetlands". Catalysis Today **151**(1–2), 114-118.

Aoudj, S., Khelifa, A., Drouiche, N., Hecini, M. and Hamitouche, H. (2010) "Electrocoagulation process applied to wastewater containing dyes from textile industry". Chemical Engineering and Processing: Process Intensification **49**(11), 1176-1182.

Araújo, C.K.C., Oliveira, G.R., Fernandes, N.S., Zanta, C.L.P.S., Castro, S.S.L., da Silva, D.R. and Martínez-Huitle, C.A. (2014) "Electrochemical removal of synthetic textile dyes from aqueous solutions using Ti/Pt anode: role of dye structure". Environmental Science and Pollution Research **21**(16), 9777-9784.

Aries, F. and Sen, T.K. (2009) "Removal of zinc metal ion ( $Zn^{2+}$ ) from its aqueous solution by kaolin clay mineral: a kinetic and equilibrium study. ". Colloids Surf A **348**(1-3), 100-108.

Arslan-Alaton, I., Gursoy, B.H. and Schmidt, J.-E. (2008) "Advanced oxidation of acid and reactive dyes: Effect of Fenton treatment on aerobic, anoxic and anaerobic processes". Dyes and Pigments **78**(2), 117-130.

Ataei-Germi, T. and Nematollahzadeh, A. (2016) "Bimodal porous silica microspheres decorated with polydopamine nano-particles for the adsorption of methylene blue in fixed-bed columns". Journal of Colloid and Interface Science **470**, 172-182.

Auta, M. and Hameed, B.H. (2013a) "Acid modified local clay beads as effective low-cost adsorbent for dynamic adsorption of methylene blue". Journal of Industrial and Engineering Chemistry **19**(4), 1153-1161.

Auta, M. and Hameed, B.H. (2014) "Chitosan–clay composite as highly effective and low-cost adsorbent for batch and fixed-bed adsorption of methylene blue". Chemical Engineering Journal **237**, 352-361.

Auta, M. and Hameed, B.H. (2013b) "Coalesced chitosan activated carbon composite for batch and fixed-bed adsorption of cationic and anionic dyes". Colloids and Surfaces B: Biointerfaces **105**(0), 199-206.

Avlonitis, S.A., Poullos, I., Sotiriou, D., Pappas, M. and Moutesidis, K. (2008) "Simulated cotton dye effluents treatment and reuse by nanofiltration". Desalination **221**(1–3), 259-267.

Azzaz, A.A., Jellali, S., Akrouf, H., Assadi, A.A. and Bousselmi, L. (2017) "Optimization of a cationic dye removal by a chemically modified agriculture by-product using response surface methodology: biomasses characterization and adsorption properties". Environmental Science and Pollution Research **24**(11), 9831-9846.

Babaei, A.A., Kakavandi, B., Rafiee, M., Kalantarhormizi, F., Purkaram, I., Ahmadi, E. and Esmaili, S. (2017) "Comparative treatment of textile wastewater by adsorption, Fenton, UV-Fenton and US-Fenton using magnetic nanoparticles-functionalized carbon (MNPs@C)". Journal of Industrial and Engineering Chemistry **56**(Supplement C), 163-174.

Balamurugan, B., Thirumarimurugan, M. and Kannadasan, T. (2011) "Anaerobic degradation of textile dye bath effluent using *Halomonas* sp". Bioresource Technology **102**(10), 6365-6369.

Baral, S.S., Das, N., Ramulu, T.S., Sahoo, S.K., Das, S.N. and Chaudhury, G.R. (2009) "Removal of Cr(VI) by thermally activated weed *Salvinia cucullata* in a fixed-bed column". Journal of Hazardous Materials **161**(2–3), 1427-1435.

Bediako, J.K., Wei, W., Kim, S. and Yun, Y.-S. (2015) "Removal of heavy metals from aqueous phases using chemically modified waste Lyocell fiber". Journal of Hazardous Materials **299**(Supplement C), 550-561.

Belala, Z., Jeguirim, M., Belhachemi, M., Addoun, F. and Trouvé, G. (2011) "Biosorption of basic dye from aqueous solutions by Date Stones and Palm-Trees Waste: Kinetic, equilibrium and thermodynamic studies". Desalination **271**(1–3), 80-87.

Bilińska, L., Gmurek, M. and Ledakowicz, S. (2016) "Comparison between industrial and simulated textile wastewater treatment by AOPs – Biodegradability, toxicity and cost assessment". Chemical Engineering Journal **306**, 550-559.

Borah, L., Goswami, M. and Phukan, P. (2015) "Adsorption of methylene blue and eosin yellow using porous carbon prepared from tea waste: Adsorption equilibrium, kinetics and thermodynamics study". Journal of Environmental Chemical Engineering **3**(2), 1018-1028.

Boruah, P., Sarma, A. and Bhattacharyya, K.G. (2015) "Removal of Ni (II) ions from aqueous solution by using low cost biosorbent prepared from jackfruit (*Artocarpus heterophyllus*) leaf powder".

Bratskaya, S.Y., Pestov, A.V., Yatluk, Y.G. and Avramenko, V.A. (2009) "Heavy metals removal by flocculation/precipitation using N-(2-carboxyethyl)chitosans". Colloids and Surfaces A: Physicochemical and Engineering Aspects **339**(1), 140-144.

Brigatti, M.F., Galán, E. and Theng, B.K.G. (2013) "Chapter 2 - Structure and Mineralogy of Clay Minerals". *Developments in Clay Science* Faiza, B. and Gerhard, L. (eds), pp. 21-81, Elsevier.

Busca, G. (2017) "Acidity and basicity of zeolites: A fundamental approach". Microporous and Mesoporous Materials **254**(Supplement C), 3-16.

Cao, D.-M., Xiao, X., Wu, Y.-M., Ma, X.-B., Wang, M.-N., Wu, Y.-Y. and Du, D.-L. (2013) "Role of electricity production in the anaerobic decolorization of dye mixture by exoelectrogenic bacterium *Shewanella oneidensis* MR-1". Bioresource Technology **136**(0), 176-181.

Cao, M., Lin, J., Lü, J., You, Y., Liu, T. and Cao, R. (2011) "Development of a polyoxometallate-based photocatalyst assembled with cucurbit[6]uril via hydrogen bonds for azo dyes degradation". Journal of Hazardous Materials **186**(1), 948-951.

Carmen, Z. and Daniela, S. (2012) "Textile Organic Dyes – Characteristics, Polluting Effects and Separation/Elimination Procedures from Industrial Effluents – A Critical Overview". *Organic Pollutants Ten Years After the Stockholm Convention -*

*Environmental and Analytical Update* T.Puzyn and Mostrag-Szlichtyng, A. (eds), IntechOpen.

Cazetta, A.L., Pezoti, O., Bedin, K.C., Silva, T.L., Paesano Junior, A., Asefa, T. and Almeida, V.C. (2016) "Magnetic activated carbon derived from biomass waste by concurrent synthesis: efficient adsorbent for toxic dyes". ACS Sustainable Chemistry & Engineering **4**(3), 1058-1068.

- Chai, W., Huang, Y., Han, G., Liu, J., Yang, S. and Cao, Y. (2017) "An Enhanced Study on Adsorption of Al(III) onto Bentonite and Kaolin: Kinetics, Isotherms, and Mechanisms". Mineral Processing and Extractive Metallurgy Review **38**(2), 106-115.
- Chakraborty, J.N. (2014) "4 - Dyeing with direct dye". Fundamentals and Practices in Colouration of Textiles, pp. 29-45, Woodhead Publishing India.
- Chander, M. and Arora, D.S. (2007) "Evaluation of some white-rot fungi for their potential to decolourise industrial dyes". Dyes and Pigments **72**(2), 192-198.
- Chantawong, V., Harvey, N.W. and Bashkin, V.N. (2003) "Comparison of Heavy Metal Adsorptions by Thai Kaolin and Ballclay". Water, Air, and Soil Pollution **148**(1), 111-125.
- Chen, H. and Zhao, J. (2009) " Adsorption study for removal of Congo red anionic dye using organo-attapulgite". Adsorption **15**, 381-389.
- Chen, S., Yue, Q., Gao, B., Li, Q., Xu, X. and Fu, K. (2012) "Adsorption of hexavalent chromium from aqueous solution by modified corn stalk: A fixed-bed column study". Bioresource Technology **113**, 114-120.
- Cheng, S., Oatley, D.L., Williams, P.M. and Wright, C.J. (2012) "Characterisation and application of a novel positively charged nanofiltration membrane for the treatment of textile industry wastewaters". Water Research **46**(1), 33-42.
- Chieng, H.I., Lim, L.B. and Priyantha, N. (2015) "Enhancing adsorption capacity of toxic malachite green dye through chemically modified breadnut peel: equilibrium, thermodynamics, kinetics and regeneration studies". Environmental technology **36**(1), 86-97.
- Chitpong, N. and Husson, S.M. (2017) "High-capacity, nanofiber-based ion-exchange membranes for the selective recovery of heavy metals from impaired waters". Separation and Purification Technology **179**(Supplement C), 94-103.
- Clark, N.N., Atkinson, C.M. and Flemmer, R.L.C. (1987) "Turbulent circulation in bubble columns". AIChE Journal **33**(3), 515-518.
- Cruz-Olivares, J., Pérez-Alonso, C., Barrera-Díaz, C., Ureña-Nuñez, F., Chaparro-Mercado, M.C. and Bilyeu, B. (2013) "Modeling of lead (II) biosorption by residue of allspice in a fixed-bed column". Chemical Engineering Journal **228**(Supplement C), 21-27.

Da Silva, J.F. and Williams, R.J.P. (2001) *The biological chemistry of the elements: the inorganic chemistry of life*, Oxford University Press.

Daâssi, D., Mechichi, T., Nasri, M. and Rodriguez-Couto, S. (2013) "Decolorization of the metal textile dye Lanaset Grey G by immobilized white-rot fungi". Journal of Environmental Management **129**(Supplement C), 324-332.

Dahri, M., Lim, L., Priyantha, N. and Chan, C. (2016) "Removal of Acid blue 25 using Cempedak Durian peel from aqueous medium: Isotherm, kinetics and thermodynamics studies". International Food Research Journal **23**(3).

Dawkar, V.V., Jadhav, U.U., Tamboli, D.P. and Govindwar, S.P. (2010) "Efficient industrial dye decolorization by *Bacillus* sp. VUS with its enzyme system". Ecotoxicology and environmental safety **73**(7), 1696-1703.

Dawood, S., Gupta, T. and Sen, T.K. (2017a) "Adsorptive Removal of Methylene Blue (MB) Dye at Kaolin Clay-Water Interface: Kinetics, Isotherm Modelling and Process Design". *Clay Minerals: Properties, Occurrence and Uses* Sen, T.K. (ed), pp. 209-236, Nova Science Publisher Inc., New York, USA.

Dawood, S. and Sen, T. (2014) "Review on Dye Removal from Its Aqueous Solution into Alternative Cost Effective and Non-Conventional Adsorbents". J Chem Proc Engg **1**(1), 1-7.

Dawood, S., Sen, T. and Phan, C. (2013) Effect of phosphoric acid and temperature profile on pine cone based activated carbon production and its effectiveness in the removal of Congo red dye by adsorption, pp. 76-82, ICEAI.

Dawood, S. and Sen, T.K. (2012a) "Author's Responses to the comment by Canzano et al and also corrigendum to "Removal of anionic dye Congo red from aqueous solution by raw pine and acid-treated pine cone powder as adsorbent: Equilibrium, thermodynamic, kinetics, mechanism and process design" published in *Water Research*, Vol. 46, pp. 1933–1946, 2012". Water Research **46**(13), 4316-4317.

Dawood, S. and Sen, T.K. (2012b) "Removal of anionic dye Congo red from aqueous solution by raw pine and acid-treated pine cone powder as adsorbent: Equilibrium, thermodynamic, kinetics, mechanism and process design". Water Research **46**(6), 1933-1946.

Dawood, S., Sen, T.K. and phan, C. (2016) "Adsorption removal of Methylene Blue (MB) dye from aqueous solution by bio-char prepared from *Eucalyptus sheathiana* bark: kinetic,

equilibrium, mechanism, thermodynamic and process design". Desalination and Water Treatment **57**(59), 28964-28980.

Dawood, S., Sen, T.K. and Phan, C. (2017b) "Synthesis and characterization of slow pyrolysis pine cone bio-char in the removal of organic and inorganic pollutants from aqueous solution by adsorption: Kinetic, equilibrium, mechanism and thermodynamic". Bioresource Technology **246**, 76-81.

Dawood, S., Sen, T.K. and Phan, C. (2014) "Synthesis and characterisation of novel-activated carbon from waste biomass pine cone and its application in the removal of congo red dye from aqueous solution by adsorption". Water, Air, and Soil Pollution **225**(1).

de Campos Ventura-Camargo, B. and Marin-Morales, M.A. (2013) "Azo dyes: characterization and toxicity—a review". Textiles and Light Industrial Science and Technology.

De Gisi, S., Lofrano, G., Grassi, M. and Notarnicola, M. (2016) "Characteristics and adsorption capacities of low-cost sorbents for wastewater treatment: A review". Sustainable Materials and Technologies **9**, 10-40.

Deng, Z., Fung, K.Y., Ng, K.M. and Wei, C. (2016) "Design of anaerobic fluidized bed bioreactor – Dyeing effluents". Chemical Engineering Science **139**(Supplement C), 273-284.

Deniz, F. and Karaman, S. (2011) "Removal of Basic Red 46 dye from aqueous solution by pine tree leaves". Chemical Engineering Journal **170**(1), 67-74.

Dhanasekaran, P., Satya Sai, P.M. and Gnanasekar, K.I. (2017) "Fixed bed adsorption of fluoride by *Artocarpus hirsutus* based adsorbent". Journal of Fluorine Chemistry **195**, 37-46.

Dill, H.G. (2016) "Kaolin: Soil, rock and ore: From the mineral to the magmatic, sedimentary and metamorphic environments". Earth-Science Reviews **161**(Supplement C), 16-129.

Ding, Z., Hu, X., Wan, Y., Wang, S. and Gao, B. (2016) "Removal of lead, copper, cadmium, zinc, and nickel from aqueous solutions by alkali-modified biochar: Batch and column tests". Journal of Industrial and Engineering Chemistry **33**(Supplement C), 239-245.

dos Santos, A.B., Cervantes, F.J. and van Lier, J.B. (2007) "Review paper on current technologies for decolourisation of textile wastewaters: Perspectives for anaerobic biotechnology". Bioresource Technology **98**(12), 2369-2385.

Dutta, B.K. (2007) Principles of mass transfer and separation processes, PHI Learning Pvt. Ltd.

El-Latif, M.M.A., Ibrahim, A.M. and El-Kady, M.F. (2010) " Adsorption equilibrium, kinetics and thermodynamics of methylene blue from aqueous solutions using biopolymer oak sawdust composite". J. Am. Sci. **6**(6), 267-283.

El-Sayed and Owes, G. (2011) "Removal of methylene blue and crystal violet from aqueous solutions by palm kernel fiber". Desalination **272**(1–3), 225-232.

El Messaoudi, N., El Khomri, M., Dbik, A., Bentahar, S., Lacherai, A. and Bakiz, B. (2016) "Biosorption of Congo red in a fixed-bed column from aqueous solution using jujube shell: Experimental and mathematical modeling". Journal of Environmental Chemical Engineering **4**(4, Part A), 3848-3855.

Eren, E. (2009) "Investigation of a basic dye removal from aqueous solution onto chemically modified Unye bentonite". Journal of Hazardous Materials **166**(1), 88-93.

Errais, E., Duplay, J., Elhabiri, M., Khodja, M., Ocampo, R., Baltenweck-Guyot, R. and Darragi, F. (2012) "Anionic RR120 dye adsorption onto raw clay: Surface properties and adsorption mechanism". Colloids and Surfaces A: Physicochemical and Engineering Aspects **403**(0), 69-78.

Ertugay, N. and Acar, F.N. (2017) "Removal of COD and color from Direct Blue 71 azo dye wastewater by Fenton's oxidation: Kinetic study". Arabian Journal of Chemistry **10**(Supplement 1), S1158-S1163.

Ezechi, E.H., Kutty, S.R.b.M., Malakahmad, A. and Isa, M.H. (2015) "Characterization and optimization of effluent dye removal using a new low cost adsorbent: Equilibrium, kinetics and thermodynamic study". Process Safety and Environmental Protection **98**, 16-32.

Fan, J., Hu, X., Xie, Z., Zhang, K. and Wang, J. (2012) "Photocatalytic degradation of azo dye by novel Bi-based photocatalyst Bi<sub>4</sub>TaO<sub>8</sub>I under visible-light irradiation". Chemical Engineering Journal **179**(0), 44-51.

Farooq, U., Khan, M.A., Athar, M. and Kozinski, J.A. (2011) "Effect of modification of environmentally friendly biosorbent wheat (*Triticum aestivum*) on the biosorptive removal of cadmium(II) ions from aqueous solution". Chemical Engineering Journal **171**(2), 400-410.

Fathy, N.A., Ahmed, S.A.S. and El-enin, R.M.M.A. (2012) "Effect of Activation Temperature on Textural and Adsorptive Properties for Activated Carbon Derived from Local Reed



Biomass: Removal of p-Nitrophenol". Environmental Research, Engineering and Management **59**(1).

Feng, N., Guo, X., Liang, S., Zhu, Y. and Liu, J. (2011) "Biosorption of heavy metals from aqueous solutions by chemically modified orange peel". Journal of Hazardous Materials **185**(1), 49-54.

Flett, D.S. (2004) "Cobalt-Nickel Separation in Hydrometallurgy: a Review". Chemistry for Sustainable Development **12**, 81-91.

Foo, K.Y. and Hameed, B.H. (2011a) "Microwave assisted preparation of activated carbon from pomelo skin for the removal of anionic and cationic dyes". Chemical Engineering Journal **173**(2), 385-390.

Foo, K.Y. and Hameed, B.H. (2011b) "Utilization of rice husks as a feedstock for preparation of activated carbon by microwave induced KOH and K<sub>2</sub>CO<sub>3</sub> activation". Bioresource Technology **102**(20), 9814-9817.

Foo, K.Y. and Hameed, B.H. (2011c) " Preparation of activated carbon from date stones by microwave induced chemical activation: Application for methylene blue adsorption". Chem. Eng. J **170**, 338-341.

Forgacs, E., Cserhádi, T. and Oros, G. (2004) "Removal of synthetic dyes from wastewaters: a review". Environment International **30**(7), 953-971.

Freundlich, H.M.F. (1906) " Ober dies adsorption in losungen". Z. Phys. Chem **57**, 385-470.

Fu, F. and Wang, Q. (2011) "Removal of heavy metal ions from wastewaters: A review". Journal of Environmental Management **92**(3), 407-418.

Fu, F., Wang, Q. and Tang, B. (2009) "Fenton and Fenton-like reaction followed by hydroxide precipitation in the removal of Ni(II) from NiEDTA wastewater: A comparative study". Chemical Engineering Journal **155**(3), 769-774.

Gao, M., Zeng, Z., Sun, B., Zou, H., Chen, J. and Shao, L. (2012) "Ozonation of azo dye Acid Red 14 in a microporous tube-in-tube microchannel reactor: Decolorization and mechanism". Chemosphere **89**(2), 190-197.

Ghaedi, M., Tavallali, H., Sharifi, M., Kokhdan, S.N. and Asghari, A. (2012) "Preparation of low cost activated carbon from Myrtus communis and pomegranate and their efficient

application for removal of Congo red from aqueous solution". Spectrochimica Acta Part A: Molecular and Biomolecular Spectroscopy **86**(0), 107-114.

Ghasemi, M., Keshtkar, A.R., Dabbagh, R. and Jaber Safdari, S. (2011) "Biosorption of uranium(VI) from aqueous solutions by Ca-pretreated *Cystoseira indica* alga: Breakthrough curves studies and modeling". Journal of Hazardous Materials **189**(1–2), 141-149.

Ghosh, A., Dastidar, M.G. and Sreekrishnan, T.R. (2016) "Recent Advances in Bioremediation of Heavy Metals and Metal Complex Dyes: Review". Journal of Environmental Engineering **142**(9), C4015003.

Gola, D., Dey, P., Bhattacharya, A., Mishra, A., Malik, A., Namburath, M. and Ahammad, S.Z. (2016) "Multiple heavy metal removal using an entomopathogenic fungi *Beauveria bassiana*". Bioresource Technology **218**(Supplement C), 388-396.

Goldhaber, S.B. (2003) "Trace element risk assessment: essentiality vs. toxicity". Regulatory Toxicology and Pharmacology **38**(2), 232-242.

Goswami, M. and Phukan, P. (2017) "Enhanced adsorption of cationic dyes using sulfonic acid modified activated carbon". Journal of Environmental Chemical Engineering **5**(4), 3508-3517.

Gupta, V. (2011) Surface charge features of kaolinite particles and their interactions, The University of Utah.

Gupta, V.K., Kumar, R., Nayak, A., Saleh, T.A. and Barakat, M.A. (2013) "Adsorptive removal of dyes from aqueous solution onto carbon nanotubes: A review". Advances in Colloid and Interface Science **193–194**(0), 24-34.

Gurten, I.I., Ozmak, M., Yagmur, E. and Aktas, Z. (2012) "Preparation and characterisation of activated carbon from waste tea using  $K_2CO_3$ ". Biomass and Bioenergy **37**(0), 73-81.

Gutha, Y., Munagapati, V.S., Naushad, M. and Abburi, K. (2015) "Removal of Ni(II) from aqueous solution by *Lycopersicon esculentum* (Tomato) leaf powder as a low-cost biosorbent". Desalination and Water Treatment **54**(1), 200-208.

Guyo, U. and Moyo, M. (2017) "Cowpea pod (*Vigna unguiculata*) biomass as a low-cost biosorbent for removal of Pb(II) ions from aqueous solution". Environmental Monitoring and Assessment **189**(2), 47.

Güzel, F., Saygılı, H., Akkaya Saygılı, G., Koyuncu, F. and Yılmaz, C. (2017) "Optimal oxidation with nitric acid of biochar derived from pyrolysis of weeds and its application in removal of hazardous dye methylene blue from aqueous solution". Journal of Cleaner Production **144**(Supplement C), 260-265.

Haddad, P.R. (2005) "ION EXCHANGE | Overview". Encyclopedia of Analytical Science (Second Edition) Editors-in-Chief: Paul, W., Alan, T. and Colin, P. (eds), pp. 440-446, Elsevier, Oxford.

Hameed, B.H. and Ahmad, A.A. (2009) "Batch adsorption of methylene blue from aqueous solution by garlic peel, an agricultural waste biomass". Journal of Hazardous Materials **164**(2-3), 870-875.

Hameed, B.H. and Daud, F.B.M. (2008) "Adsorption studies of basic dye on activated carbon derived from agricultural waste: Hevea brasiliensis seed coat". Chemical Engineering Journal **139**(1), 48-55.

Han, R., Ding, D., Xu, Y., Zou, W., Wang, Y., Li, Y. and Zou, L. (2008) "Use of rice husk for the adsorption of congo red from aqueous solution in column mode". Bioresource Technology **99**(8), 2938-2946.

Han, R., Wang, Y., Yu, W., Zou, W., Shi, J. and Liu, H. (2007) "Biosorption of methylene blue from aqueous solution by rice husk in a fixed-bed column". Journal of Hazardous Materials **141**(3), 713-718.

Hardy, B., Leifeld, J., Knicker, H., Dufey, J.E., Deforce, K. and Cornélis, J.-T. (2017) "Long term change in chemical properties of preindustrial charcoal particles aged in forest and agricultural temperate soil". Organic Geochemistry **107**, 33-45.

Harraz, F.A., Abdel-Salam, O.E., Mostafa, A.A., Mohamed, R.M. and Hanafy, M. (2013) "Rapid synthesis of titania–silica nanoparticles photocatalyst by a modified sol–gel method for cyanide degradation and heavy metals removal". Journal of Alloys and Compounds **551**(Supplement C), 1-7.

Hernández-Hernández, L.E., Bonilla-Petriciolet, A., Mendoza-Castillo, D.I. and Reynel-Ávila, H.E. (2017) "Antagonistic binary adsorption of heavy metals using stratified bone char columns". Journal of Molecular Liquids **241**, 334-346.

Hernández-Montoya, V., Pérez-Cruz, M.A., Mendoza-Castillo, D.I., Moreno-Virgen, M.R. and Bonilla-Petriciolet, A. (2013) "Competitive adsorption of dyes and heavy metals on zeolitic structures". Journal of Environmental Management **116**(0), 213-221.

Ho, Y.S. and McKay, G. (2000) "The kinetic of the sorption of divalent metal ions on to sphagnum moss peat". Water Research **34**, 735-742.

Hong, S., Wen, C., He, J., Gan, F. and Ho, Y.S. (2009) "Adsorption thermodynamics of Methylene Blue onto bentonite". Journal of Hazardous Materials **167**(1-3), 630-633.

Hor, K.Y., Chee, J.M.C., Chong, M.N., Jin, B., Saint, C., Poh, P.E. and Aryal, R. (2016) "Evaluation of physicochemical methods in enhancing the adsorption performance of natural zeolite as low-cost adsorbent of methylene blue dye from wastewater". Journal of Cleaner Production **118**(Supplement C), 197-209.

Hu, X., Ding, Z., Zimmerman, A.R., Wang, S. and Gao, B. (2015) "Batch and column sorption of arsenic onto iron-impregnated biochar synthesized through hydrolysis". Water Research **68**, 206-216.

Inyang, M., Gao, B., Ding, W., Pullammanappallil, P., Zimmerman, A.R. and Cao, X. (2011) "Enhanced lead sorption by biochar derived from anaerobically digested sugarcane bagasse". Separation Science and Technology **46**(12), 1950-1956.

Inyang, M., Gao, B., Yao, Y., Xue, Y., Zimmerman, A.R., Pullammanappallil, P. and Cao, X. (2012) "Removal of heavy metals from aqueous solution by biochars derived from anaerobically digested biomass". Bioresource Technology **110**, 50-56.

Jha, B., Basha, S., Jaiswar, S., Mishra, B. and Thakur, M.C. (2008) "Biosorption of Cd(II) and Pb(II) onto brown seaweed, *Lobophora variegata* (Lamouroux): kinetic and equilibrium studies". Biodegradation **20**(1), 1.

Jiang, C., Gao, Z., Qu, H., Li, J., Wang, X., Li, P. and Liu, H. (2013) "A new insight into Fenton and Fenton-like processes for water treatment: Part II. Influence of organic compounds on Fe(III)/Fe(II) interconversion and the course of reactions". Journal of Hazardous Materials **250–251**(0), 76-81.

Joh, D. and Mbadcam, J.K. (2015) "Adsorption of Zinc (II) ions from aqueous solution onto kaolinite and metakaolinite". Der. Pharm. Chem. **7**, 51-58.

Johari, K., Saman, N., Song, S.T., Cheu, S.C., Kong, H. and Mat, H. (2016) "Development of coconut pith chars towards high elemental mercury adsorption performance – Effect of pyrolysis temperatures". Chemosphere **156**, 56-68.

Junghanns, C., Krauss, G. and Schlosser, D. (2008) "Potential of aquatic fungi derived from diverse freshwater environments to decolourise synthetic azo and anthraquinone dyes". Bioresource Technology **99**(5), 1225-1235.

Kara, İ., Yilmazer, D. and Akar, S.T. (2017) "Metakaolin based geopolymer as an effective adsorbent for adsorption of zinc(II) and nickel(II) ions from aqueous solutions". Applied Clay Science **139**, 54-63.

Kaur, S., Rani, S. and Mahajan, R.K. (2013) " Adsorption Kinetics for the Removal of Hazardous Dye Congo Red by Biowaste Materials as Adsorbents". Journal of Chemistry **2013**, 12.

Khalid, K., Ngah, W.S., Hanafiah, M.A., Malek, N.S. and Khazaai, S.N. (2015) "Acid Blue 25 Adsorption onto Phosphoric Acid Treated Rubber Leaf Powder". American Journal of Environmental Engineering **5**(3A), 19-25.

Khan, S. and Malik, A. (2014) "Environmental and Health Effects of Textile Industry Wastewater". *Environmental Deterioration and Human Health: Natural and anthropogenic determinants* Malik, A., Grohmann, E. and Akhtar, R. (eds), pp. 55-71, Springer Netherlands, Dordrecht.

Khan, T.A., Khan, E.A. and Shahjahan (2015) "Removal of basic dyes from aqueous solution by adsorption onto binary iron-manganese oxide coated kaolinite: Non-linear isotherm and kinetics modeling". Applied Clay Science **107**(Supplement C), 70-77.

Khouni, I., Marrot, B. and Amar, R.B. (2012) "Treatment of reconstituted textile wastewater containing a reactive dye in an aerobic sequencing batch reactor using a novel bacterial consortium". Separation and Purification Technology **87**(0), 110-119.

Kılıç, M., Kırbıyık, Ç., Çepelioğullar, Ö. and Pütün, A.E. (2013) "Adsorption of heavy metal ions from aqueous solutions by bio-char, a by-product of pyrolysis". Applied Surface Science **283**, 856-862.

Kırbıyık, Ç., Pütün, A.E. and Pütün, E. (2016) "Comparative studies on adsorptive removal of heavy metal ions by biosorbent, bio-char and activated carbon obtained from low cost agro-residue". Water Science and Technology **73**(2), 423-436.

Koçer, O. and Acemioğlu, B. (2016) "Adsorption of Basic green 4 from aqueous solution by olive pomace and commercial activated carbon: process design, isotherm, kinetic and thermodynamic studies". Desalination and Water Treatment **57**(35), 16653-16669.

Kołodzyńska, D., Krukowska-Bąk, J., Kazmierczak-Razna, J. and Pietrzak, R. (2017a) "Uptake of heavy metal ions from aqueous solutions by sorbents obtained from the spent ion exchange resins". Microporous and Mesoporous Materials **244**(Supplement C), 127-136.

Kołodzyńska, D., Krukowska, J. and Thomas, P. (2017b) "Comparison of sorption and desorption studies of heavy metal ions from biochar and commercial active carbon". Chemical Engineering Journal **307**(Supplement C), 353-363.

Konicki, W., Sibera, D., Mijowska, E., Lendzion-Bieluń, Z. and Narkiewicz, U. (2013) "Equilibrium and kinetic studies on acid dye Acid Red 88 adsorption by magnetic ZnFe<sub>2</sub>O<sub>4</sub> spinel ferrite nanoparticles". Journal of Colloid and Interface Science **398**, 152-160.

Körbahti, B.K., Artut, K., Geçgel, C. and Özer, A. (2011) "Electrochemical decolorization of textile dyes and removal of metal ions from textile dye and metal ion binary mixtures". Chemical Engineering Journal **173**(3), 677-688.

Krishna, L.S., Yuzir, A., Yuvaraja, G. and Ashokkumar, V. (2017) "Removal of Acid Blue25 from aqueous solutions using Bengal gram fruit shell (BGFS) biomass". International Journal of Phytoremediation **19**(5), 431-438.

Krishnan, K.A., Sreejalekshmi, K., Vimexen, V. and Dev, V.V. (2016) "Evaluation of adsorption properties of sulphurised activated carbon for the effective and economically viable removal of Zn (II) from aqueous solutions". Ecotoxicology and environmental safety **124**, 418-425.

Kumar, A. and Jena, H.M. (2016) "Removal of methylene blue and phenol onto prepared activated carbon from Fox nutshell by chemical activation in batch and fixed-bed column". Journal of Cleaner Production **137**, 1246-1259.

Kyzas, G.Z., Deliyanni, E.A. and Lazaridis, N.K. (2014) "Magnetic modification of microporous carbon for dye adsorption". Journal of Colloid and Interface Science **430**(Supplement C), 166-173.

Labanda, J., Sabaté, J. and Llorens, J. (2009) "Modeling of the dynamic adsorption of an anionic dye through ion-exchange membrane adsorber". Journal of Membrane Science **340**(1–2), 234-240.

Lafi, R., Fradj, A., Hafiane, A. and Hameed, B.H. (2014) "Coffee waste as potential adsorbent for the removal of basic dyes from aqueous solution". Korean Journal of Chemical Engineering, 1-9.

Lagergren, S. (1898) " Zur theorie der sogenannten adsorption gelöster stoffe. Kungliga Sevenska Vetenskapakademiens". Handlingar **24**, 1-39.

Lago, A., Rocha, V., Silva, B. and Tavares, T. (2017) "Modified low cost adsorbent (cedar) for the removal of Pb (II), Ni (II) and Zn (II) from aqueous solutions".

Lakshmi, U.R., Srivastava, V.C., Mall, I.D. and Lataye, D.H. (2009) "Rice husk ash as an effective adsorbent: Evaluation of adsorptive characteristics for Indigo Carmine dye". Journal of Environmental Management **90**(2), 710-720.

Langmuir, I. (1916) "The constitution and fundamental properties of solids and liquids. Part I. Solids". The Journal of the American Chemical Society **38**(2), 2221-2295.

Lee, K.M., Lai, C.W., Ngai, K.S. and Juan, J.C. (2016a) "Recent developments of zinc oxide based photocatalyst in water treatment technology: A review". Water Research **88**, 428-448.

Lee, L.Y., Gan, S., Yin Tan, M.S., Lim, S.S., Lee, X.J. and Lam, Y.F. (2016b) "Effective removal of Acid Blue 113 dye using overripe Cucumis sativus peel as an eco-friendly biosorbent from agricultural residue". Journal of Cleaner Production **113**(Supplement C), 194-203.

Leyh, R.G., Kofidis, T., Struber, M., Fischer, S., Knobloch, K., Wachsmann, B., Hagl, C., Simon, A.R. and Haverich, A. (2003) "Methylene blue: the drug of choice for catecholamine-refractory vasoplegia after cardiopulmonary bypass?". J Thorac Cardiovasc Surg **125**(6), 1426-1431.

Li, T., Hu, X., Liu, C., Tang, C., Wang, X. and Luo, S. (2016a) "Efficient photocatalytic degradation of organic dyes and reaction mechanism with Ag<sub>2</sub>CO<sub>3</sub>/Bi<sub>2</sub>O<sub>2</sub>CO<sub>3</sub> photocatalyst under visible light irradiation". Journal of Molecular Catalysis A: Chemical **425**, 124-135.

Li, W.-H., Yue, Q.-Y., Gao, B.-Y., Ma, Z.-H., Li, Y.-J. and Zhao, H.-X. (2011a) "Preparation and utilization of sludge-based activated carbon for the adsorption of dyes from aqueous solutions". Chemical Engineering Journal **171**(1), 320-327.

Li, W., Yue, Q., Tu, P., Ma, Z., Gao, B., Li, J. and Xu, X. (2011b) "Adsorption characteristics of dyes in columns of activated carbon prepared from paper mill sewage sludge". Chemical Engineering Journal **178**, 197-203.

Li, Y., Meas, A., Shan, S., Yang, R. and Gai, X. (2016b) "Production and optimization of bamboo hydrochars for adsorption of Congo red and 2-naphthol". Bioresource Technology **207**(Supplement C), 379-386.

Liao, P., Malik Ismael, Z., Zhang, W., Yuan, S., Tong, M., Wang, K. and Bao, J. (2012) "Adsorption of dyes from aqueous solutions by microwave modified bamboo charcoal". Chemical Engineering Journal **195–196**, 339-346.

Liu, D., Yuan, W., Yuan, P., Yu, W., Tan, D., Liu, H. and He, H. (2013) "Physical activation of diatomite-templated carbons and its effect on the adsorption of methylene blue (MB)". Applied Surface Science (0).

Liu, S.-H., Zeng, G.-M., Niu, Q.-Y., Liu, Y., Zhou, L., Jiang, L.-H., Tan, X.-f., Xu, P., Zhang, C. and Cheng, M. (2017a) "Bioremediation mechanisms of combined pollution of PAHs and heavy metals by bacteria and fungi: A mini review". Bioresource Technology **224**(Supplement C), 25-33.

Liu, T., Han, X., Wang, Y., Yan, L., Du, B., Wei, Q. and Wei, D. (2017b) "Magnetic chitosan/anaerobic granular sludge composite: Synthesis, characterization and application in heavy metal ions removal". Journal of Colloid and Interface Science **508**, 405-414.

Liu, X., Sun, J., Duan, S., Wang, Y., Hayat, T., Alsaedi, A., Wang, C. and Li, J. (2017c) "A Valuable Biochar from Poplar Catkins with High Adsorption Capacity for Both Organic Pollutants and Inorganic Heavy Metal Ions". Scientific Reports **7**(1), 10033.



- Magdy, A., Fouad, Y.O., Abdel-Aziz, M.H. and Konsowa, A.H. (2017) "Synthesis and characterization of Fe<sub>3</sub>O<sub>4</sub>/kaolin magnetic nanocomposite and its application in wastewater treatment". Journal of Industrial and Engineering Chemistry **56**(Supplement C), 299-311.
- Mahmoodi, N.M., Hayati, B., Arami, M. and Lan, C. (2011) "Adsorption of textile dyes on Pine Cone from colored wastewater: Kinetic, equilibrium and thermodynamic studies ". Desalination **268**(1-3), 117-125.
- Mahmoud, D.K., Salleh, M.A.M., Karim, W.A.W.A., Idris, A. and Abidin, Z.Z. (2012) "Batch adsorption of basic dye using acid treated kenaf fibre char: Equilibrium, kinetic and thermodynamic studies". Chemical Engineering Journal **181–182**(0), 449-457.
- Mane, V.S. and Babu, P.V.V. (2011) "Studies on the adsorption of Brilliant Green dye from aqueous solution onto low-cost NaOH treated saw dust". Desalination **273**(2), 321-329.
- Mane, V.S. and Vijay Babu, P.V. (2013) "Kinetic and equilibrium studies on the removal of Congo red from aqueous solution using Eucalyptus wood (*Eucalyptus globulus*) saw dust". Journal of the Taiwan Institute of Chemical Engineers **44**(1), 81-88.
- Maneerung, T., Liew, J., Dai, Y., Kawi, S., Chong, C. and Wang, C.-H. (2016) "Activated carbon derived from carbon residue from biomass gasification and its application for dye adsorption: Kinetics, isotherms and thermodynamic studies". Bioresource Technology **200**, 350-359.
- Marrakchi, F., Ahmed, M.J., Khanday, W.A., Asif, M. and Hameed, B.H. (2017) "Mesoporous-activated carbon prepared from chitosan flakes via single-step sodium hydroxide activation for the adsorption of methylene blue". International Journal of Biological Macromolecules **98**, 233-239.
- Matilainen, A., Vepsäläinen, M. and Sillanpää, M. (2010) "Natural organic matter removal by coagulation during drinking water treatment: A review". Advances in Colloid and Interface Science **159**(2), 189-197.
- Merzouk, B., Gourich, B., Madani, K., Vial, C. and Sekki, A. (2011) "Removal of a disperse red dye from synthetic wastewater by chemical coagulation and continuous electrocoagulation. A comparative study". Desalination **272**(1–3), 246-253.

- Mikhailov, I., Komarov, S., Levina, V., Gusev, A., Issi, J.-P. and Kuznetsov, D. (2017) "Nanosized zero-valent iron as Fenton-like reagent for ultrasonic-assisted leaching of zinc from blast furnace sludge". Journal of Hazardous Materials **321**(Supplement C), 557-565.
- Mishra, A. and Malik, A. (2014) "Novel fungal consortium for bioremediation of metals and dyes from mixed waste stream". Bioresource Technology **171**(Supplement C), 217-226.
- Momčilović, M., Purenović, M., Bojić, A., Zarubica, A. and Ranđelović, M. (2011) "Removal of lead(II) ions from aqueous solutions by adsorption onto pine cone activated carbon". Desalination **276**(1), 53-59.
- Muneeb Ur Rahman Khattak, M., Zahoor, M., Muhammad, B., Khan, F.A., Ullah, R. and AbdEI-Salam, N.M. (2017) "Removal of Heavy Metals from Drinking Water by Magnetic Carbon Nanostructures Prepared from Biomass". Journal of Nanomaterials **2017**.
- Nandi, B.K., Goswami, A. and Purkait, M.K. (2009) "Adsorption characteristics of brilliant green dye on kaolin". Journal of Hazardous Materials **161**(1), 387-395.
- Nandi, B.K., Uppaluri, R. and Purkait, M.K. (2008) "Preparation and characterization of low cost ceramic membranes for micro-filtration applications". Applied Clay Science **42**(1-2), 102-110.
- Nasuha, N., Zurainan, H.Z., Maarof, H.I., Zubir, N.A. and Amri, N. (2011) Effect of cationic and anionic dye adsorption from aqueous solution by using chemically modified papaya seed, pp. 50-54.
- Nautiyal, P., Subramanian, K.A. and Dastidar, M.G. (2016) "Adsorptive removal of dye using biochar derived from residual algae after in-situ transesterification: Alternate use of waste of biodiesel industry". Journal of Environmental Management **182**(Supplement C), 187-197.
- Nawaz, S., Bhatti, H.N., Bokhari, T.H. and Sadaf, S. (2014) "Removal of Novacron Golden Yellow dye from aqueous solutions by low-cost agricultural waste: Batch and fixed bed study". Chemistry and Ecology **30**(1), 52-65.
- Nomura, S., Nishioka, H. and Sen, T.K. (2017) "Synthesis and Arsenic Adsorptive Characteristics of a Novel Magnetic Adsorbent". Journal of Environmental Conservation Engineering **46**(3), 35-42.

- Okoli, C.P., Diagboya, P.N., Anigbogu, I.O., Olu-Owolabi, B.I. and Adebowale, K.O. (2016) "Competitive biosorption of Pb(II) and Cd(II) ions from aqueous solutions using chemically modified moss biomass (*Barbula lambarenensis*)". *Environmental Earth Sciences* **76**(1), 33.
- Omorogie, M.O., Babalola, J.O., Unuabonah, E.I., Song, W. and Gong, J.R. (2016) "Efficient chromium abstraction from aqueous solution using a low-cost biosorbent: *Nauclea diderrichii* seed biomass waste". *Journal of Saudi Chemical Society* **20**(1), 49-57.
- Önal, E., Özbay, N., Yargıç, A.Ş., Şahin, R.Z.Y. and Gök, Ö. (2014) "Performance Evaluation of the Bio-char Heavy Metal Removal Produced from Tomato Factory Waste". *Progress in Exergy, Energy, and the Environment*, pp. 733-740, Springer.
- Özbay, İ., Özdemir, U., Özbay, B. and Veli, S. (2013) "Kinetic, thermodynamic, and equilibrium studies for adsorption of azo reactive dye onto a novel waste adsorbent: charcoal ash". *Desalination and Water Treatment* **51**(31-33), 6091-6100.
- Padhi, B. (2012) "Pollution due to synthetic dyes toxicity & carcinogenicity studies and remediation". *International Journal of Environmental Sciences* **3**(3), 940.
- Paduraru, C., Tofan, L., Teodosiu, C., Bunia, I., Tudorachi, N. and Toma, O. (2015) "Biosorption of zinc (II) on rapeseed waste: equilibrium studies and thermogravimetric investigations". *Process Safety and Environmental Protection* **94**, 18-28.
- Pal, S., Patra, A.S., Ghorai, S., Sarkar, A.K., Mahato, V., Sarkar, S. and Singh, R.P. (2015) "Efficient and rapid adsorption characteristics of templating modified guar gum and silica nanocomposite toward removal of toxic reactive blue and Congo red dyes". *Bioresource Technology* **191**(Supplement C), 291-299.
- Pang, Y.L. and Abdullah, A.Z. (2013) "Current Status of Textile Industry Wastewater Management and Research Progress in Malaysia: A Review". *CLEAN – Soil, Air, Water*
- Peng, X., Huang, D., Odoom-Wubah, T., Fu, D., Huang, J. and Qin, Q. (2014) "Adsorption of anionic and cationic dyes on ferromagnetic ordered mesoporous carbon from aqueous solution: Equilibrium, thermodynamic and kinetics". *Journal of Colloid and Interface Science* **430**(Supplement C), 272-282.
- Phalakornkule, C., Polgumhang, S., Tongdaung, W., Karakat, B. and Nuyut, T. (2010) "Electrocoagulation of blue reactive, red disperse and mixed dyes, and application in treating textile effluent". *Journal of Environmental Management* **91**(4), 918-926.

Priyadharsan, A., Vasanthakumar, V., Karthikeyan, S., Raj, V., Shanavas, S. and Anbarasan, P.M. (2017) "Multi-functional properties of ternary CeO<sub>2</sub>/SnO<sub>2</sub>/rGO nanocomposites: Visible light driven photocatalyst and heavy metal removal". Journal of Photochemistry and Photobiology A: Chemistry **346**(Supplement C), 32-45.

Purkait, M.K., Maiti, A., DasGupta, S. and De, S. (2007) "Removal of congo red using activated carbon and its regeneration". Journal of Hazardous Materials **145**(1–2), 287-295.

Putra, W.P., Kamari, A., Yusoff, S.N.M., Ishak, C.F., Mohamed, A., Hashim, N. and Isa, I.M. (2014) "Biosorption of Cu (II), Pb (II) and Zn (II) ions from aqueous solutions using selected waste materials: Adsorption and characterisation studies". Journal of Encapsulation and Adsorption Sciences **4**(01), 25.

Qu, Y., Cao, X., Ma, Q., Shi, S., Tan, L., Li, X., Zhou, H., Zhang, X. and Zhou, J. (2012) "Aerobic decolorization and degradation of Acid Red B by a newly isolated *Pichia* sp. TCL". Journal of Hazardous Materials **223-224**, 31-38.

Quan, X., Luo, D., Wu, J., Li, R., Cheng, W. and Ge, s. (2017) "Ozonation of acid red 18 wastewater using O<sub>3</sub>/Ca(OH)<sub>2</sub> system in a micro bubble gas-liquid reactor". Journal of Environmental Chemical Engineering **5**(1), 283-291.

Ragupathy, S., Raghu, K. and Prabu, P. (2015) "Synthesis and characterization of TiO<sub>2</sub> loaded cashew nut shell activated carbon and photocatalytic activity on BG and MB dyes under sunlight radiation". Spectrochimica Acta Part A: Molecular and Biomolecular Spectroscopy **138**, 314-320.

Ribas, M.C., Adebayo, M.A., Prola, L.D.T., Lima, E.C., Cataluña, R., Feris, L.A., Puchana-Rosero, M.J., Machado, F.M., Pavan, F.A. and Calvete, T. (2014) "Comparison of a homemade cocoa shell activated carbon with commercial activated carbon for the removal of reactive violet 5 dye from aqueous solutions". Chemical Engineering Journal **248**(0), 315-326.

Rida, K., Bouraoui, S. and Hadnine, S. (2013a) "Adsorption of methylene blue from aqueous solution by kaolin and zeolite". Applied Clay Science **83-84**(Supplement C), 99-105.

Rida, K., Bouraoui, S. and Hadnine, S. (2013b) "Adsorption of methylene blue from aqueous solution by kaolin and zeolite". Applied Clay Science **83-84**, 99-105.

Robinson, T., McMullan, G., Marchant, R. and Nigam, P. (2001) "Remediation of dyes in textile effluent: a critical review on current treatment technologies with a proposed alternative". Bioresource Technology **77**(3), 247-255.

Roohani, N., Hurrell, R., Kelishadi, R. and Schulin, R. (2013) "Zinc and its importance for human health: An integrative review". Journal of Research in Medical Sciences : The Official Journal of Isfahan University of Medical Sciences **18**(2), 144-157.

Sadaf, S. and Bhatti, H.N. (2014) "Evaluation of peanut husk as a novel, low cost biosorbent for the removal of Indosol Orange RSN dye from aqueous solutions: batch and fixed bed studies". Clean Technologies and Environmental Policy **16**(3), 527-544.

Sadaf, S., Bhatti, H.N., Ali, S. and Rehman, K.-u. (2014) "Removal of Indosol Turquoise FBL dye from aqueous solution by bagasse, a low cost agricultural waste: batch and column study". Desalination and Water Treatment **52**(1-3), 184-198.

Saeed, A., Sharif, M. and Iqbal, M. (2010) "Application potential of grapefruit peel as dye sorbent: Kinetics, equilibrium and mechanism of crystal violet adsorption". Journal of Hazardous Materials **179**(1), 564-572.

Safarik, I., Ashoura, N., Maderova, Z., POSOIKOVA, K., Baldikova, E. and Safarikova, M. (2016) "Magnetically modified Posidonia oceanica biomass as an adsorbent for organic dyes removal". Mediterranean Marine Science **17**(2), 351-358.

Said, A.E.-A.A., Aly, A.A.M., Goda, M.N., Abd El-Aal, M. and Abdelazim, M. (2017) "Modified Sugarcane Bagasse with Tartaric Acid for Removal of Diazonium Blue from Aqueous Solutions". Journal of Polymers and the Environment.

Saif Ur Rehman, M., Kim, I., Rashid, N., Adeel Umer, M., Sajid, M. and Han, J.I. (2016) "Adsorption of Brilliant Green dye on biochar prepared from lignocellulosic bioethanol plant waste". CLEAN–Soil, Air, Water **44**(1), 55-62.

Sajab, M.S., Chia, C.H., Zakaria, S., Jani, S.M., Ayob, M.K., Chee, K.L., Khiew, P.S. and Chiu, W.S. (2011) "Citric acid modified kenaf core fibres for removal of methylene blue from aqueous solution". Bioresource Technology **102**(15), 7237-7243.

Salleh, M.A.M., Mahmoud, D.K., Karim, W.A. and Idris, A. (2011) "Cationic and anionic dye adsorption by agricultural solid wastes: a comprehensive review". Desalination **280**(1-3), 1-13.

Samanta, A.K. and Konar, A. (2011) "Dyeing of textiles with natural dyes". Natural dyes, InTech.

San Keskin, N.O., Celebioglu, A., Sarioglu, O.F., Uyar, T. and Tekinay, T. (2018) "Encapsulation of living bacteria in electrospun cyclodextrin ultrathin fibers for bioremediation of heavy metals and reactive dye from wastewater". Colloids and Surfaces B: Biointerfaces **161**(Supplement C), 169-176.

Sangi, M.R., Shahmoradi, A., Zolgharnein, J., Azimi, G.H. and Ghorbandoost, M. (2008) "Removal and recovery of heavy metals from aqueous solution using *Ulmus carpinifolia* and *Fraxinus excelsior* tree leaves". Journal of Hazardous Materials **155**(3), 513-522.

Sarma, G.K., Sen Gupta, S. and Bhattacharyya, K.G. (2016) "Adsorption of Crystal violet on raw and acid-treated montmorillonite, K10, in aqueous suspension". Journal of Environmental Management **171**, 1-10.

Saruchi and Kumar, V. (2016) "Adsorption kinetics and isotherms for the removal of rhodamine B dye and Pb<sup>+2</sup> ions from aqueous solutions by a hybrid ion-exchanger". Arabian Journal of Chemistry.

Sen, T.K., Afroze, S. and Ang, H.M. (2011) "Equilibrium, kinetics and mechanism of removal of methylene blue from aqueous solution by adsorption onto pine cone biomass of *Pinus radiata*". Water Air Soil Pollut **218**, 499-515.

Sen, T.K., Thi, M.T., Afroze, S., Phan, C. and Ang, M. (2012) "Removal of anionic surfactant sodium dodecyl sulphate from aqueous solution by adsorption onto pine cone biomass of *Pinus Radiata*: equilibrium, thermodynamic, kinetics, mechanism and process design". Desalination and Water Treatment **45**(1-3), 263-275.

Senthil Kumar, P., Palaniyappan, M., Priyadharshini, M., Vignesh, A.M., Thanjiappan, A., Sebastina Anne Fernando, P., Tanvir Ahmed, R. and Srinath, R. (2014) "Adsorption of basic dye onto raw and surface-modified agricultural waste". Environmental Progress & Sustainable Energy **33**(1), 87-98.

Senthil Kumar, P., Ramalingam, S., Abhinaya, R.V., Kirupha, S.D., Murugesan, A. and Sivanesan, S. (2012) "Adsorption of metal ions onto the chemically modified agricultural waste". CLEAN-Soil, Air, Water **40**(2), 188-197.

Sewu, D.D., Boakye, P., Jung, H. and Woo, S.H. (2017a) "Synergistic dye adsorption by biochar from co-pyrolysis of spent mushroom substrate and *Saccharina japonica*". Bioresource Technology **244**(Part 1), 1142-1149.

Sewu, D.D., Boakye, P. and Woo, S.H. (2017b) "Highly efficient adsorption of cationic dye by biochar produced with Korean cabbage waste". Bioresource Technology **224**, 206-213.

Shaban, M., Abukhadra, M.R., Shahien, M. and Ibrahim, S.S. (2017) "Novel bentonite/zeolite-NaP composite efficiently removes methylene blue and Congo red dyes". Environmental Chemistry Letters, 1-6.

Shahid, M., Shahid ul, I. and Mohammad, F. (2013) "Recent advancements in natural dye applications: a review". Journal of Cleaner Production **53**(0), 310-331.

Shak, A., Dawood, S. and Sen, T.K. (2017) "Performance and dynamic modelling of mixed biomass-kaolin packed bed adsorption column for the removal of aqueous phase methylene blue (MB) dye". Desalination and Water Treatment **82**, 67-80.

Shakoor, S. and Nasar, A. (2016) "Removal of methylene blue dye from artificially contaminated water using citrus limetta peel waste as a very low cost adsorbent". Journal of the Taiwan Institute of Chemical Engineers **66**, 154-163.

Sharma, S., Buddhdev, J., Patel, M. and Ruparelia, J.P. (2013) "Studies on Degradation of Reactive Red 135 Dye in Wastewater using Ozone". Procedia Engineering **51**(0), 451-455.

Sheshdeh, R.K., Nikou, M.R.K., Badii, K., Limaee, N.Y. and Golkarnarenji, G. (2014) "Equilibrium and kinetics studies for the adsorption of Basic Red 46 on nickel oxide nanoparticles-modified diatomite in aqueous solutions". Journal of the Taiwan Institute of Chemical Engineers **45**(4), 1792-1802.

Shi, Q., Zhang, J., Zhang, C., Li, C., Zhang, B., Hu, W., Xu, J. and Zhao, R. (2010) "Preparation of activated carbon from cattail and its application for dyes removal". Journal of Environmental Sciences **22**(1), 91-97.

Shi, X., Leong, K.Y. and Ng, H.Y. (2017) "Anaerobic treatment of pharmaceutical wastewater: A critical review". Bioresource Technology **245**(Part A), 1238-1244.

Singha, A.S. and Guleria, A. (2015) "Utility of chemically modified agricultural waste okra biomass for removal of toxic heavy metal ions from aqueous solution". Engineering in Agriculture, Environment and Food **8**(1), 52-60.

Slejko, F.L. (1985) Adsorption technology: A step-by-step approach to process evaluation and application Tall Oaks Publishing, Inc.

Sočo, E. and Kalembkiewicz, J. (2013) "Adsorption of nickel(II) and copper(II) ions from aqueous solution by coal fly ash". Journal of Environmental Chemical Engineering **1**(3), 581-588.

Sousa, F.W., Oliveira, A.G., Ribeiro, J.P., Rosa, M.F., Keukeleire, D. and Nascimento, R.F. (2010) "Green coconut shells applied as adsorbent for removal of toxic metal ions using fixed-bed column technology". Journal of Environmental Management **91**(8), 1634-1640.

Sreelatha, G., Ageetha, V., Parmar, J. and Padmaja, P. (2011) "Equilibrium and kinetic studies on reactive dye adsorption using palm shell powder and chitosan". J. Chem. Eng. Data **56**, 35-42.

Sreńscek-Nazzal, J., Narkiewicz, U., Morawski, A.W., Wróbel, R.J. and Michalkiewicz, B. (2016) "The Increase of the Microporosity and CO<sub>2</sub> Adsorption Capacity of the Commercial Activated Carbon CWZ-22 by KOH Treatment". *Microporous and Mesoporous Materials* Dariani, R.S. (ed), p. Ch. 01, InTech, Rijeka.

Stavropoulos, G.G., Skodras, G.S. and Papadimitriou, K.G. (2015) "Effect of solution chemistry on cyanide adsorption in activated carbon". Applied Thermal Engineering **74**(Supplement C), 182-185.

Su, C.-C., Pukdee-Asa, M., Ratanatamskul, C. and Lu, M.-C. (2011) "Effect of operating parameters on decolorization and COD removal of three reactive dyes by Fenton's reagent using fluidized-bed reactor". Desalination **278**(1-3), 211-218.

Suhas, V., Carrott, P., Singh, R., Chaudhary, M. and Kushwaha, S. (2016) "Cellulose: A review as natural, modified and activated carbon adsorbent: biomass, bioenergy, biowastes, conversion technologies, biotransformations, production technologies". Bioresource Technology **216**, 1066-1076.



Suksabye, P. and Thiravetyan, P. (2012) "Cr(VI) adsorption from electroplating plating wastewater by chemically modified coir pith". Journal of Environmental Management **102**(Supplement C), 1-8.

Talaiekhosani, A. and Rezania, S. (2017) "Application of photosynthetic bacteria for removal of heavy metals, macro-pollutants and dye from wastewater: A review". Journal of Water Process Engineering **19**(Supplement C), 312-321.

Tan, L., Ning, S., Zhang, X. and Shi, S. (2013) "Aerobic decolorization and degradation of azo dyes by growing cells of a newly isolated yeast *Candida tropicalis* TL-F1". Bioresource Technology **138**(0), 307-313.

Tanyildizi, M.Ş. (2011) "Modeling of adsorption isotherms and kinetics of reactive dye from aqueous solution by peanut hull". Chemical Engineering Journal **168**(3), 1234-1240.

Tchounwou, P.B., Yedjou, C.G., Patlolla, A.K. and Sutton, D.J. (2012) "Heavy Metals Toxicity and the Environment". EXS **101**, 133-164.

Thomas, H.C. (1944) "Heterogeneous ion exchange in a flowing system". Journal of the American Chemical Society **66**(10), 1664-1666.

Tony, B.D., Goyal, D. and Khanna, S. (2009) "Decolorization of textile azo dyes by aerobic bacterial consortium". International Biodeterioration & Biodegradation **63**(4), 462-469.

Tran, H.N., You, S.-J. and Chao, H.-P. (2016) "Thermodynamic parameters of cadmium adsorption onto orange peel calculated from various methods: A comparison study". Journal of Environmental Chemical Engineering **4**(3), 2671-2682.

Tran, H.N., You, S.-J., Hosseini-Bandegharai, A. and Chao, H.-P. (2017) "Mistakes and inconsistencies regarding adsorption of contaminants from aqueous solutions: A critical review". Water Research **120**(Supplement C), 88-116.

Turhan, K., Durukan, I., Ozturkcan, S.A. and Turgut, Z. (2012) "Decolorization of textile basic dye in aqueous solution by ozone". Dyes and Pigments **92**(3), 897-901.

Uçar, S., Erdem, M., Tay, T. and Karagöz, S. (2015) "Removal of lead (II) and nickel (II) ions from aqueous solution using activated carbon prepared from rapeseed oil cake by Na<sub>2</sub>CO<sub>3</sub> activation". Clean Technologies and Environmental Policy **17**(3), 747-756.

Uddin, M.T., Rahman, M.A., Rukanuzzaman, M. and Islam, M.A. (2017) "A potential low cost adsorbent for the removal of cationic dyes from aqueous solutions". Applied Water Science **7**(6), 2831-2842.

Uğurlu, M., Gürses, A. and Açıkyıldız, M. (2008) "Comparison of textile dyeing effluent adsorption on commercial activated carbon and activated carbon prepared from olive stone by ZnCl<sub>2</sub> activation". Microporous and Mesoporous Materials **111**(1–3), 228-235.

Vağzoğullar, A.Ğ., Uğurlu, M. and Kula, Ğ. (2015) "Comparing adsorption activity of raw Sepiolite and CTAB modified Sepiolite: kinetic and adsorption study for removal of Hg<sup>+</sup>". International Journal of Environment **4**(4), 19-31.

Vasudevan, S., Lakshmi, J. and Vanathi, R. (2010) "Electrochemical Coagulation for Chromium Removal: Process Optimization, Kinetics, Isotherms and Sludge Characterization". CLEAN – Soil, Air, Water **38**(1), 9-16.

Vasudevan, S. and Oturan, M.A. (2014) "Electrochemistry: as cause and cure in water pollution—an overview". Environmental Chemistry Letters **12**(1), 97-108.

Velho, S.R.K., Brum, L.F.W., Petter, C.O., dos Santos, J.H.Z., Šimunić, Š. and Kappa, W.H. (2017) "Development of structured natural dyes for use into plastics". Dyes and Pigments **136**, 248-254.

Venkatesh, S., Venkatesh, K. and Quaff, A.R. (2017) "Dye decomposition by combined ozonation and anaerobic treatment: Cost effective technology". Journal of Applied Research and Technology **15**(4), 340-345.

Vidal, J., Villegas, L., Peralta-Hernández, J.M. and Salazar González, R. (2016) "Removal of Acid Black 194 dye from water by electrocoagulation with aluminum anode". Journal of Environmental Science and Health, Part A **51**(4), 289-296.

Vieira, M.L.G., Esquerdo, V.M., Nobre, L.R., Dotto, G.L. and Pinto, L.A.A. (2014) "Glass beads coated with chitosan for the food azo dyes adsorption in a fixed bed column". Journal of Industrial and Engineering Chemistry **20**(5), 3387-3393.

Vijayaraghavan, K., Premkumar, Y. and Jegan, J. (2016) "Malachite green and crystal violet biosorption onto coco-peat: characterization and removal studies". Desalination and Water Treatment **57**(14), 6423-6431.

Vilvanathan, S. and Shanthakumar, S. (2017) "Column adsorption studies on nickel and cobalt removal from aqueous solution using native and biochar form of *Tectona grandis*". Environmental Progress & Sustainable Energy.

Weber, J. and Morriss, J.C. (1963) " Kinetics of adsorption on carbon from solution.". J. Saint. Eng. Div. Am. Soc. Civ. Eng **89**, 31-60.

Woiseschläger, D., Humpl, B., Koncar, M. and Siebenhofer, M. (2013) "Electrochemical oxidation of wastewater – opportunities and drawbacks". Water Science and Technology **68**(5), 1173-1179.

Wu, J.-S., Liu, C.-H., Chu, K.H. and Suen, S.-Y. (2008) "Removal of cationic dye methyl violet 2B from water by cation exchange membranes". Journal of Membrane Science **309**(1–2), 239-245.

Wu, Y., Fan, Y., Zhang, M., Ming, Z., Yang, S., Arkin, A. and Fang, P. (2016) "Functionalized agricultural biomass as a low-cost adsorbent: Utilization of rice straw incorporated with amine groups for the adsorption of Cr(VI) and Ni(II) from single and binary systems". Biochemical Engineering Journal **105**(Part A), 27-35.

Xu, Z., Cai, J.-G. and Pan, B.-C. (2013) "Mathematically Modelling Fixed-Bed Adsorption in Aqueous Systems". Journal of Zhejiang University-Science A (Applied Physics & Engineering) **14**(3), 155-176.

Yagub, M.T., Sen, T.K., Afroze, S. and Ang, H.M. (2015) "Fixed-bed dynamic column adsorption study of methylene blue (MB) onto pine cone". Desalination and Water Treatment **55**(4), 1026-1039.

Yagub, M.T., Sen, T.K., Afroze, S. and Ang, H.M. (2014a) "Dye and its removal from aqueous solution by adsorption: A review". Advances in Colloid and Interface Science **209**(0), 172-184.

Yagub, M.T., Sen, T.K. and Ang, H.M. (2012) "Equilibrium, kinetics, and thermodynamics of methylene blue adsorption by pine tree leaves". Water, Air, and Soil Pollution **223**(8), 5267-5282.

Yagub, M.T., Sen, T.K. and Ang, M. (2014b) "Removal of cationic dye methylene blue (MB) from aqueous solution by ground raw and base modified pine cone powder". Environmental Earth Sciences **71**(4), 1507-1519.

Yakkala, K., Yu, M.-R., Roh, H., Yang, J.-K. and Chang, Y.-Y. (2013) "Buffalo weed (*Ambrosia trifida* L. var. *trifida*) biochar for cadmium (II) and lead (II) adsorption in single and mixed system". *Desalination and Water Treatment* **51**(40-42), 7732-7745.

Yaneva, Z.L. and Georgieva, N.V. (2012) "Insights into Congo Red Adsorption on Agro-Industrial Materials - Spectral, Equilibrium, Kinetic, Thermodynamic, Dynamic and Desorption Studies. A Review". *International Review of Chemical Engineering* **4**(2), 127-146.

Yavuz, Ö. and Saka, C. (2013) "Surface modification with cold plasma application on kaolin and its effects on the adsorption of methylene blue". *Applied Clay Science* **85**, 96-102.

Yoon, Y.H. and Nelson, J.H. (1984) "Application of Gas Adsorption Kinetics I. A Theoretical Model for Respirator Cartridge Service Life". *American Industrial Hygiene Association Journal* **45**(8), 509-516.

Yurekli, Y., Yildirim, M., Aydin, L. and Savran, M. (2017) "Filtration and removal performances of membrane adsorbers". *Journal of Hazardous Materials* **332**(Supplement C), 33-41.

Zazycki, M.A., Godinho, M., Perondi, D., Foletto, E.L., Collazzo, G.C. and Dotto, G.L. (2018) "New biochar from pecan nutshells as an alternative adsorbent for removing reactive red 141 from aqueous solutions". *Journal of Cleaner Production* **171**(Supplement C), 57-65.

Zhang, L., Hu, P., Wang, J. and Huang, R. (2016) "Adsorption of Amido Black 10B from aqueous solutions onto Zr (IV) surface-immobilized cross-linked chitosan/bentonite composite". *Applied Surface Science* **369**, 558-566.

Zhang, T., Zhu, X., Shi, L., Li, J., Li, S., Lü, J. and Li, Y. (2017) "Efficient removal of lead from solution by celery-derived biochars rich in alkaline minerals". *Bioresource Technology* **235**, 185-192.

Zhang, Y., Xu, S., Luo, Y., Pan, S., Ding, H. and Li, G. (2011a) "Synthesis of mesoporous carbon capsules encapsulated with magnetite nanoparticles and their application in wastewater treatment". *Journal of Materials Chemistry* **21**(11), 3664-3671.

Zhang, Z., Moghaddam, L., O'Hara, I.M. and Doherty, W.O.S. (2011b) "Congo Red adsorption by ball-milled sugarcane bagasse". *Chemical Engineering Journal* **178**(0), 122-128.

Zhao, B., Xiao, W., Shang, Y., Zhu, H. and Han, R. (2014a) "Adsorption of light green anionic dye using cationic surfactant-modified peanut husk in batch mode". Arabian Journal of Chemistry **10**(Supplement 2), 3595-3602.

Zhao, Y., Xia, Y., Yang, H., Wang, Y. and Zhao, M. (2014b) "Synthesis of glutamic acid-modified magnetic corn straw: equilibrium and kinetic studies on methylene blue adsorption". Desalination and Water Treatment **52**(1-3), 199-207.

Zhou, N., Chen, H., Xi, J., Yao, D., Zhou, Z., Tian, Y. and Lu, X. (2017) "Biochars with excellent Pb(II) adsorption property produced from fresh and dehydrated banana peels via hydrothermal carbonization". Bioresource Technology **232**, 204-210.

Zhu, C., Liu, F., Xu, C., Gao, J., Chen, D. and Li, A. (2015) "Enhanced removal of Cu(II) and Ni(II) from saline solution by novel dual-primary-amine chelating resin based on anion-synergism". Journal of Hazardous Materials **287**(Supplement C), 234-242.

Zhu, L., Wang, Y., He, T., You, L. and Shen, X. (2016) "Assessment of Potential Capability of Water Bamboo Leaves on the Adsorption Removal Efficiency of Cationic Dye from Aqueous Solutions". Journal of Polymers and the Environment **24**(2), 148-158.

Zhu, M. and Diao, G. (2011) "Review on the progress in synthesis and application of magnetic carbon nanocomposites". Nanoscale **3**(7), 2748-2767.

Zhu, X., Liu, Y., Zhou, C., Zhang, S. and Chen, J. (2014) "Novel and high-performance magnetic carbon composite prepared from waste hydrochar for dye removal". ACS Sustainable Chemistry & Engineering **2**(4), 969-977.

Zou, W., Bai, H., Gao, S. and Li, K. (2013) "Characterization of modified sawdust, kinetic and equilibrium study about methylene blue adsorption in batch mode". Korean Journal of Chemical Engineering **30**(1), 111-122.

*Every reasonable effort has been made to acknowledge the owners of copyright material. I would be pleased to hear from any copyright owner who has been omitted or incorrectly acknowledged.*

# **CHAPTER 3**

## **MATERIALS, CHARACTERISATION AND EXPERIMENTAL METHODS**

### 3.1 Introduction

This chapter provides detailed description on the chemicals and adsorbents used in this study. Pine cone bio-char and Eucalyptus bark bio-char were synthesized through slow pyrolysis process at various temperature profile. Also, the effectiveness of kaolin clay in the removal of Methylene blue dye is investigated in this research study. The effectiveness of synthesized biochar and kaolin in the removal of organic and inorganic pollutants from aqueous solution were explored through batch kinetics, isotherm adsorption and packed bed column experiments. Further, the physical, chemical and morphological characterisation of the synthesized biochar and kaolin were utilised through the use of Malvern particle sizer, SEM, EDS, XRD, CHN-O analyse, BET surface area, FT-IR,  $\text{pH}_{\text{pzc}}$ , bio-char yield and bulk density.

### 3.2 Adsorbents

#### 3.2.1 Pine cone, eucalyptus bark and kaolin clay collection

Eucalyptus (*sheathiana*) bark and pine cone (*P. radiate*) biomasses were obtained from Curtin University Bentley campus, Western Australia between January and April of 2014 as shown in Fig.3.1 (a) and (b) respectively. Both biomasses are widely available in Australia at no cost and larger amount of eucalyptus bark and pine cone are disposed each year (Blue Mountains City Council 2009, Morton 1980). The biomasses were placed separately and washed three times with deionized water to remove dust, dirt and insoluble contaminations. The raw biomasses dried at 75°C for 24 h and collected in a labelled plastic bags. Kaolin is a white clay mineral and it is also known as kaolinite with a formula of  $\text{Al}_2\text{Si}_2\text{O}_5(\text{OH})_4$  and molecular weight of 258.16 g/mol. In this research kaolin clay is obtained by Chem.-supply, Gillman SA, Australia. The clay was oven dried at 75°C to eliminate moisture then stored in a labelled plastic container as shown in Fig.3.1 (c).

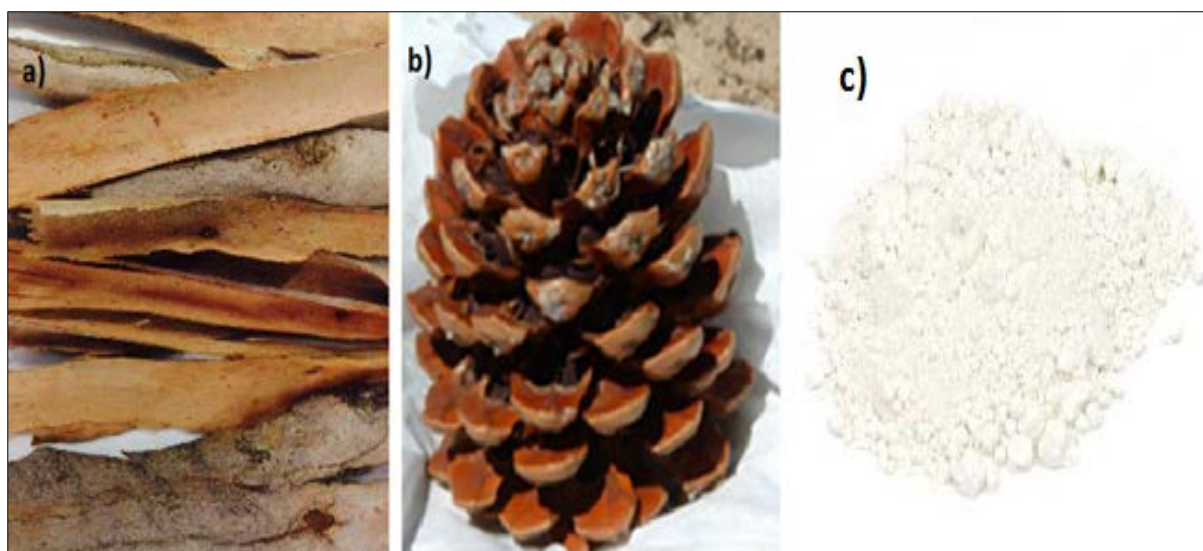


**Figure 3.1:** a) Raw eucalyptus bark, b) raw pine cone and c) kaolin clay powder.

### **3.2.2 Synthesis of slow pyrolysis EB and pine cone bio-chars**

The dried biomasses were cut into small pieces and then placed separately in a closed crucibles inside a muffle furnace under limited oxygen content and atmospheric pressure. The temperature profile was increased at the rate of  $10^{\circ}\text{C}/\text{min}$  until it reached the set point of  $300^{\circ}\text{C}$ ,  $400^{\circ}\text{C}$ ,  $500^{\circ}\text{C}$ ,  $600^{\circ}\text{C}$  and  $700^{\circ}\text{C}$  respectively and kept at the set point temperature up-to 2.5 hrs. The synthesized pine cone biochar and EB biochar were cooled down gradually at room temperature for a period of 5 hrs then grounded using a mechanical grinder (manufactured by 135 RETSCH, GmbH & Co. KG, West Germany). The resultants bio-char powders were passed through a British Standard Sieve (BSS) of  $106\ \mu\text{m}$  and stored in a labelled containers. Schematic diagram of the production of EB biochar was shown in Fig.3.2. Similar procedure was carried out in the production of pine cone bio-char.



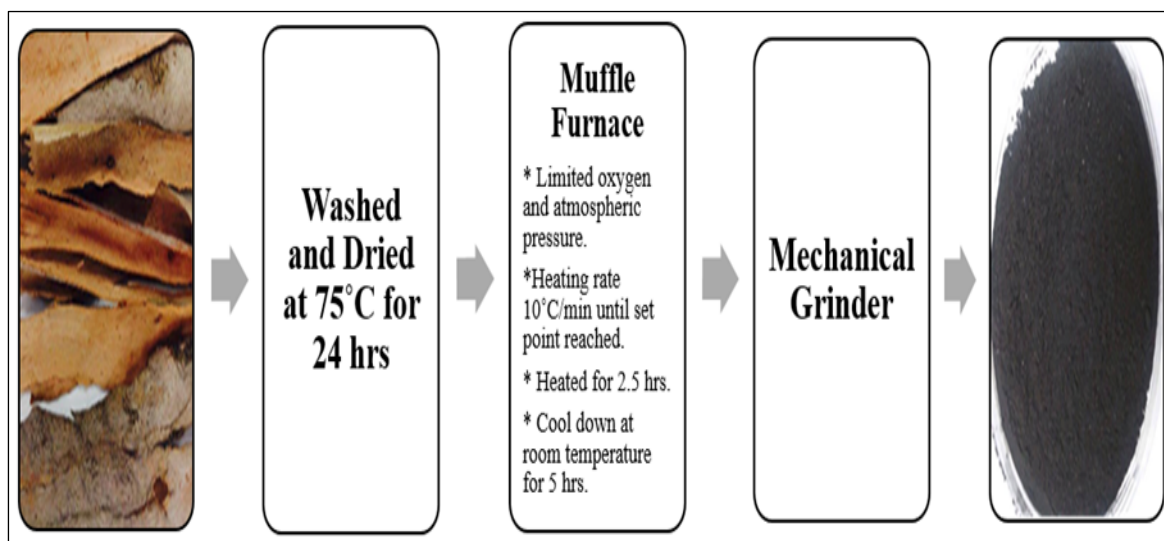


**Figure 3.2:** Schematic diagram of the production of EB bio-char.

### 3.3 Adsorbates and other chemicals

#### 3.3.1 Methylene Blue (MB) Dye

The cationic dye, Methylene Blue dye of an analytical grade is used as the model adsorbate in this research study. Methylene blue has dark green color and when diluted with water, the solution turns into dark blue due to presence of oxygen as shown in Fig.3.3 (a). The scientific name of MB dye is 3,7-Bis (dimethylamino) phenothiazin-5-ium chloride with the molecular weight of 319.85g/mol and a chemical formula:  $C_{16}H_{18}N_3SCl$ . It was obtained from Sigma Aldrich with 99.9% purity. A stock solution of 1000 mg/L was prepared by dissolving 1000 mg of MB powder in 1000 ml volumetric flask and filled it with ultra-pure water. Various dye concentrations of 1- 150 mg/L were prepared by diluting the stock solution with ultra-pure water. The spectrophotometer SP-8001 UV/VIS presented in Fig 3.3 (b) was used to measure the concentration of MB dye in solution where the maximum adsorption for the dye solution was measured at wavelength of  $\lambda = 668$  nm. The calibration curve was plotted between the absorbance and concentration of MB dye solution to obtain the linear calibration equation as shown in Fig 3.4. The concentration of the MB dye was measured from the calibration plot. Chemical risk assessment was carried out through the use of material safety data to detect and regulate any hazards associated with the use of MB dye.

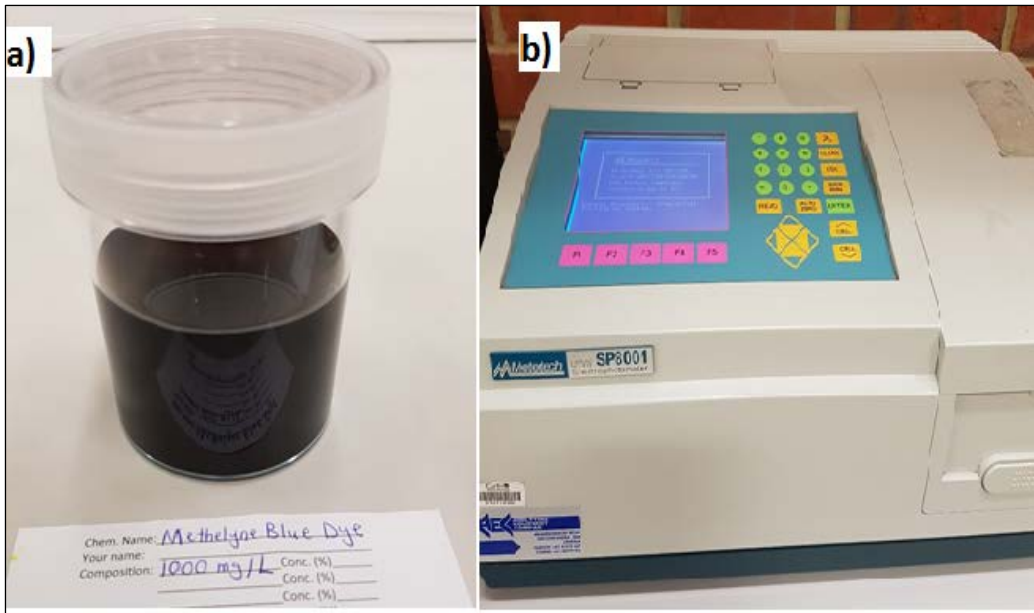


**Figure 3.3:** a) MB dye of 1000 mg/L, b) SP-8001 UV/VIS Spectrophotometer.

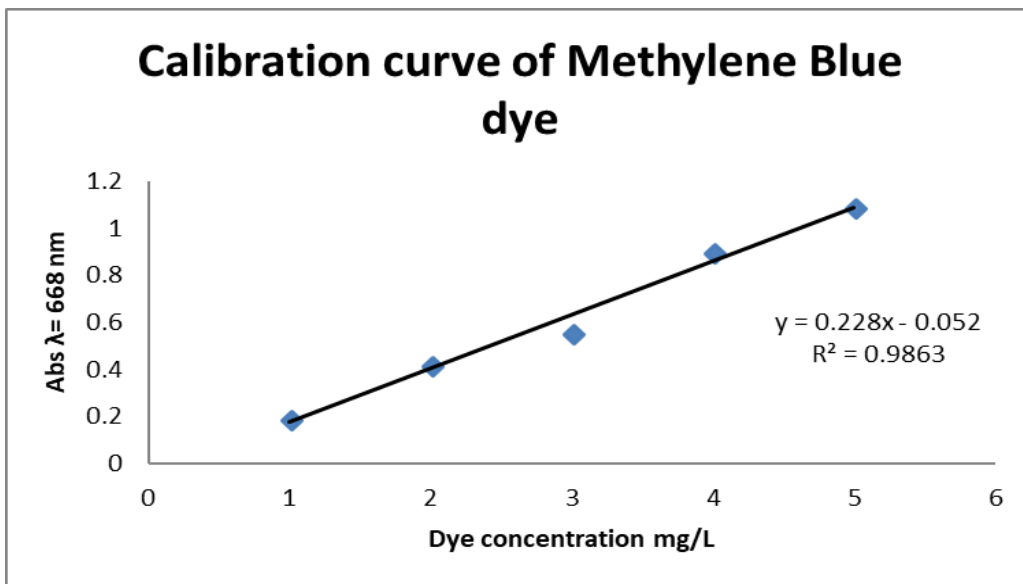


**Figure 3.4:** The calibration curve for various MB dye concentration.

### 3.3.2 Nickel metal ions ( $\text{Ni}^{2+}$ )

Nickel metal ions was used as another model adsorbate in this research study and it is presented in the form of  $\text{Ni}(\text{NO}_3)_2 \cdot 6\text{H}_2\text{O}$  salt with a molecular weight of 290.79 g/mol. A stock solution of 1000 mg/L ( $\text{Ni}^{2+}$ ) was prepared by adding 4.953 g of  $\text{Ni}(\text{NO}_3)_2 \cdot 6\text{H}_2\text{O}$  salt into 1000 ml volumetric flask containing an ultra-pure water as shown in Fig.3.5 (a). Various metal ions concentrations of 1- 70 mg/L were prepared by diluting the stock solution with deionized water. Atomic Absorption Spectrophotometer (AAS) (model AA-7000) as shown in Fig.3.5 (b) was used to measure concentration of nickel ions in solution. The calibration curve shown in Fig 3.6 was plotted between the absorbance and concentration of nickel ions solution to obtain the linear calibration equation. The concentration of the Ni (II) ions was measured from the calibration plot. Chemical risk assessment was carried out through the use of material safety data to detect and regulate any hazards associated with the use of Ni (II) ions.

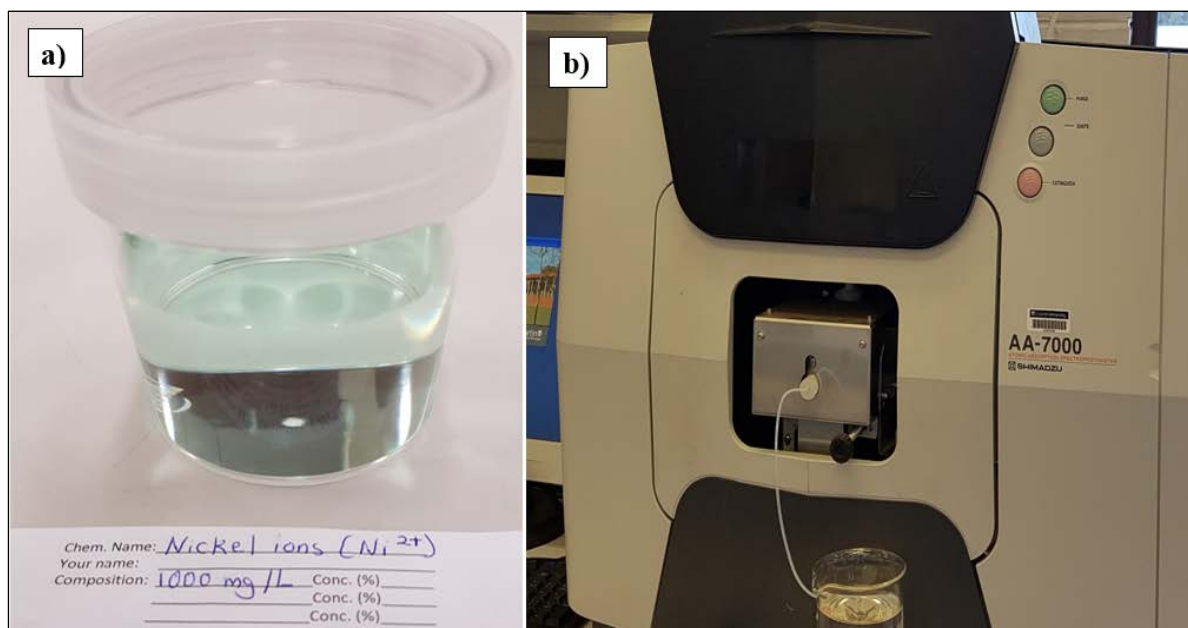


**Figure 3.5:** a) Nickel ions stock solution of 1000 mg/L, b) Atomic Absorption Spectrometer AAS-7000

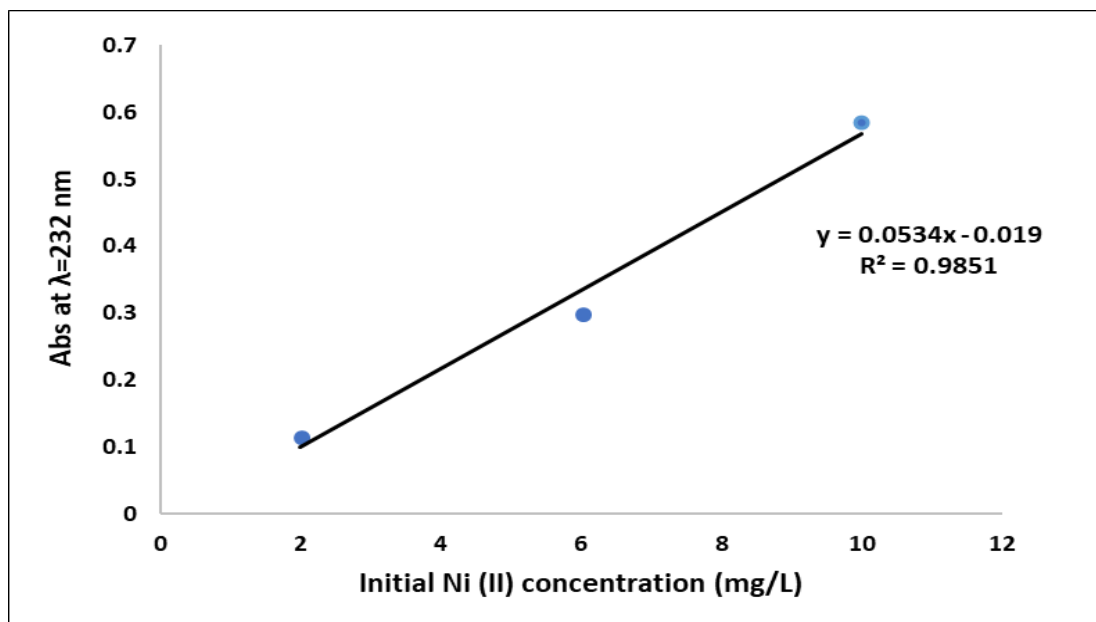


**Figure 3.6:** Calibration curve for various nickel ( $\text{Ni}^{2+}$ ) ions concentration

### 3.3.3 Other chemicals

Hydrochloric acid (HCL) solution is used in this research study to modify the solution pH of cationic dye and heavy metal ions. Hydrochloric acid stock solution 37.5% was obtained from Sigma Aldrich. The 0.1 M hydrochloric acid was prepared by diluting a known volume of the stock solution with deionized water to make 1000 ml of 0.1 M HCL solution. The prepared solution is kept in a glass labelled bottle.

Sodium hydroxide (NaOH) solution is used in this research study to adjust the solution pH of MB dye and nickel ions. In this study sodium hydroxide solution of an analytical grade is obtained from Orica (Australia). 0.1 M of ammonium hydroxide ( $\text{NH}_4\text{OH}$ ) solution was used to adjust the pH solution of nickel ions ( $\text{Ni}^{2+}$ ) instead of sodium hydroxide to avoid the formation of sodium ions ( $\text{Na}^+$ ) ions which may competes with the available bind sites on the bio-char surface. Chemical risk assessments were carried out through the use of material safety data to detect and regulate any hazards associated with the use of these chemicals.

### **3.4 Adsorbents characterizations**

#### **3.4.1 CHNS Analysis**

CHN-O analysis is used to determine the amount of carbon, hydrogen, nitrogen and oxygen presented in different substances. In this project, CHN-O Analysis was carried out by PerkinElmer model- CHNS-O analyser 2400 as shown in Fig 3.7. CHN-O analysis was carried out to measure mainly the amount of carbon (C) presented in the raw feedstocks such as raw EB and pine cone as well as the synthesised bio-char.

Further, bio-char synthesised under various temperature profiles as discussed in section 3.2.2 were also examined to evaluate the amount of carbon, hydrogen and nitrogen produced from the precursor as shown in Table 3.1. CHN analysis found that raw EB biomass contains 41 % carbon, 5.4% hydrogen and 0.3 nitrogen. The amount of carbon presented was increasing from 51.7% EB bio-char (300°C) to 60% EB bio-char (500°C) while the amount of hydrogen decreases from 3.1% to 1.68 % for the same samples. However, the amount of nitrogen presence remains almost constant. EB samples produced at temperature profile higher than 500°C were mainly formed as ash thus very low carbon content was assumed. CHN analysis shows that raw pine cone biomass contains 47.1 % carbon, 5.5 % hydrogen and 0.4 nitrogen. Pine cone bio-char produced at higher temperature profile results in higher percentage carbon of 60.2 %, 66.6 % and 75.1% for pine cone bio-char produced at 300°C - 500°C respectively. Hydrogen percentage decreased from 5.5% (raw pine cone) to 2.5% for pine cone bio-char (500°C) while nitrogen content was slightly increased from 0.4% to 0.84% for the same samples. Pine cone bio-char produced at temperature profile higher than 500°C were mainly formed as ash thus very low carbon content was assumed. Results obtained in this study are comparative to other published bio-char, charcoal and activated carbon and indicated the applicability of EB and pine cone wastes as excellent precursor in the production of bio-char as presented in Table.3.1. The highest amount of carbon yield is based on the production of bio-char at temperature profile of 500°C as shown in Table 3.1. Therefore, EB biochar and pine cone bio-char produced bio-char at temperature profile of 500°C were chosen as adsorbents in this research study.



**Figure 3.7:** CHNS Analysis by PerkinElmer (CHNS-O analyser 2400).

**Table 3.1:** Element comparative analysis of various char, charcoal and activated carbon.

<b>Adsorbent</b>	<b>(C) %</b>	<b>(H) %</b>	<b>(N) %</b>	<b>Reference</b>
Raw EB	40.9	5.4	0.29	This study
EB bio-char (300°C)	51.7	3.1	0.27	This study
EB bio-char (400°C)	53.4	2.1	0.27	This study
EB bio-char (500°C)	60.0	1.68	0.25	This study
Raw pine cone	47.1	5.5	0.36	This study
pine cone bio-char (300°C)	61.2	3.8	0.65	This study

---

pine cone bio-char (400°C)	66.6	2.9	0.73	This study
pine cone bio-char (500°C)	75.1	2.5	0.83	This study
Banana biochar	71.4	6.3	0.6	(Zhou et al. 2017)
Rice straw biochar	56.9	0.9	0	(Sewu et al. 2017b)
Korean cabbage biochar	46.4	1.1	0.9	(Sewu et al. 2017b)
Bamboo hydrochar	63.6	3.7	0.6	(Li et al. 2016)
Weed biochar	65.9	2.5	3.1	(Güzel et al. 2017)
Pecan nut activated carbon	76.5	0.9	-	(Aguayo-Villarreal et al. 2017)
Empty fruit activated carbon	71.4	2.5	1.5	(Isahak et al. 2012)
Commercial charcoal	73.6	4.8	1.4	(Isahak et al. 2012)
Palm shell activated carbon	60.0	0.3	0.03	(Yin et al. 2007)

---

### 3.4.2 Fourier-Transform Infrared (FT-IR)

Understanding the surface functional groups presented in the adsorbents is significant to evaluate the adsorption characteristics of the adsorbent and the interaction of the adsorbate-adsorbent. Fourier-transform infrared (FTIR) spectrum from Perkin Elmer (Version 6.3.4) is used to study the functional groups presented in EB bio-char, Pine cone bio-char and kaolin clay respectively. FTIR spectrometer is used to investigate the functional groups presented in the EB biochar, pine cone biochar and kaolin clay before and after MB dye adsorption shown in Fig. (3.8- 3.10) respectively.

From Fig.3.8, the absorption band at  $3500\text{--}3300\text{ cm}^{-1}$  is presented with a peak band about  $3337\text{ cm}^{-1}$  and thus indicates the presence of O-H vibrations of alcohols, phenols and carboxylic acids in the cellulose and lignin (Liang et al. 2010). Therefore, it suggests that phenolic and acidic groups are responsible for MB dye adsorption on EB bio-char. Two peaks were found at  $11607\text{ cm}^{-1}$  and  $1315\text{ cm}^{-1}$  which indicates N-H bending. Also, a small peak of  $2162\text{ cm}^{-1}$  suggests the presence of  $\text{C}\equiv\text{C}$  stretching band. Another peak of  $1400\text{ cm}^{-1}$  is found and it suggests the presence of C-H scissoring and bending absorption band. C-N stretching is detected at the peak of  $1315\text{ cm}^{-1}$  where N-H bending band is detected at  $900\text{--}650\text{ cm}^{-1}$  band.

The FTIR analysis of EB bio-char after the adsorption of MB dye suggests the presence of N-H stretching band at  $3500\text{--}3300\text{ cm}^{-1}$ . Strong peaks noted at  $1592\text{ cm}^{-1}$  and  $1387\text{ cm}^{-1}$  suggest the presence of C=C stretch aromatic ring and C-H scissoring and bending absorption bands respectively. From Fig.3.8, the presence of MB dye on EB bio-char has shifted peak bands at  $1607\text{ cm}^{-1}$  and  $1315\text{ cm}^{-1}$  shifted to  $1591\text{ cm}^{-1}$  and  $1325\text{ cm}^{-1}$  respectively while the functional groups presented at  $2162\text{ cm}^{-1}$  and  $780\text{ cm}^{-1}$  of EB bio-char which suggest the aggregation of MB molecules with their functional groups of EB bio-char. Furthermore, a peak at  $1400\text{ cm}^{-1}$  has shifted to  $1387\text{ cm}^{-1}$  suggests that carboxyl group took part in the adsorption process. Also, the O-H stretching peak of  $3337\text{ cm}^{-1}$  has increased to  $3349\text{ cm}^{-1}$  after adsorption of MB dye which indicates significant hydrogen- bonding interaction in alkaline conditions.



The FTIR spectrum of the pine cone bio-char presented in Fig.3.9 shows a weak peak band at  $3336\text{ cm}^{-1}$  and this is due to O-H stretch of carboxylic acids presented in the origin biomass. Peaks observed at  $1558\text{ cm}^{-1}$  and  $1407\text{ cm}^{-1}$  presented aromatic (C=C) and (C-H) stretching groups respectively. Sharp peak shown at  $873\text{ cm}^{-1}$  indicate the presence of aromatic C-H bending. The presence of low intensity bands at  $3336$ ,  $1710$ ,  $1558$ , and  $1316\text{ cm}^{-1}$  indicate that the volatile matters were removed supporting the biochar yield thus increased the pine cone bio-char surface area (Zazycki et al. 2018). The existence of various weak peaks on pine cone bio-char reveals that the surface functional groups were decreasing with increases of pyrolysis temperature which is consistent with the change of carbon and hydrogen amount. A peak at  $1407\text{ cm}^{-1}$  demonstrated the presence of O-H bend from carboxylic acids group indicate the existence of acidic oxygen containing functional groups that increase the adsorption capacity of MB dye and Ni (II) ions (Van Vinh et al. 2015). FTIR spectrum of pine cone biochar loaded with Ni (II) ions and pine cone biochar loaded with MB dye as shown in Fig.3.8 show two weak peaks at ( $1786\text{-}1784\text{ cm}^{-1}$ ) and ( $1235\text{-}1229\text{ cm}^{-1}$ ) which indicate the presence of (C=O) and (C-O-C) stretching groups respectively.

The FTIR analysis of kaolin clay before and after MB dye adsorption as shown in Fig 3.10 exhibits sharp absorption peak bands at  $3687$  and  $3619\text{ cm}^{-1}$  which suggest the presence of O-H and Si-O stretching vibration of Silanol group. This is due to the presence of intramolecular hydrogen bonding. Also, these peaks are presented due to the stretching vibration of O-H groups coordinated to the  $\text{Al}^{3+}$  ions (Mukherjee et al. 2015). FT-IR of raw kaolin and kaolin loaded with MB dye show sharp peaks absorption band at  $1023\text{ cm}^{-1}$ ,  $994\text{ cm}^{-1}$ ,  $909\text{ cm}^{-1}$  which suggest the presence of  $\nu$  (Si-O) planer stretching, O-H deformation and Si-O Stretching respectively (Mukherjee et al. 2015). However, new weak peaks has been found on Kaolin after the MB dye adsorption at  $1605\text{ cm}^{-1}$  and  $1391\text{ cm}^{-1}$  which presents central ring stretching C=N and multiple ring stretching respectively (Ji et al. 2011). These form peaks suggest the aggregation of MB molecules into Kaolin surface during adsorption process.

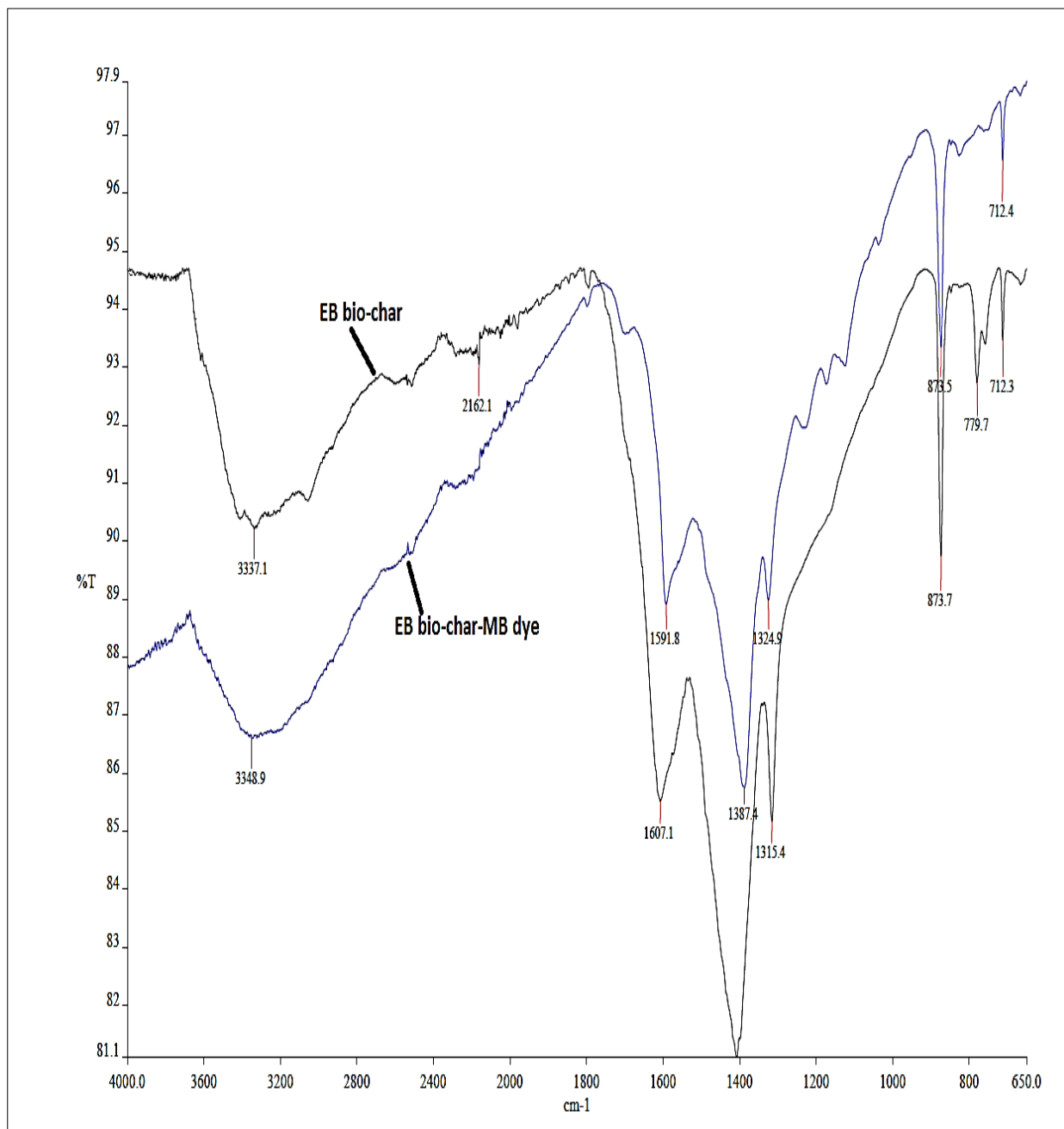


**Figure 3.8:** FTIR of EB biochar and EB biochar after MB dye adsorption.

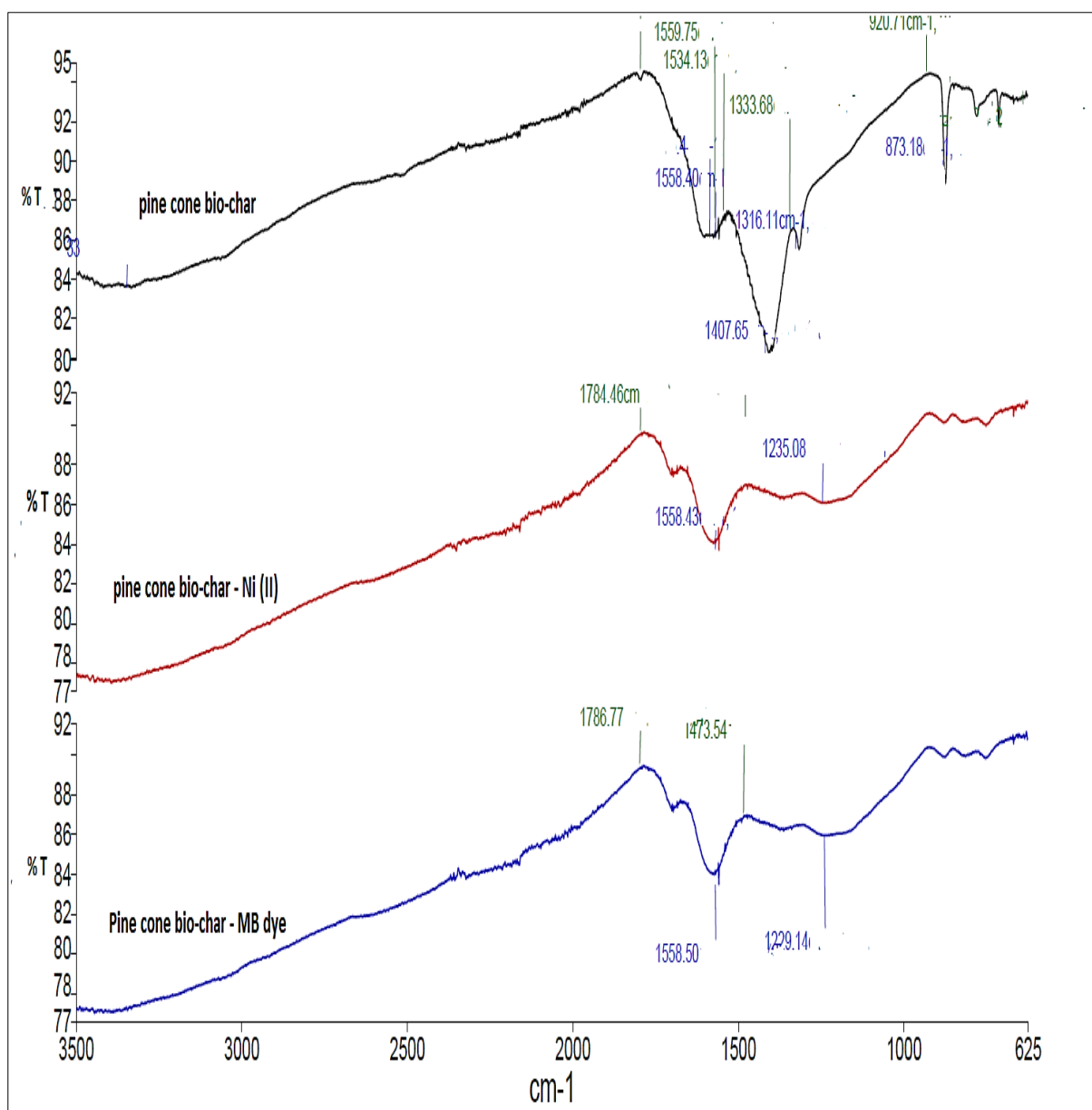


**Figure 3.9:** FTIR of pine cone bio-char, pine cone biochar-MB dye and pine cone biochar-Ni (II) adsorption.

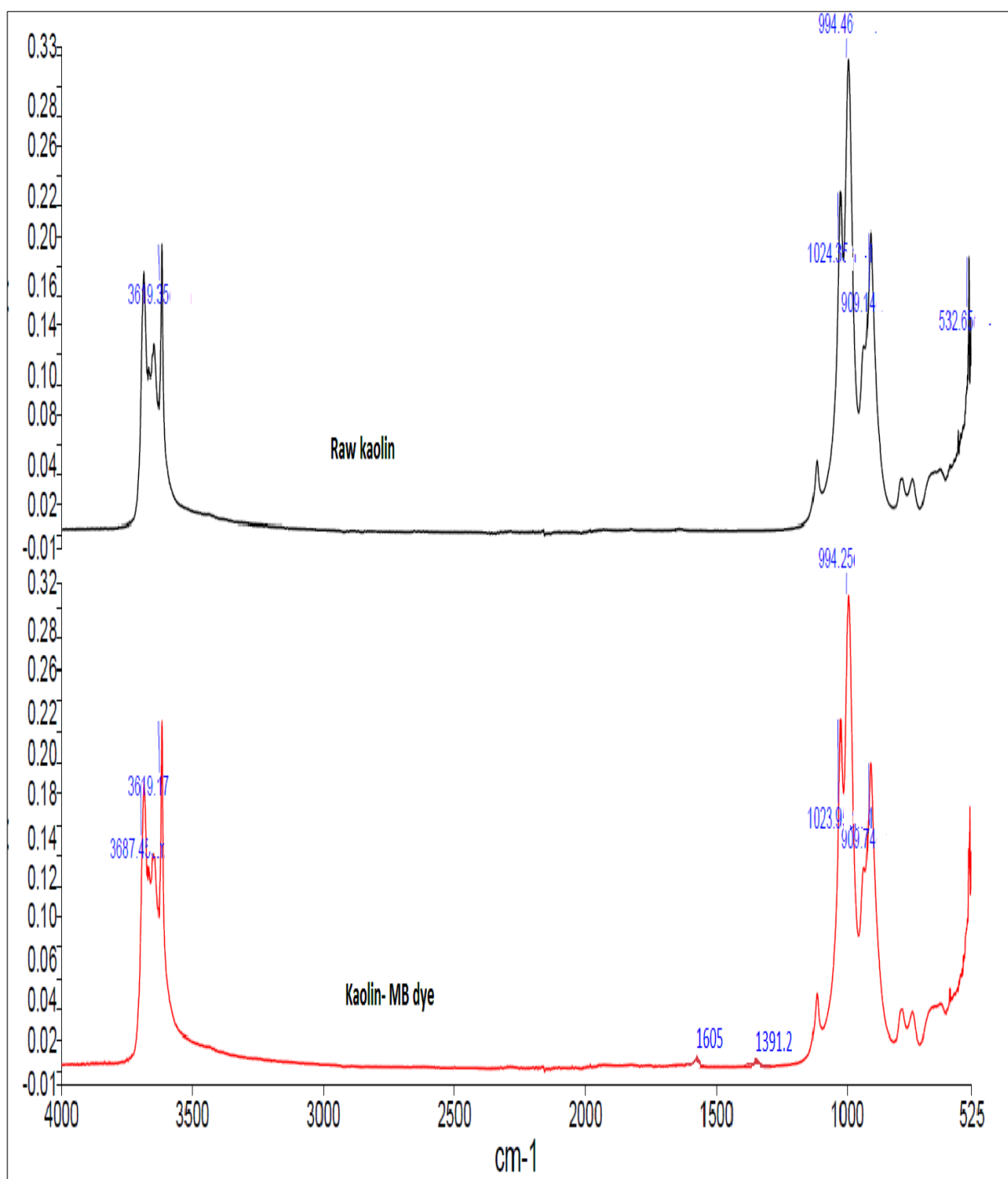


**Figure 3.10:** FTIR of kaolin clay before and after MB dye adsorption.

### 3.4.3 Scanning Electron Microscope (SEM) and Energy Dispersive X-ray Spectroscopy (EDS)

SEM and EDS analysis were used to study the adsorbent surface morphology. SEM analysis was carried out using SEM instrument with Evo-40XVP model. Static electric charge on the adsorbent's surface may affect the accuracy of SEM images therefore prior to the analysis, the adsorbents were coated with a layer of platinum for both biochar samples while kaolin clay was coated with a thin layer of carbon. The samples were kept under vacuum to remove accumulation of static electric charge on the adsorbents. SEM/ EDS of EB bio-char, pine cone bio-char and kaolin clay are shown in Fig (3.11- 3.13) respectively.

EB bio-char before and after MB dye adsorption are presented in Fig.3.11 (a) and (b) respectively. EB biochar shows a well-developed and heterogeneous structure with high porosity. From Fig. 3.11 (b), the porous structures were reduced which indicates the binding of dye's molecules into the surface of biochar particles. Also, EDS analysis of EB biochar indicates that carbon, oxygen and calcium were the main components presented as shown in Fig.3.11 (c). Furthermore, pine cone bio-char before adsorption presents a honey comb like bio-char particle structure with clearly distributed visible pores across the bulk surface as shown in Fig 3.12 (a). The structured pores can be attributed due to the elimination of volatile matters presented in pine cone biomass during the pyrolysis process (Hu et al. 2015). MB dye loaded into pine biochar was presented in Fig 3.12 (b) where the visible pores were reduced due to MB dye binding at the surface of the adsorbent. EDS analysis of pine cone biochar shows that carbon and oxygen were the main components presented as shown in Fig.3.12 (c). However, sodium is also detected but in low proportion. SEM analysis of kaolin clay before and after adsorption are shown as per Fig.3.13 (a) and (b) respectively. Kaolin particles were found to be clustered, irregular in shape and having a porous texture and thus enhances the adsorption of MB dye's molecules into the kaolin surface. Also, from EDS analysis as shown in Fig.3.13 (c) that aluminium, silicon, oxygen and titanium were the main components presenting in kaolin clay. The presence of impurities such as titanium dioxide was reported by other researchers (Fabbri et al. 2013, González and del C. Ruiz 2006).

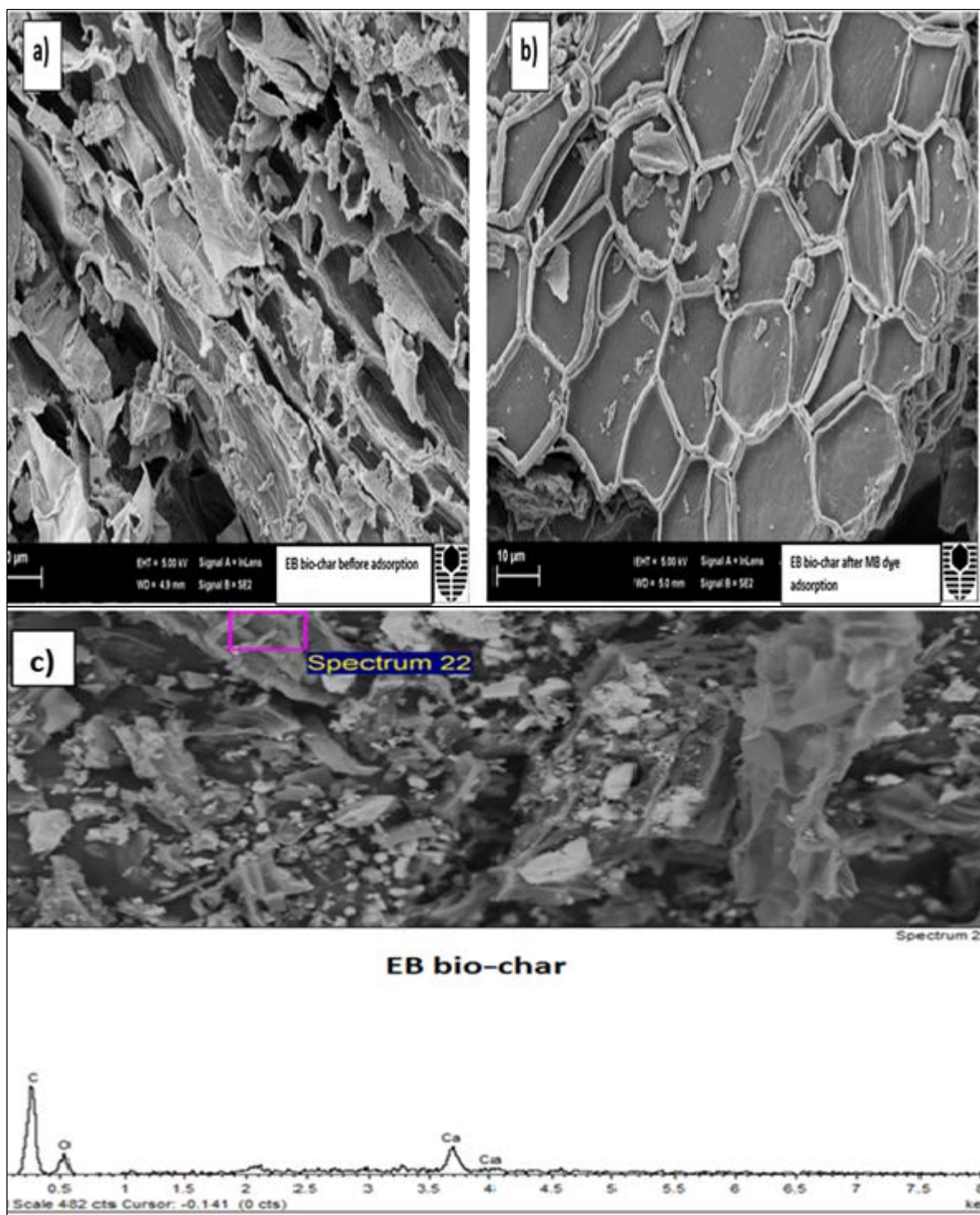


**Figure 3.11:** a) SEM of EB bio-char before adsorption (2000x), b) SEM of EB bio-char after MB dye adsorption (2000x), c) EDS of EB bio-char.

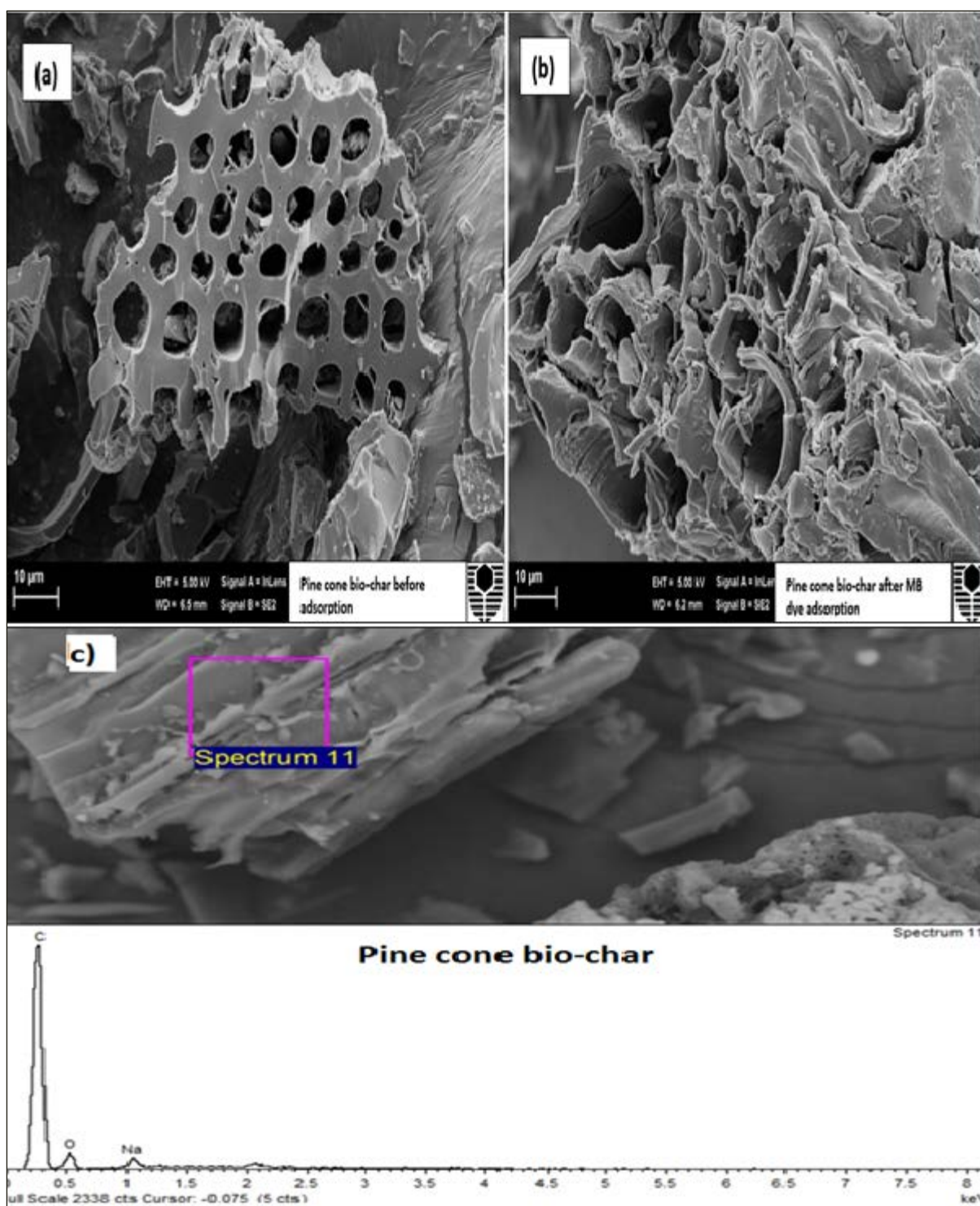


**Figure 3.12:** a) SEM of pine cone bio-char before adsorption (2000x), b) SEM of pine cone bio-char after MB dye adsorption (2000x), c) EDS of pine cone bio-char.

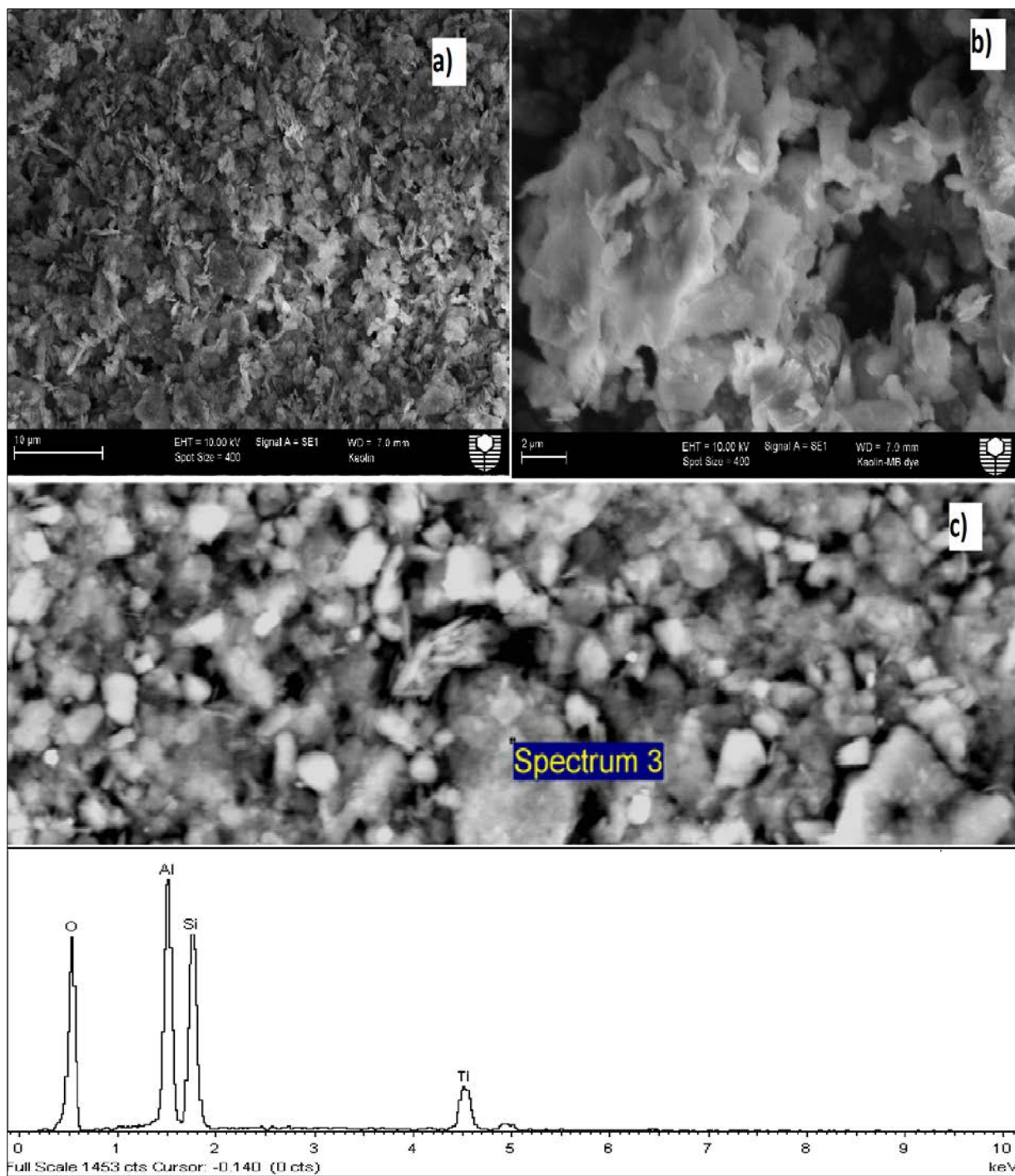


**Figure 3.13:** a) SEM of kaolin clay before adsorption (2000x), b) SEM of kaolin after MB dye adsorption (10000x), c) EDS of kaolin clay.



### 3.4.4 X-Ray Diffraction spectrum (XRD)

X-ray Diffraction (XRD) analysis is a method used to identify and quantify the crystalline structure of materials. Also, powder X-ray diffraction (XRD) is used to evaluate the lattice planes, their dimensions and epitaxial growth of crystallites within the materials (Afroze et al. 2016b). The chemical analysis and crystalline structure of EB biochar, pine cone biochar and kaolin clay were studied using XRD analysis as shown in Fig.3.14 (a), (b) and (c) respectively. The samples were analysed in the region of  $2\theta$  and angle range of  $0^\circ - 80^\circ$  at room temperature using Cu  $K\alpha$  radiation. Peaks attained from the XRD were analysed using EVA software. From Fig 3.14 (a), various peaks were observed at  $14.9^\circ$ ,  $23.1^\circ$ ,  $24.7^\circ$ ,  $29.5^\circ$ ,  $36.1^\circ$ ,  $39.5^\circ$ ,  $43.2^\circ$  and  $48.5^\circ$  which indicate the presence of organic matters and crystalline cellulose in EB biochar (Afroze et al. 2016a). XRD analysis of pine cone biochar detected a very weak peak at  $20.7^\circ$  which may indicates the presence of cellulose retained from raw pine cone powder as shown in Fig 3.14 (b) (Zhao and Lang 2018). Moreover, kaolin clay adsorbent has been analysed using XRD as shown in Fig 3.14 (c). Three major peaks were observed at  $12.2^\circ$ ,  $25.0^\circ$  and  $27.8^\circ$  which indicate the presence of silica oxides ( $\text{SiO}_2$ ) in the form of quartz and titanium oxides ( $\text{TiO}_2$ ). The presence of these compounds agreed with the theoretical chemical compositions of kaolin clay (Aries and Sen 2009, Dill 2016).

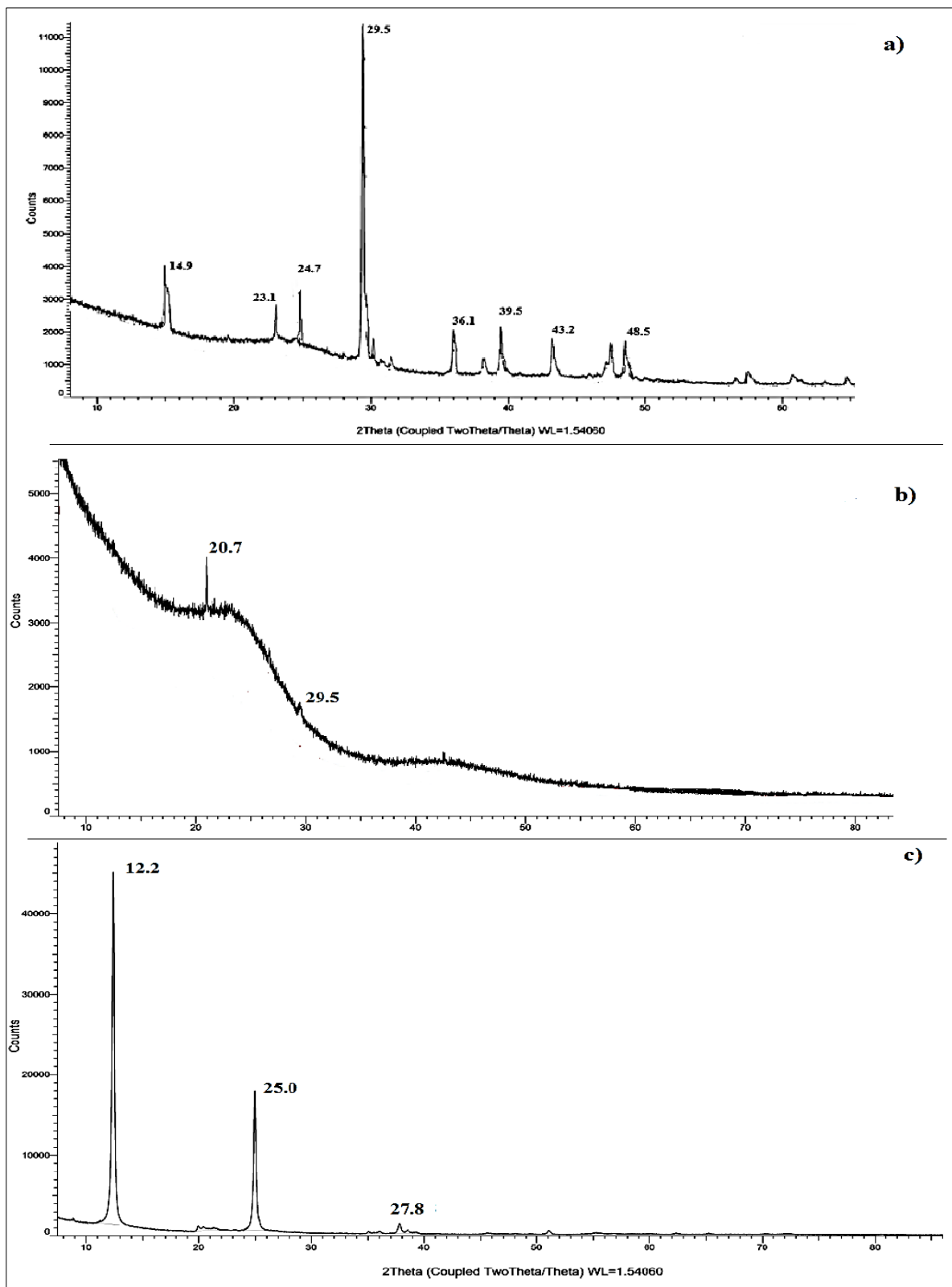


**Figure 3.14:** XRD analysis of (a) EB biochar, (b) pine cone biochar and (c) kaolin clay.

### 3.4.5 Brunauer–Emmett–Teller (BET) Surface Area and Malvern particle sizer

BET surface area is used to explain the physical adsorption of N<sub>2</sub> gas molecules on the monolayer solid surface of the adsorbents. The micromeritics (TriStar II 3020) is used to measure the surface area and pore volume of the adsorbents. Synthesized bio-char were degassed at 200°C for 24 hours to eliminate any trace of volatile elements. The samples were taken from the degas chamber and cool down at room temperature before placed into the Tristar nitrogen adsorption chamber at temperature of -196 °C. BET surface area for EB bio-char and pine cone bio-char and kaolin were calculated as 73 m<sup>2</sup>/g, 335 m<sup>2</sup>/g and 30.5 m<sup>2</sup>/g respectively as shown in Table 3.2. BET surface area was increased significantly from 15.5 m<sup>2</sup>/g for pine cone biomass to 335 m<sup>2</sup>/g synthesized pine cone biochar. This is due to the removal of volatile matters during pyrolysis thus pores and cavities are formed hence the surface area increased. Similar trend is observed for EB bio-char. Further, Table 3.2 presents the surface area for various biochar which are comparative with the synthesized biochar thus suggests the feasibility of EB biochar, pine cone biochar and kaolin clay as adsorbents in the removal of organic and inorganic wastewater pollutants. Also, the adsorption average pore diameter was found as 5.1 nm and 3.1 nm for EB bio-char and pine cone bio-char respectively.

Malvern master sizer (Hydro 2000S) instrument is used to measure the surface weighted mean particle size distribution, specific surface area and volume weighted mean of the various adsorbents particles using laser diffraction technique. The particle size and the specific surface area are significant properties in any adsorption process. The particle size distribution for EB bio-char, pine cone bio-char and kaolin are shown in Fig.3.15 (a), (b) and (c) respectively. It was found that EB bio-char has a specific surface area of 0.56 m<sup>2</sup>/g and particle size of 10.68 μm while pine cone bio-char which has a specific surface area of 0.26 m<sup>2</sup>/g and particle size of 23.0 μm. Kaolin particles were also analysed by Malvern particle sizer and the specific surface area and particle size were calculated as 1.80 m<sup>2</sup>/g and 6.38μm respectively.

**Table 3.2:** BET surface area for the synthesized bio-char, kaolin and other published biochar.

<b>Adsorbents</b>	<b>BET surface area (m<sup>2</sup>/g)</b>	<b>Reference</b>
Raw EB	7.1	This study
EB bio-char	73	This study
Raw pine cone	15.5	This study
Pine cone bio-char	335	This study
Kaolin	30.5	This study
Kaolin	28.3	(Aries and Sen 2009)
Pecan nutshell biochar	93.0	(Zazycki et al. 2018)
Rice stalk biochar	34.7	(Sewu et al. 2017b)
Chitosan activated carbon	318.4	(Marrakchi et al. 2017)
Oxidized weed char	40.5	(Güzel et al. 2017)
Banana peel biochar	31.7	(Zhou et al. 2017)
Kelp seaweed biochar	312	(Sewu et al. 2017a)

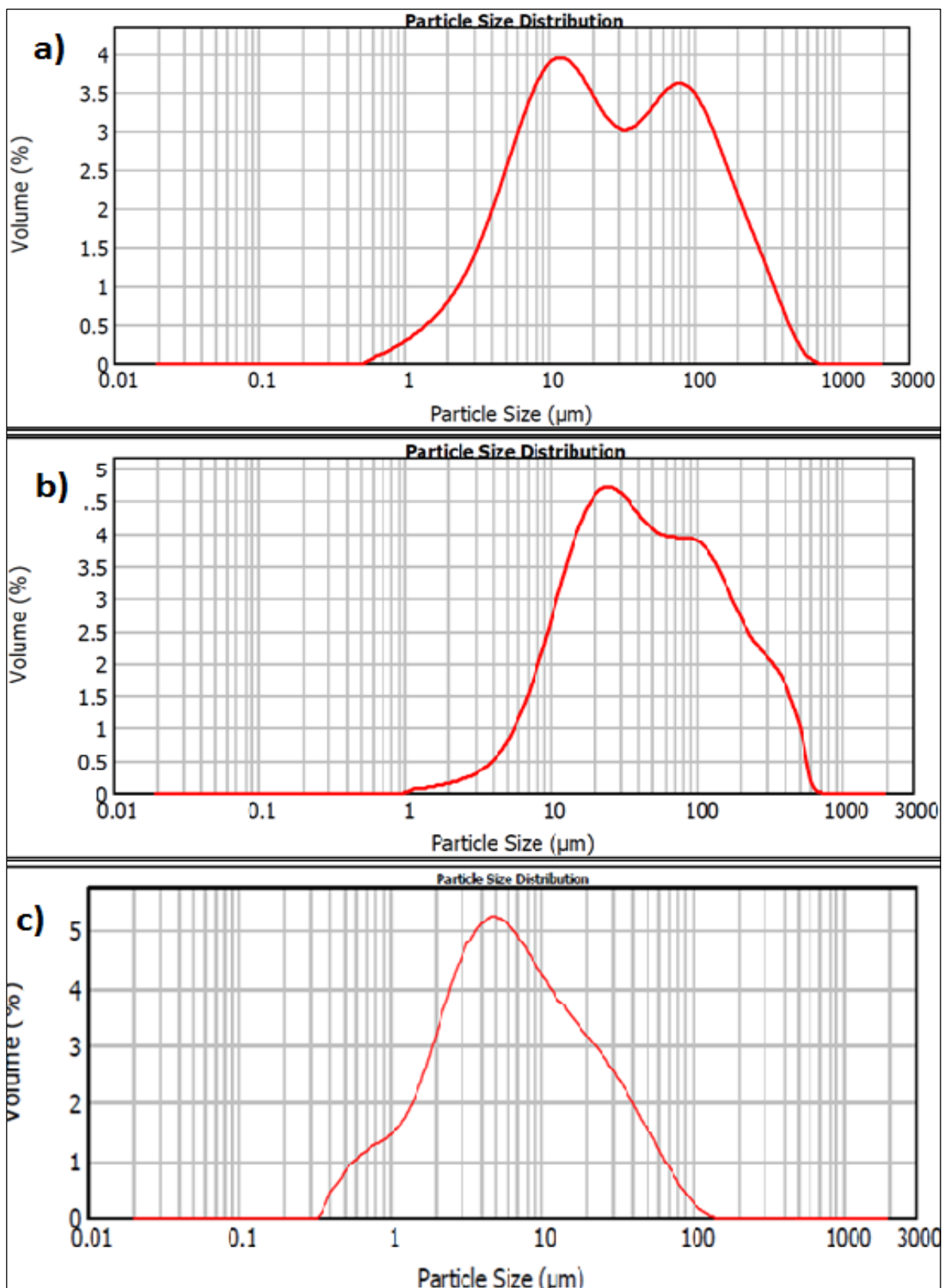


**Figure 3.15:** Malvern particle sizer analysis (a) EB biochar, (b) pine cone biochar and (c) kaolin clay.

### 3.4.6 Point of zero charge ( $\text{pH}_{\text{zpc}}$ )

The point of zero charge ( $\text{pH}_{\text{zpc}}$ ) is used to determine when the electrical charge density on the adsorbent surface is zero. The  $\text{pH}_{\text{zpc}}$  for the various adsorbents used in this research project were determined as per solid addition method described by Nawaz et al., (Nawaz et al. 2014). A fixed amount of adsorbent (10 mg) is added to 50 ml of 0.1M of  $\text{KNO}_3$  solution (solution pH 2-12). The adsorbent- potassium nitrate mixture are placed in thermo line scientific Orbital Shaker Incubator at speed of 130 rpm for 24 hrs. The final solution pH was measured and the point of zero charge ( $\text{pH}_{\text{pzc}}$ ) for each adsorbent is calculated from the plot  $\text{pH}_{\text{(initial)}}$  (X-axis) vs.  $\Delta \text{pH}_{\text{(initial-final)}}$  (Y-Aix) as shown in Fig.3.16. The point of zero charge ( $\text{pH}_{\text{pzc}}$ ) for EB biochar and pine cone biochar were calculated as 9.5 and 8.5 respectively as shown in Fig 3.16 (a) and (b) . These results are similar with other point of zero charge for various published bio-char adsorbents such as Weed char ( $\text{pH}_{\text{pzc}}= 8.0$ ) (Güzel et al. 2017) and Rice stalk biochar ( $\text{pH}_{\text{pzc}}= 8.6$ ) (Sewu et al. 2017b). Further, the point of zero charge for kaolin clay was observed from Fig.3.16(c) as 6.5 which is consistent with other published (Aries and Sen 2009)

When the solution pH is lower than ( $\text{pH}_{\text{pzc}}$ ), the solution tends to donate more protons than hydroxide groups. Thus, the number of positively charged sites increases on the adsorbent's surface hence it favours an anionic dye adsorption due to electrostatic attraction force. Higher solution pH than the point of zero charge, the number of negatively charged sites increases and hence it does favour cationic dye and metal ions adsorptions due to electrostatic force attraction.

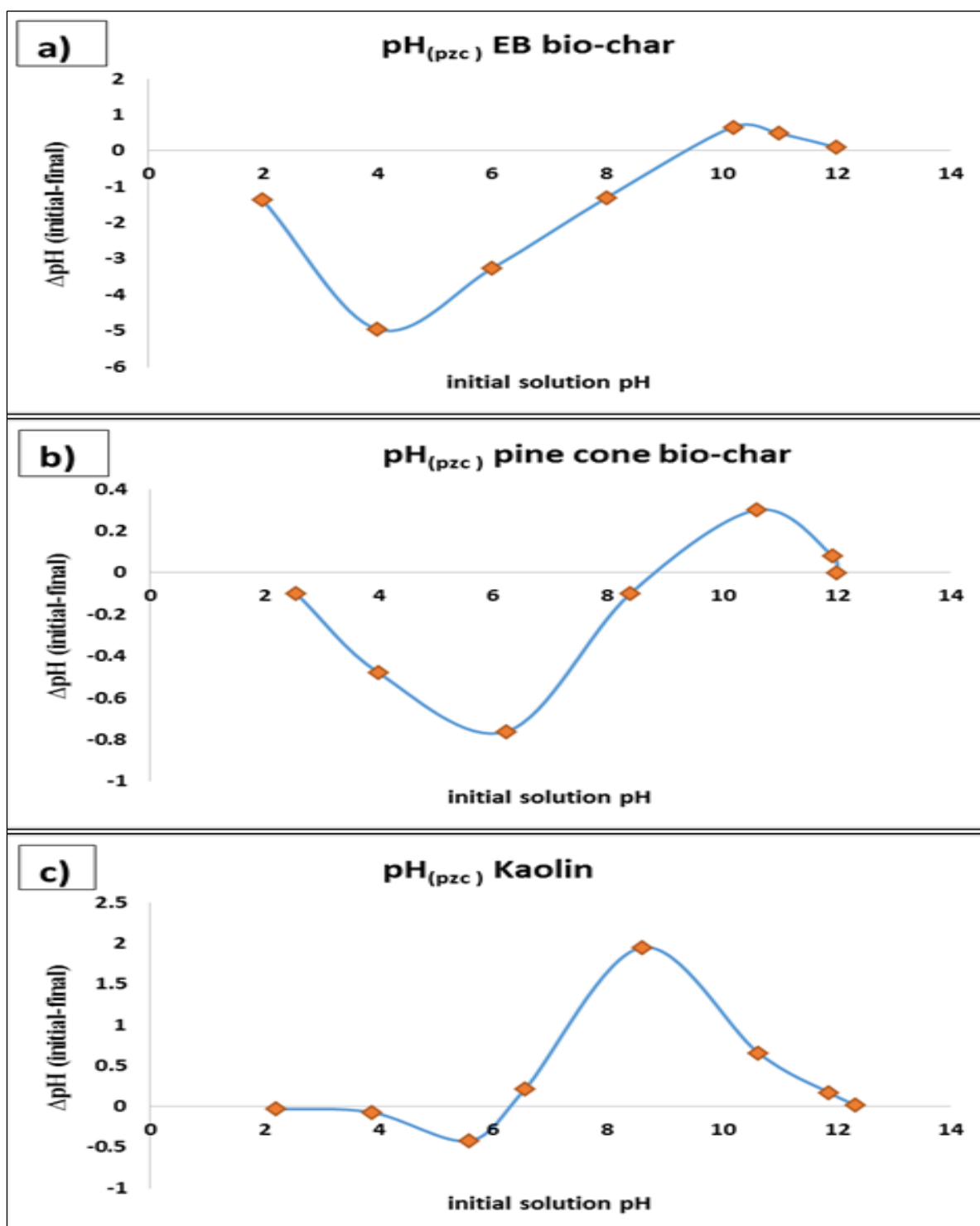


**Figure 3.16:** The point of zero charge pH pzc, a) EB bio-char, b) pine cone bio-char and c) kaolin. Mass of Adsorbent 10 mg, Volume of 0.1M  $KNO_3$  Solution 50 ml, Temp 30 °C, Shaker Speed 130 rpm and time=24 hrs.

### 3.4.7 Bulk density and yield percentage

Bulk density is the weight of powder (g) in a given unit volume (ml). It is used in this research to measure the bulk density of EB bio-char, pine cone bio-char and kaolin adsorbents by adding the adsorbent powder to fill a volumetric cylinder of a 2 ml total volume. The cylinder was tapped gently few times to ensure a smooth distribution of the adsorbent's powder. The amount of adsorbent used to fill the cylinder was measured and the bulk density was calculated as per equation (3.1). Bulk density is an important parameter for consideration in the designing of adsorption towers for use in pilot plant structure as well as large commercial application. The bulk density of EB bio-char was calculated as 0.42 g/cm<sup>3</sup> while pine cone bio-char was measured as 0.54 g/cm<sup>3</sup>. Also, kaolin bulk density is calculated as 0.67g/cm<sup>3</sup>.The American Water Work Association has set a lower limit on bulk density at 0.25 g/cm<sup>3</sup> for practical use Therefore, the bulk density of the synthesised EB and pine cone bio-char as well as kaolin suggests their applicability as practical adsorbents. Further, the Synthesised bio-char yield percentage is calculated as per equation (3.2).

$$\text{Bulk Density} = \frac{\text{mass of dry sample(g)}}{\text{total volume used (ml)}} \quad (3.1)$$

$$\text{Yield (\%)} = \frac{w_c}{w_o} \times 100 \quad (3.2)$$

Where  $w_c$  is the dry weight (g) of the synthesised bio-char and  $w_o$  is the dry weight (g) of precursor. The yield percentage of EB bio-char and pine cone bio-char were presented in Table 3.3 and calculated as 36% and 33.5% respectively. Table 3.3 compares the percentage yield for various biochar thus indicates the validity and applicability of synthesized EB biochar and pine cone biochar.



**Table 3.3:** Bulk density and percentage yield for EB bio-char, pine cone bio-char and kaolin.

<b>Adsorbents</b>	<b>Bulk density (g/cm<sup>3</sup>)</b>	<b>Bio-char Yield %</b>	<b>Reference</b>
EB bio-char	0.42	36	This study
Pine cone bio-char	0.54	33.5	This study
Kaolin	0.67	-----	This study
Banana peel biochar	-----	15.6	(Zhou et al. 2017)
Celery derived biochar	-----	33.6	(Zhang et al. 2017)
Rice stalk biochar	-----	29.8	(Sewu et al. 2017b)
Kelp seaweed biochar	-----	28.5	(Sewu et al. 2017a)
Pine cone Activated carbon	0.36	49	(Dawood et al. 2014)

### 3.5 Batch Adsorption Experiments

Batch adsorption experiments were conducted by varying the operational parameters such as the initial solution pH, adsorbent dose, initial dye concentration, ionic strength, contact time and temperature at predetermined time interval. A fixed amount of the adsorbent is mixed with 50 ml (0.05 L) of adsorbate such as Methylene blue dye or Ni (II) ions of predetermined initial concentration in a series of 125 ml plastic bottles. The mixture was placed on Thermo line scientific Orbital Shaker Incubator at constant temperature profile of 35°C and shaken speed of 130 rpm as shown in Fig.3.17. At predetermined time interval, the suspensions were taken out and filtered using micro filter of pore size 0.47 µm for Ni (II) and the filtrates were analysed using Atomic Absorption Spectrophotometer (AAS) while MB dye suspensions were

centrifuged at speed of 4700 RPM for 10 mins and the residual MB concentration was measured using UV-spectrophotometer.

The amount of MB dye and nickel ions adsorbed onto the adsorbent at time  $t$ ,  $q_t$  (mg/g) and percentage dye removal were calculated from equations (3.3) and (3.4) respectively:

$$q_t = \frac{(C_o - C_t)V}{m} \quad (3.3)$$

$$\% \text{ Adsorption} = \frac{(C_o - C_t)}{C_o} \times 100 \quad (3.4)$$

Where  $C_o$  is the initial concentration (mg/L),  $C_t$  is the concentration at any time  $t$ ,  $V$  is the volume of solution in (0.05 L) and  $m$  is the mass of the adsorbents in (g). All experiments measurements are repeated twice with  $\pm 10\%$  accuracy.



**Figure 3.17:** Thermo line scientific Orbital Shaker Incubator.

### 3.6 Isotherm Experiment

Equilibrium adsorption studies were conducted by mixing 50 ml of each MB dye (10-100 mg/L) and  $\text{Ni}^{2+}$  (10-70 mg/L) with 20 mg adsorbent powder in 125 ml plastic bottles at optimum solution pH, solution temperature and rotating speed of 130 rpm. The samples were kept for a period of up-to 210 mins which were more than sufficient to reach equilibrium. The suspensions were taken out and filtered using micro filter of pore size 0.47  $\mu\text{m}$  for Ni (II) ions while MB dye samples were centrifuged. The residual adsorbates concentration were measured by AAS for nickel ions and UV spectrophotometer for MB dye. The amount of MB dye and nickel ions adsorbed onto the adsorbent at time  $t$ ,  $q_t$  (mg/g) and % Adsorption were calculated from equations (3.3) and (3.4) respectively. All experiments measurements are repeated twice with  $\pm 10\%$  accuracy.

### 3.7 Desorption Process

Desorption studies help to explain the adsorption mechanism, recovery of the adsorbate and adsorbent regeneration. Adsorbent regeneration is very important in real and practical adsorption system as it helps to minimise the waste and recovery of the adsorbent for further use. The MB loaded adsorbent was separated from dye solution by centrifugation and dried in the oven at temperature profile of 75  $^{\circ}\text{C}$  for a period of 5 hrs. Fixed amount of dried- dye saturated adsorbent was agitated with 25 ml desorbing solution for predetermined equilibrium time using Orbital Shaker Incubator with similar conditions as obtained in the adsorption study. The final dye concentration of the supernatant is measured using the UV Spectrophotometer. The desorbing solutions used were acetone and deionized water at various solution pH (1.7-11).

### **3.8 Packed-Bed Column Adsorption Design and Experimental Procedure**

The continuous flow packed-bed column adsorption experiments were conducted in a vertical Perspex glass column with an internal diameter of 2.5 cm and height of 30 cm. The column was packed with two separated layers of pine cone bio-char and kaolin adsorbents at a volume ratio of 1:1 respectively. A known quantity of each adsorbent was added into the packed bed column to the total desired bed height of 3, 5 and 7 cm. The adsorbents were supported by two supporting layers of pre-equilibrated glass wool to ensure a securely packed arrangement as shown in Fig.3.18. A thin layer (~2 mm) of sand is placed at the top of the adsorbents to avoid bed fluidized due to the adsorbent fine particle size. Circular caps were used to enclose both ends of the column. A variable speed peristaltic pump (supplied by ProMinent Fluid Controls, NSW, and Australia) was placed at the bottom of the packed bed column to inject influent MB dye solution into the packed bed column at a constant inlet flow rate. The column experiments were conducted at room temperature. The effect of bed height (3, 5 and 7 cm), inlet flow rate (13, 15 and 17 ml/min) and initial MB dye concentration (50, 100 and 150 mg/L) on the BTCs were investigated. Effluent samples were collected at predetermined time intervals and the final MB concentration were measured using the UV Spectrophotometer. The BTCs obtained under various process conditions were fitted against various kinetics models was explained in section 2.11.

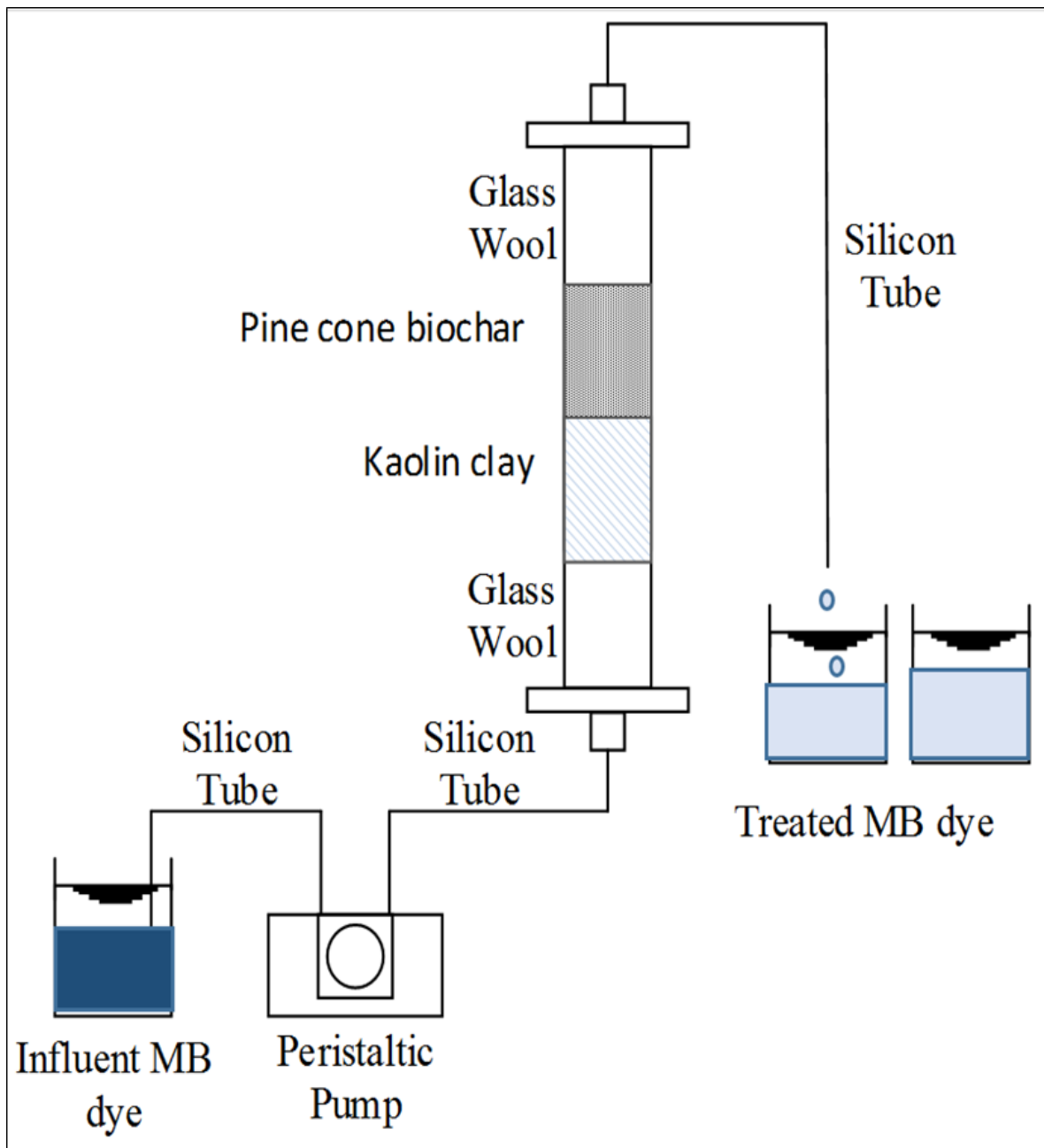


**Figure 3.18:** Schematic diagram of packed pine cone biochar and kaolin bed column

### 3.9 Summary

Chapter three provides detailed description on biochar synthesis process, kaolin clay and other chemical used in the removal of organic Methylene blue dye and Ni (II) ions from wastewater by adsorption. Pine cone bio-char and EB bio-char were synthesized through a slow pyrolysis process at various temperature profiles. Also, kaolin clay was selected as another adsorbent in the removal of organic Methylene blue dye in this study. The effectiveness of the synthesized biochar and kaolin adsorbents in the removal of organic MB dye were explored through batch adsorption kinetics and isotherm adsorption experiments. Also, the removal of inorganic Ni (II) ions from its aqueous solution into pine cone bio-char has been evaluated through a batch adsorption study. Further, packed pine cone biochar and kaolin bed column experiments has been carried out in the removal of MB dye from its aqueous phase as shown in Fig 3.18. Batch adsorption kinetics and isotherm experimental results are presented in the following chapters.

The physical and chemical characterization of the synthesized EB bio-char, pine cone biochar and kaolin were utilised through the use of various instruments such as Malvern particle sizer, SEM-EDS, XRD, CHN-O analyser, BET surface area, FT-IR, point of zero charge, bio-char yield and bulk density. CHN-O analyser was found that the amount of carbon presented in EB biochar and pine cone biochar produced at temperature profile of 500°C were 60 % and 75.1 % respectively. Also, from, BET surface area analyser, it was found that pine cone bio-char has a surface area of 335 m<sup>2</sup>/g and EB bio-char surface area was calculated as 73 m<sup>2</sup>/g. Kaolin clay surface area has been calculated as 30.573 m<sup>2</sup>/g. Further, the point of zero charge (pH<sub>zpc</sub>) was calculated as 9.5, 8.5 and 6.5 for EB biochar, pine cone biochar and kaolin respectively. The physical and chemical characterization of the selected biochar and kaolin clay indicate their applicability in the removal of organic and inorganic contamination from wastewater by adsorption process.

### 3. 10 References

Afroze, S., Sen, T.K. and Ang, H.M. (2016a) "Adsorption removal of zinc (II) from aqueous phase by raw and base modified Eucalyptus sheathiana bark: Kinetics, mechanism and equilibrium study". Process Safety and Environmental Protection **102**, 336-352.

Aguayo-Villarreal, I.A., Bonilla-Petriciolet, A. and Muñiz-Valencia, R. (2017) "Preparation of activated carbons from pecan nutshell and their application in the antagonistic adsorption of heavy metal ions". Journal of Molecular Liquids **230**, 686-695.

Aries, F. and Sen, T.K. (2009) " Removal of zinc metal ion (Zn<sup>2+</sup>) from its aqueous solution by kaolin clay mineral: a kinetic and equilibrium study. ". Colloids Surf A **348**(1-3), 100-108.

Blue Mountains City Council (2009) Weeds of the Blue Mountains, <http://www.bmcc.nsw.gov.au/index.cfm>.

Dawood, S., Sen, T.K. and Phan, C. (2014) "Synthesis and characterisation of novel-activated carbon from waste biomass pine cone and its application in the removal of congo red dye from aqueous solution by adsorption". Water, Air, and Soil Pollution **225**(1).

Dill, H.G. (2016) "Kaolin: Soil, rock and ore: From the mineral to the magmatic, sedimentary and metamorphic environments". Earth-Science Reviews **161**(Supplement C), 16-129.

Fabbri, B., Gualtieri, S. and Leonardi, C. (2013) "Modifications induced by the thermal treatment of kaolin and determination of reactivity of metakaolin". Applied Clay Science **73**, 2-10.

González, J.A. and del C. Ruiz, M. (2006) "Bleaching of kaolins and clays by chlorination of iron and titanium". Applied Clay Science **33**(3), 219-229.

Güzel, F., Saygılı, H., Akkaya Saygılı, G., Koyuncu, F. and Yılmaz, C. (2017) "Optimal oxidation with nitric acid of biochar derived from pyrolysis of weeds and its application in removal of hazardous dye methylene blue from aqueous solution". Journal of Cleaner Production **144**(Supplement C), 260-265.

Hu, X., Ding, Z., Zimmerman, A.R., Wang, S. and Gao, B. (2015) "Batch and column sorption of arsenic onto iron-impregnated biochar synthesized through hydrolysis". Water Research **68**, 206-216.

Isahak, W.N.R.W., Hisham, M.W.M. and Yarmo, M.A. (2012) "Highly porous carbon materials from biomass by chemical and carbonization method: A comparison study". Journal of Chemistry **2013**.

Ji, F., Li, C., Zhang, J. and Deng, L. (2011) "Efficient decolorization of dye pollutants with  $\text{LiFe}(\text{WO}_4)_2$  as a reusable heterogeneous Fenton-like catalyst". Desalination **269**(1-3), 284-290.

Li, Y., Meas, A., Shan, S., Yang, R. and Gai, X. (2016) "Production and optimization of bamboo hydrochars for adsorption of Congo red and 2-naphthol". Bioresource Technology **207**(Supplement C), 379-386.

Liang, S., Guo, X., Feng, N. and Tian, Q. (2010) "Isotherms, kinetics and thermodynamic studies of adsorption of  $\text{Cu}^{2+}$  from aqueous solutions by  $\text{Mg}^{2+}/\text{K}^{+}$  type orange peel adsorbents". Journal of Hazardous Materials **174**(1-3), 756-762.

Marrakchi, F., Ahmed, M.J., Khanday, W.A., Asif, M. and Hameed, B.H. (2017) "Mesoporous-activated carbon prepared from chitosan flakes via single-step sodium hydroxide activation for the adsorption of methylene blue". International Journal of Biological Macromolecules **98**, 233-239.

Morton, J.F. (1980) The Australian pine or beefwood (*Casuarina equisetifolia* L.) an invasive "weed" tree in Florida, pp. 87-95.

Mukherjee, K., Kedia, A., Jagajjanani Rao, K., Dhir, S. and Paria, S. (2015) "Adsorption enhancement of methylene blue dye at kaolinite clay-water interface influenced by electrolyte solutions". RSC Advances **5**(39), 30654-30659.

Nawaz, S., Bhatti, H.N., Bokhari, T.H. and Sadaf, S. (2014) "Removal of Novacron Golden Yellow dye from aqueous solutions by low-cost agricultural waste: Batch and fixed bed study". Chemistry and Ecology **30**(1), 52-65.



Sewu, D.D., Boakye, P., Jung, H. and Woo, S.H. (2017a) "Synergistic dye adsorption by biochar from co-pyrolysis of spent mushroom substrate and *Saccharina japonica*". Bioresource Technology **244**(Part 1), 1142-1149.

Sewu, D.D., Boakye, P. and Woo, S.H. (2017b) "Highly efficient adsorption of cationic dye by biochar produced with Korean cabbage waste". Bioresource Technology **224**, 206-213.

Van Vinh, N., Zafar, M., Behera, S.K. and Park, H.-S. (2015) "Arsenic(III) removal from aqueous solution by raw and zinc-loaded pine cone biochar: equilibrium, kinetics, and thermodynamics studies". International Journal of Environmental Science and Technology **12**(4), 1283-1294.

Yin, C.Y., Aroua, M.K. and Daud, W.M.A.W. (2007) "Impregnation of palm shell activated carbon with polyethyleneimine and its effects on Cd<sup>2+</sup> adsorption". Colloids and Surfaces A: Physicochemical and Engineering Aspects **307**(1-3), 128-136.

Zazycki, M.A., Godinho, M., Perondi, D., Foletto, E.L., Collazzo, G.C. and Dotto, G.L. (2018) "New biochar from pecan nutshells as an alternative adsorbent for removing reactive red 141 from aqueous solutions". Journal of Cleaner Production **171**(Supplement C), 57-65.

Zhang, T., Zhu, X., Shi, L., Li, J., Li, S., Lü, J. and Li, Y. (2017) "Efficient removal of lead from solution by celery-derived biochars rich in alkaline minerals". Bioresource Technology **235**, 185-192.

Zhao, H. and Lang, Y. (2018) "Adsorption behaviors and mechanisms of florfenicol by magnetic functionalized biochar and reed biochar". Journal of the Taiwan Institute of Chemical Engineers **88**, 152-160.

Zhou, N., Chen, H., Xi, J., Yao, D., Zhou, Z., Tian, Y. and Lu, X. (2017) "Biochars with excellent Pb(II) adsorption property produced from fresh and dehydrated banana peels via hydrothermal carbonization". Bioresource Technology **232**, 204-210.

*Every reasonable effort has been made to acknowledge the owners of copyright material. I would be pleased to hear from any copyright owner who has been omitted or incorrectly acknowledged.*

# **CHAPTER 4**

**ADSORPTIVE REMOVAL OF  
METHYLENE BLUE DYE FROM  
AQUEOUS SOLUTION BY  
EUCALYPTUS BARK BIO-CHAR:  
KINETICS, ISOTHERM,  
THERMODYNAMIC AND PROCESS  
DESIGN STUDY.**

## ABSTRACT\*

Eucalyptus bark biomass based bio-char adsorbent was synthesized and tested its effectiveness in the removal of aqueous phase Methylene blue dye by batch adsorption. The synthesized bio-char adsorbent was characterized by SEM-EDS, XRD, FTIR and CHN analyzer. Various textural characteristics such as BET surface area, pore size, bulk density, point of zero charge were also determined. The effects of various temperature profile on the production of EB bio-char were studied and the optimum temperature of 500°C was identified. Batch adsorption kinetics study showed that the amount of dye adsorbed  $q_t$  (mg/g) depends on various physicochemical process parameters such as initial solution pH, dye concentration, temperature, adsorbent dose, salt concentration and presence of SDS surfactant. It was found that the extent of MB dye adsorption by EB bio-char increased with the increase of initial dye concentration, contact time, temperature and solution pH, but decreased with the increase of adsorbent dose and salt concentration. The optimum adsorption conditions were found at an initial dye concentration of 100 mg/L, initial solution pH of 11.3, adsorbent dose of 10 mg and solution temperature of 55°C. Furthermore, pseudo-first-order, pseudo-second-order and intra-particle diffusion models were fitted to examine the adsorption kinetics and mechanism of adsorption. Equilibrium data were best represented by Langmuir isotherm model and the maximum adsorption capacity of bio-char was determined which is comparative to commercial activated carbon. Thermodynamic parameters suggested that the adsorption process was an endothermic, spontaneous and physical in nature. Furthermore, a single-stage batch adsorber design for the MB dye onto EB bio-char particles was presented based on the Langmuir isotherm model equation. These results indicated EB biomass was a good and cheap precursor for the production of effective and environmental friendly bio-char adsorbent.

---

\*This work has been published in Desalination and Water Treatment Journal (Dawood, S., Sen, T.K. and Phan, C., 2016. Adsorption removal of Methylene Blue (MB) dye from aqueous solution by bio-char prepared from Eucalyptus *sheathiana* bark: kinetic, equilibrium, mechanism, thermodynamic and process design. Desalination and Water Treatment 57(59), 28964-28980. DOI:10.1080/19443994.2016.1188732).

## 4.1 Introduction

This chapter investigates the potential effectiveness of eucalyptus bark based bio-char as an adsorbent in the removal of organic Methylene blue dye from its aqueous solution by adsorption process. The production of bio-char does not require the use of chemicals such as acids and bases and hence it is considered to be environmental friendly adsorbent. The synthesized EB bio-char under various production temperature were studied and the most efficient temperature profile was identified at 500°C as described in section 3.4.1 of chapter 3. Batch adsorption kinetics study was carried out as described in section 3.5 and 3.6 of chapter 3 under various physicochemical process parameters such as initial solution pH, dye concentration, temperature and adsorbent dosage. Also, the effect of salt concentration was studied due to its presence in a textile effluent. Batch experimental data were analysed with pseudo-first-order, pseudo-second-order and intra-particle diffusion models to determine the adsorption kinetics and mechanism of adsorption. Further, to understand the adsorption isotherm and MB dye-EB bio-char interaction, the equilibrium data were simulated by Langmuir and Freundlich isotherm models. The EB bio-char effectiveness in the removal of MB dye under various physicochemical parameters were compared to other published adsorbents including commercial activated carbon. Thermodynamic parameters were studied to determine the process feasibility. Also, desorption study was carried out to determine the reusable capacity of EB bio-char and to identify the mechanism of adsorption. Furthermore, a single-stage batch adsorber was designed for the MB dye-EB bio-char based on equilibrium experimental data to gain insight into the process dynamics.

## 4.2 Results and discussion

### 4.2.1 Effect of initial solution pH on MB dye adsorption.

The effect of solution pH on the MB dye adsorption from its aqueous solution by EB bio-char was studied in the pH range of 4.8-11.3 as shown in Fig.4.1. It was found that the amount of dye adsorbed  $q_t$  (mg/g) and percentage dye removal were increased with the increase of contact time and then slowed down until equilibrium reached at 150 mins as shown in Fig.4.1 (a) and (b) respectively. Further, it was found that the amount of MB dye adsorbed,  $q_e$  (mg/g) was increased from 26.7 mg/g to 40.3 mg/g with the increase of the solution pH of 4.8-11.3 as shown in Fig.4.1 (c). Also, it was found that the amount of dye removal efficiency increased from 53.4 % to 80.5 % with the increases in solution pH from 4.8 to 11.3 for a fixed initial dye concentration of 20 mg/L and adsorbent dose of 0.02 g as shown in Fig.4.1 (c). EB bio-char was determined from solid addition method which is described in section 3.4.6 of chapter 3 and was calculated as 9.5.

EB biochar becomes more negatively charged at solution pH higher than 9.5 due to dissociation of oxygenated group and formation of MB– oxygen binding sites. In contrast, at lower solution pH, the adsorbent becomes more positively charged. With the increase in solution pH, the number of negatively charged sites increases and hence it does favour for a cationic MB dye adsorption due to electrostatic attraction forces. Lower solution acidic pH gives lower adsorption of MB dye which is due to presences of excess  $H^+$  ions thus competing with the cationic group of dye for the adsorption sites. A similar MB dye adsorption behaviour was reported by various adsorbents such as wheat straw biochar (Liu et al. 2012), mango leaf (Uddin et al. 2017) and weed biochar (Güzel et al. 2017). The experimental data and detailed calculation on the adsorption capacity  $q_t$  (mg/g) and percentage dye removal are presented in Appendix A-1.

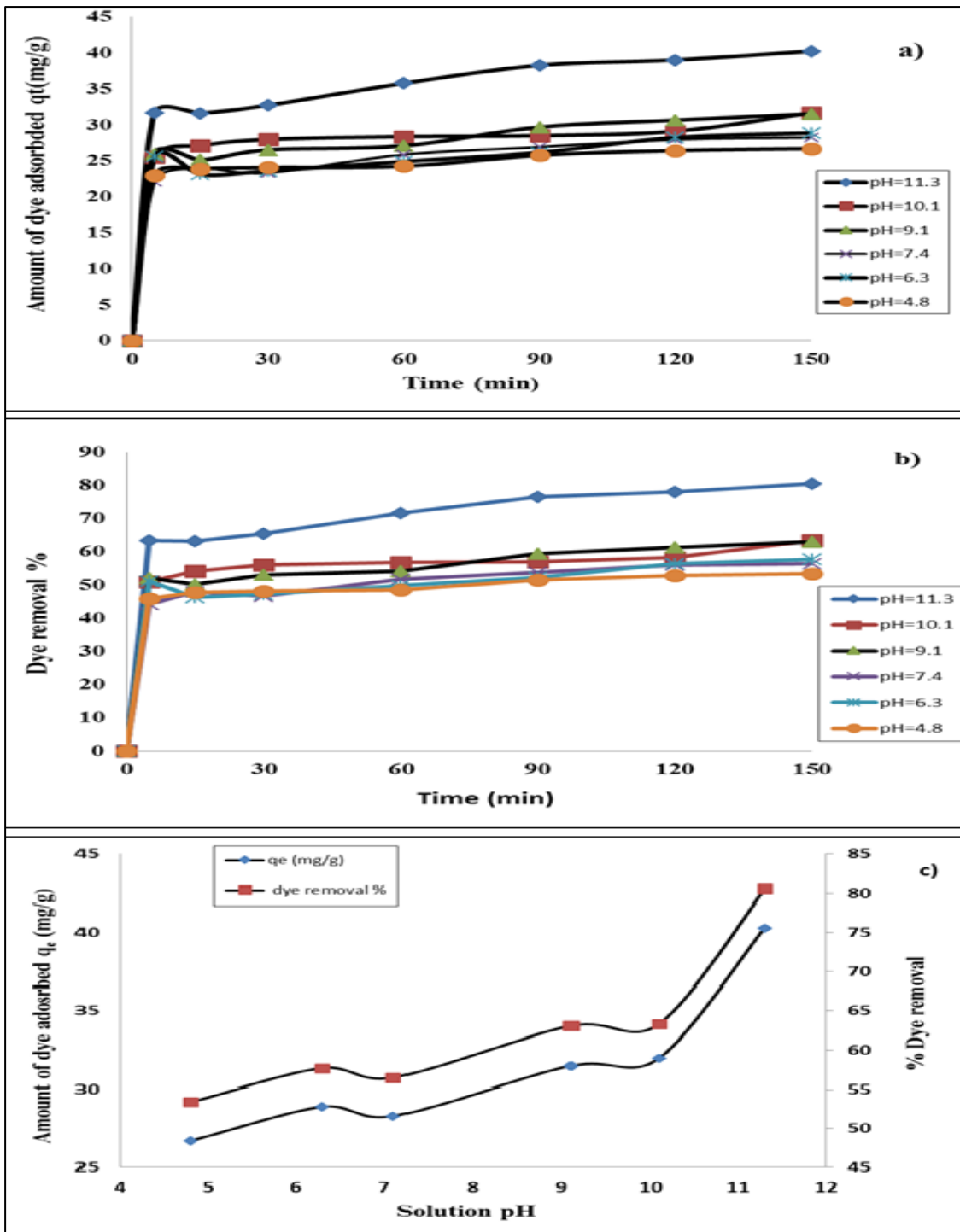


**Figure 4.1:** Effect of initial solution pH on the adsorption of MB dye on EB bio-char. (a) amount of dye adsorbed  $q_t$  (m/g) at time  $t$ , (b) percentage dye removal at time  $t$  and (c) amount of dye adsorbed  $q_e$  (m/g) and dye removal at equilibrium. Adsorbent dose=20 mg, V= 50 ml, Initial dye Concentration =20 mg/L, T= 35 °C and rotating Speed= 130 rpm.

#### 4.2.2 Effect of EB bio-char dosage on MB dye adsorption

The effectiveness of various EB bio-char doses on MB dye adsorption were studied to determine the most economical minimum dosage. It was found that the amount of dye adsorbed  $q_t$  (mg/g) and percentage dye removal were increased rapidly with the increase of contact time and then slowed down until equilibrium reached at 150 mins as shown in Fig.4.2 (a) and (b) respectively. Also, it was observed that the increase in EB bio-char dose from 10 mg to 30 mg resulted in decreased in amount of dye adsorbed ( $q_e$ ) from 56.8 mg/g to 25.5 mg/g while the percentage dye removal was increased from 56.8 % to 80.5 % for the same adsorbent dose range as shown in Fig.4.2 (c). Furthermore, it was observed a slight decrease in the dye removal percentage from 80.5% to 76.6 % upon the increases of EB biochar dose form 20 mg to 30 mg. This experiment was carried out at alkaline solution pH of 11.3 thus higher removal efficiency was observed.

The decreases in amount of dye adsorbed  $q_e$  (mg/g) with increasing the adsorbent mass as shown in Fig.4.2 (c) is due to the split in the flux or the concentration gradient between solute concentration in the solution and the solute concentration in the surface of the adsorbent (Dawood et al. 2014, Vadivelan and Kumar 2005). Also, higher EB bio-char doses lead to a very fast adsorption of MB dye on the adsorbent surface which gives a lower adsorbate concentration in bulk solution compared to low adsorbent dose situation. Thus, with increasing adsorbent dose, the amount of MB dye adsorbed per unit mass of adsorbent  $q_e$  (mg/g) decreased (Han et al. 2009). At lower adsorbent dose, the adsorbate dye molecules are more easily accessible hence the dye removal per unit mass of adsorbent is high. The increases in the percentage dye removal with the increases of adsorbent dosage could be attributed to the increase in the adsorbent surface areas hence the number of available active sites due to the increase in the adsorbent mass. A similar behaviour was reported for MB dye adsorption by various biomass and biomass based biochar and activated carbon such as waste tea activated carbon (Gokce and Aktas 2014), pine tree leaves (Yagub et al. 2012) and raw eucalyptus bark (Afroze et al. 2016). The experimental data and detailed calculation on the adsorption capacity  $q_t$  (mg/g) and percentage dye removal are presented in Appendix A-2.

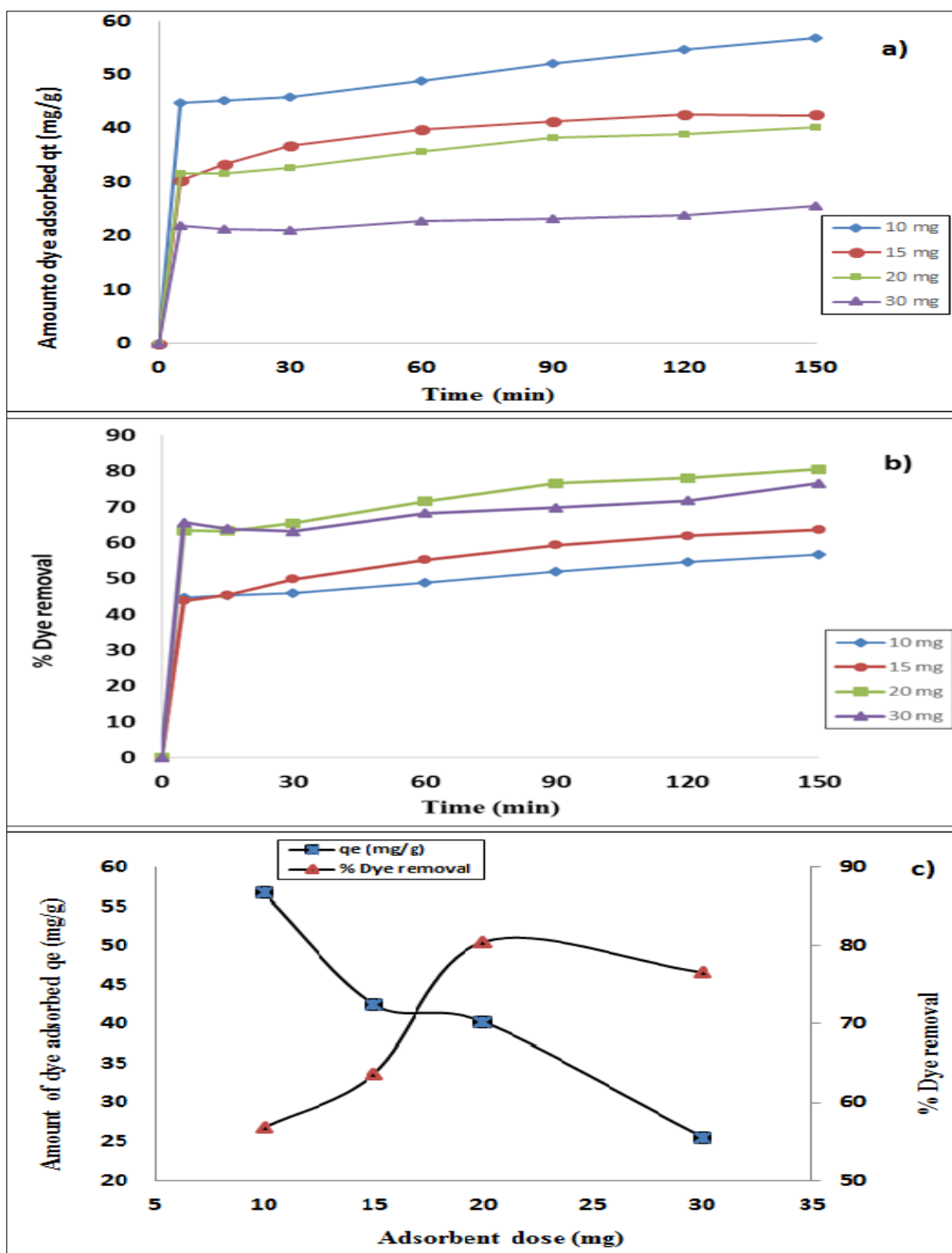


**Figure 4.2:** Effect of adsorbent dose on MB dye adsorption. (a) Amount of dye adsorbed  $q_t$  (m/g) at time  $t$ , (b) percentage dye removal at time  $t$  and (c) amount of dye adsorbed  $q_e$  (m/g) and dye removal at equilibrium. Solution pH= 11.3, V= 50 ml, Initial dye Concentration =20 mg/L, T= 35 °C and rotating Speed= 130 rpm.



### 4.2.3 Effect of contact time and initial MB dye concentration

The initial dye concentration has a significant effect on its removal from aqueous solutions. In this research work, MB dye concentration was varied from 10 to 100 mg/L while other process parameters were kept constant. The effects of various initial MB dye concentration and contact time on the amount of dye adsorbed  $q_t$  (mg/g) and percentage dye removal were studied and results are presented in Fig.4.3 (a) and (b) respectively. It was observed from Fig 4.3 (a) and (b) that the amount of adsorption capacity  $q_t$  (mg/g) and percentage dye removal were increased rapidly with increasing contact time at all initial dye concentrations and then slowed down with the increases of contact time till equilibrium is attained within 150 min.

Further, from Fig.4.3 (c), it is observed that the amount of dye adsorbed  $q_e$  (mg/g) increased from 19.3 mg/g to 92.1 mg/g with increasing MB dye concentration from 10 mg/L to 100 mg/L respectively. The initial dye concentration provides a high driving force to overcome the resistance to the mass transfer of dye between the aqueous solution and the solid phase of a fixed adsorbent dose. Simultaneously the percentage MB dye removal was decreased from almost 80.5 % to 36.8 % with increasing initial concentration of MB dye from 10 mg/L to 100 mg/L as shown in Fig.4.3 (c). Higher initial dye concentration causes the accumulation of dye molecules on the surface of the sorbent and thus leads to the saturation of available active sites and hence decreases the amount of dye removal (Dawood and Sen 2012, Yagub et al. 2014). Also, an increase in initial dye concentration enhances the interaction between the adsorbate and adsorbent and thus leads to an increase in amount of dye adsorbed. Similar observation in the removal of MB dye by various adsorbents was reported by other researchers such as weed biochar (Güzel et al. 2017), water bamboo leaf (Zhu et al. 2016), tea waste activated carbon (Borah et al. 2015) and kenaf fibre char (Mahmoud et al. 2012). The experimental data and detailed calculation on the adsorption capacity  $q_t$  (mg/g) and percentage dye removal are presented in Appendix A-3.

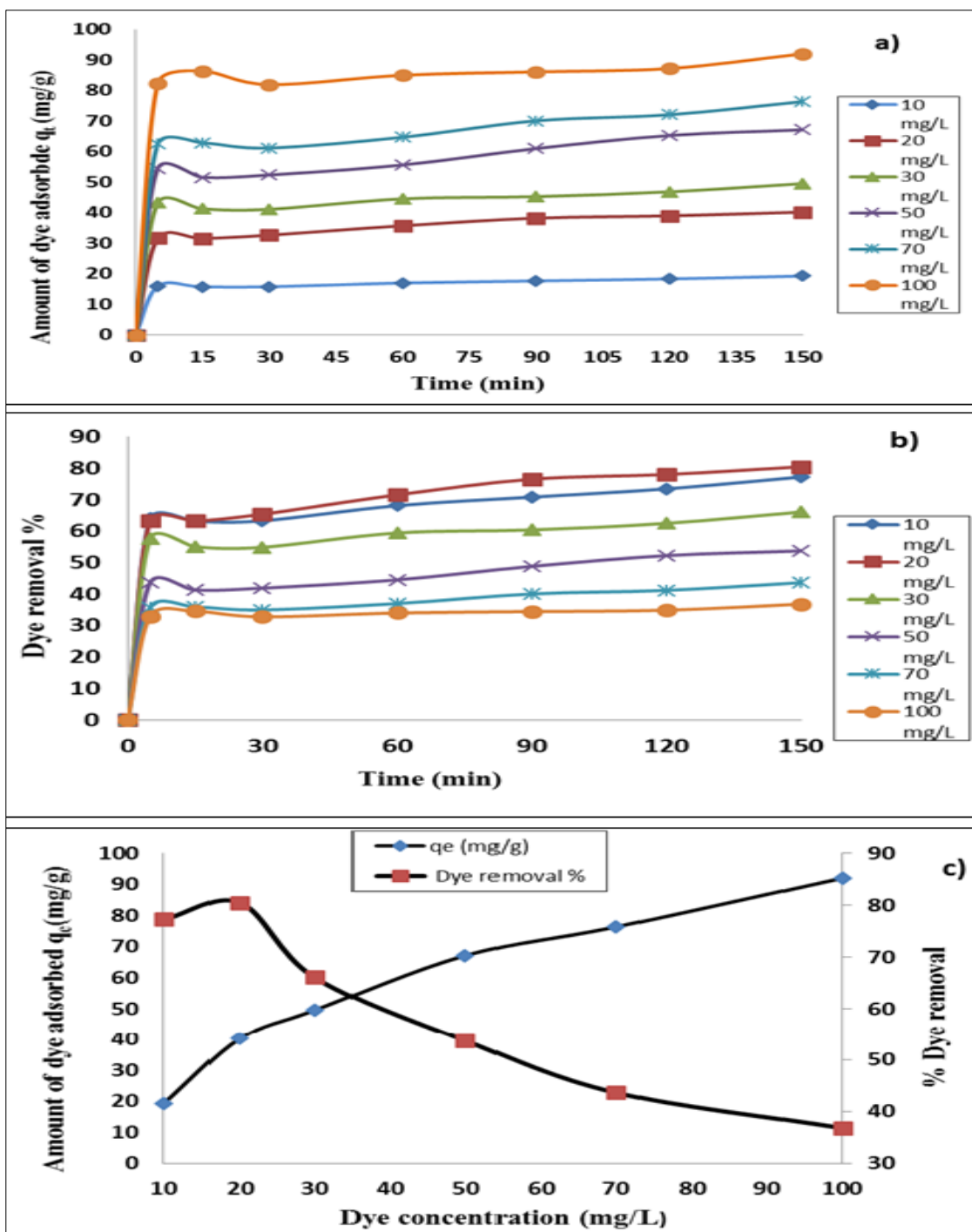


**Figure 4.3:** Effect of MB dye concentration and contact time on MB dye adsorption by EB bio-char. (a) amount of dye adsorbed  $q_t$  (m/g) at time  $t$ , (b) percentage dye removal at time  $t$  and (c) amount of dye adsorbed  $q_e$  (m/g) and dye removal at equilibrium. Adsorbent dose=20 mg, V= 50 ml, solution pH=11.3, T= 35 °C and rotating Speed= 130 rpm.

#### 4.2.4 Effect of solution temperature and thermodynamics studies

Textile wastewater Industrial effluents are generally being discharged at high temperature of 35°C to 45°C (Ghaly et al. 2014). The adsorption kinetics and the thermodynamic behaviour of MB dye adsorption on EB bio-char were determined by varying MB dye solution temperature from 25°C to 55°C while other process parameters were kept constant as shown in Fig 4.4. The amount of MB dye adsorbed  $q_t$  (mg/g) was increased from 29.0 mg/g to 44.0 mg/g with the increase of solution temperature respectively as shown in Fig.4.4. Also, it was found that the increase the solution temperature of MB dye solution from 25°C to 55°C resulted in an increase in percentage dye removal from 57.9% to 87.9% respectively. Increasing the adsorption capacity with the increase of temperature indicates an endothermic adsorption process. This is also supported by thermodynamic parameter  $\Delta G^0$  which is decreased with increases in solution temperature as shown in Table 4.1. Increasing solution temperature leads to increase the mobility of the dye molecules and thus enhance the mass transfer of dye molecules from its liquid phase to the solid phase of sorbent (Salleh et al. 2011, Yagub et al. 2014).

The thermodynamics parameters include Gibb's free energy change ( $\Delta G^0$ ), entropy change ( $\Delta S^0$ ) and enthalpy changes ( $\Delta H^0$ ) were calculated from Fig 4.5 as per equation (2.16) and (2.17) respectively and are presented in Table 4.1. Generally, The Gibbs energy change ( $\Delta G^0$ ) plays a significant factor for determining the degree of spontaneity of the adsorption process. Gibb's free energy change ( $\Delta G^0$ ) value was found to decrease from -20.65 KJ/mole to -26.82 KJ/mole with the increase of solution temperature from 25 °C to 55 °C respectively. Higher negative value ( $\Delta G^0$ ) indicates an energetically favourable and spontaneous adsorption proFrom Table 4.1, the enthalpy change ( $\Delta H^0$ ) was calculated as 40.61 kJ mol<sup>-1</sup> which indicates a physical adsorption controlled by Van der Waals force of interaction. The positive value of enthalpy change ( $\Delta H^0$ ) indicates the adsorption was an endothermic process in nature.

An endothermic adsorption process of Methylene blue (MB) dye removal by various adsorbents were also reported such as Chitosan based activated carbon (Marrakchi et al. 2017), raw eucalyptus bark (Afroze et al. 2016), pine tree leaves (Yagub et al. 2012) and citrus peel (Shakoor and Nasar 2016). The entropy change value ( $\Delta S^0$ ) was calculated as 0.21 KJ /mole.K which indicates favorable randomness at the solid/liquid interface. Similar trend has been reported in the removal of MB dye by various adsorbents such as citrus peel (Shakoor and Nasar 2016), tea waste activated carbon (Borah et al. 2015) and palm tree based activated carbon (AlOthman et al. 2014). The experimental data and detailed calculation on the adsorption capacity  $q_t$  (mg/g) and percentage dye removal are presented in Appendix A-4.

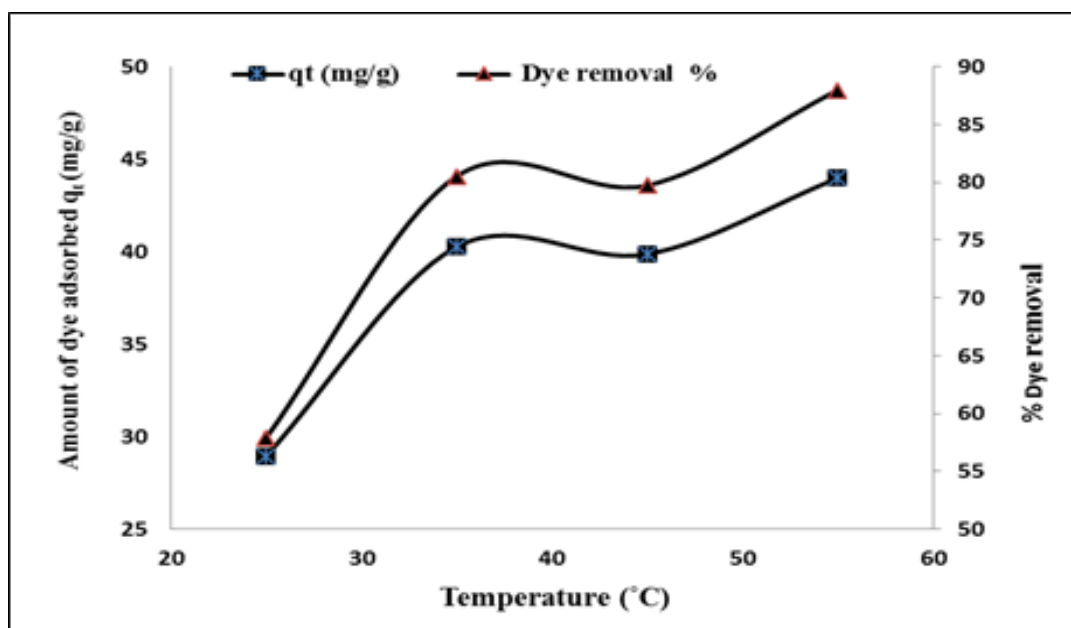


**Figure 4.4:** Effect of solution temperature on MB dye adsorption capacity  $q_e$  (m/g) and percentage dye removal. Solution pH=11.3, V= 50 ml, Initial dye Concentration =20 mg/L, adsorbent dose= 20 mg and rotating Speed= 130 rpm.

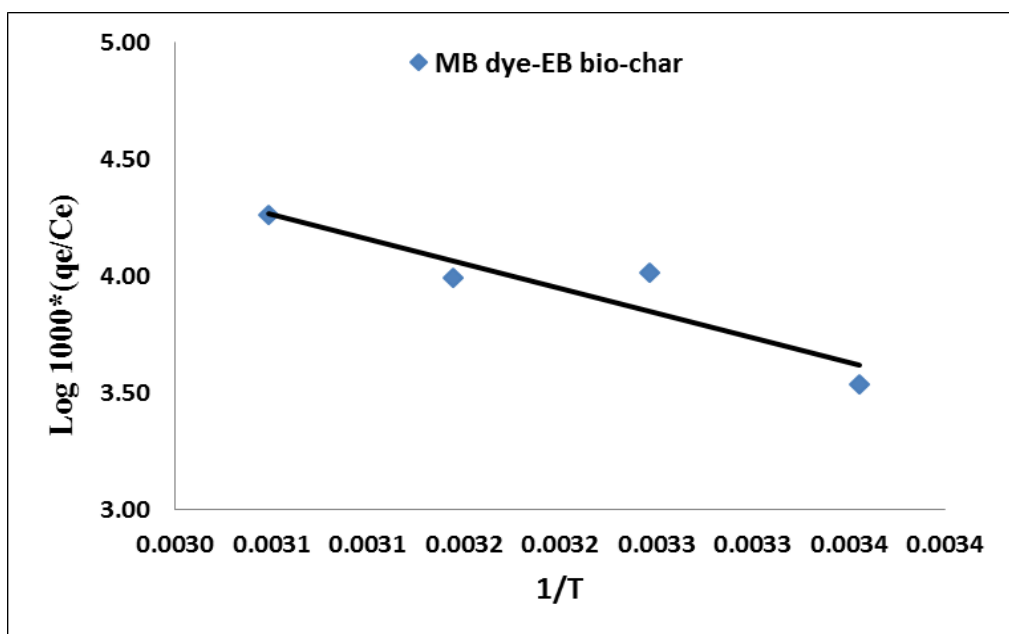


**Figure 4.5:** Plot of Van't Hoff equation for MB dye- EB bio-char adsorption.

**Table 4.1:** Thermodynamics parameters for MB dye adsorption onto EB bio-char at various solution temperature.

Temp (K)	$\Delta G^\circ$ (KJ/mole)	$\Delta H^\circ$ (KJ /mole)	$\Delta S^\circ$ (KJ /mole.K)
298	-20.65	40.61	0.21
308	-22.71	40.61	0.21
318	-24.76	40.61	0.21
328	-26.82	40.61	0.21

#### 4.2.5 Effect of monovalent and divalent presence of salts on adsorption

Dye bearing effluents from textile industries contain significant amount of salts and hence the effect of salt on the adsorption process must be considered. The presence of these salts in dye effluents affects both electrostatic and non-electrostatic interactions between the adsorbent surface and dye molecules and therefore affects the adsorption capacity (Afroze et al. 2015). The effect of salts presented in MB dye effluent has been evaluated in this project by using monovalent sodium chloride salt (NaCl) and divalent calcium chloride (CaCl<sub>2</sub>) salt respectively. Kinetic experiments have been carried out by mixing initial salt concentrations of 150 mg/L, 250 mg/L and 400 mg/L with MB dye solution at a fixed volume ratio of 1:9 respectively for 150 mins. Other process parameters such as solution pH, adsorbent dose, temperature, initial dye concentration and shaker speed were kept constant. It was found from Fig. 4.6 (a) the amount of MB dye adsorbed  $q_e$  (mg/g) was decreased from 40.3 mg/g to 32.6 with the increase of initial sodium chloride concentration from 0 mg/L to 400 mg/L respectively. Also, increasing the initial calcium chloride salt concentration from 0 mg/L to 400 mg/L decreased the amount of MB dye adsorbed  $q_t$  from 40.3 mg/g to 29.8 mg/g as shown in Fig 4.6 (a). Further, the percentage dye removal was decreased from 80.5% to 65.3% and from 80.5% to 59.6% upon the increases of monovalent and divalent initial salt concentration from 0 mg/L to 400 mg/L respectively as shown in Fig.4.6 (b).

This trend indicates that the presence of external ionic strength in the aqueous solution could be attributed to the competitive effect between the cationic MB dye and the cations from the salts (Na<sup>+</sup> and Ca<sup>2+</sup>) for the available active site which governs the adsorption process (Li et al. 2011). Also, the increase in the salt concentration (Na<sup>+</sup>) may changes the equilibrium constant between the interface and the bulk of the liquid thus affecting the adsorption operation. Generally, at the adsorbent inner sphere, the overall electrostatic interaction with bulk surface is not affected by ionic presence while at the outer sphere structure, the ions remain bonded to its original position and the attraction electrostatic is affected significantly to the presence of ionic strength. Also, the presence of (Na<sup>+</sup>) and (Ca<sup>2+</sup>) ions have a limited effect on the binding efficiency between the adsorbent and the adsorbate as the ions presence may compete with the adsorbate for binding sites on the adsorbent surface and hence reduce the adsorption capacity. Further, the molecular weight size, atomic radii and

atomic charge of ions contribute significantly towards the efficiency of the adsorption process. Calcium ions have higher contribution to ionic strength and positive charge compared to sodium ions and hence the effect of  $\text{Ca}^{2+}$  ions on adsorption process is more serious than  $\text{Na}^+$ . The decreases of MB dye adsorption onto various adsorbents upon the increase of ionic strength concentration were reported such as kaolin and zeolite clays (Rida et al. 2013), pine tree leaves (Yagub et al. 2012) and modified sawdust (Zou et al. 2013). The experimental data and detailed calculation on the adsorption capacity  $q_t$  (mg/g) and percentage dye removal are presented in Appendix A-5.

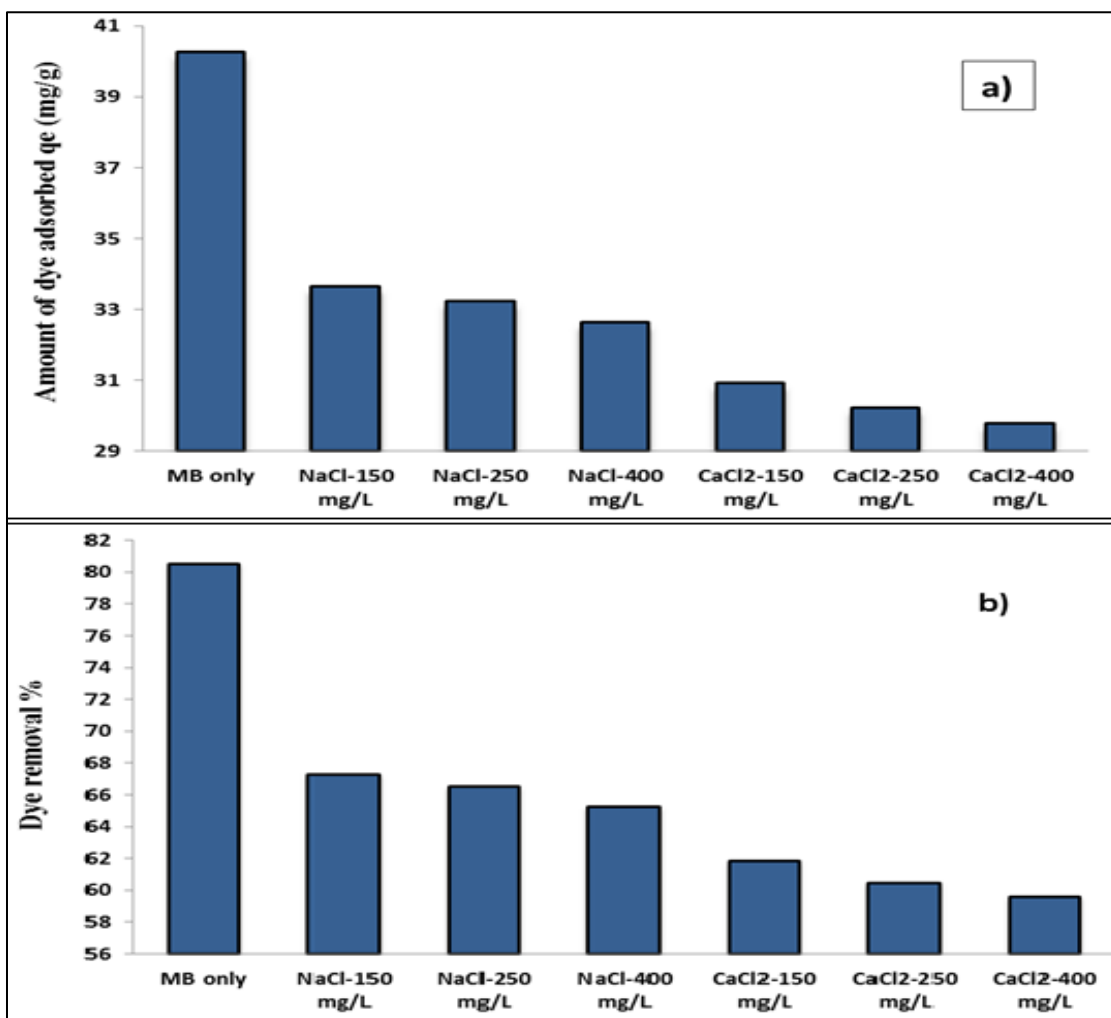


**Figure 4.6:** Effect of NaCl and CaCl<sub>2</sub> salts on MB dye adsorption, a) Amount of dye adsorbed  $q_e$  (mg/g), b) Percentage Dye removal. Adsorbent dose=20 mg, initial dye concentration= 20 mg/L, V= 50 ml, solution pH=11.3, T= 35 °C and rotating Speed= 130 rpm.

## 4.3 Applications of Adsorption Kinetic Models

In order to understand the mechanism of adsorption, rate of reaction and the transient behaviour of dye adsorption process, adsorption kinetics must be studied under various physio-chemical process parameters such as adsorbent dose, initial adsorbate concentration, ionic strength, solution pH, and temperature and contact time. Lagergren Pseudo-first-order, Pseudo-second-order and Intra-particles-diffusion kinetic models were fitted with the experimental data to determine the suitability of these models. The theory of these models was described in section 2.8 of chapter 2. The linear regression coefficient ( $R^2$ ) and the error function Chi-square ( $\chi^2$ ) were used to test the validity of these models. Chi-square ( $\chi^2$ ) is a statistic test used to evaluate the accuracy and the applicability of Pseudo-first-order and Pseudo-second-order kinetics models by determine the error between experimental ( $q_e$ ) and calculated ( $q_e$ ) and it is calculated from equation (2.4).

### 4.3.1 Application of pseudo-first-order adsorption kinetic model

Analysing the batch adsorption kinetic experiments play a major role in the designing, optimisation and performance of industrial adsorption column. The nature of the adsorption process depends on physical and chemical characteristics of the adsorbent and on the system conditions (Dawood and Sen 2012). The applicability of pseudo-first-order model was tested by fitting the experimental data under various physico-chemical process parameters into equation (2.6). The calculated amount of dye adsorbed  $q_e$  (mg/g) values were obtained from the intercept of the linearized form of the plots  $\log (q_e - q_t)$  verses time ( $t$ ) as shown in Fig.4.7 and the fitted kinetic parameters were presented in Table 4.2. It was observed that the adsorption capacity  $q_e$  (mg/g) was increased with the increase in initial dye concentration, solution pH and temperature but decreased with the increase of adsorbent dose and ionic strength. The linear regression coefficient ( $R^2$ ) values were found in the range of 0.64 to 0.84 and the calculated ( $q_e$ ) values were significantly lower than the experimental equilibrium adsorption capacity ( $q_e$ ) as shown in Table 4.2. Low linear regression coefficient ( $R^2$ ) values, lower calculated adsorption capacity  $q_{e(calculated)}$  in compare to experimental adsorption capacity  $q_{e(exp)}$  as well as the high error value from ( $\chi^2$ ) test indicate



the inaccuracy and inapplicability of pseudo-first-order model kinetic model to the experimental data.

**Table 4.2:** Fitted pseudo-first-order kinetic parameters under various process conditions in the removal of MB dye by EB biochar.

<b>System Parameters</b>	<b><math>q_e</math> (mg/g), Experimental</b>	<b><math>K_f</math> (<math>\text{min}^{-1}</math>)</b>	<b><math>q_e</math> (mg/g), Calculated</b>	<b><math>(\chi^2)</math></b>	<b><math>R^2</math></b>
<b>Initial dye Concentration (mg/L)</b>					
<b>10</b>	19.3	0.03	2.8	97	0.719
<b>20</b>	40.3	0.04	4.2	305	0.774
<b>30</b>	49.6	0.04	4.3	473	0.639
<b>50</b>	61.1	0.04	5.8	530	0.711
<b>70</b>	76.5	0.04	5.9	831	0.634
<b>100</b>	92.1	0.04	4.9	1564	0.587
<b>Solution pH</b>					
<b>11.3</b>	40.3	0.02	3.3	415	0.774
<b>10.1</b>	31.7	0.04	3.3	243	0.647
<b>9.1</b>	30.2	0.04	3.9	180	0.711
<b>7.4</b>	31.9	0.04	3.5	228	0.845
<b>6.3</b>	27.9	0.05	3.9	145	0.657
<b>4.8</b>	26.7	0.02	2.3	264	0.640
<b>Solution temperature</b>					
<b>25<sup>0</sup>C</b>	28.9	0.04	2.9	228	0.510
<b>35<sup>0</sup>C</b>	40.3	0.04	4.2	305	0.774
<b>45<sup>0</sup>C</b>	39.9	0.05	5.3	226	0.742
<b>55<sup>0</sup>C</b>	44.0	0.04	5.3	284	0.710
<b>Initial adsorbent dosage (mg)</b>					
<b>10</b>	56.8	0.04	5.1	518	0.704
<b>15</b>	42.5	0.04	4.9	282	0.770
<b>20</b>	40.3	0.04	4.2	305	0.773
<b>30</b>	25.5	0.04	3.2	153	0.640
<b>Initial NaCl concentration(mg/L)</b>					
<b>150</b>	33.6	0.01	2.5	388	0.640
<b>250</b>	33.3	0.04	3.1	290	0.679
<b>400</b>	32.6	0.02	2.6	354	0.682
<b>Initial CaCl<sub>2</sub> concentration (mg/L)</b>					
<b>150</b>	30.9	0.03	2.5	318	0.609
<b>250</b>	30.2	0.05	4.1	168	0.689
<b>400</b>	29.8	0.04	2.7	275	0.759

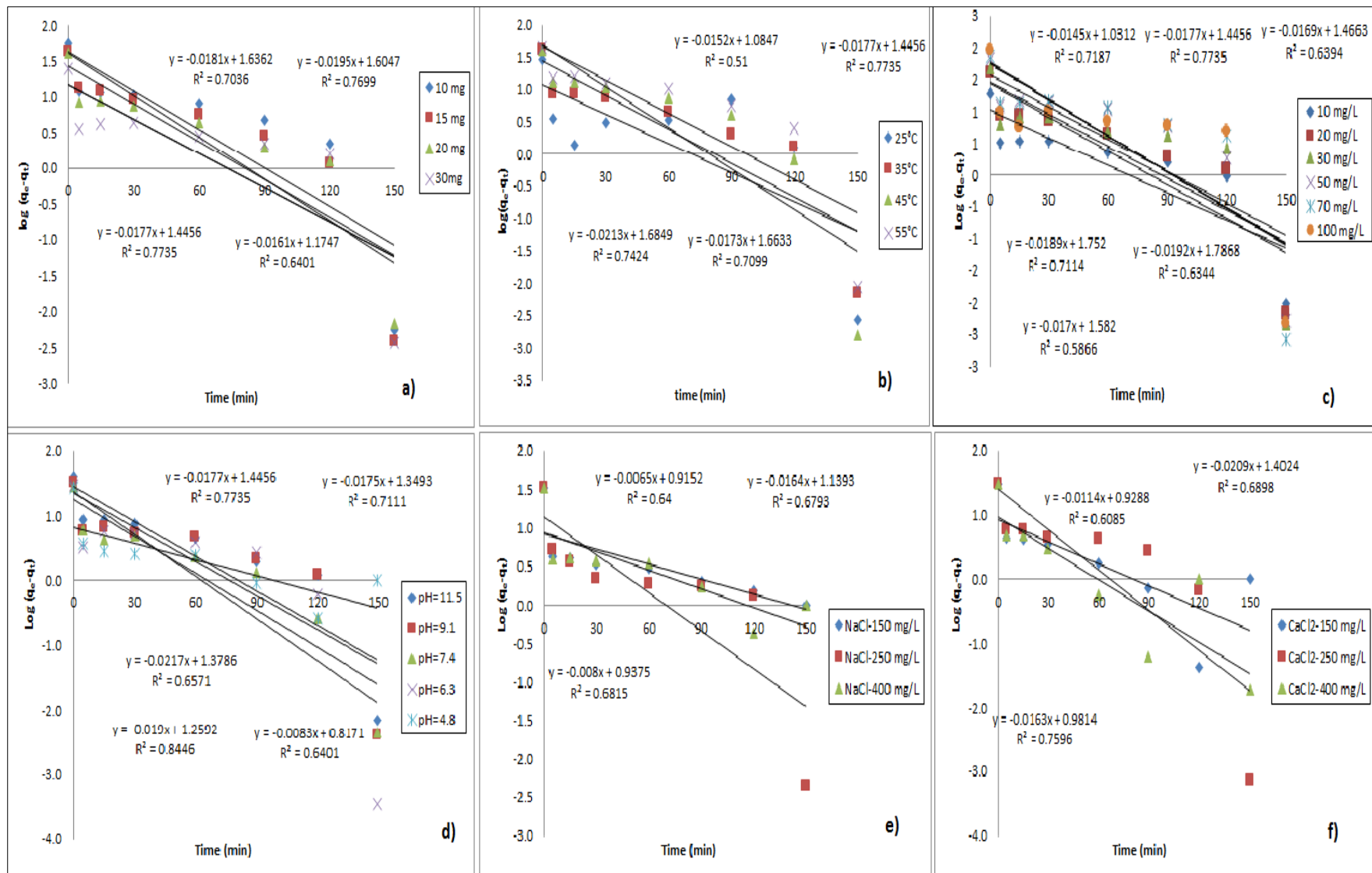


**Figure 4.7:** Pseudo-first-order kinetic model fitting for MB dye adsorption by EB bio-char at various a) adsorbent dosage, b) solution temperature, c) initial MB concentration, d) solution pH, e) initial NaCl concentration and f) initial CaCl<sub>2</sub> concentration.

### 4.3.2 Application of pseudo-second-order kinetic model

The applicability of pseudo-second-order model was tested by fitting the experimental data under various physico-chemical process parameters into equation (2.8). The calculated amount of dye adsorbed  $q_e$  (mg/g) was obtained from the slope of the linearized plots of  $(t/q_t)$  vs. time ( $t$ ) as shown in Fig.4.8. The various pseudo-second-order fitted parameters under different physio-chemical process parameters are tabulated in Table.4.3. It was observed from Table 4.3 that the calculated amount of dye adsorbed ( $q_e$ ) values were almost identical to the experimental amount of dye adsorbed ( $q_e$ ). Also, it was observed from Table 4.3, the adsorption capacity of MB dye on EB bio-char increased with the increase in initial dye concentration, solution pH and temperature and decreases with the increase of adsorbent dose and ionic strength. Pseudo-second order rate constant  $K_s$  (g/mg.min) was found to decrease with the increases of solution temperature and initial dye concentration up to 70 mg/L. This may be due to the lower competition for the sorption sites at lower concentration. At higher dye concentrations and solution temperature, the competition for the surface-active sites will be high and hence lower adsorption rates are attained. The initial adsorption rate  $h$  (mg/g.min) was calculated as per equation (2.9) and it was increased with the increase of adsorbent dose. Furthermore, higher linear regression coefficients ( $R^2$ ) values were found in range of 0.97 to 0.99 as presented in Table 4.3. Also, Chi-square ( $\chi^2$ ) values were found to be lower than 0.045 for various process parameters as shown in Table4.3. Therefore, high linear regression coefficient ( $R^2$ ) values and low error values presented from Chi-square ( $\chi^2$ ) test indicate the accuracy and applicability pseudo-second-order model.

**Table 4.3:** Fitted pseudo-second-order kinetic parameters at various process conditions in the removal of MB dye by EB biochar.

System Parameters	$q_e$ (mg/g), Experimental	$K_s$ (g/mg.min)	$q_e$ (mg/g), Calculated	$h$ (mg/g.min)	$(\chi^2)$	$R^2$
<b>Adsorbent Dosage (mg)</b>						
10	56.8	0.004	56.5	13.9	0.001	0.996
15	42.5	0.005	42.9	8.5	0.005	0.996
20	40.3	0.007	40.3	10.9	0.000	0.997
30	25.5	0.013	25.1	8.2	0.009	0.996
<b>Initial dye Concentration (mg/L)</b>						
10	19.3	0.015	19.1	5.5	0.002	0.996
20	40.3	0.007	40.3	10.9	0.000	0.996
30	49.6	0.007	48.8	16.2	0.014	0.997
50	67.2	0.003	67.1	13.8	0.000	0.996
70	76.5	0.003	75.2	19.3	0.021	0.995
100	92.1	0.006	90.1	52.6	0.045	0.998
<b>Solution pH</b>						
11.3	40.3	0.007	40.3	10.9	0.000	0.997
10.1	30.2	0.020	29.9	18.0	0.005	0.999
9.1	31.9	0.008	31.8	8.2	0.001	0.996
7.4	28.3	0.011	28.5	9.1	0.002	0.998
6.3	28.9	0.009	28.7	7.5	0.001	0.995
4.8	26.7	0.017	26.7	12.5	0.000	0.999
<b>Solution temperature</b>						
25 <sup>o</sup> C	28.9	0.013	27.6	9.5	0.063	0.997
35 <sup>o</sup> C	40.3	0.007	40.3	10.9	0.000	0.996
45 <sup>o</sup> C	39.9	0.004	40.3	6.1	0.005	0.998
55 <sup>o</sup> C	43.9	0.003	43.9	5.9	0.000	0.995
<b>Initial NaCl concentration (mg/L)</b>						
150	33.6	0.015	33.1	16.0	0.008	0.998
250	33.3	0.020	32.7	21.0	0.006	0.999
400	32.6	0.012	32.6	13.0	0.000	0.998
<b>Initial CaCl<sub>2</sub> concentration (mg/L)</b>						
150	30.9	0.015	31.2	14.8	0.002	0.999
250	30.2	0.009	30.1	8.3	0.000	0.996
400	29.8	0.018	30.3	16.3	0.008	0.999

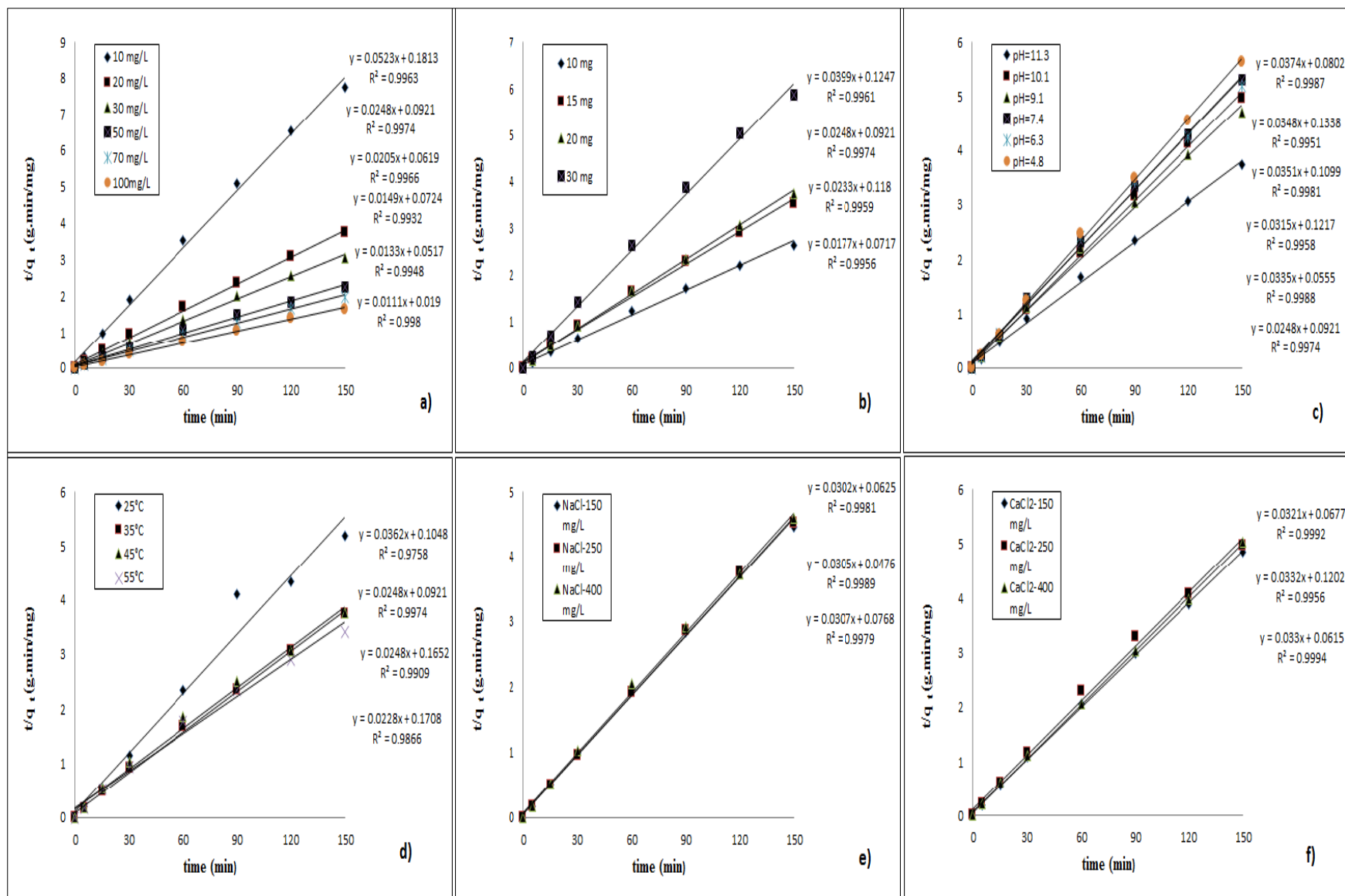


**Figure 4.8:** Pseudo-second-order kinetic model fitting for MB dye adsorption by EB bio-char at various a) initial MB concentration, b) adsorbent dosage, c) solution pH, d) solution temperature, e) initial NaCl concentration, and f) initial CaCl<sub>2</sub> concentration.

### 4.3.3 Intra-particles-diffusion model and mechanisms of adsorption

The sorption process of solid/liquid phases is generally identified by either an external mass transfer occurred on the boundary layers of the adsorbent or through an intra-particle diffusion or both. The most commonly used technique for identifying the mechanism involved in the sorption process is presented by fitting the experimental data onto Intra-particle diffusion model as per equation (2.10) where  $k_{id}$  ( $\text{mg/g min}^{0.5}$ ) is the intra-particle diffusion rate constant. Intra-particle adsorption process consist of multi steps where migration of the dye molecules from the bulk solution to the surface of the sorbent take place, diffusion through the boundary layer to the surface of the sorbent, adsorption at sites and followed by intra-particle diffusion into the interior of the sorbent (Konicki et al. 2013). The adsorption mechanism and the dynamic behaviour of methylene blue dye adsorption onto EB bio-char have been evaluated by fitting the experimental data into Intra-particle diffusion model. Intra-particle diffusion plots of the amount of dye adsorbed ( $q_t$ ) versus the square roots of contact ( $t$ )<sup>0.5</sup> for various process parameters such as initial dye concentration, solution pH, adsorbent dose, temperature and ionic strength of monovalent and divalent salts are presented in Fig4.9.

It was found that the removal of MB dye by EB bio-char adsorbent was rapid at the initial period of contact time and then became slow and almost stable with the increases in contact time. This trend indicates the multistage of adsorption where the MB dye solution is adsorbed due to the external mass transfer followed by intra particle diffusion respectively (Arias and Sen 2009, Sen et al. 2011). The overall rate of adsorption is controlled by the slowest step, which may be either film diffusion or pore diffusion. All the plots presented in Fig.4.9 give two or more intercepting lines depending on the actual mechanism where none of these plots give linear straight line segment passing through the origin. This trend shows that both film diffusion and intra-particle diffusion occurred simultaneously and the adsorption of MB dye onto EB bio-char particles is controlled by a fast rate film diffusion at earlier stages.

Furthermore, the diffusion coefficient ( $D_p$ ) depends on the surface properties of adsorbents and it was calculated from equation (2.11) where ( $r_0$ ) is the radius of the adsorbent particle (cm). The half-life ( $t^{0.5}$ ) was calculated from equation (4.1) where  $K_s$  is the pseudo-second order rate constant (g/mg.min).

$$t^{0.5} = \frac{1}{K_s q_e} \quad (4.1)$$

The surface weighted mean diameter of EB bio-char particle was found as 10.68  $\mu\text{m}$  (radius= 5.34  $\mu\text{m}$  x 0.0001 cm = 0.000534 cm). The intra particle diffusion coefficient ( $D_p$ ) ( $\text{cm}^2/\text{s}$ ) was calculated as  $4.1 \times 10^{-11}$ ,  $3.8 \times 10^{-11}$ ,  $4.7 \times 10^{-11}$ ,  $2.9 \times 10^{-11}$ ,  $3.7 \times 10^{-11}$ ,  $8.3 \times 10^{-11}$   $\text{cm}^2/\text{s}$  for 10, 20, 30, 50, 70 and 100 mg/L respectively. Values of pore diffusion rate constants were found to be in the range of  $2.9 \times 10^{-11}$  to  $8.3 \times 10^{-11}$   $\text{cm}^2/\text{s}$  for all the adsorbent samples. Therefore, the pore diffusion role is important in this study. Furthermore, the intercept (C) values obtained from the plots presented by equation (2.10) are shown in Fig 4.9. It describes the boundary layer effect where higher C values are an indicative of higher boundary layer effect. From Fig.4.9, C values were high in the range of (8.1- 44.7) thus indicates the inapplicability of pore diffusion as the only rate-determining step in describing the dynamics of the adsorption process (Sewu et al. 2017). Moreover, the linear regression coefficient values ( $R^2$ ) shown in Table 4.4 were calculated lower than 0.722 which indicates the inaccuracy of intra-particle diffusion model. However, the influence of this model cannot be totally neglected.

**Table 4.4:** Fitted intra-particle-diffusion model parameters under different process conditions in the removal of MB dye by EB biochar.

<b>System Parameters</b>	<b><math>q_e</math> (mg/g), Experimental</b>	<b><math>K_{id}</math> (mg/g min<sup>0.5</sup>)</b>	<b><math>R^2</math></b>
<b>Adsorbent Dosage (mg)</b>			
10	56.75	3.25	0.605
15	42.46	2.88	0.722
20	40.26	2.37	0.601
30	25.53	1.37	0.523
<b>Initial dye Concentration (mg/L)</b>			
10	19.32	1.07	0.559
20	40.26	2.37	0.621
30	49.61	2.65	0.515
50	61.07	3.84	0.606
70	76.45	4.21	0.563
100	92.11	4.69	0.443
<b>Solution pH</b>			
11.3	40.26	2.37	0.621
10.1	31.67	1.63	0.497
9.1	30.22	1.80	0.581
7.4	31.89	1.66	0.599
6.3	27.98	1.57	0.529
4.8	26.71	1.47	0.511
<b>Solution temperature</b>			
25 <sup>0</sup> C	28.95	1.36	0.387
35 <sup>0</sup> C	40.26	2.37	0.621
45 <sup>0</sup> C	39.87	2.54	0.754
55 <sup>0</sup> C	44.00	2.75	0.761
<b>Initial NaCl concentration (mg/L)</b>			
150	33.64	1.78	0.488
250	33.25	1.80	0.498
400	32.63	1.77	0.504
<b>Initial CaCl<sub>2</sub> concentration (mg/L)</b>			
150	30.92	1.75	0.537
250	30.22	1.71	0.576
400	29.80	1.79	0.582



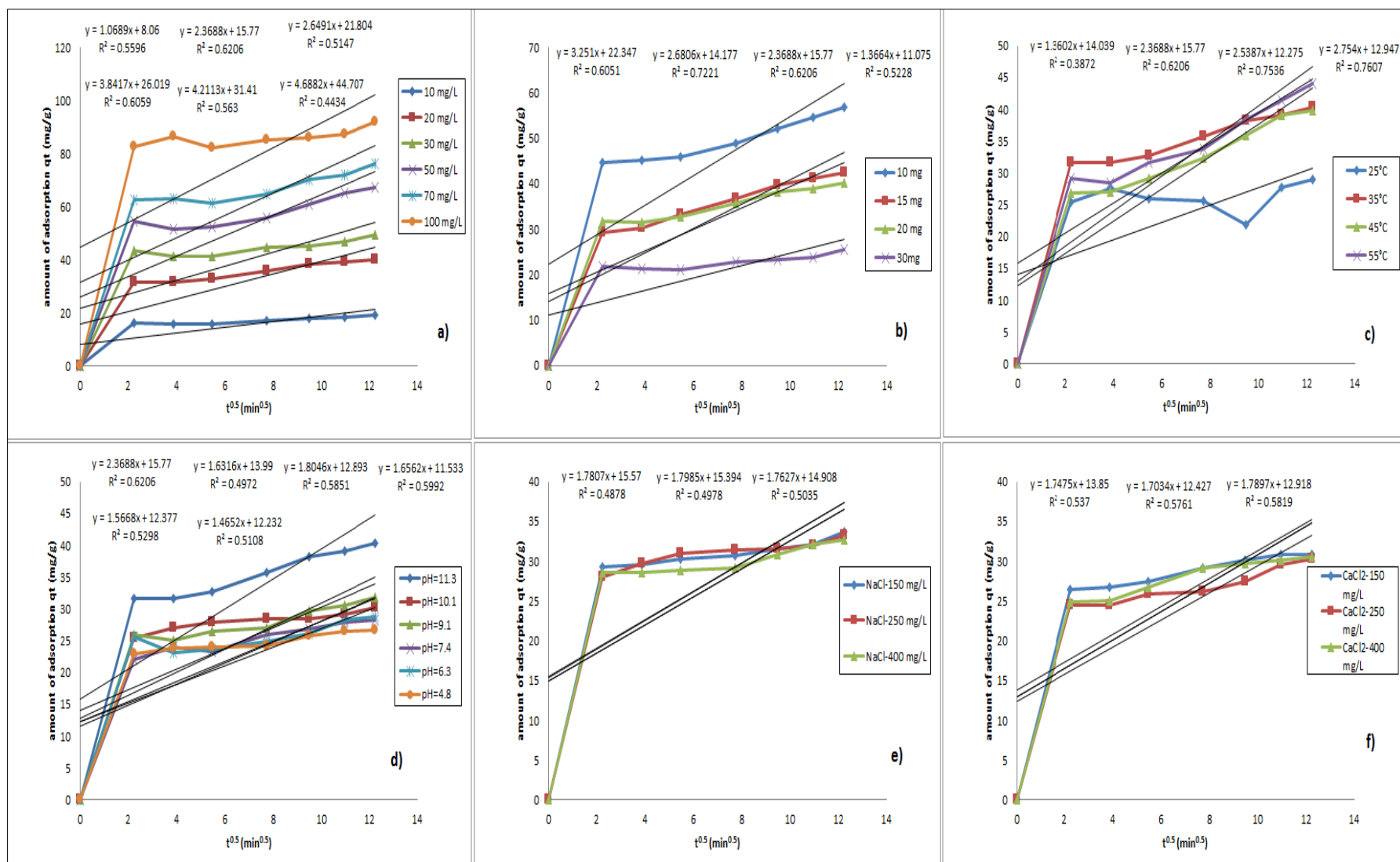


**Figure 4.9:** Intra-particle-diffusion model fitting for the adsorption of MB dye by EB bio-char at various a) initial MB concentration, b) adsorbent dosage, c) solution temperature, d) solution pH, e) initial NaCl concentration, and f) initial CaCl<sub>2</sub> concentration.

## 4.4 Adsorption Equilibrium Isotherm

The adsorption equilibrium isotherm explains the specific relationship between the concentration of adsorbate and its degree of accumulation onto adsorbent surface at constant temperature (Liu and Zhang 2015). Experimental data have been fitted into Langmuir and Freundlich isotherm models to evaluate the applicability of these models for MB-EB bio-char adsorption process. The best fitted model was determined by high linear regression coefficient ( $R^2$ ). The isotherm experiment was carried out as per section 3.6 of chapter 3 and the theory of these models are detailed in section 2.8 of chapter 2.

Langmuir isotherm is valid for monolayer adsorption onto the adsorbent surface containing a finite number of identical active sites. The equilibrium experimental data were fitted into equations (2.13) and (2.14). It was found that Langmuir (I) isotherm gives a higher linear regression coefficient ( $R^2$ ) of 0.97 compared to 0.80 for Langmuir (II) isotherm as shown in Table 4.5. The maximum adsorption capacity,  $q_m$  (mg/g) and Langmuir constant  $K_L$  (L/mg) were calculated from the slope and intercept of equations (2.13) and (2.14) as shown in Fig.4.10 (a) and (b) respectively. Further, the maximum adsorption capacity ( $q_m$ ) and Langmuir constant  $K_L$  were calculated as 104.2 mg/g and 0.09 L/g for Langmuir (I) and 94.3 mg/g and 0.12 L/g for Langmuir (II) isotherm models respectively. Also, the low separation factor ( $R_L$ ) values for various initial dye concentrations were calculated as per equation (2.15). The  $R_{(L-I)}$  for Langmuir (I) values were found to decrease from 0.53 to 0.10 with the increase of initial MB dye concentration from 10 mg/L to 100 mg/L respectively. Similar trend is observed for  $R_{(L-II)}$ . The dimensionless factor ( $R_L$ ) were found to be  $0 < R_L < 1$  thus indicates a feasible and physical adsorption process (Kaur et al. 2013).

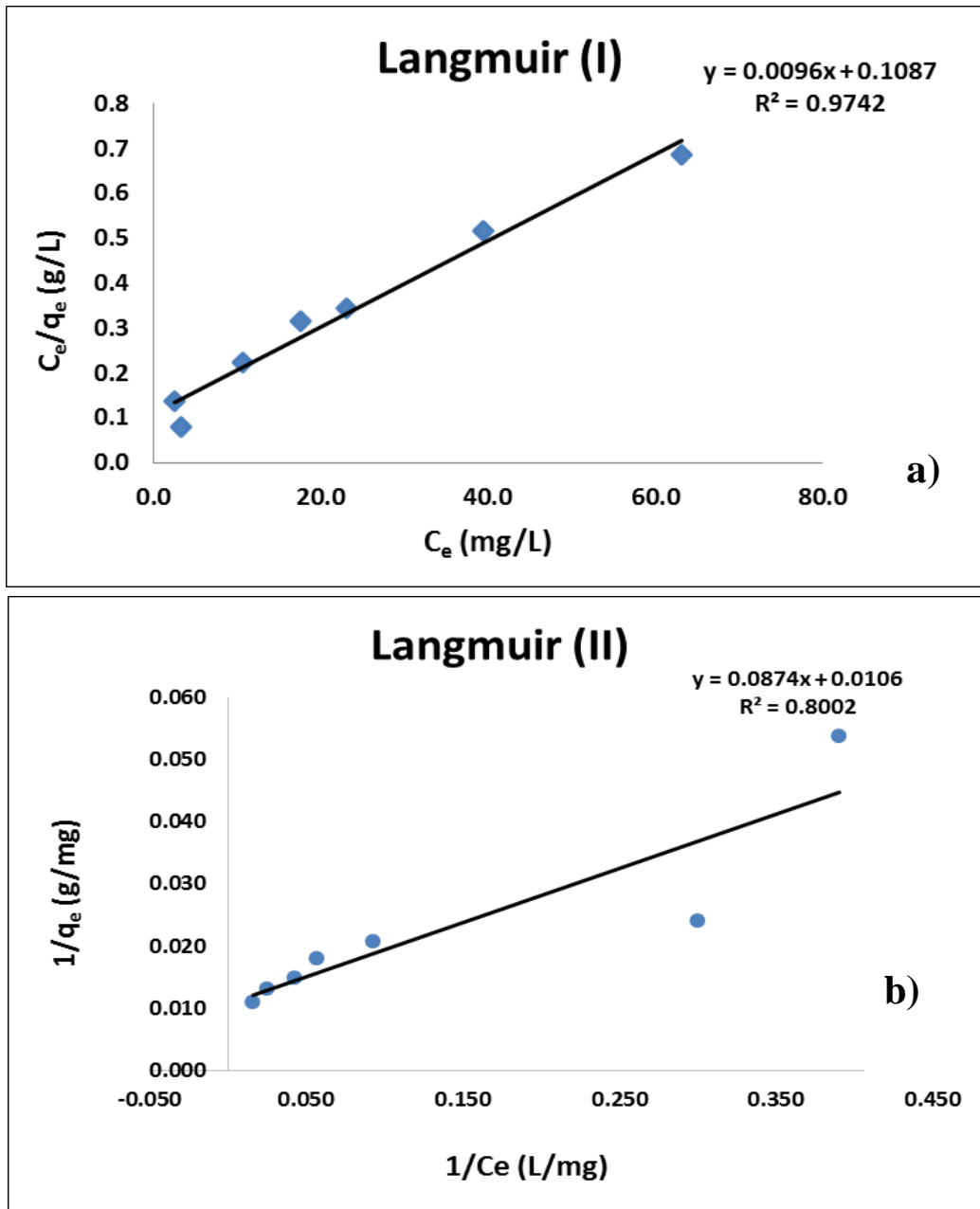


**Figure 4.10:** Langmuir isotherm plots. a) Langmuir (I) , b) Langmuir (II) , pH solution =11.3, V =50 ml, adsorbent dose=20mg, T =35 °C, rotating Speed = 130 rpm and t =210 min.

Freundlich isotherm model is valid for multilayer adsorption and is derived by assuming a heterogeneous surface with interaction between adsorbed molecules with a non-uniform distribution of heat of sorption over the surface. The equilibrium experimental data were fitted into equation (2.12). It was found that Freundlich isotherm gives lower linear regression coefficient ( $R^2$ ) of 0.85 which is lower compared to ( $R^2$ ) of 0.97 for Langmuir (I) isotherm model as shown in Table 4.5 which indicates its inapplicability of this model. The adsorption capacity of the system,  $K_f(L/g)$  and the heterogeneity factor  $1/n$  can be calculated from slope and intercept of the linear plot of  $\ln(q_e)$  versus  $\ln(C_e)$  as shown in Fig.4.11.

It can be concluded that the isotherm experimental data are well fitted with Langmuir (I) thus indicates the applicability of this model. The adsorption capacity of MB dye onto EB bio-char has been compared with other bio-char, biomass based activated carbon and commercial activated carbon under similar experimental conditions as presented in Table 4.6. From Table.4.6, it shows that EB bio-char studied in this work has a comparative adsorption capacity compared to other adsorbents.

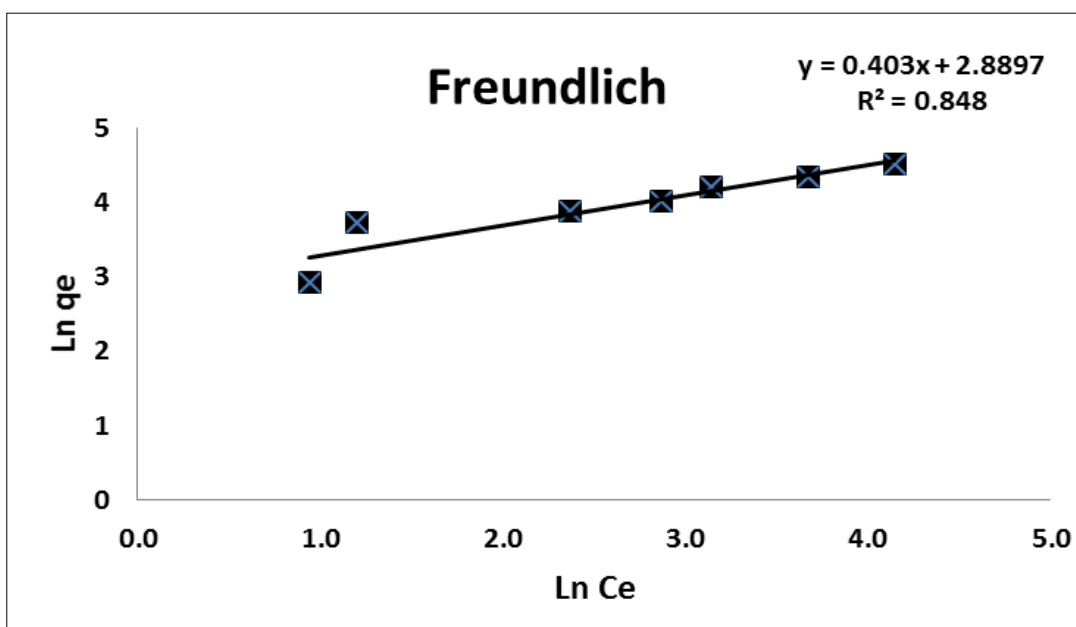


**Figure 4.11:** Freundlich isotherm plot for MB dye on EB bio-char, pH solution =11.3, V =50 ml, adsorbent dose=20mg, T =35 °C, rotating Speed =130 rpm at t=210 min.

**Table 4.5:** Calculated values for Freundlich and Langmuir isotherm models.

<b>Freundlich</b>		
<b><math>K_f</math> (L/g)</b>	<b>n</b>	<b><math>R^2</math></b>
17.99	2.48	0.848
<b>Langmuir (I)</b>		
<b><math>q_m</math> (mg/g)</b>	<b><math>K_L</math> (L/g)</b>	<b><math>R^2</math></b>
104.17	0.09	0.974
<b>Langmuir (II)</b>		
<b><math>q_m</math> (mg/g)</b>	<b><math>K_L</math> (L/g)</b>	<b><math>R^2</math></b>
94.34	0.12	0.80

**Table 4.6:** Comparison of adsorption capacities of various adsorbents in the removal of MB dye.

<b>Adsorbents</b>	<b><math>q_{max}</math> (mg/g)</b>	<b>References</b>
Chitosan activated carbon	143.5	(Marrakchi et al. 2017)
Oxidized weed biochar	161.3	(Güzel et al. 2017)
Base modified orange tree waste	78.7	(Azzaz et al. 2017)
Nut shell activated carbon	5.3	(Ragupathy et al. 2015)
Macoře fruit shell activated carbon	10.6	(Aboua et al. 2015)
Waste tea activated carbon	402	(Borah et al. 2015)
Palm tree activated carbon	128	(AlOthman et al. 2014)
Bio-char Ash	178	(Özbay et al. 2013)

Wheat straw bio-char	12.03	(Liu et al. 2012)
Kenaf fibre char	22.7	(Mahmoud et al. 2012)
Granular activated carbon	21.5	(Yener et al. 2008)
Wood apple shell activated carbon	37	(Malarvizhi and Sulochana 2008)
Powdered activated carbon	91	(Yener et al. 2008)
EB bio-char	104.2	Present study

#### 4.5 Design of Single Stage Batch Adsorber from Isotherm Data

It was found that Langmuir isotherm model is fitted well with the equilibrium data. Adsorption isotherms can be used to predict the design of a single batch adsorption system (Dawood et al. 2014, Sen et al. 2011). Due to lack of extensive experimental data, empirical design procedures based on batch adsorption isotherm study is used to predict the optimum process parameter such as the adsorber size and performance. The design objective was to decrease the initial MB initial dye concentration from  $C_0$  to  $C_t$  (mg/L) for which total volume of dye solution is  $V$  (L). The amount of added adsorbent was  $m$  (g) and the solute loading changes from  $q_0$  (mg/g) to  $q_t$  (mg/g). The MB dye concentration on solid changes from  $q_0 = 0$  to  $q_t$  due to added adsorbent into the system. The mass balance for the MB dye in the single-stage operation under equilibrium is presented as per equation (4.2). Langmuir adsorption isotherm data has been utilised in this study to design a single-stage batch adsorption system as per method developed by (Kumar et al. 2010). Rearranging equations (2.13) and (4.2) thus can be written as per equation (4.3).

$$V (C_0 - C_e) = m (q_e - q_0) = m \cdot q_e \quad (4.2)$$

$$\frac{m}{V} = \frac{C_0 - C_e}{q_e} = \frac{C_0 - C_e}{q_m K_a C_e / (1 + K_a C_e)} \quad (4.3)$$

Figure.4.12 shows series of plots derived from equation (4.3) between the predicted amount of EB bio-char particles required to remove Methylene Blue dye of initial concentrations of 100 mg/L for 50%, 60%, 70% , 80% and 90% dye removal at different solution volumes (L) for a single-stage batch adsorption. For example, to obtain 90% MB dye removal, it is required 0.97, 1.93, 2.91, 3.88, 4.84, 5.81, 6.78, 7.75, 8.72 and 9.69 g of EB bio-char to remove 1-10 L MB dye solution respectively.

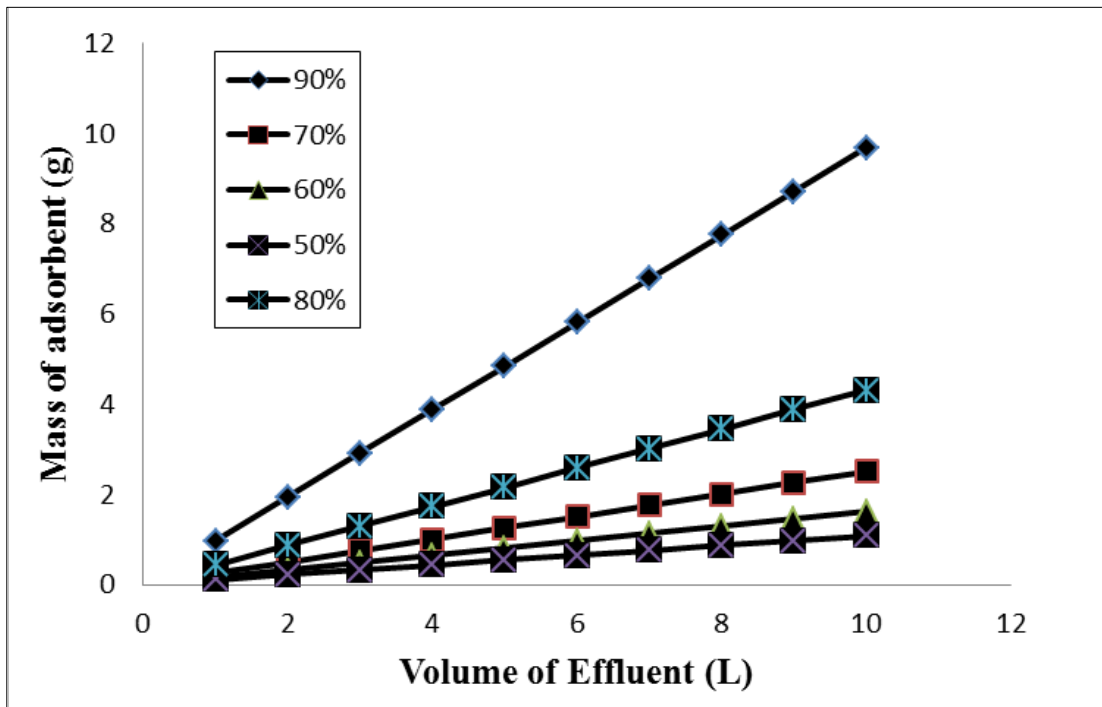


**Figure 4.12:** Design of single stage batch adsorber - Adsorbent mass (m) against volume of solution treated (L).

## 4.6 Desorption Study

Desorption study has been performed to explain the adsorption mechanism and regeneration of the adsorbent. The MB loaded EB bio-char was separated from dye solution by centrifugation and dried. Fixed amount of 10 mg loaded dried adsorbent was agitated with 25 ml of acetone and distilled water at various pH values for predetermined equilibrium time of the adsorption process as described in section 3.7 of chapter 3. It was found that the amount of dye regenerated is increased with the decreases of solution pH as shown in Fig4.13. Desorption tests showed that amounts of dye released were 44%, 43%, 31%, 30% and 28% achieved in aqueous solution at pH of 1.7, 2.3, 3, 5 and 11 respectively. The point of zero charge ( $pH_{pzc}$ ) of EB bio-char was determined at solution pH of 9.5, therefore the amount MB dye released from the loaded EB bio-char is higher with the decreases of solution pH due to the enhanced electrostatic repulsion between the adsorbent and the adsorbate. Also, lower solution pH tends to give higher dye released percentage as the protons in solution replace the MB ions on the bio-char surface, while poor recovery of almost 28% is observed in high solution pH due to the coordinating ligands being deprotonated; hence, bound-dye ions find it difficult to be detached from the adsorbent (Afroze et al. 2015). Also, it was found that the maximum dye releasing of 78% was achieved in an aqueous solution of acetone. Acetone is an organic compound contains carbonyl groups which have both positive and negative centres and hence played the pivotal role in desorbing the adsorbed MB dye molecules from the EB bio-char sites. (Chowdhury et al. 2009). Also, this result indicates the dye has been held by the adsorbent through a chemisorption process.



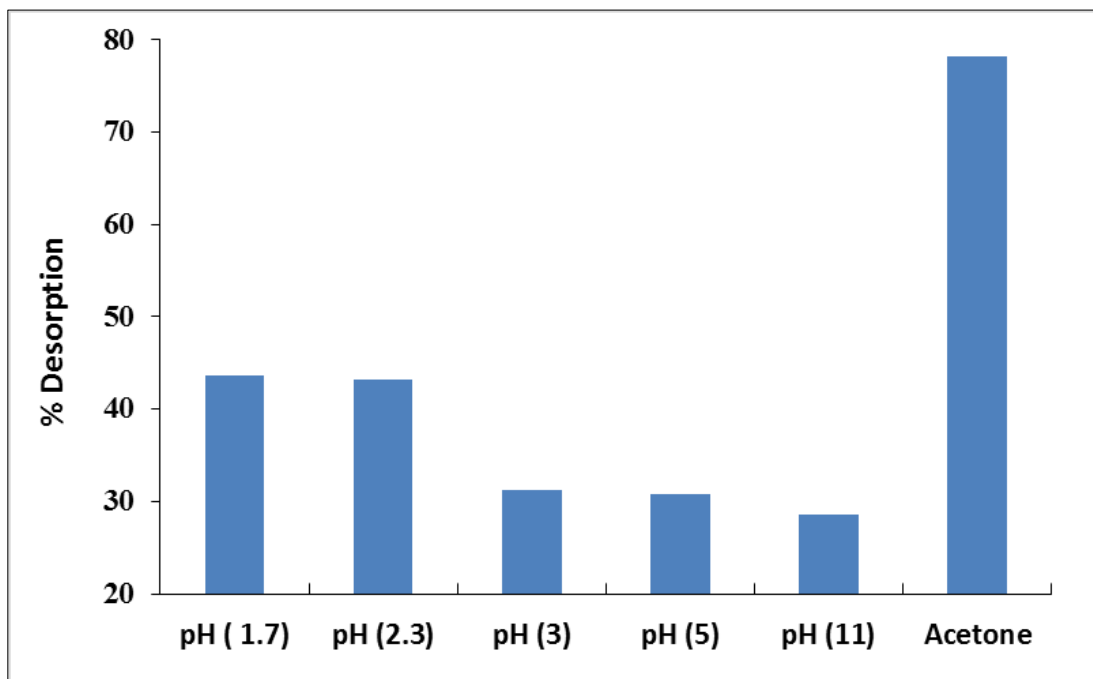


**Figure 4.13:** Batch desorption study of MB dye from EB bio-char by various solution pH and acetone solvent.

## 4.7 Conclusion

In the present study, the synthesized (EB) bio-char was tested as an effective and low cost adsorbent in the removal of Methylene blue dye from aqueous solution by adsorption process. Agricultural by-product eucalyptus barks waste was considered as substance raw materials to produce bio-char. It was found that the extent of MB dye adsorption on EB bio-char increased with the increasing initial dye concentration, contact time, temperature, and solution pH but decreased with the increase of adsorbent dose and salt concentration. Kinetic experiments clearly indicated that adsorption of Methylene blue on EB bio-char are multi step processes: a rapid adsorption of dye onto the external surface followed by intra-particle diffusion into the interior of adsorbent which has also been confirmed by intra-particle diffusion model. Overall, the kinetic studies showed that the Methylene blue dye adsorption process followed pseudo-second -order. Equilibrium data were fitted well with Langmuir adsorption isotherm model and Langmuir maximum adsorption capacity  $q_m$  was calculated as 104.2 mg/g. Based on the thermodynamic analysis and Langmuir isotherm data, it was observed that the adsorption system was endothermic and physical processes in nature. The positive value of  $\Delta S^0$  indicated also greater stability of an adsorption process with no structural changes at the solid-liquid interface. The present works also highlighted that eucalyptus barks bio-char is a good low cost adsorbent in the removal of MB dye. Further, the utilization of eucalyptus barks waste will add economic value and help to reduce the cost of agricultural solid waste disposal and provide a potentially inexpensive alternative bio-char adsorbent to commercial activated carbon.

## 4.8 References

- Aboua, K.N., Yobouet, Y.A., Yao, K.B., Goné, D.L. and Trokourey, A. (2015) "Investigation of dye adsorption onto activated carbon from the shells of Macoré fruit". Journal of Environmental Management **156**, 10-14.
- Afroze, S., Sen, T.K., Ang, M. and Nishioka, H. (2015) "Adsorption of methylene blue dye from aqueous solution by novel biomass Eucalyptus sheathiana bark: equilibrium, kinetics, thermodynamics and mechanism". Desalination and Water Treatment.
- Afroze, S., Sen, T.K., Ang, M. and Nishioka, H. (2016) "Adsorption of methylene blue dye from aqueous solution by novel biomass Eucalyptus sheathiana bark: equilibrium, kinetics, thermodynamics and mechanism". Desalination and Water Treatment **57**(13), 5858-5878.
- AlOthman, Z.A., Habila, M.A., Ali, R., Abdel Ghafar, A. and El-din Hassouna, M.S. (2014) "Valorization of two waste streams into activated carbon and studying its adsorption kinetics, equilibrium isotherms and thermodynamics for methylene blue removal". Arabian Journal of Chemistry **7**(6), 1148-1158.
- Arias, F. and Sen, T.K. (2009) "Removal of zinc metal ion ( $Zn^{2+}$ ) from its aqueous solution by kaolin clay mineral: A kinetic and equilibrium study". Colloids and Surfaces A: Physicochemical and Engineering Aspects **348**(1-3), 100-108.
- Azzaz, A.A., Jellali, S., Akrouf, H., Assadi, A.A. and Bousselmi, L. (2017) "Optimization of a cationic dye removal by a chemically modified agriculture by-product using response surface methodology: biomasses characterization and adsorption properties". Environmental Science and Pollution Research **24**(11), 9831-9846.
- Borah, L., Goswami, M. and Phukan, P. (2015) "Adsorption of methylene blue and eosin yellow using porous carbon prepared from tea waste: Adsorption equilibrium, kinetics and thermodynamics study". Journal of Environmental Chemical Engineering **3**(2), 1018-1028.
- Chowdhury, A.K., Sarkar, A.D. and Bandyopadhyay, A. (2009) "Rice Husk Ash as a Low Cost Adsorbent for the Removal of Methylene Blue and Congo Red in Aqueous Phases". CLEAN – Soil, Air, Water **37**(7), 581-591.

Dawood, S. and Sen, T.K. (2012) "Removal of anionic dye Congo red from aqueous solution by raw pine and acid-treated pine cone powder as adsorbent: Equilibrium, thermodynamic, kinetics, mechanism and process design". Water Research **46**(6), 1933-1946.

Dawood, S., Sen, T.K. and Phan, C. (2014) "Synthesis and characterisation of novel-activated carbon from waste biomass pine cone and its application in the removal of congo red dye from aqueous solution by adsorption". Water, Air, and Soil Pollution **225**(1).

Ghaly, A.E., Ananthashankar, R., M., A. and Ramakrishnan, V.V. (2014) "Production, Characterization and Treatment of Textile Effluents: A Critical Review". J Chem Eng Process Technol **5**, 182.

Gokce, Y. and Aktas, Z. (2014) "Nitric acid modification of activated carbon produced from waste tea and adsorption of methylene blue and phenol". Applied Surface Science **313**, 352-359.

Güzel, F., Saygılı, H., Akkaya Saygılı, G., Koyuncu, F. and Yılmaz, C. (2017) "Optimal oxidation with nitric acid of biochar derived from pyrolysis of weeds and its application in removal of hazardous dye methylene blue from aqueous solution". Journal of Cleaner Production **144**(Supplement C), 260-265.

Han, R., Zhang, J., Han, P., Wang, Y., Zhao, Z. and Tang, M. (2009) "Study of equilibrium, kinetic and thermodynamic parameters about methylene blue adsorption onto natural zeolite". Chemical Engineering Journal **145**(3), 496-504.

Kaur, S., Rani, S. and Mahajan, R.K. (2013) " Adsorption Kinetics for the Removal of Hazardous Dye Congo Red by Biowaste Materials as Adsorbents". Journal of Chemistry **2013**, 12.

Konicki, W., Sibera, D., Mijowska, E., Lendzion-Bieluń, Z. and Narkiewicz, U. (2013) "Equilibrium and kinetic studies on acid dye Acid Red 88 adsorption by magnetic ZnFe<sub>2</sub>O<sub>4</sub> spinel ferrite nanoparticles". Journal of Colloid and Interface Science **398**, 152-160.

Kumar, P., Ramalingam, S., Senthamarai, C., Niranjanaa, M., Vijayalakshmi, P. and Sivanesan, S. (2010) "Adsorption of dye from aqueous solution by cashew nut shell: Studies on equilibrium isotherm, kinetics and thermodynamics of interactions". Desalination **261**(1–2), 52-60.

Li, W.-H., Yue, Q.-Y., Gao, B.-Y., Ma, Z.-H., Li, Y.-J. and Zhao, H.-X. (2011) "Preparation and utilization of sludge-based activated carbon for the adsorption of dyes from aqueous solutions". Chemical Engineering Journal **171**(1), 320-327.

Liu, X. and Zhang, L. (2015) "Removal of phosphate anions using the modified chitosan beads: Adsorption kinetic, isotherm and mechanism studies". Powder Technology **277**, 112-119.

Liu, Y., Zhao, X., Li, J., Ma, D. and Han, R. (2012) "Characterization of bio-char from pyrolysis of wheat straw and its evaluation on methylene blue adsorption". Desalination and Water Treatment **46**(1-3), 115-123.

Mahmoud, D.K., Salleh, M.A.M., Karim, W.A.W.A., Idris, A. and Abidin, Z.Z. (2012) "Batch adsorption of basic dye using acid treated kenaf fibre char: Equilibrium, kinetic and thermodynamic studies". Chemical Engineering Journal **181–182**(0), 449-457.

Malarvizhi, R. and Sulochana, N. (2008) "Sorption isotherm and kinetic studies of methylene blue uptake onto activated carbon prepared from wood apple shell". Journal of Environmental Protection Science **2**, 40-46.

Marrakchi, F., Ahmed, M.J., Khanday, W.A., Asif, M. and Hameed, B.H. (2017) "Mesoporous-activated carbon prepared from chitosan flakes via single-step sodium hydroxide activation for the adsorption of methylene blue". International Journal of Biological Macromolecules **98**, 233-239.

Özbay, İ., Özdemir, U., Özbay, B. and Veli, S. (2013) "Kinetic, thermodynamic, and equilibrium studies for adsorption of azo reactive dye onto a novel waste adsorbent: charcoal ash". Desalination and Water Treatment **51**(31-33), 6091-6100.

Ragupathy, S., Raghu, K. and Prabu, P. (2015) "Synthesis and characterization of TiO<sub>2</sub> loaded cashew nut shell activated carbon and photocatalytic activity on BG and MB dyes under sunlight radiation". Spectrochimica Acta Part A: Molecular and Biomolecular Spectroscopy **138**, 314-320.

Rida, K., Bouraoui, S. and Hadnine, S. (2013) "Adsorption of methylene blue from aqueous solution by kaolin and zeolite". Applied Clay Science **83-84**(Supplement C), 99-105.

Salleh, M.A.M., Mahmoud, D.K., Karim, W.A. and Idris, A. (2011) "Cationic and anionic dye adsorption by agricultural solid wastes: a comprehensive review". Desalination **280**(1-3), 1-13.

Sen, T.K., Afroze, S. and Ang, H.M. (2011) "Equilibrium, kinetics and mechanism of removal of methylene blue from aqueous solution by adsorption onto pine cone biomass of *Pinus radiata*". Water Air Soil Pollut **218**, 499-515.

Sewu, D.D., Boakye, P. and Woo, S.H. (2017) "Highly efficient adsorption of cationic dye by biochar produced with Korean cabbage waste". Bioresource Technology **224**, 206-213.

Shakoor, S. and Nasar, A. (2016) "Removal of methylene blue dye from artificially contaminated water using citrus limetta peel waste as a very low cost adsorbent". Journal of the Taiwan Institute of Chemical Engineers **66**, 154-163.

Tran, H.N., You, S.-J., Hosseini-Bandegharai, A. and Chao, H.-P. (2017) "Mistakes and inconsistencies regarding adsorption of contaminants from aqueous solutions: A critical review". Water Research **120**(Supplement C), 88-116.

Uddin, M.T., Rahman, M.A., Rukanuzzaman, M. and Islam, M.A. (2017) "A potential low cost adsorbent for the removal of cationic dyes from aqueous solutions". Applied Water Science **7**(6), 2831-2842.

Vadivelan, V. and Kumar, K.V. (2005) " Equilibrium, kinetics, mechanism and process design for the sorption of methylene blue onto rice husk". J. Colloid Interface Sci **286**, 90-100.

Yagub, M.T., Sen, T.K., Afroze, S. and Ang, H.M. (2014) "Dye and its removal from aqueous solution by adsorption: A review". Advances in Colloid and Interface Science **209**(0), 172-184.

Yagub, M.T., Sen, T.K. and Ang, H.M. (2012) "Equilibrium, kinetics, and thermodynamics of methylene blue adsorption by pine tree leaves". Water, Air, and Soil Pollution **223**(8), 5267-5282.

Yener, J., Kopac, T., Dogu, G. and Dogu, T. (2008) "Dynamic analysis of sorption of methylene blue dye on granular and powdered activated carbon". Chemical Engineering Journal **144**(3), 400-406.

Zhu, L., Wang, Y., He, T., You, L. and Shen, X. (2016) "Assessment of Potential Capability of Water Bamboo Leaves on the Adsorption Removal Efficiency of Cationic Dye from Aqueous Solutions". Journal of Polymers and the Environment **24**(2), 148-158.

Zou, W., Bai, H., Gao, S. and Li, K. (2013) "Characterization of modified sawdust, kinetic and equilibrium study about methylene blue adsorption in batch mode". Korean Journal of Chemical Engineering **30**(1), 111-122.

*Every reasonable effort has been made to acknowledge the owners of copyright material. I would be pleased to hear from any copyright owner who has been omitted or incorrectly acknowledged.*

# **CHAPTER 5**

**REMOVAL OF ORGANIC MB DYE AND  
INORGANIC NI (II) IONS FROM  
AQUEOUS SOLUTION BY PINE CONE  
BIOCHAR ADSORBENT**



## ABSTRACT\*

Pine cone based bio-char was synthesis and used as an effective adsorbent in the removal of organic MB dye and inorganic Ni (II) ions from wastewater. BET surface area, bulk density, point of zero charge, SEM, FT-IR and CHN elemental analysis were used to evaluate the adsorbent characteristics. The adsorption potential of pine cone bio-char in the removal of cationic dye Methylene Blue and Ni (II) ions from aqueous solutions was studied. Batch adsorption kinetic study was carried out and found that the amount of dye adsorbed  $q_t$  (mg/g) depends on various physicochemical process parameters such as initial solution pH, dye concentration, temperature, adsorbent dose and contact time. Batch experimental data were fitted with pseudo-first-order, pseudo-second-order and intra-particle diffusion adsorption kinetics models. Also, equilibrium data fitted into Langmuir and Freundlich isotherm models and Langmuir maximum adsorption capability was found as 106 mg/g and 117.4 mg/g for MB dye and Ni (II) ions respectively. Thermodynamic parameters suggested that the adsorption was an endothermic and spontaneous. These results indicated the applicability of pine cone as a cheap precursor for the production of cost-effective and environmental friendly bio-char adsorbent. Furthermore, a single-stage batch adsorber design for the MB dye onto pine cone bio-char particles was presented based on the Langmuir isotherm model equation.

---

\*This work has been published in Bioresource Technology Journal (Dawood, S., Sen, T.K. and phan, C., 2017. Synthesis and characterization of slow pyrolysis pine cone bio-char in the removal of organic and inorganic pollutants from aqueous solution by adsorption: Kinetic, equilibrium, mechanism and thermodynamic. Bioresource Technology, (246): 76-81. DOI: 10.1016/j.biortech.2017.07.019).

## 5.1 Introduction

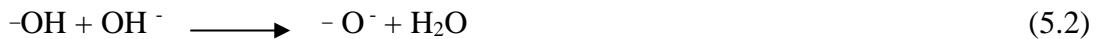
This chapter examines the potential efficiency of pine cone based bio-char as an adsorbent in the removal of organic MB dye and inorganic Ni (II) ions from their aqueous solution. Pine cone (*Pinus radiata*) tree is available in large quantities in nature. Pine cone is widely available in Australia, New Zealand, Spain, Chile and United States. In Australia, pine cone has no economic value and according to Blue Mountains City Council in New South Wales state, pine cone is considered as weed thus its removal is encouraged (Blue Mountains City Council 2009). The production of bio-char does not require the use of chemicals such as acids and bases thus it is considered to be environmental friendly. The synthesized pine cone based bio-char under various production temperature profiles were studied and the most efficient temperature profile was identified at 500°C as described in section 3.4.1 of chapter 3. Batch adsorption kinetic study was carried out as described in section 3.5 and 3.6 of chapter 3 under various physicochemical process parameters such as initial solution pH, dye concentration, temperature and adsorbent dosage. Detailed experimental procedure Batch experimental data were analysed with pseudo-first-order, pseudo-second-order and intra-particle diffusion models to determine the adsorption kinetics and mechanism of adsorption. Further, to understand the adsorption isotherm and MB dye-pine cone bio-char interaction, the equilibrium data were fitted into Langmuir and Freundlich isotherm models. The adsorptive efficiency of pine cone bio-char in the removal of these organic and inorganic pollutants under various physiochemical parameters were compared to other published adsorbents including commercial activated carbon. Thermodynamic parameters were studied to determine the process feasibility. Furthermore, a single-stage batch adsorber was designed for both organic MB dye and inorganic Ni (II) ions removal onto pine cone bio-char based on equilibrium experimental data to gain insight into the process dynamics.

## 5.2 Results and discussion

### 5.2.1 Effect of initial solution pH on MB dye and Ni (II) ions adsorption

Pine cone bio-char was used in the removal of MB dye and Ni (II) from aqueous solution under different initial solution pH of 5.1 to 11.3 where the other parameters were kept constant as shown in Fig 5.1. It was found that the amount of MB dye adsorbed,  $q_e$  (mg/g) and percentage dye removal are increasing significantly from 21.4 mg/g to 41.1 mg/g and from 42.8% to 82.3% with the increase of the solution pH from 5.1 to 11.3 respectively as shown in Fig.5.1. Also, the amount of Ni (II) ions adsorbed  $q_t$  was found to increase from 5.2 mg/g to 37.5 mg/g with the increases of solution pH from 5.1 to 9.4 and decreases to 20.9 mg/g at solution pH of 11.3 as shown in Fig.5.1. Similar trend was observed upon the percentage Ni (II) ions removal where the percentage removal was increased from 10.5 % to 75.1 % with the increases of solution pH from 5.1 to 9.4 and then decreases to 42.0 % at solution pH of 11.3.

Pine cone bio-char point of zero charge ( $\text{pH}_{\text{pzc}}$ ) was calculated as 8.5 as per method described in section 3.4.5 of chapter 3. At initial solution pH higher than ( $\text{pH}_{\text{zpc}} = 8.5$ ) the stretching hydroxyl ( $-\text{OH}$ ) and carboxyl ( $-\text{COOH}$ ) groups presented on the surface of pine cone bio-char were deprotonated and became more negatively charged as shown in equations (5.1) and (5.2) respectively (Maneerung et al. 2016). Therefore, the adsorption MB dye and Ni (II) ions onto bio-char tends to increase rapidly due to the increase of electrostatic interaction of cationic dye and metal ions and with the negatively charged pine cone bio-char surface to form a solid surface complex.



However, as seen from Fig.5.1, the adsorption capacity and percentage removal of Ni (II) ions were decreased rapidly after solution pH of 9.1. This may be due to the formation of soluble hydroxylated complexes of the nickel ions and their competition with the active sites of the bio-char surface. Where at lower solution pH, the adsorption capacity of MB dye and Ni (II) by pine cone bio-char tends to decrease due to presences of hydronium ( $H_3O^+$ ) ions thus competing with the cationic dye and metal ions for the adsorption sites respectively. A similar adsorption behaviour was reported by various adsorbents in the removal of MB dye and Ni (II) ions such as wheat straw biochar (Liu et al. 2012), mango leaf (Uddin et al. 2017), rapeseed cake activated carbon (Uçar et al. 2015), coal fly ash (Sočo and Kalembkiewicz 2013) and weed biochar (Güzel et al. 2017). The experimental data and detailed calculation on the adsorption capacity  $q_t$  (mg/g) and percentage adsorbate removal are presented in Appendix B-1.

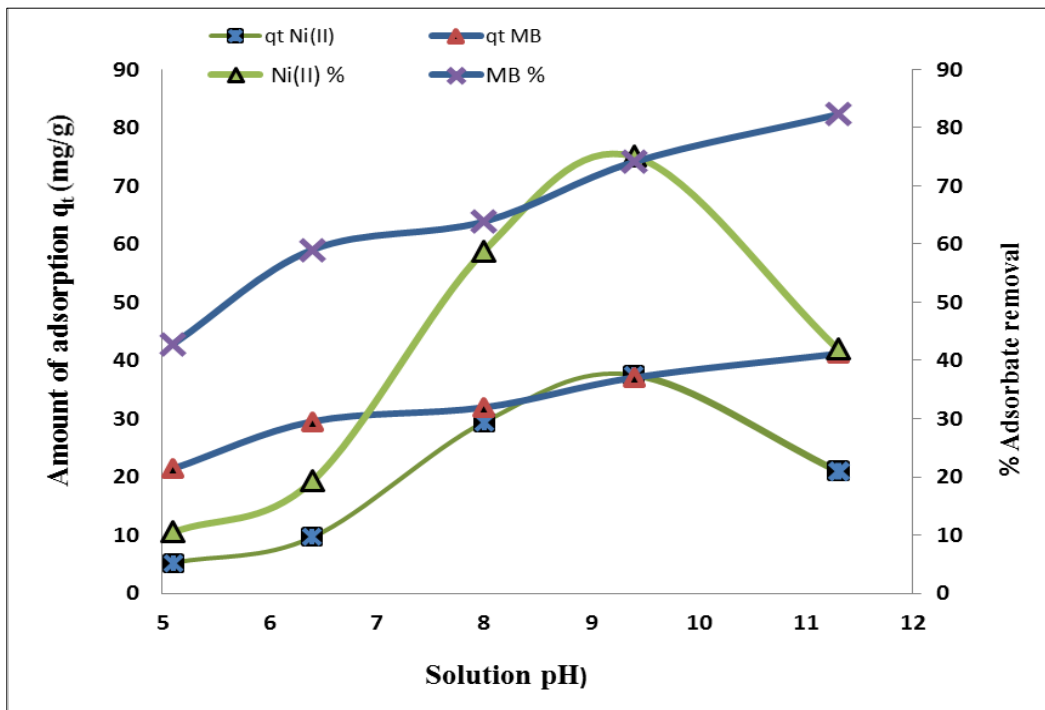


**Figure 5.1:** Effect of initial solution pH into MB dye and Ni (II) ions adsorption. pine cone bio-char dose= 20 mg, V= 50 ml, adsorbate concentration = 20 mg/L, T= 35 °C, rotating Speed 130 rpm and time=120 mins.

### 5.2.2 Effect of pine cone bio-char dosage on adsorption process

Adsorbent dose is an important parameter for adsorber design. Therefore effect of various pine cone bio-char doses of 10 to 50 mg in the removal of both MB dye and Ni (II) ions from aqueous solution were studied and presented in Fig.5.2. Other process parameters were kept constant with 50 ml of initial adsorbate concentration of 20 mg/L and solution pH value of 11.3 for MB dye and 9.4 for Ni (II) ions. The samples were shaken constantly at speed of 130 rpm and temperature of 35°C for a period of up-to 120 min. It was found that amount of MB dye and Ni (II) ions adsorbed  $q_t$  (mg/g) increased rapidly with the increase of contact time and then slowed down until equilibrium reached at 120 mins.

Also, it was observed that the increase in pine cone bio-char dose from 10 mg to 50 mg results in decreased amount of dye adsorbed ( $q_e$ ) from 66.58 mg/g to 17.18 mg/g for MB dye and from 55.75 mg/g to 15.15 mg/g for Ni (II) ions as shown in Fig.5.2. Simultaneously, with the increases of adsorbent dosage from 10mg to 40 mg, the percentage adsorbate removal was increased from 66.6 % to 87.7 % for MB dye and from 55.8 % to 77.5 % for Ni (II) ions as shown in Fig.5.2. Furthermore, it was observed from Fig.5.2, a slight decrease in the adsorbate percentage removal from 87.7 % to 85.9 % for MB dye and from 77.5 % to 75.8 % for Ni (II) ions with the increases of pine cone biochar dose form 40 mg to 50 mg. The decreases in amount of adsorbate adsorbed  $q_e$  (mg/g) with increasing the adsorbent mass as shown in Fig.5.2 is due to the split in the flux or the concentration gradient between solute concentration in the solution and the solute concentration in the surface of the adsorbent (Dawood et al. 2014, Vadivelan and Kumar 2005). Also, higher pine cone bio-char doses lead to a very fast adsorption of MB dye and Ni (II) ions on the adsorbent surface which gives a lower adsorbate concentration in bulk solution compared to low adsorbent dose situation. Thus, with increasing adsorbent dose, the amount of MB dye and Ni (II) ions adsorbed per unit mass of adsorbent  $q_e$  (mg/g) decreased (Han et al. 2009). At lower adsorbent dose, the adsorbate-adsorbate' molecules are more easily accessible hence the adsorbate removal per unit weigh of adsorbent is high. Also, the increases in the percentage removal of MB dye and Ni (II) ions with the increases of adsorbent dosage could be attributed to the increase in the availability of the active sites on the adsorbent surface due to the increase in the adsorbent mass. A similar behaviour was also reported in MB dye and Ni (II) ions adsorption on biomass and biomass based carbon such as waste tea activated carbon (Gokce and Aktas 2014), pine tree leaves (Yagub et al. 2012) and raw eucalyptus bark (Afroze et al. 2016b). The experimental data and detailed calculation on the adsorption capacity  $q_t$  (mg/g) and percentage adsorbate removal are presented in Appendix B-2.

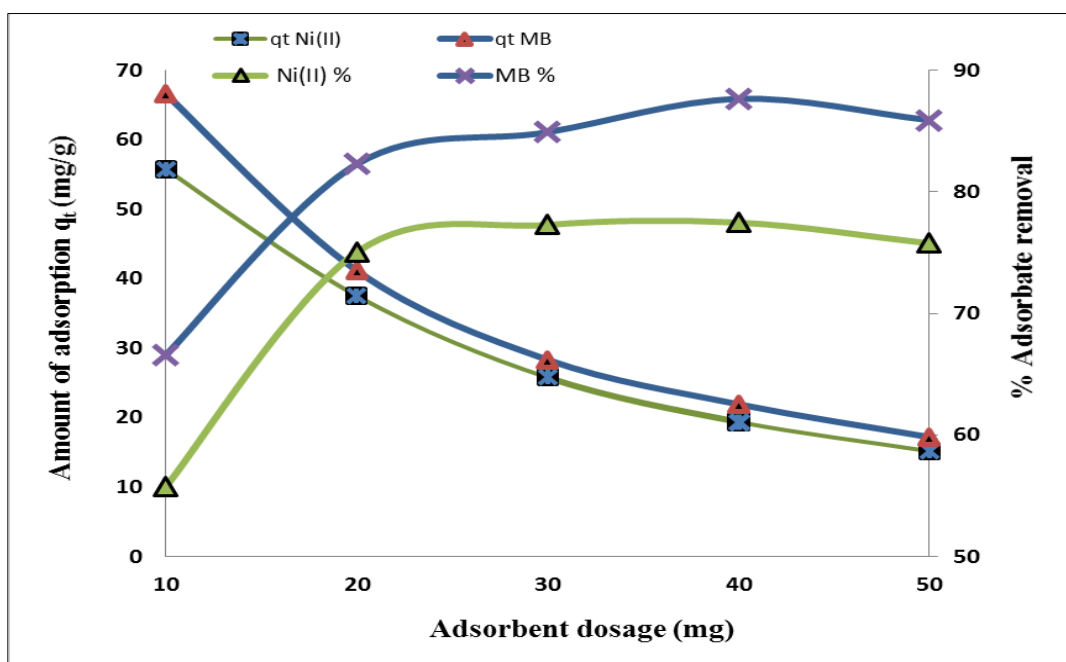


**Figure 5.2:** Effect of adsorbent dose into MB dye and Ni (II) ions adsorption. Amount of adsorbate=20 mg/L, V= 50 ml, solution pH (MB= 11.3) (Ni (II)=9.4), T= 35 °C, rotating Speed 130 rpm and time=120 min.

### 5.2.3 Effect of contact time and initial adsorbate concentration

The effects of initial MB dye and Ni (II) ions concentration and contact time on the amount of adsorbate adsorbed  $q_t$  (mg/g) and percentage adsorbate removal were investigated and results are presented in Fig.5.3 (a), (b) and (c) respectively. In this project, MB dye and Ni (II) ions concentration were varied from 10 to 70 mg/L as shown in Fig 5.3. The other process parameters were kept constant such as solution pH ( MB=11.3 and Ni (II)=9.4), solution temperature of 35°C , rotating speed of 130 rpm 35°C for a period of up-to 120 min. It was observed from Fig 5.3 (a) and (b) that the amount of adsorption capacity  $q_t$  (mg/g) was increased rapidly with increasing contact time at all initial adsorbate concentrations and slowed down with the increases of contact time till equilibrium is attained within 120 min. From Fig. 5.3 (c), the

amount of MB dye adsorbed  $q_t$  (mg/g) increased rapidly from 21.9 mg/g to 93.8 mg/g with the increases of initial dye concentration (10–70 mg/L). Concurrently, percentage dye removal decreased from 87.5% to % 53.6.8 for the same initial MB dye concentration. Furthermore, the amount of Ni (II) ions adsorbed  $q_t$  (mg/g) increased from 20.1 mg/g to 89.6 mg/g with the increases of initial nickel metal ions concentration (10–70 mg/L) while the percentage removal efficiency decreased from % 80.4 to % 51.2 for the same initial nickel metal ions concentration. The high initial adsorbate concentration provides a high driving force to overcome the resistance to the mass transfer of adsorbate between the aqueous solution and the solid pine cone bio-char. Also, it was observed that the amount of adsorption  $q_t$  (mg/g) increased rapidly with contact time at all adsorbate initial concentrations and equilibrium was attained within 120 min as shown in Fig.5.3 (a) and (b). This indicates that overall adsorption process is consisted of multi steps process where a very rapid adsorption of MB dye and Ni(II) occurred on the bio-char external surface followed by slow and intra-particle diffusion in the interior of the adsorbent surface (Afroze et al. 2016a).

Higher initial MB dye and Ni (II) ions concentration tends to increase the adsorbate sorption at the initial stages however after initial adsorption stage, the adsorbate concentration gradient reduces and causes the accumulation of adsorbate's molecules on the surface of the adsorbent. This is due to the saturation of available active sites on adsorbent surface and hence decreased the amount of adsorbate removal (Dawood and Sen 2012, Yagub et al. 2014a). Similar observation was reported by other researchers in the removal of Methylene blue (MB) dye and Ni (II) ions by various adsorbents such as weed biochar (Güzel et al. 2017), water bamboo leaf (Zhu et al. 2016), Hickory wood bio-char (Ding et al. 2016), tea waste activated carbon (Borah et al. 2015), Almond shell biochar (Kılıç et al. 2013) and kenaf fibre char (Mahmoud et al. 2012). The experimental data and detailed calculation on the adsorption capacity  $q_t$  (mg/g) and percentage adsorbate removal are presented in Appendix B-3.



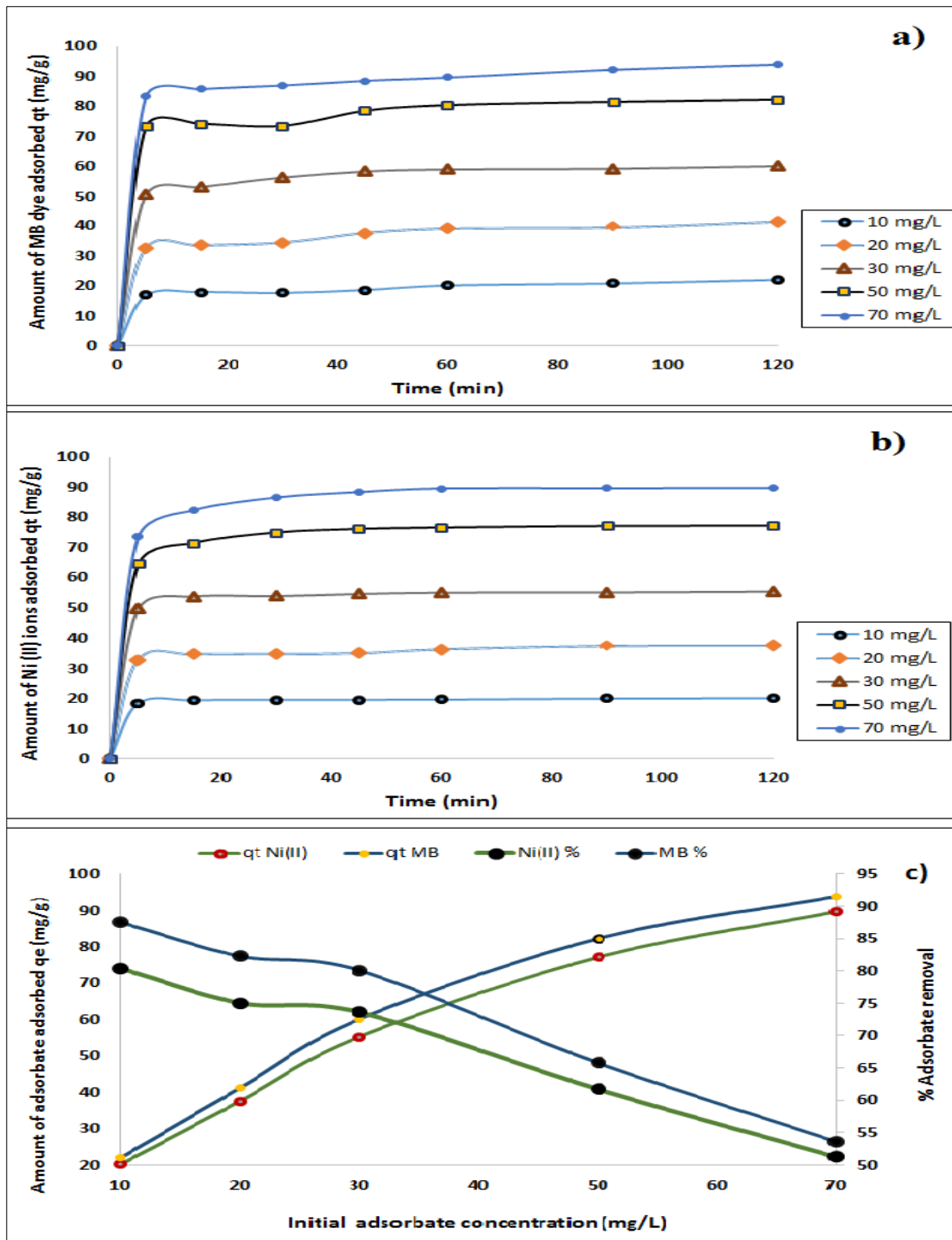


**Figure 5.3:** Effect of initial adsorbate concentration and contact time onto pine cone bio-char adsorption a) Amount of MB dye adsorbed  $q_t$  (mg/g) vs contact time, b) Amount of Ni (II) ions adsorbed  $q_t$  (mg/g) vs contact time, c) Amount adsorbate adsorbed  $q_t$  (mg/g) and percentage removal at  $t = 120$  min. Where  $V = 50$  ml, solution pH (MB = 11.3 and Ni (II) = 9.4), adsorbent dose = 20 mg,  $T = 35$  °C and rotating Speed 130 rpm.

#### 5.2.4 Effect of solution temperature and thermodynamics studies

To investigate the effect of solution temperature on the adsorption process, MB dye and Ni (II) ions batch adsorption studies on pine cone biochar were extended at three different temperatures profile of 25– 45°C while other process parameters were kept constant as shown in Fig 5.4. A 50 ml solution of 20 mg/L initial adsorbate concentration was added to 20 mg pine cone based biochar at solution pH of 11.3 for MB dye and 9.4 for Ni (II) ions and rotating speed of 130 rpm for a period of up-to 125 min to determine the optimum solution temperature and the thermodynamic behaviour of MB dye and Ni (II) ions adsorption by pine cone biochar. Generally, textile wastewater Industrial effluents are being discharged at high temperature of 35°C to 45°C (Ghaly et al. 2014). From Fig 5.4, it was found that the percentage adsorbate removal was increased from 57.5 % to 83.6 % for MB dye and from 61.2 % to 78.2 % for Ni (II) ions with the increase of solution temperature. Also from the same figure, it was observed that the amount of adsorbate adsorbed  $q_t$  (mg/g) was increased from 28.8 mg/g to 41.8 mg/g for MB dye and from 30.6 mg/g to 39.1 mg/g for Ni (II) ions with the increase of solution temperature.

Increasing the adsorption capacity with the increases of temperature indicates an endothermic adsorption process in nature. This is also supported by Gibb's free energy change ( $\Delta G^0$ ) which is decreasing with the increases of solution temperature as shown in Table.5.1. Further, it indicates that increasing the temperature increases the mobility of the adsorbate molecules and hence enhances the mass transfer of MB dye and Ni (II) ions molecules from its liquid phase to the solid phase (Salleh et al. 2011, Yagub et al. 2014a). Further, increasing the reaction temperature tends to increase the amount of non-protonated functional groups presented on the adsorbent due to the increase in the dissociation constant of the protonated carboxyl groups which can causes a swelling effect within the internal surface of the adsorbent (Afroze et al. 2016b, Yagub et al. 2014b).

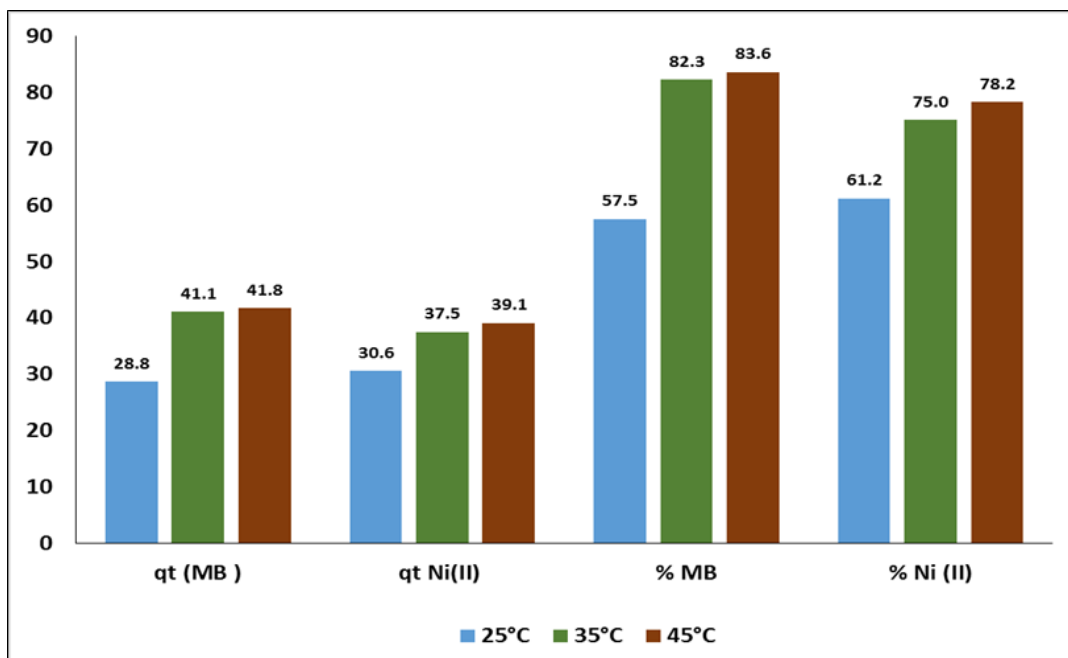


**Figure 5.4:** Effect of solution temperature of MB and Ni (II) ions adsorption onto pine cone biochar: pH solution = 11.3 for MB, 9.4 for Ni (II), V=50 ml, Initial dose=20mg, initial adsorbate concentration =20 mg/L, rotating speed= 130 rpm at time=120 min.

The thermodynamics parameters include Gibb's free energy change ( $\Delta G^0$ ), entropy change ( $\Delta S^0$ ) and enthalpy change ( $\Delta H^0$ ) were calculated from Fig 5.5 and from Van't Hoff equation (2.16) and equation (2.17) respectively. These results are tabulated and presented in Table 5.1. Generally, The Gibbs energy change ( $\Delta G^0$ ) plays a significant factor for determining the degree of spontaneity of the adsorption process. Gibb's free energy change ( $\Delta G^0$ ) values were found to be in the range of -20.7 kJ/mole to -24.3 kJ/mole for Ni (II)-pine cone biochar system and from -3.4 kJ/mole to -7.4 kJ/-mole for MB- pine cone biochar system with the increase of temperature from 25°C to 45°C respectively. Higher negative value of ( $\Delta G^0$ ) indicates an energetically favourable and spontaneous adsorption process (Tran et al. 2016). The enthalpy change ( $\Delta H^0$ ) of MB-pine cone biochar and Ni-pine cone biochar were calculated as 56.3 kJ/mole and 32.68 kJ/mole respectively as presented in Table.5.1. The adsorption process is usually considered as a physical adsorption if the enthalpy change ( $\Delta H^0$ ) <84 kJ/mole (Yaneva and Georgieva 2012) therefore it can concluded that MB dye-pine cone biochar and

Ni (II)-pine cone biochar adsorption systems are physical adsorption controlled by Van der Waals interaction. Also, the positive value of ( $\Delta H^0$ ) indicates an endothermic adsorption process. The positive entropy change ( $\Delta S^0$ ) value as shown in Table.5.1 suggests that a high affinity of the sorbent for the sorbate thus randomness at the solid/liquid interface occurs in the internal structure of the adsorbent. Similar observations were reported by various researchers in the removal in the methylene blue (MB) dye and Ni (II) ions by kaolin clay (Kara et al. 2017), Chitosan based activated carbon (Marrakchi et al. 2017), raw eucalyptus bark (Afroze et al. 2016b), Almond shell biochar (Kılıç et al. 2013), pine tree leaves (Yagub et al. 2012) and citrus peel (Shakoor and Nasar 2016). The experimental data and detailed calculations on the adsorption capacity  $q_t$  (mg/g) and percentage dye removal were presented in Appendix B-4.

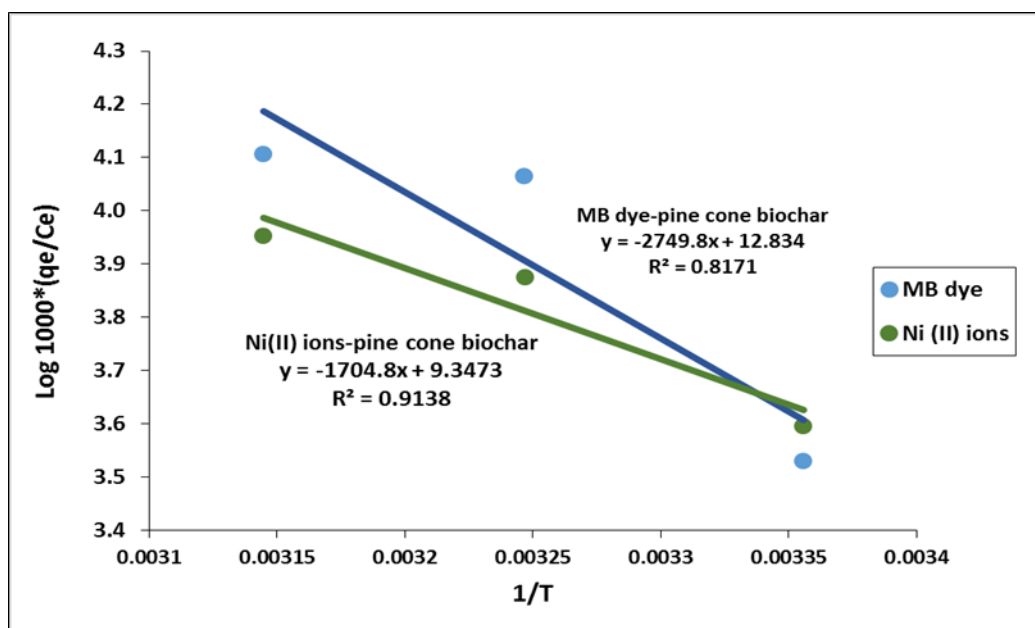


**Figure 5.5:** Plot of Van't Hoff equation for MB dye and Ni (II) ions adsorption onto pine cone bio-char adsorption.

**Table 5.1:** Thermodynamics parameters for MB dye and Ni (II) ions adsorption onto pine cone bio-char at various temperature profiles.

<b>Temp (K)</b>	<b>Ni (II) ions</b>			<b>MB dye</b>		
	$\Delta G^\circ$ (kJ/mole)	$\Delta H^\circ$ (kJ/mole)	$\Delta S^\circ$ (kJ/mole.K)	$\Delta G^\circ$ (kJ/mole)	$\Delta H^\circ$ (kJ/mole)	$\Delta S^\circ$ (kJ/mole.K)
<b>298</b>	-20.70	32.64	0.18	-3.42	56.25	0.25
<b>308</b>	-22.49	32.64	0.18	-5.42	56.25	0.25
<b>318</b>	-24.28	32.64	0.18	-7.43	56.25	0.25

### 5.3 Applications of Adsorption Kinetic Models

In order to understand the mechanism of adsorption, rate of control and the transient behaviour of MB dye and Ni (II) ions adsorption process, adsorption kinetics must be studied under various physio-chemical process parameters such as adsorbent dose, initial adsorbate concentration, solution pH, temperature and contact time. Lagergren Pseudo-first-order, Pseudo-second-order and Intra particles diffusion kinetic models are used to determine the most suitable and practical model in term of high adsorption capacity and fast adsorption rate. The theory of these models are described in section 2.8 of chapter 2. Also, Chi-square ( $\chi^2$ ) is a statistic test used to evaluate the accuracy and the applicability of Pseudo-first-order and Pseudo-second-order kinetics models by determine the error between experimental ( $q_e$ ) and calculated ( $q_e$ ) and it is calculated from equation (2.4).

### 5.3.1 Pseudo first order adsorption kinetics model

The applicability of pseudo-first-order model was tested to investigate the adsorption nature of MB dye and Ni (II) ions onto pine cone bio-char as per equation (2.6). Experimental data at various physico-chemical process parameters were fitted into Pseudo-first-order kinetic model. The calculated amount of MB dye and Ni (II) ions adsorbed  $q_e$  (mg/g) values were obtained from the intercept of the linearized form of the plot  $\log (q_e - q_t)$  verses time ( $t$ ) as shown in Fig.5.6 and Fig.5.7 and the fitted parameters were tabulated and presented in Table.5.2 and Table 5.3 respectively. It was observed that the adsorption capacity  $q_e$  (mg/g) increased with increase initial dye concentration, solution pH and temperature but decreased with the increase of adsorbent dosage. Also, it was found that the adsorption capacity  $q_e$  (mg/g) increased with increase initial Ni (II) ions concentration, solution pH up to 9.4 and temperature but decreased with the increase of adsorbent dosage. The linear regression coefficient ( $R^2$ ) values for both MB dye and Ni (II) ions were found to be in the range of 0.243 to 0.942 and the calculated ( $q_e$ ) values were significantly lower than the experimental equilibrium adsorption capacity ( $q_e$ ). For example, the experimental results presented in Table 5.2 show that the amount of MB dye adsorbed  $q_e$  (mg/g) were 21.9, 41.1, 60.1, 82.2 and 93.8 mg/g for an initial dye concentration of 10, 20, 30, 50 and 70 mg/L respectively while the calculated amount of dye adsorbed  $q_e$  (mg/g) were 3.6, 3.2, 4.3, 3.7 and 3.8 mg/g for the same initial dye concentration respectively. Similar trend was observed for Ni (II) ions removal and the experimental results are presented in Table 5.3. From Table 5.3, it was found that the experimental amount of Ni (II) adsorbed  $q_e$  (mg/g) were 55.8, 37.5, 25.8, 19.4 and 15.2 mg/g for an initial pine cone biochar dosage of 10, 20, 30, 40 and 50 mg respectively while the calculated amount of metal ions adsorbed  $q_e$  (mg/g) were 4.7, 3.8, 1.8, 2.3 and 1.4 mg/g for the same initial adsorbent dosage respectively. Therefore, Low value of linear regression coefficient ( $R^2$ ) and large error values resulted from Chi-square test indicate the inaccuracy and inapplicability of pseudo-first-order model kinetic model.

**Table 5.2:** Fitted pseudo-first-order kinetic model parameters for MB dye adsorption onto pine cone bio-char.

<b>System Parameters</b>	<b><math>q_e</math> (mg/g), Experimental</b>	<b><math>K_f</math> (<math>\text{min}^{-1}</math>)</b>	<b><math>q_e</math> (mg/g), Calculated</b>	<b>Chi square</b>	<b><math>R^2</math></b>
<b>Initial MB Concentration (mg/L)</b>					
<b>10</b>	21.89	0.05	3.56	94.44	0.758
<b>20</b>	41.14	0.02	3.23	445.57	0.824
<b>30</b>	60.07	0.06	4.33	716.99	0.857
<b>50</b>	82.21	0.03	3.65	1691.32	0.765
<b>70</b>	93.79	0.03	3.84	2104.64	0.768
<b>Solution pH</b>					
<b>5.1</b>	21.40	0.02	2.21	166.65	0.630
<b>6.4</b>	29.52	0.06	4.09	158.30	0.786
<b>8</b>	31.93	0.08	5.67	121.58	0.801
<b>9.4</b>	37.06	0.03	3.30	345.99	0.870
<b>11.3</b>	41.14	0.02	3.23	445.57	0.824
<b>Solution temperature</b>					
<b>25<sup>0</sup>C</b>	28.77	0.02	2.17	325.71	0.539
<b>35<sup>0</sup>C</b>	41.14	0.02	3.23	445.57	0.824
<b>45<sup>0</sup>C</b>	41.80	0.06	5.05	267.65	0.737
<b>Initial pine cone biochar dosage (mg)</b>					
<b>10</b>	66.58	0.07	6.45	560.32	0.673
<b>20</b>	41.14	0.02	3.23	445.57	0.824
<b>30</b>	28.30	0.05	3.62	168.62	0.797
<b>40</b>	21.91	0.06	2.85	127.56	0.942
<b>50</b>	17.18	0.03	1.84	128.18	0.502

**Table 5.3:** Fitted pseudo-first-order kinetic model parameters for Ni (II) ions adsorption onto pine cone bio-char.

<b>System Parameters</b>	<b><math>q_e</math> (mg/g), Experimental</b>	<b><math>K_f</math> (<math>\text{min}^{-1}</math>)</b>	<b><math>q_e</math> (mg/g), Calculated</b>	<b>Chi square</b>	<b><math>R^2</math></b>
<b>Initial Ni (II) Concentration (mg/L)</b>					
<b>10</b>	20.11	0.05	2.03	161.19	0.816
<b>20</b>	37.52	0.07	3.81	298.17	0.902
<b>30</b>	55.21	0.03	2.14	1318.83	0.474
<b>50</b>	77.11	0.06	1.75	3250.09	0.739
<b>70</b>	89.63	0.03	1.41	5536.20	0.243
<b>Solution pH</b>					
<b>5.1</b>	5.24	0.01	1.42	10.25	0.068
<b>6.4</b>	9.64	0.02	1.84	33.19	0.064
<b>8</b>	29.40	0.03	2.94	237.98	0.829
<b>9.4</b>	37.52	0.07	3.81	298.10	0.902
<b>11.3</b>	20.97	0.02	1.84	199.15	0.503
<b>Solution temperature</b>					
<b>25<sup>0</sup>C</b>	30.59	0.09	4.32	159.59	0.859
<b>35<sup>0</sup>C</b>	37.52	0.07	3.81	298.17	0.902
<b>45<sup>0</sup>C</b>	39.11	0.03	2.53	529.70	0.542
<b>Initial pine cone biochar dosage (mg)</b>					
<b>10</b>	55.75	0.07	4.72	552.09	0.877
<b>20</b>	37.52	0.07	3.81	298.17	0.902
<b>30</b>	25.76	0.03	1.81	315.97	0.417
<b>40</b>	19.37	0.06	2.32	125.51	0.898
<b>50</b>	15.15	0.03	1.41	134.40	0.328



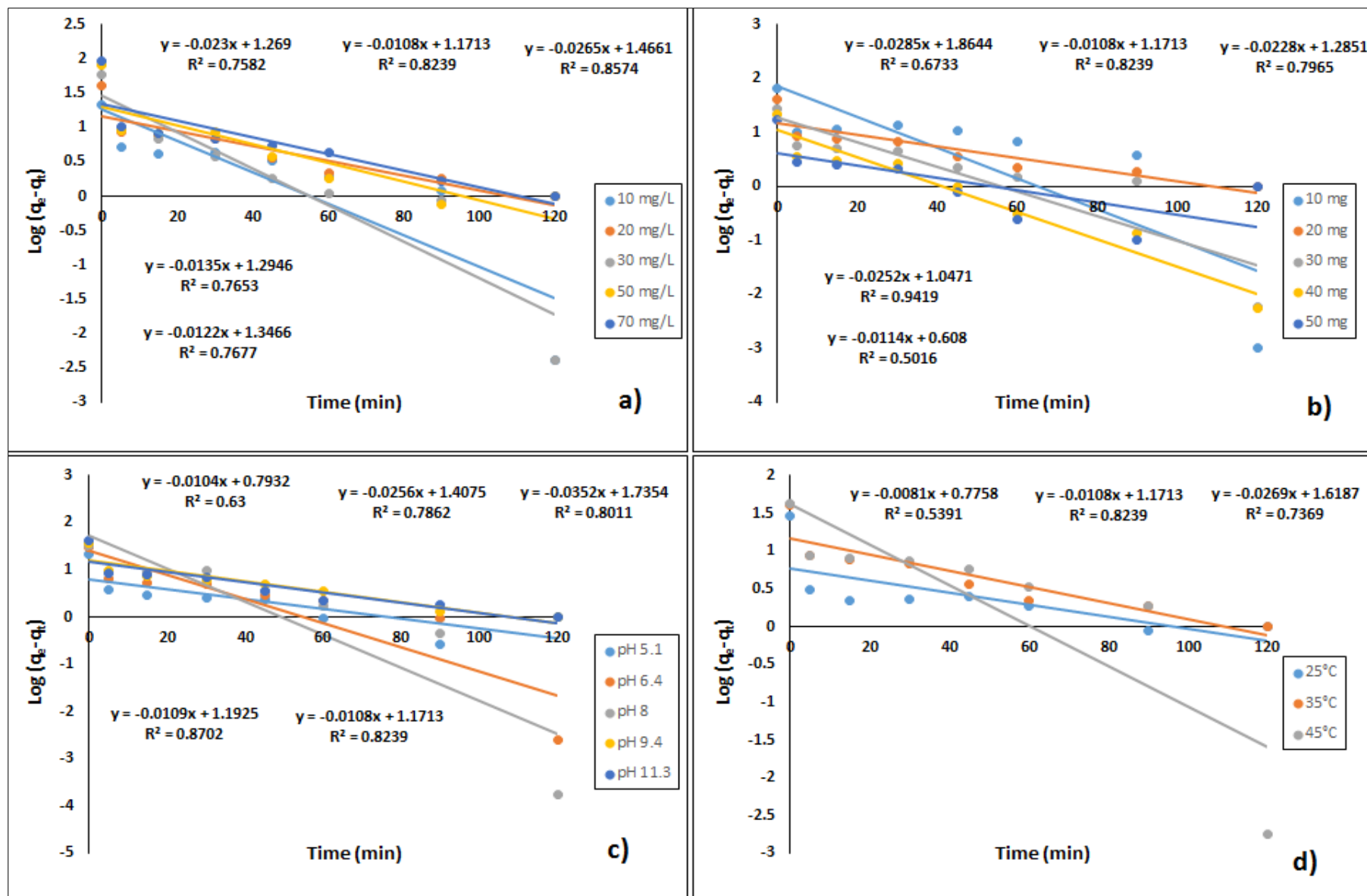


**Figure 5.6:** Fitted pseudo-first-order kinetic model for the adsorption of MB dye onto pine cone bio-char at a) initial MB concentration, b) adsorbent dosage c) solution pH and d) solution temperature.

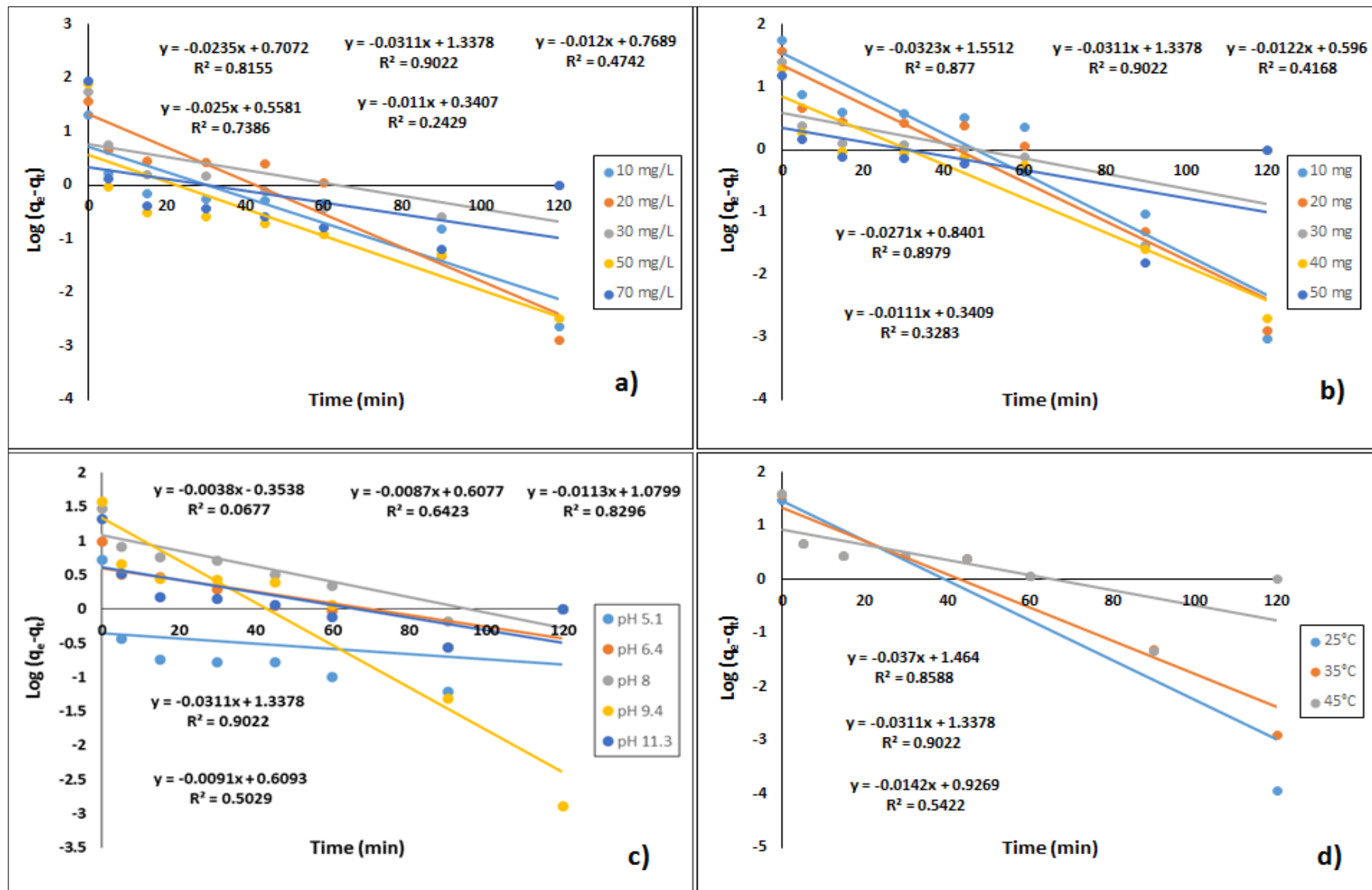


**Figure 5.7:** Fitted pseudo-first-order kinetic model for the adsorption of Ni (II) ions onto pine cone bio-char at a) initial MB concentration, b) adsorbent dosage c) solution pH and d) solution temperature.

### 5.3.2 Application of pseudo-second order kinetic model

Pseudo-second-order kinetics model was applied to investigate the applicability of MB dye and Ni (II) ions adsorption nature onto pine cone bio-char as per equation (2.8). Experimental data were fitted into pseudo-second order kinetic model and the calculated amount of MB dye and Ni (II) ions adsorbed  $q_e$  (mg/g) values were obtained from the intercept of the linearized form where  $(t/q_t)$  versus time (t) as shown in Fig.5.8 and Fig.5.9 and the fitted parameters were tabulated and presented in Table.5.4 and Table 5.5 respectively.

It was observed from Table 5.4, the adsorption capacity  $q_e$  (mg/g) for MB dye adsorption by pine cone bio-char was increased with increase in initial dye concentration, solution pH and temperature and decreased with the increase of adsorbent dosage. Also, pseudo-second order rate constant  $K_s$  (g/mg.min) was found to be decreased with the increase of solution temperature and increased with the increase of adsorbent dosage. This may be due to the lower competition for the sorption sites at lower concentration. The initial adsorption rate  $h$  (mg/g.min) was calculated as per equation (2.9) and it was observed to increase with the increases of initial dye concentration and decrease with the increases of solution temperature. Furthermore, higher linear regression coefficients ( $R^2$ ) values of 0.99 or higher were obtained as shown in Table 5.4. Also, low Chi-square ( $\chi^2$ ) values were calculated lower than 0.028 for various process parameters as shown in Table 5.4. Therefore, high linear regression coefficient values and low error value presented from chi square test indicate the accuracy and applicability of Pseudo-second-order kinetics model in the removal of MB dye by pine cone biochar. Similar trend was observed in the removal of Ni (II) ions where the calculated amount of metal ions adsorbed ( $q_e$ ) values were almost equivalent to the amount of Ni (II) ions adsorbed  $q_e$  obtained from the experimental values as shown in Table 5.5. Also, it was observed from Table 5.5, the adsorption capacity of Ni (II) ions onto pine cone bio-char was increased with the increase in initial dye concentration, solution pH and temperature and decreased with the increase of adsorbent dosage. Also, pseudo-second order rate constant  $K_s$  (g/mg.min) was found to increase with the increases of adsorbent dosage. This may be

due to the lower competition for the sorption sites at lower concentration. The initial adsorption rate  $h$  (mg/g.min) was calculated as per equation (2.9) and it was observed to be increased with increase of initial dye concentration and solution temperature but decreased with the increase of adsorbent dosage. Furthermore, higher linear regression coefficients ( $R^2$ ) values of  $> 0.99$  were obtained as shown in Table 5.5. Also, low Chi-square ( $\chi^2$ ) values were calculated lower than 0.004 for various process parameters as shown in Table 5.5. Therefore, high linear regression coefficient values and low error value presented from chi square test indicate the accuracy and applicability of Pseudo-second-order kinetics model in the removal of Ni (II) ions as well.

**Table 5.4:** Fitted pseudo-second-order kinetic model parameters for MB dye adsorption onto pine cone bio-char.

<b>System Parameters</b>	<b>q<sub>e</sub> (mg/g), Experimental</b>	<b>K<sub>s</sub> (g/mg-min)</b>	<b>q<sub>e</sub> (mg/g), Calculated</b>	<b>h (mg/g.min)</b>	<b>χ<sup>2</sup></b>	<b>R<sup>2</sup></b>
<b>Pine cone bio-char Dose (mg)</b>						
10	66.578	0.004	66.23	17.36	0.002	0.993
20	41.140	0.008	41.15	14.03	0.000	0.997
30	28.300	0.013	28.33	10.36	0.000	0.997
40	21.910	0.024	22.17	11.56	0.003	0.999
50	17.180	0.029	17.39	8.86	0.003	0.999
<b>Initial MB dye Concentration (mg/L)</b>						
10	21.89	0.011	21.65	5.29	0.003	0.995
20	41.14	0.008	41.15	14.03	0.000	0.997
30	60.07	0.013	60.24	46.08	0.001	0.999
50	82.21	0.008	82.64	53.19	0.002	0.999
70	93.79	0.007	93.46	65.36	0.001	0.999
<b>Solution pH</b>						
5.1	21.40	0.018	21.55	8.57	0.001	0.997
6.4	29.52	0.011	29.67	9.35	0.001	0.997
8	31.93	0.006	32.89	6.26	0.028	0.991
9.4	37.06	0.007	37.17	10.13	0.000	0.996
11.3	41.14	0.008	41.15	14.03	0.000	0.997
<b>Solution temperature</b>						
25 <sup>0</sup> C	28.77	0.021	28.57	17.12	0.001	0.998
35 <sup>0</sup> C	41.14	0.008	41.15	14.03	0.000	0.997
45 <sup>0</sup> C	41.80	0.007	41.84	11.92	0.000	0.996

**Table 5.5:** Fitted pseudo-second-order kinetic model parameters for Ni (II) ions adsorption onto pine cone bio-char.

System Parameters	$q_e$ (mg/g), Experimental	$K_s$ (g/mg-min)	$q_e$ (mg/g), Calculated	$h$ (mg/g.min)	$\chi^2$	$R^2$
<b>Pine cone bio-char Dosage (mg)</b>						
10	55.75	0.013	55.87	39.68	0.000	0.993
20	37.52	0.018	37.74	26.18	0.001	0.999
30	25.76	0.041	25.84	27.17	0.000	0.997
40	19.37	0.054	19.42	20.45	0.000	0.999
50	15.15	0.068	15.20	15.65	0.000	0.996
<b>Initial Ni (II) Concentration (mg/L)</b>						
10	20.11	0.077	20.12	31.25	0.000	0.999
20	37.52	0.018	37.74	26.18	0.001	0.999
30	55.21	0.035	55.25	107.53	0.000	0.999
50	77.11	0.188	76.92	1111.11	0.000	0.999
70	89.63	0.139	89.29	1111.11	0.001	0.999
<b>Solution pH</b>						
5.1	5.24	0.293	5.24	8.02	0.000	0.999
6.4	9.64	0.021	9.80	2.04	0.003	0.995
8	29.40	0.009	29.76	8.30	0.004	0.997
9.4	37.52	0.018	37.74	26.18	0.001	0.999
11.3	20.97	0.035	21.01	15.34	0.000	0.999
<b>Solution temperature</b>						
25 <sup>0</sup> C	30.590	0.018	30.77	17.06	0.001	0.999
35 <sup>0</sup> C	37.519	0.018	37.74	26.18	0.001	0.999
45 <sup>0</sup> C	39.110	0.018	39.37	28.49	0.002	0.999

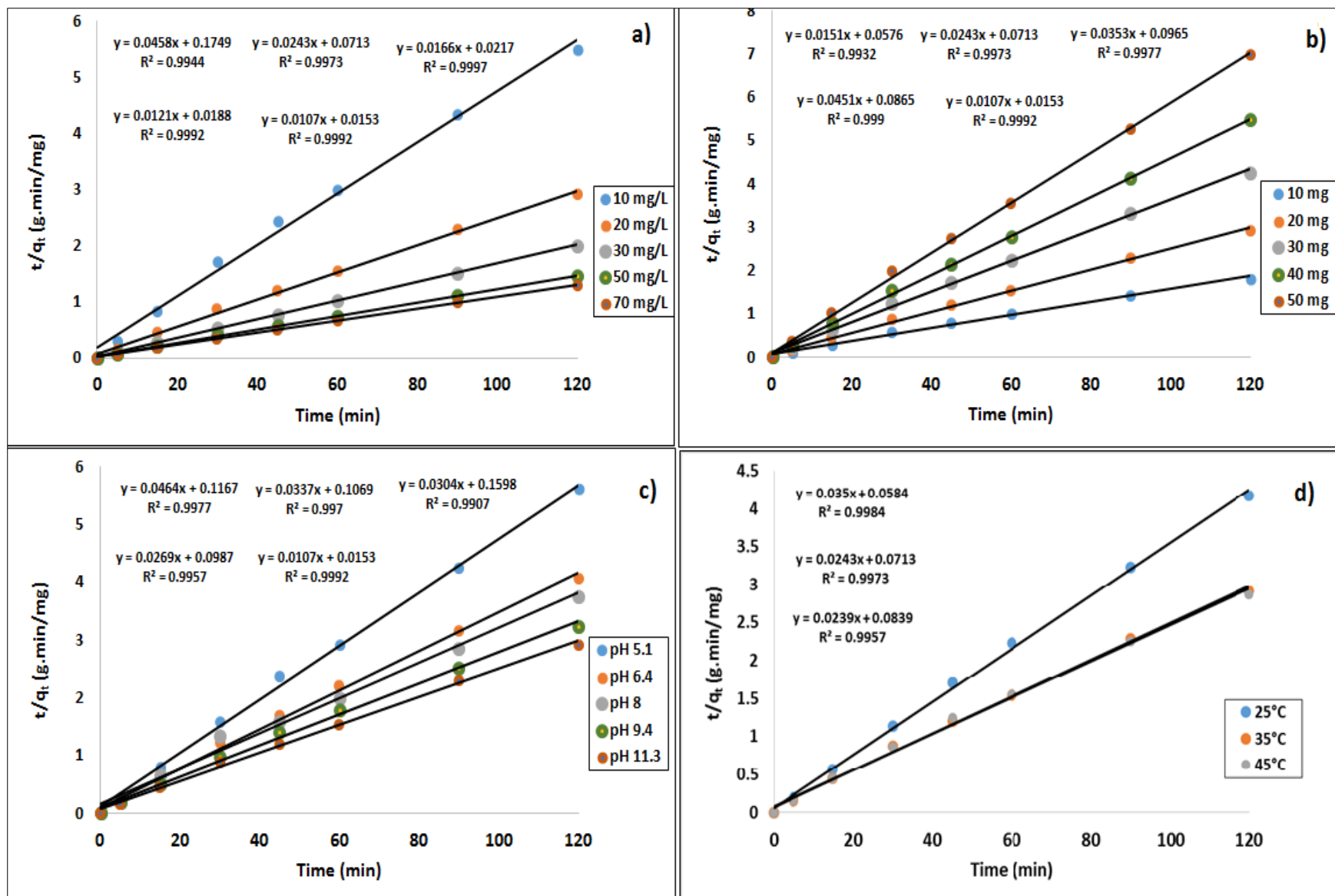


**Figure 5.8:** Fitted pseudo-second-order kinetic model for the adsorption of MB dye onto EB bio-char at various a) initial MB concentration, b) adsorbent dosage, c) solution pH, d) solution temperature.

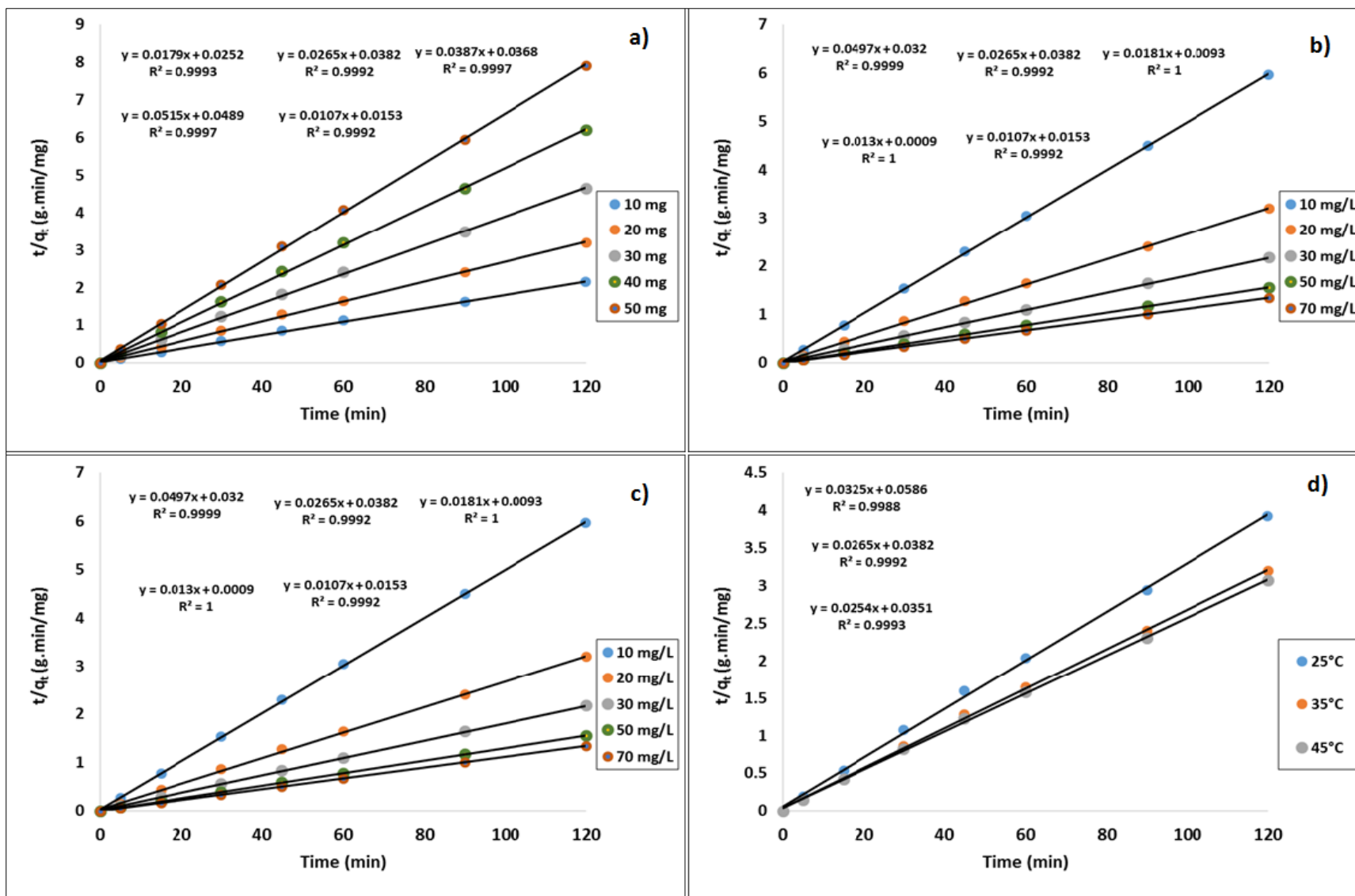


**Figure 5.9:** Fitted pseudo-second-order kinetic model for the adsorption of Ni (II) ions onto EB bio-char at various, a) adsorbent dosage, b) initial Ni concentration c) solution pH, d) solution temperature.



### 5.3.3 Intra Particles Diffusion Model and Mechanisms of Adsorption

The sorption process of solid/liquid phases is generally identified either by an external mass transfer occurred on the boundary layers of the adsorbent or through an intra-particle diffusion or both. The most commonly used technique for identifying the mechanism involved in the adsorption process is presented by fitting the experimental data onto Intra-particle diffusion model as per equation (2.10) where  $k_{id}$  ( $\text{mg/g min}^{0.5}$ ) is the intra-particle diffusion rate constant. Intra-particle adsorption process is consisted of multi steps where migration of the dye molecules from the bulk solution to the surface of the sorbent, diffusion through the boundary layer to the surface of the sorbent, adsorption at sites and intra-particle diffusion into the interior of the sorbent (Konicki et al. 2013). The adsorption mechanism and the dynamic behaviour of MB dye and Ni (II) ions adsorption onto pine cone bio-char have been examined by fitting the experimental data into Intra-particle diffusion model as shown in Fig 5.10 and Fig.5.11 respectively. Intra-particle diffusion plots of the amount of MB dye and Ni (II) ions adsorbed ( $q_t$ ) versus the square roots of contact time ( $t$ )<sup>0.5</sup> for various process parameters such as initial dye concentration, solution pH, adsorbent dose and temperature are presented in Fig 5.10 and Fig.5.11 respectively. It was found from in from Fig 5.10 and Fig.5.11 that the amount of adsorbates adsorbed  $q_t$  ( $\text{mg/g}$ ) were rapid at the initial period of contact time and then became slow and almost stable with the increases in contact time. This trend indicates the multistage of adsorption where the adsorbate solution is adsorbed due to the external mass transfer followed by intra particle diffusion respectively (Dawood et al. 2014). The overall rate of adsorption is controlled by the slowest step, which may be either film diffusion or pore diffusion. All the plots presented in Fig.5.10 and Fig.5.11 give two or more intercepting lines depending on the actual mechanism where none of these plots give linear straight line segment passing through the origin. This trend shows that both film diffusion and intra-particle diffusion occurred simultaneously and the adsorption of

MB dye and Ni (II) ions onto pine cone bio-char particles are controlled by a fast film diffusion at earlier stages (Sen et al. 2011). Generally, the adsorbate molecules move from bulk solution to the surface of the sorbent, through the boundary layer followed by mesopores intra-particle diffusion into the interior of the sorbent. Furthermore, the diffusion coefficient ( $D_p$ ) depends on the surface properties of adsorbents and it was calculated from equation (2.11) where ( $r_0$ ) is the radius of the adsorbent particle (cm). The half-life ( $t^{0.5}$ ) was calculated from equation (5.3) where  $K_s$  is the pseudo-second order rate constant (g/mg.min).

$$t^{0.5} = \frac{1}{K_s q_e} \quad (5.3)$$

The surface weighted mean diameter of pine cone bio-char particle was found as 23  $\mu\text{m}$  (radius= 11.5  $\mu\text{m}$  x 0.0001 cm = 0.00115 cm). The intra-particle-diffusion coefficient ( $D_p$ ) ( $\text{cm}^2/\text{s}$ ) was calculated as  $9.8 \times 10^{-9}$ ,  $1.4 \times 10^{-8}$ ,  $3 \times 10^{-8}$ ,  $2.5 \times 10^{-8}$  and  $2.8 \times 10^{-8}$   $\text{cm}^2/\text{s}$  for an initial MB dye concentration of 10, 20, 30, 50 and 70 mg/L respectively. Therefore, the pore diffusion role is important in this study. Further,  $C$  values describes the boundary layer effect where higher  $C$  values are an indicative of higher boundary layer effect. It was found that  $C$  values were high and ranging from 7.1 to 41.9 in the removal of MB dye as shown in Table 5.6 and 2.5 to 45.9 for Ni (II) ions as presented in Table 5.7 and thus indicates the inapplicability of pore diffusion as the only rate-determining step in describing the dynamics of the adsorption process (Sewu et al. 2017) and suggests a higher contribution of the surface sorption in the rate limiting step. It was further observed from Table 5.6 that  $K_{id}$  ( $\text{mg}/\text{g min}^{0.5}$ ) and constant ( $C$ ) for MB dye increased with the increases of initial adsorbate concentration, solution pH and temperature and decreased with the increases of pine cone biochar dose. From Table 5.7, that  $K_{id}$  ( $\text{mg}/\text{g min}^{0.5}$ ) and constant ( $C$ ) for Ni (II) ions increased with the increases of initial adsorbate concentration and temperature but decreased with the increase of pine cone biochar doses. Also, that  $K_{id}$  ( $\text{mg}/\text{g min}^{0.5}$ ) and constant ( $C$ ) for Ni (II) ions adsorption increased with the increases of initial solution pH up to a pH of 9.4 then decreased significantly at a solution pH of 11.3. The linear regression coefficient ( $R^2$ ) values were calculated lower than 0.763 for both adsorbates as shown in Table 5.6 and Table 5.7 respectively and thus suggest the

inaccuracy of intra-particle diffusion model. However, the influence of this model cannot be totally neglected.

**Table 5.6:** Intra particle diffusion model parameters for MB dye adsorption onto pine cone bio-char.

<b>System Parameters</b>	<b><math>q_e</math> (mg/g), Experimental</b>	<b><math>K_{id}</math> (mg/g min<sup>0.5</sup>)</b>	<b>C</b>	<b>R<sup>2</sup></b>
<b>Adsorbent Dosage (mg)</b>				
<b>10</b>	66.58	4.37	25.72	0.579
<b>20</b>	41.14	2.87	15.43	0.629
<b>30</b>	28.30	1.96	10.84	0.617
<b>40</b>	21.91	1.52	8.99	0.584
<b>50</b>	17.18	1.2	7.01	0.587
<b>Initial dye Concentration (mg/L)</b>				
<b>10</b>	21.89	1.51	7.87	0.644
<b>20</b>	41.14	2.87	15.43	0.629
<b>30</b>	60.07	4.12	25.62	0.559
<b>50</b>	82.21	5.46	36.2	0.527
<b>70</b>	93.79	6.12	41.91	0.513
<b>Solution pH</b>				
<b>5.1</b>	21.40	1.467	8.59	0.588
<b>6.4</b>	29.52	2.07	10.92	0.638
<b>8</b>	31.93	2.42	9.75	0.735
<b>9.4</b>	37.06	2.63	13.04	0.667
<b>11.3</b>	41.14	2.87	15.43	0.629
<b>Solution temperature</b>				
<b>25<sup>0</sup>C</b>	28.77	1.83	12.91	0.498
<b>35<sup>0</sup>C</b>	41.14	2.87	15.43	0.629
<b>45<sup>0</sup>C</b>	41.80	2.88	15.42	0.631

**Table 5.7:** Intra particle diffusion model parameters for Ni (II) ions adsorption onto pine cone bio-char.

<b>System Parameters</b>	<b>q<sub>e</sub> (mg/g), Experimental</b>	<b>K<sub>id</sub> (mg/g min<sup>0.5</sup>)</b>	<b>C</b>	<b>R<sup>2</sup></b>
<b>Adsorbent Dosage (mg)</b>				
<b>10</b>	55.75	22	24.65	0.527
<b>20</b>	37.52	2.49	16.66	0.523
<b>30</b>	25.76	1.67	11.99	0.489
<b>40</b>	19.37	1.26	9.02	0.489
<b>50</b>	15.15	0.98	7.04	0.491
<b>Initial dye Concentration (mg/L)</b>				
<b>10</b>	20.11	1.29	9.58	0.472
<b>20</b>	37.52	2.49	16.66	0.523
<b>30</b>	55.21	3.61	26.06	0.485
<b>50</b>	77.11	4.76	39.61	0.416
<b>70</b>	89.63	5.54	45.93	0.417
<b>Solution pH</b>				
<b>5.1</b>	5.24	0.33	2.52	0.463
<b>6.4</b>	9.64	0.74	2.87	0.762
<b>8</b>	29.40	2.15	10.1	0.689
<b>9.4</b>	37.52	2.49	16.66	0.523
<b>11.3</b>	20.97	1.41	9.14	0.537
<b>Solution temperature</b>				
<b>25<sup>0</sup>C</b>	30.59	2.06	13.06	0.5511
<b>35<sup>0</sup>C</b>	37.52	2.49	16.66	0.523
<b>45<sup>0</sup>C</b>	39.11	2.59	17.48	0.518

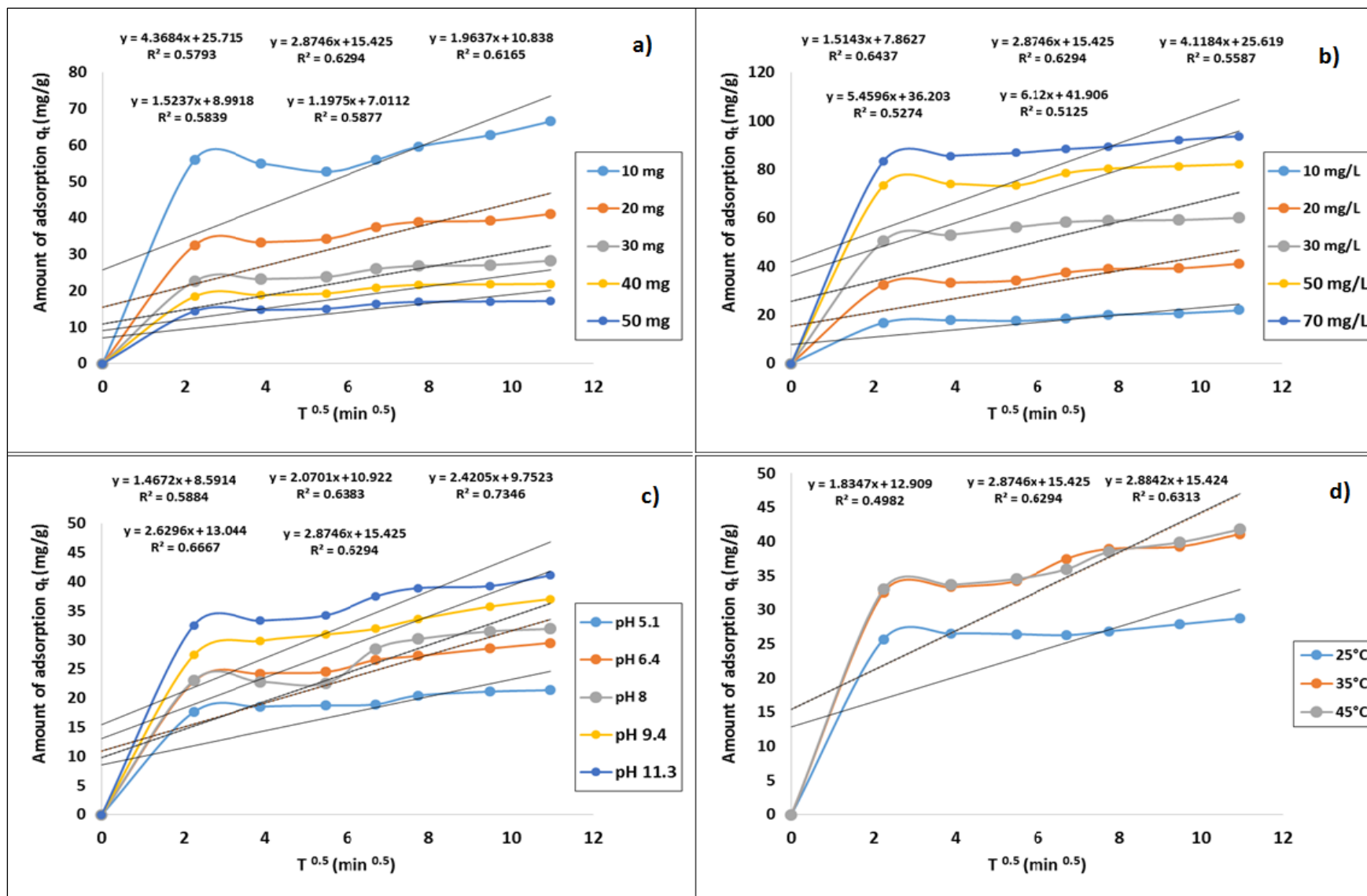


**Figure 5.10:** Intra particle diffusion model for the adsorption of MB dye onto pine cone bio-char at various a) adsorbent dosage, b) initial MB concentration, c) solution pH, d) solution temperature.

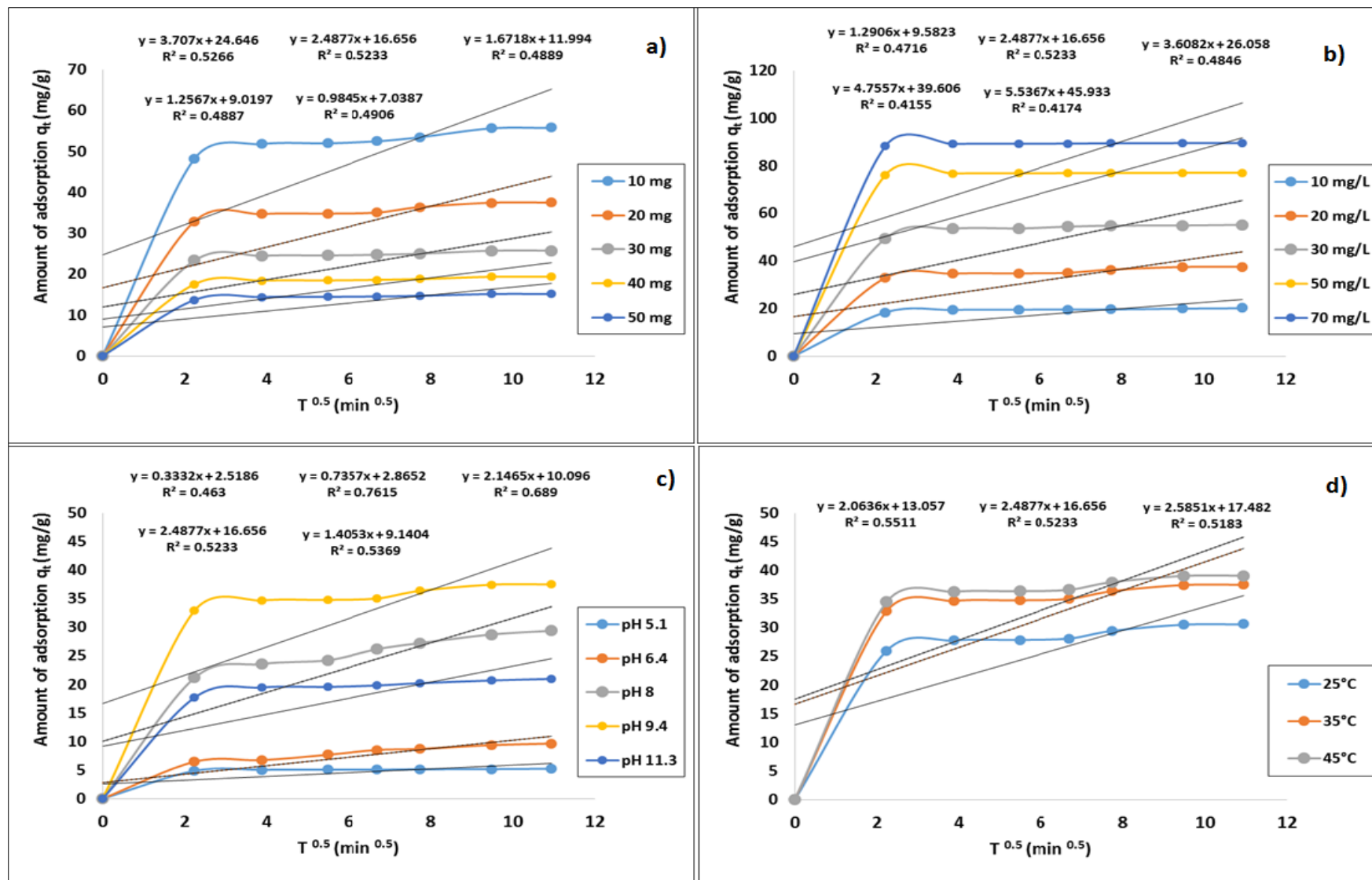


**Figure 5.11:** Intra particle diffusion model for the adsorption of Ni (II) onto pine cone bio-char at various a) adsorbent dosage, b) initial MB concentration, c) solution pH, d) solution temperature.

## 5.4 Application of Adsorption Equilibrium Models

The adsorption equilibrium model explains the specific relationship between the concentration of adsorbate and its degree of accumulation onto adsorbent surface at constant temperature (Liu and Zhang 2015). The adsorbent surface phase may be considered as a monolayer or multilayer. Experimental data have been fitted with Langmuir and Freundlich isotherm models to evaluate the applicability of these models for MB dye and Ni (II) ions onto pine cone bio-char adsorption process. The best fitted model was determined by high linear regression coefficient ( $R^2$ ). The isotherm experiment was carried out as per section (3.6) and the theory of these models are detailed in section 2.9 of chapter 2.

Langmuir isotherm is valid for monolayer adsorption onto the adsorbent surface containing a finite number of identical sites. The equilibrium experimental data were fitted as per equations (2.13) and (2.14). It was found that Langmuir isotherm gives a higher linear regression coefficient of 0.999 in the removal of MB dye and 0.994 in the removal of Ni (II) ions as shown in Table 5.8. The maximum adsorption capacity  $q_m$  (mg/g) and Langmuir constant  $K_L$  (L/mg) were calculated from the slope and intercept of plot between ( $C_e$ ) vs. ( $C_e/q_e$ ) as per equation (2.13) as shown in Fig.5.12 (a) and (b). Langmuir constant  $K_L$  (L/mg) for MB dye and Ni (II) ions was calculated as 0.20 and 0.11 respectively while the maximum adsorption capacity  $q_m$  was calculated as 106.38 mg/g for MB dye and 117.65 mg/g for Ni (II) ions as shown in Table 5.8. Also, the low separation factor ( $R_L$ ) values for various initial adsorbate concentrations were calculated as per equation (2.15). The  $R_L$  values for MB dye were found in the range of 0.07 to 0.33 and 0.11 to 0.47 for Ni (II) ions. The dimensionless factor ( $R_L$ ) values were found to be  $0 < R_L < 1$  for both adsorbates and thus indicate a feasible and physical adsorption process (Kaur et al. 2013).

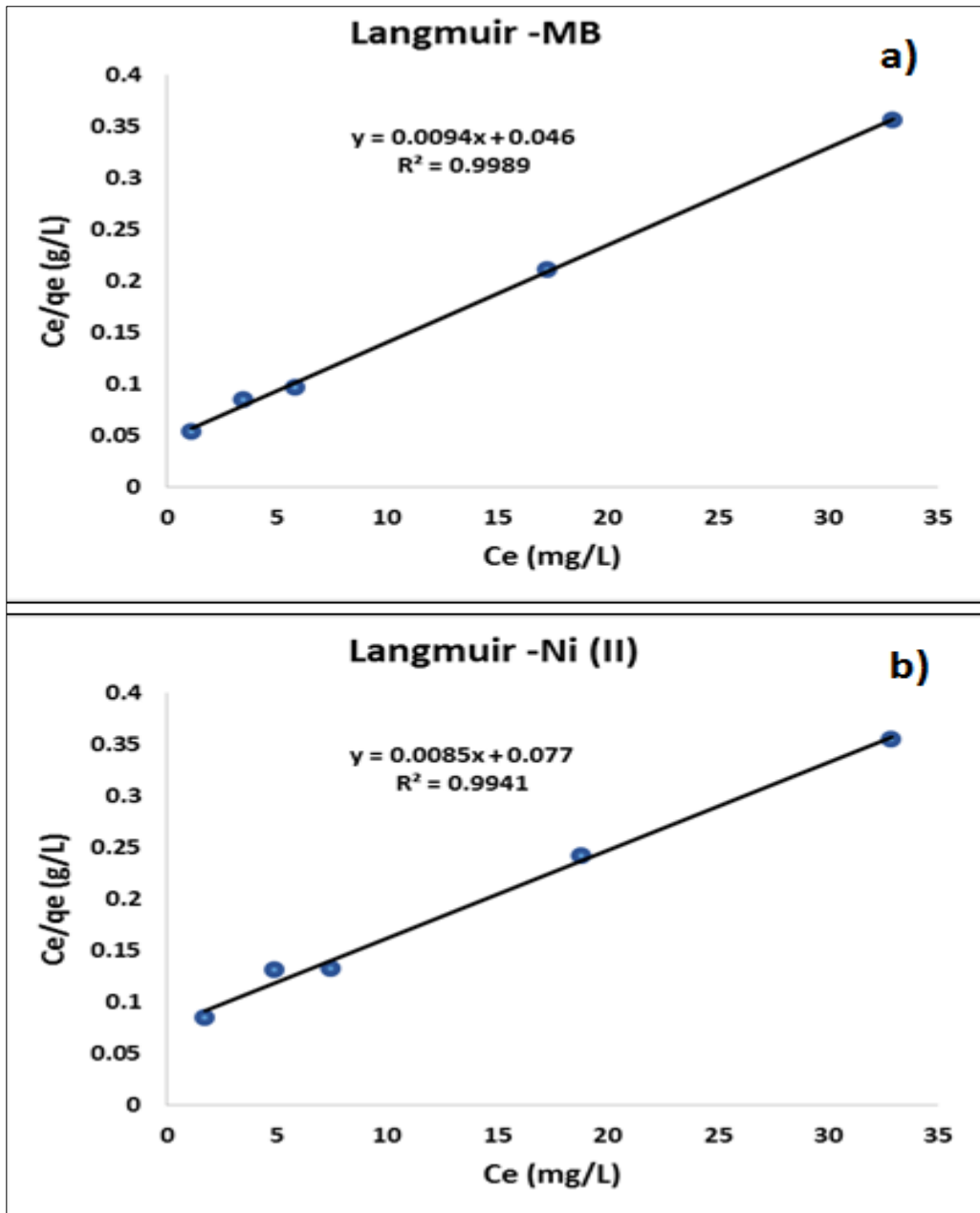


**Figure 5.12:** a) Langmuir plot for MB dye , b) Langmuir plot for Ni (II), pH solution (MB=11.3,Ni= 9.4) Volume =50 ml, Initial dose=20mg, temperature =35 °C, Shaker Speed 130 rpm at time=180 min.



The applicability of Freundlich model was tested by fitting the equilibrium experimental data as per equation (2.12) and as shown in Fig.5.13. The results were tabulated and presented in Table.5.8. It was found that Freundlich isotherm gives a high linear regression coefficient value of 0.947 for MB dye and 0.968 for Ni (II) removal systems respectively as shown in Table 5.8. The adsorption capacity of the system,  $K_f$  (L/g) and the heterogeneity factor  $1/n$  can be calculated from slope and intercept of the linear plot of  $\ln(q_e)$  versus  $(\ln C_e)$  as shown in Fig.5.13. The adsorption capacity of the system,  $K_f$  was calculated as 23.19 L/g for MB dye and 16.68 L/g for Ni (II) ions. Further, Freundlich constant  $n$  was found to be higher than unity for MB dye and Ni (II) removal which indicates a favourable and a physical adsorption process (Tran et al. 2017). Finally, it can be concluded that the removal of MB dye and Ni (II) ions onto pine cone biochar fit well with both the Langmuir and Freundlich isotherm models. The adsorption capacity of MB dye and Ni (II) ions onto pine cone bio-char have been compared with various adsorbents carbon under similar experimental conditions as presented in Table 5.9. From Table.5.9, it shows that pine cone bio-char studied in this work has a comparative adsorption capacity compared to other adsorbents.

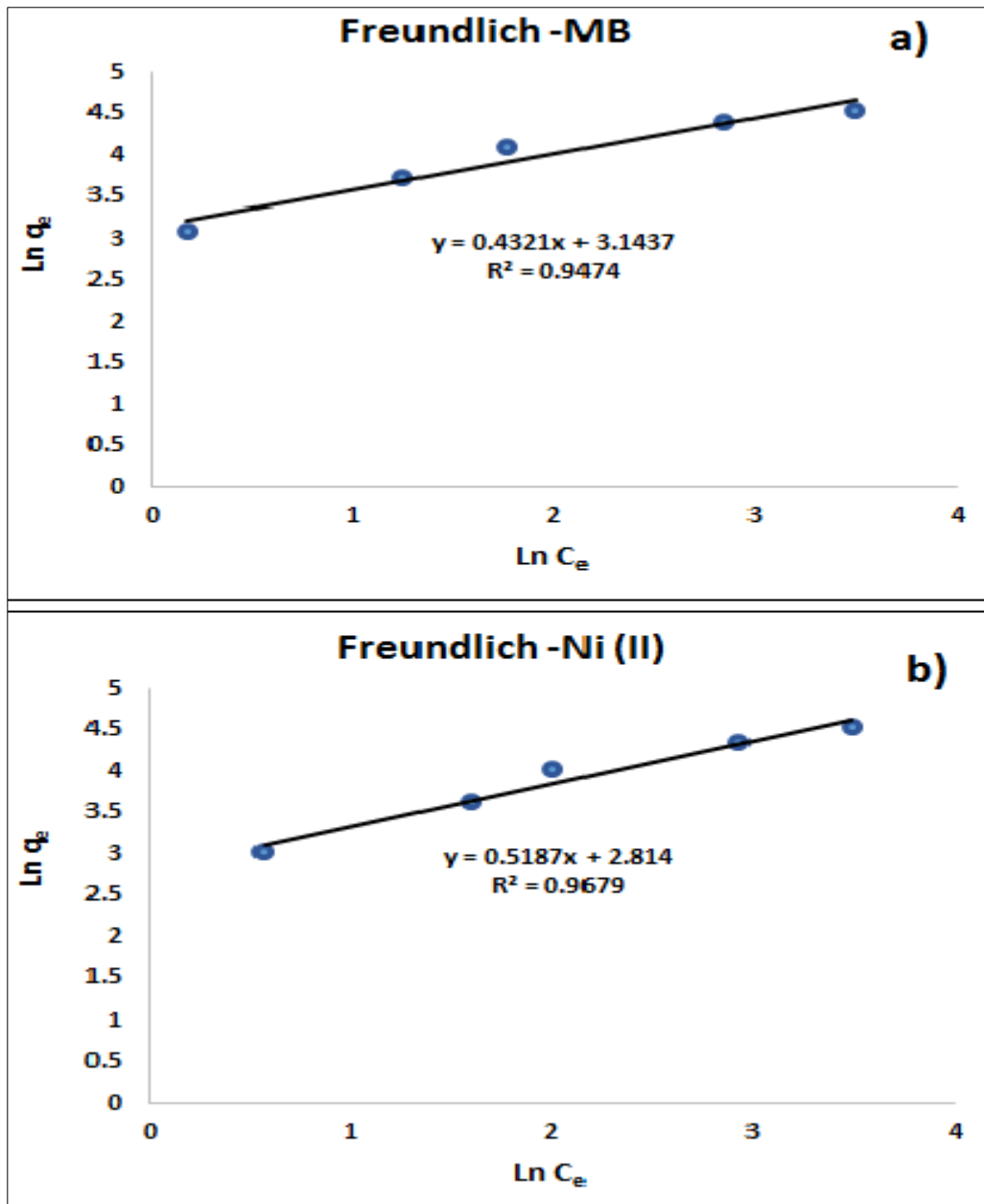


**Figure 5.13:** Freundlich isotherm model for MB dye and Ni (II) onto pine cone bio-char, pH solution (MB=11.3,Ni= 9.4) Volume =50 ml, Initial dose=20mg, temperature =35 °C, Shaker Speed 130 rpm at time=180 min.

**Table 5.8:** Calculated values for Freundlich and Langmuir isotherm models.

		Ni (II) ions	MB dye
Freundlich	$K_f$ (L/g)	16.68	23.19
	$n$	1.92	2.33
	$R^2$	0.968	0.947
Langmuir	$q_m$ (mg/g)	117.65	106.38
	$K_L$ (L/mg)	0.11	0.20
	$R^2$	0.994	0.999
	$R_L$ range	(0.11-0.47)	(0.07-0.33)

**Table 5.9:** Comparison of adsorption capacities in the removal of MB dye and Ni (II) ions by various adsorbents.

Adsorbents	Adsorbate	$q_{max}$ (mg/g)	References
bentonite/zeolite composite	MB dye	36.2	(Shaban et al. 2017)
Chitosan activated carbon	MB dye	143.5	(Marrakchi et al. 2017)
Oxidized weed biochar	MB dye	161.3	(Güzel et al. 2017)
Metkaolin (Geopolymer)	Ni (II)	42.6	(Kara et al. 2017)
Magnetic palm seed biochar	Ni (II)	28.0	(Gazi et al. 2017)
Nut shell activated carbon	MB dye	5.3	(Ragupathy et al. 2015)
Macoře fruit shell activated carbon	MB dye	10.6	(Aboua et al. 2015)
Waste tea activated carbon	MB dye	402	(Borah et al. 2015)
Palm tree activated carbon	MB dye	128	(AlOthman et al. 2014)
rapeseed oil cake activated carbon	Ni (II)	133.3	(Uçar et al. 2015)

Bio-char Ash	MB dye	178	(Özbay et al. 2013)
Clinoptilolite (Zeolite)	Ni (II)	186.1	(Hernández-Montoya et al. 2013)
kaolin	MB dye	45	(Rida et al. 2013)
Wheat straw bio-char	MB dye	12.03	(Liu et al. 2012)
Natural bentonite	Ni (II)	33	(Alandis et al. 2010)
Granular activated carbon	MB dye	21.5	(Yener et al. 2008)
Pine cone bio-char	MB dye	106.38	Present study
Pine cone bio-char	Ni (II)	117.65	Present study

## 5.5 Design of Single Stage Batch Adsorber from Isotherm Data

It was found that Langmuir isotherm model is fitted well with the equilibrium data. Adsorption isotherms can be used to predict the design of single batch adsorption system (Afroze et al. 2016b). Due to lack of extensive experimental data, empirical design procedures based on a batch adsorption isotherm study is used to predict the optimum process parameter such as the adsorber size and performance. The design objective was to decrease the initial adsorbate concentration from  $C_0$  to  $C_t$  (mg/L) for which the total adsorbate solution is  $V$  (L). The amount of added adsorbent (Pine cone biochar) is  $m$  (g) and the solute loading changes from  $q_0$  (mg/g) to  $q_t$  (mg/g). The initial adsorbate concentration on solid changes from  $q_0$  (mg/g) to  $q_t$  (mg/g) due to added adsorbent into the system. At time  $t = 0$ ,  $q_0 = 0$  and as time proceeds, the mass balance equates the MB dye and Ni (II) removal from the liquid phase to the adsorbed by pine cone biochar. The mass balance for MB dye and Ni (II) in the single-stage

operation under equilibrium are presented as per equation (5.4). Langmuir adsorption isotherm data has been utilised in this study to design a single-stage batch adsorption system as per method developed by (Kumar et al. 2010). Rearranging equations (2.13) and (5.4) thus can be written as per equation (5.5).

$$V (C_0 - C_e) = m (q_e - q_0) = m \cdot q_e \quad (5.4)$$

$$\frac{m}{V} = \frac{C_0 - C_e}{q_e} = \frac{C_0 - C_e}{q_m K_a C_e / (1 + K_a C_e)} \quad (5.5)$$

The predicted amount of pine cone bio-char particles required to remove MB dye and Ni (II) ions of initial concentrations of 100 mg/L for 50%, 60%, 70%, 80% and 90% adsorbate removal at different solution volumes (L) were presented in Fig 5.14 (a) and (b) respectively. For example, from Fig.5.14 (a), to obtain 90% MB dye removal, it is required 0.42, 0.84, 1.26, 1.68, 2.10, 2.51, 2.93, 3.35, 3.77 and 4.19 g of pine cone bio-char to remove 1-10 L of MB dye solution respectively. From Fig.5.14 (b), to achieve 90% Ni (II) ions removal, it is required 0.69, 1.38, 2.01, 2.76, 3.45, 4.14, 4.83, 5.52, 6.21 and 6.90g of pine cone bio-char to remove 1-10 L of nickel ions solution respectively.

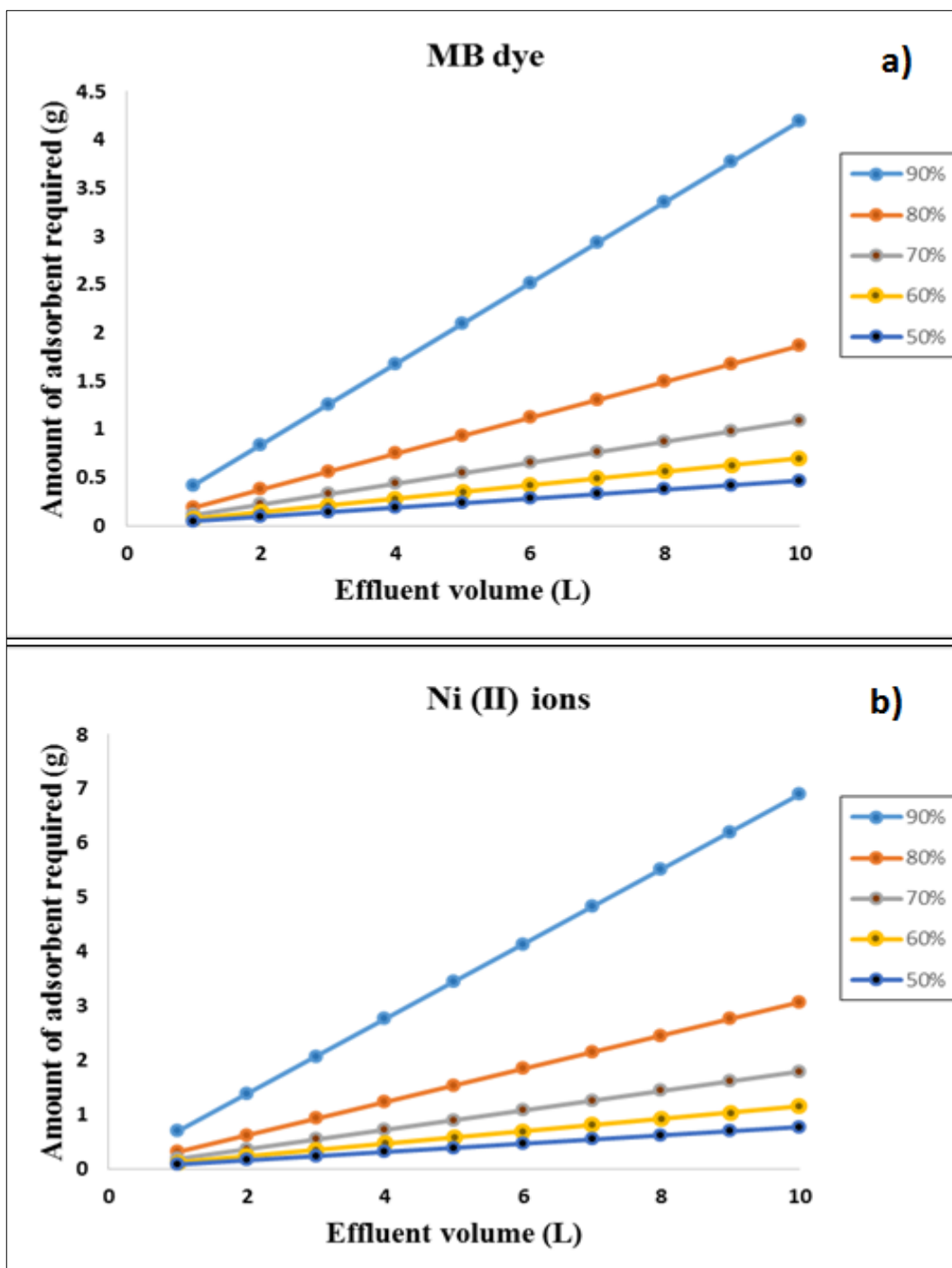


**Figure 5.14:** Design of single stage batch adsorber for a) MB dye, b) Ni (II) ions, Adsorbent mass (m) against volume of solution treated (L).

## 5.6 Conclusion

In the present study, pine cone biomass was utilized as a low cost feedstock in the production of pine cone based bio-char. The effectiveness of synthesized bio-char in the removal of Methylene blue dye and Ni (II) ions from their aqueous solution by adsorption process was tested here. It was found that the extent of both adsorbates adsorption onto pine cone bio-char increased with the increasing of initial adsorbate concentration, contact time, solution temperature and solution pH but decreased with the increase of adsorbent dose. Batch kinetics data were fitted into pseudo-first-order, pseudo-second order and intra particle diffusion models. Overall, the kinetic studies showed that the adsorption process for both MB dye and Ni (II) ions followed pseudo-second order kinetic and consisted of multi-steps processes: a rapid adsorption of adsorbate onto the external surface followed by intra-particle diffusion into the interior of adsorbent which has also been confirmed by intra-particle diffusion model. Equilibrium data were fitted with both Langmuir and Freundlich adsorption isotherm models and Langmuir maximum adsorption capacity  $q_m$  was calculated as 106.38 mg/g and 117.65 mg/g for MB dye and Ni (II) ions respectively. Based on the thermodynamic analysis and Langmuir isotherm data, it was observed that the adsorption system was endothermic and physical processes in nature. The positive value of ( $\Delta S^0$ ) indicated greater stability of an adsorption process with no structural changes at the solid-liquid interface. Therefore, it can be concluded that pine cone bio-char is a good low cost adsorbent in the removal of organic and inorganic pollutants from wastewater. Further, the utilization of pine cone waste will add economic value and help to reduce the cost of agricultural solid waste disposal and provide a potentially inexpensive alternative bio-char adsorbent to commercial activated carbon.

## 5.7 References

Aboua, K.N., Yobouet, Y.A., Yao, K.B., Goné, D.L. and Trokourey, A. (2015) "Investigation of dye adsorption onto activated carbon from the shells of Macoré fruit". Journal of Environmental Management **156**, 10-14.

Afroze, S., Sen, T.K. and Ang, H.M. (2016a) "Adsorption removal of zinc (II) from aqueous phase by raw and base modified Eucalyptus sheathiana bark: Kinetics, mechanism and equilibrium study". Process Safety and Environmental Protection **102**, 336-352.

Afroze, S., Sen, T.K., Ang, M. and Nishioka, H. (2016b) "Adsorption of methylene blue dye from aqueous solution by novel biomass Eucalyptus sheathiana bark: equilibrium, kinetics, thermodynamics and mechanism". Desalination and Water Treatment **57**(13), 5858-5878.

Alandis, N., Aldayel, O., Mekhemer, W., Hefne, J. and Jokhab, H. (2010) "Thermodynamic and kinetic studies for the adsorption of Fe (III) and Ni (II) ions from aqueous solution using natural bentonite". Journal of dispersion science and technology **31**(11), 1526-1534.

AlOthman, Z.A., Habila, M.A., Ali, R., Abdel Ghafar, A. and El-din Hassouna, M.S. (2014) "Valorization of two waste streams into activated carbon and studying its adsorption kinetics, equilibrium isotherms and thermodynamics for methylene blue removal". Arabian Journal of Chemistry **7**(6), 1148-1158.

Blue Mountains City Council (2009) Weeds of the Blue Mountains, <http://www.bmcc.nsw.gov.au/index.cfm>.

Borah, L., Goswami, M. and Phukan, P. (2015) "Adsorption of methylene blue and eosin yellow using porous carbon prepared from tea waste: Adsorption equilibrium, kinetics and thermodynamics study". Journal of Environmental Chemical Engineering **3**(2), 1018-1028.

Dawood, S. and Sen, T.K. (2012) "Removal of anionic dye Congo red from aqueous solution by raw pine and acid-treated pine cone powder as adsorbent: Equilibrium,



thermodynamic, kinetics, mechanism and process design". Water Research **46**(6), 1933-1946.

Dawood, S., Sen, T.K. and Phan, C. (2014) "Synthesis and characterisation of novel-activated carbon from waste biomass pine cone and its application in the removal of congo red dye from aqueous solution by adsorption". Water, Air, and Soil Pollution **225**(1).

Ding, S., Yang, Y., Li, C., Huang, H. and Hou, L.-a. (2016) "The effects of organic fouling on the removal of radionuclides by reverse osmosis membranes". Water Research **95**, 174-184.

Gazi, M., Oladipo, A.A. and Azalok, K.A. (2017) "Highly efficient and magnetically separable palm seed-based biochar for the removal of nickel". Separation Science and Technology, 1-8.

Ghaly, A.E., Ananthashankar, R., M., A. and Ramakrishnan, V.V. (2014) "Production, Characterization and Treatment of Textile Effluents: A Critical Review". J Chem Eng Process Technol **5**, 182.

Gokce, Y. and Aktas, Z. (2014) "Nitric acid modification of activated carbon produced from waste tea and adsorption of methylene blue and phenol". Applied Surface Science **313**, 352-359.

Güzel, F., Saygılı, H., Akkaya Saygılı, G., Koyuncu, F. and Yılmaz, C. (2017) "Optimal oxidation with nitric acid of biochar derived from pyrolysis of weeds and its application in removal of hazardous dye methylene blue from aqueous solution". Journal of Cleaner Production **144**(Supplement C), 260-265.

Han, R., Zhang, J., Han, P., Wang, Y., Zhao, Z. and Tang, M. (2009) "Study of equilibrium, kinetic and thermodynamic parameters about methylene blue adsorption onto natural zeolite". Chemical Engineering Journal **145**(3), 496-504.

Hernández-Montoya, V., Pérez-Cruz, M.A., Mendoza-Castillo, D.I., Moreno-Virgen, M.R. and Bonilla-Petriciolet, A. (2013) "Competitive adsorption of dyes and heavy metals on zeolitic structures". Journal of Environmental Management **116**(0), 213-221.

Kara, İ., Yilmazer, D. and Akar, S.T. (2017) "Metakaolin based geopolymer as an effective adsorbent for adsorption of zinc(II) and nickel(II) ions from aqueous solutions". Applied Clay Science **139**, 54-63.

Kaur, S., Rani, S. and Mahajan, R.K. (2013) " Adsorption Kinetics for the Removal of Hazardous Dye Congo Red by Biowaste Materials as Adsorbents". Journal of Chemistry **2013**, 12.

Kılıç, M., Kırbıyık, Ç., Çepelioğullar, Ö. and Pütün, A.E. (2013) "Adsorption of heavy metal ions from aqueous solutions by bio-char, a by-product of pyrolysis". Applied Surface Science **283**, 856-862.

Konicki, W., Sibera, D., Mijowska, E., Lenzion-Bieluń, Z. and Narkiewicz, U. (2013) "Equilibrium and kinetic studies on acid dye Acid Red 88 adsorption by magnetic ZnFe<sub>2</sub>O<sub>4</sub> spinel ferrite nanoparticles". Journal of Colloid and Interface Science **398**, 152-160.

Kumar, P., Ramalingam, S., Senthamarai, C., Niranjanaa, M., Vijayalakshmi, P. and Sivanesan, S. (2010) "Adsorption of dye from aqueous solution by cashew nut shell: Studies on equilibrium isotherm, kinetics and thermodynamics of interactions". Desalination **261**(1-2), 52-60.

Liu, X. and Zhang, L. (2015) "Removal of phosphate anions using the modified chitosan beads: Adsorption kinetic, isotherm and mechanism studies". Powder Technology **277**, 112-119.

Liu, Y., Zhao, X., Li, J., Ma, D. and Han, R. (2012) "Characterization of bio-char from pyrolysis of wheat straw and its evaluation on methylene blue adsorption". Desalination and Water Treatment **46**(1-3), 115-123.

Mahmoud, D.K., Salleh, M.A.M., Karim, W.A.W.A., Idris, A. and Abidin, Z.Z. (2012) "Batch adsorption of basic dye using acid treated kenaf fibre char: Equilibrium, kinetic and thermodynamic studies". Chemical Engineering Journal **181-182**(0), 449-457.

- Maneerung, T., Liew, J., Dai, Y., Kawi, S., Chong, C. and Wang, C.-H. (2016) "Activated carbon derived from carbon residue from biomass gasification and its application for dye adsorption: Kinetics, isotherms and thermodynamic studies". Bioresource Technology **200**, 350-359.
- Marrakchi, F., Ahmed, M.J., Khanday, W.A., Asif, M. and Hameed, B.H. (2017) "Mesoporous-activated carbon prepared from chitosan flakes via single-step sodium hydroxide activation for the adsorption of methylene blue". International Journal of Biological Macromolecules **98**, 233-239.
- Özbay, İ., Özdemir, U., Özbay, B. and Veli, S. (2013) "Kinetic, thermodynamic, and equilibrium studies for adsorption of azo reactive dye onto a novel waste adsorbent: charcoal ash". Desalination and Water Treatment **51**(31-33), 6091-6100.
- Ragupathy, S., Raghu, K. and Prabu, P. (2015) "Synthesis and characterization of TiO<sub>2</sub> loaded cashew nut shell activated carbon and photocatalytic activity on BG and MB dyes under sunlight radiation". Spectrochimica Acta Part A: Molecular and Biomolecular Spectroscopy **138**, 314-320.
- Rida, K., Bouraoui, S. and Hadnine, S. (2013) "Adsorption of methylene blue from aqueous solution by kaolin and zeolite". Applied Clay Science **83-84**(Supplement C), 99-105.
- Salleh, M.A.M., Mahmoud, D.K., Karim, W.A. and Idris, A. (2011) "Cationic and anionic dye adsorption by agricultural solid wastes: a comprehensive review". Desalination **280**(1-3), 1-13.
- Sen, T.K., Afroze, S. and Ang, H.M. (2011) "Equilibrium, kinetics and mechanism of removal of methylene blue from aqueous solution by adsorption onto pine cone biomass of *Pinus radiata*". Water Air Soil Pollut **218**, 499-515.
- Sewu, D.D., Boakye, P. and Woo, S.H. (2017) "Highly efficient adsorption of cationic dye by biochar produced with Korean cabbage waste". Bioresource Technology **224**, 206-213.

Shaban, M., Abukhadra, M.R., Shahien, M. and Ibrahim, S.S. (2017) "Novel bentonite/zeolite-NaP composite efficiently removes methylene blue and Congo red dyes". Environmental Chemistry Letters, 1-6.

Shakoor, S. and Nasar, A. (2016) "Removal of methylene blue dye from artificially contaminated water using citrus limetta peel waste as a very low cost adsorbent". Journal of the Taiwan Institute of Chemical Engineers **66**, 154-163.

Sočo, E. and Kalembkiewicz, J. (2013) "Adsorption of nickel(II) and copper(II) ions from aqueous solution by coal fly ash". Journal of Environmental Chemical Engineering **1**(3), 581-588.

Tran, H.N., You, S.-J. and Chao, H.-P. (2016) "Thermodynamic parameters of cadmium adsorption onto orange peel calculated from various methods: A comparison study". Journal of Environmental Chemical Engineering **4**(3), 2671-2682.

Tran, H.N., You, S.-J., Hosseini-Bandegharai, A. and Chao, H.-P. (2017) "Mistakes and inconsistencies regarding adsorption of contaminants from aqueous solutions: A critical review". Water Research **120**(Supplement C), 88-116.

Uçar, S., Erdem, M., Tay, T. and Karagöz, S. (2015) "Removal of lead (II) and nickel (II) ions from aqueous solution using activated carbon prepared from rapeseed oil cake by Na<sub>2</sub>CO<sub>3</sub> activation". Clean Technologies and Environmental Policy **17**(3), 747-756.

Uddin, M.T., Rahman, M.A., Rukanuzzaman, M. and Islam, M.A. (2017) "A potential low cost adsorbent for the removal of cationic dyes from aqueous solutions". Applied Water Science **7**(6), 2831-2842.

Vadivelan, V. and Kumar, K.V. (2005) " Equilibrium, kinetics, mechanism and process design for the sorption of methylene blue onto rice husk". J. Colloid Interface Sci **286**, 90-100.

Yagub, M.T., Sen, T.K., Afroze, S. and Ang, H.M. (2014a) "Dye and its removal from aqueous solution by adsorption: A review". Advances in Colloid and Interface Science **209**(0), 172-184.

Yagub, M.T., Sen, T.K. and Ang, H.M. (2012) "Equilibrium, kinetics, and thermodynamics of methylene blue adsorption by pine tree leaves". Water, Air, and Soil Pollution **223**(8), 5267-5282.

Yagub, M.T., Sen, T.K. and Ang, M. (2014b) "Removal of cationic dye methylene blue (MB) from aqueous solution by ground raw and base modified pine cone powder". Environmental Earth Sciences **71**(4), 1507-1519.

Yaneva, Z.L. and Georgieva, N.V. (2012) "Insights into Congo Red Adsorption on Agro-Industrial Materials - Spectral, Equilibrium, Kinetic, Thermodynamic, Dynamic and Desorption Studies. A Review". International Review of Chemical Engineering **4**(2), 127-146.

Yener, J., Kopac, T., Dogu, G. and Dogu, T. (2008) "Dynamic analysis of sorption of methylene blue dye on granular and powdered activated carbon". Chemical Engineering Journal **144**(3), 400-406.

Zhu, L., Wang, Y., He, T., You, L. and Shen, X. (2016) "Assessment of Potential Capability of Water Bamboo Leaves on the Adsorption Removal Efficiency of Cationic Dye from Aqueous Solutions". Journal of Polymers and the Environment **24**(2), 148-158.

*Every reasonable effort has been made to acknowledge the owners of copyright material. I would be pleased to hear from any copyright owner who has been omitted or incorrectly acknowledged.*

# **CHAPTER 6**

## **ADSORPTIVE REMOVAL OF METHYLENE BLUE DYE ONTO KAOLIN CLAY BY ADSORPTION PROCESS THROUGH BATCH AND ISOTHERM STUDY.**

## ABSTRACT\*

In this research raw kaolin was utilized as an adsorbent to investigate its effectiveness in the removal of cationic Methylene Blue dye from aqueous solution. Kaolin is a low cost natural clay with crystalline structure and it is available worldwide. The amount of dye adsorbed  $q_t$  (mg/g) and percentage of dye removal were determined under various physico-chemical process parameters such as initial solution pH, dye concentration, temperature and adsorbent dose. It was observed that the amount of dye adsorbed  $q_t$  (mg/g) by kaolin increased with the increase of initial dye concentration, solution pH and temperature but decreased with the increase of adsorbent dose. Furthermore, pseudo-first-order, pseudo-second-order and Intra-particle diffusion adsorption kinetic models were examined and it was observed that experimental data are well fitted with pseudo-second-order model with a linear regression coefficients values of 0.99 and Chi square values lower than 0.006. This suggests the applicability of pseudo-second-order kinetics model. Equilibrium data were best represented by both Freundlich and Langmuir isotherm models with a Langmuir maximum adsorption capacity ( $q_m$ ) of 80.65 (mg/g). Thermodynamic parameters such as entropy change ( $\Delta S^\circ$ ) and enthalpy change ( $\Delta H^\circ$ ) suggested that the adsorption was an endothermic, spontaneous and physical in nature. These results indicate the feasibility of kaolin clay as a cost-effective adsorbent in the removal of cationic Methylene Blue dye.

---

\*Partial results of this work has been published as a book chapter and cited as (Dawood, S., T. Gupta, and T. K. Sen. 2017. "Adsorptive Removal of Methylene Blue (MB) Dye at Kaolin Clay-Water Interface: Kinetics, Isotherm Modelling and Process Design." In Clay Minerals: Properties, Occurrence and Uses Sen, T. K., 209-236 New York, USA: Nova Publishers Inc).

## 6.1 Introduction

This chapter investigates the potential efficiency of raw kaolin clay as an adsorbent in the removal of organic Methylene blue dye from its aqueous solution by adsorption process. Wastewater effluents containing organic dyes may cause a prospective hazard to the environment. Methylene Blue dye is a toxic cationic dye and it is widely used in the textile industry. Exposing to high dosage of MB dye affects skin, eyes, cardiac arrhythmias, coronary vasoconstriction, decreased cardiac output, renal blood flow and mesenteric blood flow (Leyh et al. 2003, Shakoor and Nasar 2016). Therefore, the removal of MB dye from wastewater effluent is essential. Kaolin is non-metallic low cost natural clays, available worldwide in rocks as crystalline structure. Kaolin is also known as Kaolinite and it has various applications in ceramic, brick, finest chinaware and pharmaceutical industries. In this present chapter, batch adsorption in the removal of MB dye from its aqueous phase by kaolin clay has been studied as described in section 3.5 and 3.6 of chapter 3 under various physicochemical process parameters such as initial solution pH, dye concentration, temperature and adsorbent dosage. Batch experimental data were analysed with pseudo-first-order, pseudo-second-order and intra-particle-diffusion models to determine the various adsorption kinetic parameters and mechanism of adsorption. Further, to understand the adsorption isotherm and the interaction behaviour of MB dye- kaolin clay, the equilibrium data were fitted into Langmuir and Freundlich isotherm models and thermodynamics properties were investigated. A single-stage batch adsorber was designed for MB dye removal onto kaolin based on equilibrium experimental data to gain insight into the process dynamics.



## 6.2 Results and Discussion

### 6.2.1 Effect of Kaolin dosage on MB dye adsorption

Various doses of kaolin clay on MB dye adsorption were performed to determine the most economical minimum dosage by keeping all other process parameters constant and varying the adsorbent dosage as shown in Fig 6.1. The other process parameters were kept constant where 50 ml of 20 mg/L MB dye solution mixed with 20 mg kaolin clay and rotated at speed of 130 rpm and temperature of 35°C for a period of up-to 125 min. It was found that the amount of dye adsorbed  $q_t$  (mg/g) and percentage dye removal were increased rapidly with the increase of contact time then slowed down until equilibrium reached at 125 mins as shown in Fig.6.1 (a) and (b) respectively while Fig.6.1 (c) shows the amount of MB dye adsorbed  $q_t$  (mg/g) and dye removal efficiency (%) against adsorbent concentration (mg) at time interval of 125 mins. Initially, the percentage dye removal was found to be rapid then became almost constant as the dose increased. From Fig.6.1, it was observed that the increase in adsorbent dosage from 10 mg to 50 mg resulted in decrease of amount of dye adsorbed ( $q_t$ ) from 51.5 (mg/g) to 16.2 (mg/g) while the percentage dye removal increased from 51.5 % to 81.2 % respectively. The decrease in amount of dye adsorbed  $q_t$  (mg/g) with increasing adsorbent mass is due to the split in the flux or the concentration gradient between solute concentration in the solution and the solute concentration in the surface of the adsorbent (Sen et al. 2011). Upon the increases in the kaolin dosage, the adsorption of MB dye on the kaolin surface was very fast which gives a lower adsorbate concentration in bulk solution compared to low adsorbent dose situation. Thus, with increasing adsorbent dosage, the amount of dye per unit mass of adsorbent  $q_e$  (mg/g) decreased whereas at low adsorbent dose, the adsorbate dye molecules are more easily accessible and hence the dye removal per unit weight of adsorbent is high. The increases in the percentage dye removal with the increases of adsorbent dosage could be attributed to the increase in the adsorbent surface areas hence the number of available active sites due to the increase in the adsorbent mass. A similar observation was reported for cationic dye adsorption on kaolin by various researchers (Nandi et al. 2009a, b, Rida et al. 2013a). The experimental data and detailed calculation on the adsorption capacity  $q_t$  (mg/g) and percentage dye removal percentage are presented in Appendix C-2.

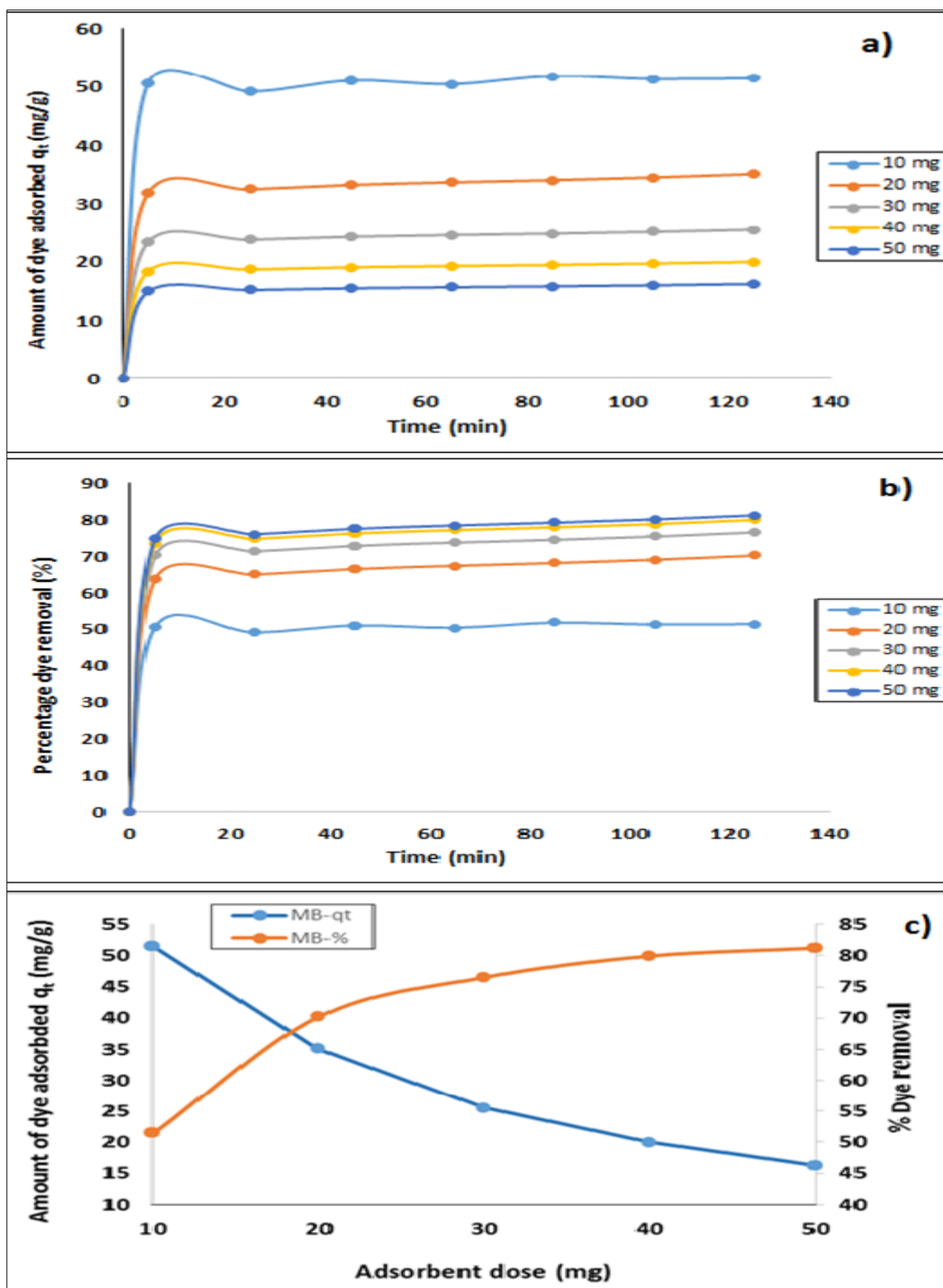
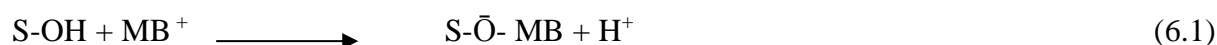


**Figure 6.1:** Effect of kaolin dose on MB dye adsorption. a) Amount of MB dye adsorbed, b) percentage dye removal c) Amount of dye adsorbed and dye removal at time=125 min. Where V= 50 ml, solution pH 11.3, MB = 20 mg/L, T= 35 °C and Shaker Speed 130 rpm.

## 6.2.2 Effect of initial solution pH on MB dye adsorption

The effect of solution pH on the adsorption of MB dye from its aqueous solution by kaolin clay was studied in the range of solution pH of 2.3 to 11.3 while the other process parameters were kept constant as shown in Fig.6.2. A fixed amount of 20 mg/L MB dye solution mixed with 20 mg kaolin clay and rotated at speed of 130 rpm and temperature of 35°C for a period of up-to 125 min. It was found that amount of dye adsorbed  $q_t$  (mg/g) was increasing rapidly with the increase of contact time then slowed down until equilibrium reached at 125 mins as shown in Fig.6.1 (a) while Fig.6.1 (b) shows the amount of MB dye adsorbed  $q_t$  (mg/g) and percentage dye removal against adsorbent concentration (mg) at time interval of 125 mins. It was found that the amount of dye adsorbed,  $q_t$  (mg/g) increased from 17.6 mg/g to 35.1 mg/g and the percentage dye removal increased from 35.1 % to 70.2 % with the increase in solution pH as shown in Fig.6.2 (b). The solution pH effect on MB dye adsorption by kaolin clay can be explained by the distribution of solid surface functional groups and  $\text{pH}_{\text{pzc}}$  (point of zero charge) of kaolin. Kaolin clay ( $\text{pH}_{\text{pzc}}$ ) was determined as 6.5 as per method described in section 3.4.5 of chapter 3. Higher solution pH above  $\text{pH}_{\text{pzc}}$ , the adsorbent becomes more negatively charged due to dissociation of oxygenated group which enhances the formation of MB – surface hydroxyl group complex as per following equation:



Where S-OH is the surface hydroxyl group of kaolin. With the increase in solution pH, the number of negatively charged sites increases and hence it does favour for a cationic dye adsorption due to electrostatic attraction force and surface complex formation as per equation (6.1). From the above equation, it is clear that  $\text{H}^+$  ions also generated during complex formation and hence final solution pH was decreased as noticed by this study. At higher solution pH, siloxane bond in kaolin clay surface is converted to Silanol group and Silanol group forms hydrogen bond with one amine group of MB dye and another amine group forms ionic bond with Si–O, molecules thus enhances the adsorption process (Mukherjee et al. 2015). Lower solution acidic pH gives lower adsorption of MB dye which is due to presences of excess  $\text{H}^+$  ions thus competing with the cationic group of dye for the adsorption sites. The experimental data and detailed calculation on the adsorption capacity  $q_t$  (mg/g) and percentage dye removal are presented in Appendix C-1.

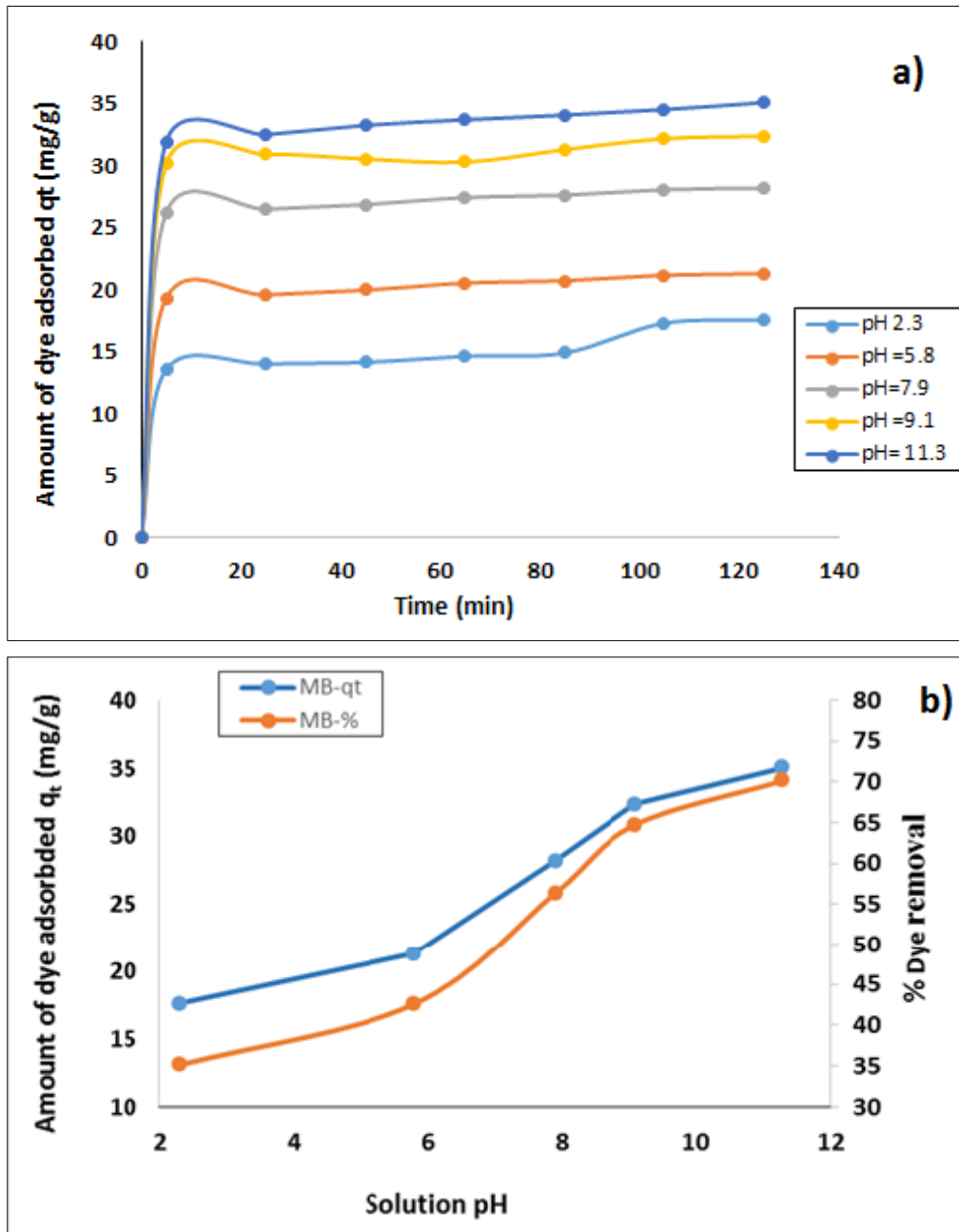


**Figure 6.2:** Effect of solution pH MB dye adsorption. a) Amount of MB dye adsorbed, b) Amount of dye adsorbed and dye removal at time=125 min. Where V= 50 ml, kaolin dose=20 mg, MB concentration= 20 mg/L, T= 35 °C and Shaker Speed 130 rpm.

### 6.2.3 Effect of initial MB dye concentration and contact time on adsorption.

The effect of initial dye concentrations has a significant effect on the development of sorbent-based water technology. In this project, MB dye concentration was varied from 10 to 70 mg/L while other process parameters were kept constant with 50 ml, pH value of 11.3 agitated at 130 rpm and temperature of 35°C for a period of up-to 125 min as shown in Fig 6.3. It was found that the amount of dye adsorbed  $q_t$  (mg/g) and percentage dye removal were increased rapidly with the increase of contact time and then slowed down until equilibrium reached at 125 mins as shown in Fig.6.3 (a) and (b) respectively while Fig.6.3 (c) shows the amount of MB dye adsorbed  $q_t$  (mg/g) and percentage dye removal (%) against MB dye concentration (mg/L) at time of 125 mins.

From Fig. 6.3 (a) and (c), the amount of dye adsorbed  $q_t$  (mg/g) was increased from 19.8 mg/g to 73.4 mg/g with increasing initial concentration of MB dye from 10 mg/L to 70 mg/L respectively. This is because higher initial dye concentration provides a high driving force to overcome the resistance to the mass transfer of dye between the aqueous solution and the solid phase for a fixed adsorbent dose, hence enhances the interaction process between the adsorbent and dye molecules. Concurrently the percentage of MB dye removal was decreased from almost 79.1 % to 42.0 % with increasing initial concentration of MB dye from 10 mg/L to 70 mg/L as shown in Fig.6.3 (b) and (c) respectively. This is because higher initial dye concentration causes the accumulation of dye molecules on the surface of the kaolin particle which leads to the saturation of available active adsorption sites and hence decreases the amount of dye removal (Yagub et al. 2014). Also, the increases of adsorption capacity  $q_t$  (mg/g) with the increases of contact time till equilibrium is attained within 125 min at all initial dye concentrations indicates two-step process: rapid adsorption from the bulk of solution to the adsorbent external surface followed by slow intra-particle diffusion in the interior of the adsorbent. Similar observation was also found by other researchers in the removal of Methylene blue (MB) dye by various adsorbents such as weed biochar (Güzel et al. 2017) and kenaf fibre char (Mahmoud et al. 2012). The experimental data and detailed calculation on the adsorption capacity  $q_t$  (mg/g) and percentage dye removal are presented in Appendix C-3.

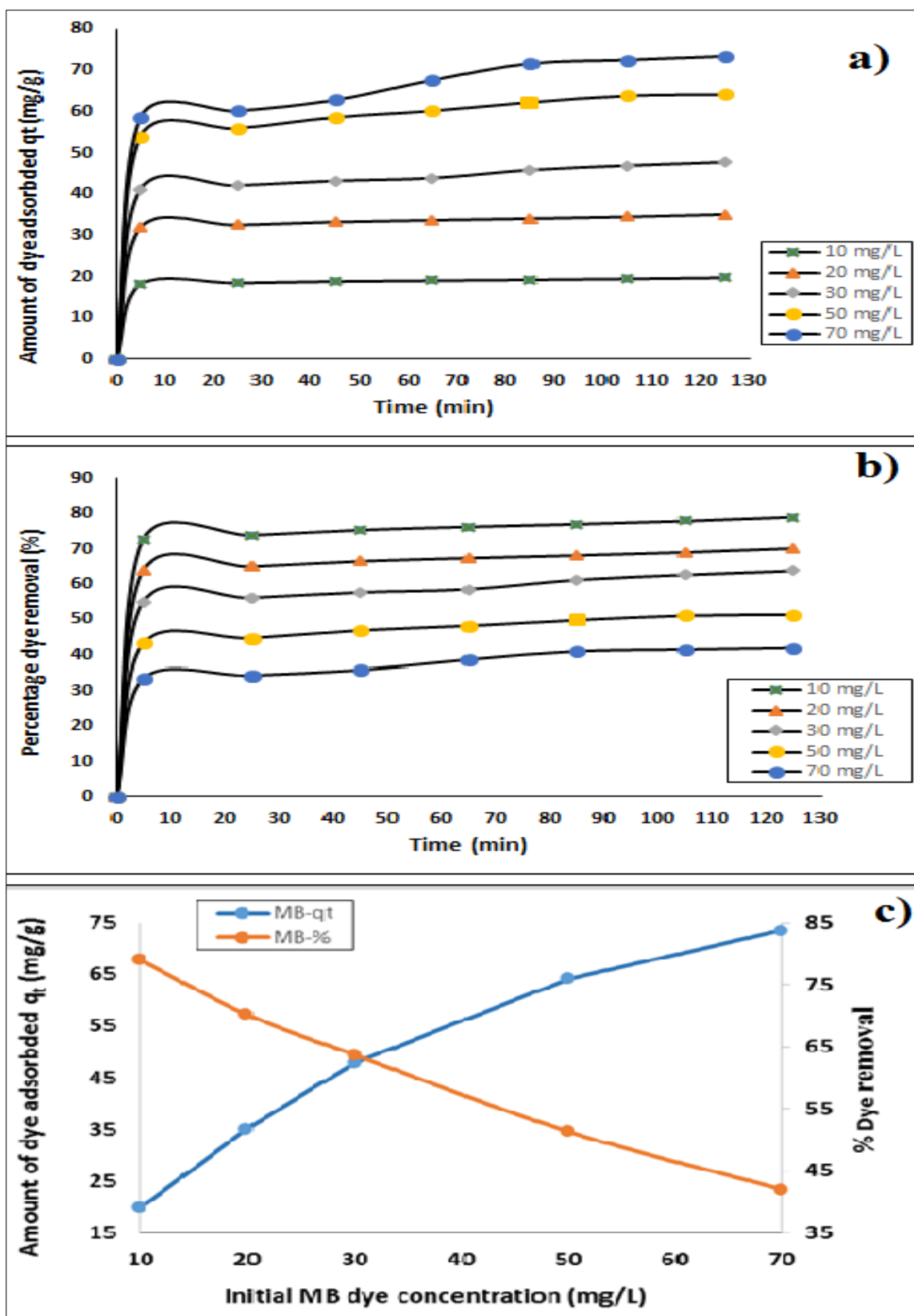


**Figure 6.3:** Effect of initial MB dye concentration and contact time on adsorption. a) Amount of MB dye adsorbed, b) percentage dye removal c) Amount of dye adsorbed and dye removal at time=125 min. Where V = 50 ml, solution pH 11.3, kaolin dose= 20 mg, T= 35 °C and Shaker Speed 130 rpm.

## 6.2.4 Effect of solution temperature and thermodynamics studies

The batch experiment has been evaluated under different solution temperatures of 25°C to 45°C while other process parameters were kept constant. A 50 ml solution of 20 mg/L initial dye concentration was added to 20 mg kaolin at solution pH of 11.3 and rotating speed of 130 rpm for a period of up-to 125 min to determine the optimum solution temperature and the thermodynamic behaviour of MB dye adsorption on kaolin clay. From Fig 6.4, it was found that the amount of dye adsorbed on kaolin clay was increased from 29.3 mg/g to 36.9 mg/g and the percentage dye removal was also increase from 58.5 % to 73.7 % with increasing the solution temperature respectively. Increasing the adsorption capacity with increase of temperature indicates an endothermic process in nature. This is also supported by thermodynamic parameter  $\Delta G^0$  which is decreasing with the increases of temperature as shown in Table.6.1.

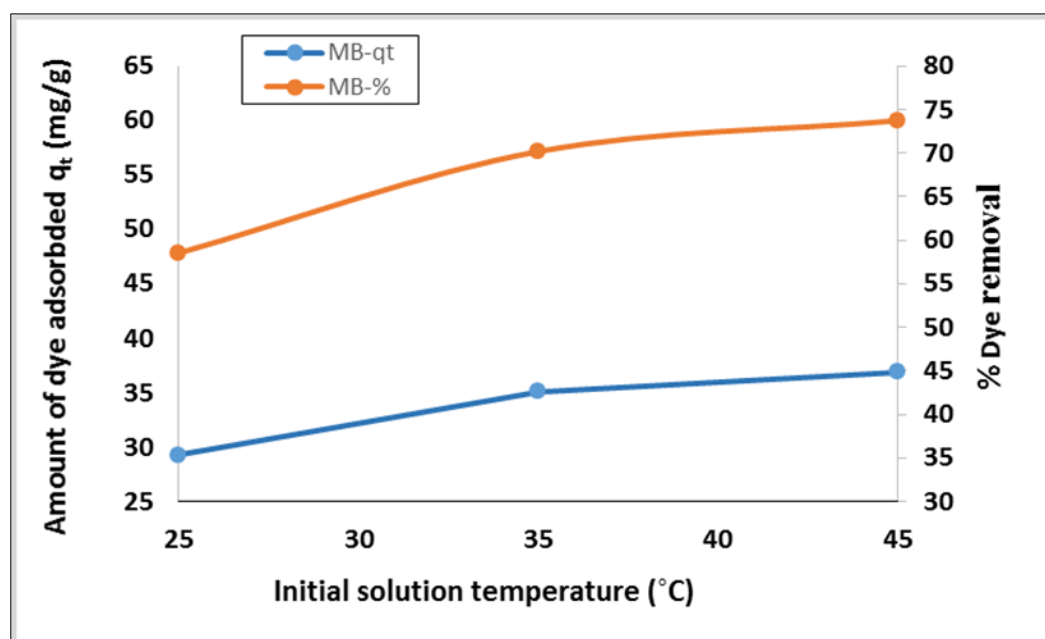


**Figure 6.4:** Effect of solution temperature on Kaolin adsorption of MB dye: MB conc=20 mg/L, adsorbent dose= 20 mg, MB volume 50 ml, solution pH=11.3, Shaker Speed 130 rpm and time=125 min.

The thermodynamics parameters include Gibb's free energy change ( $\Delta G^0$ ), entropy change ( $\Delta S^0$ ) and enthalpy change ( $\Delta H^0$ ) were calculated from Fig 6.5 as per equation (2.16) and (2.17) respectively and results are shown in Table 6.1. Gibb's free energy change ( $\Delta G^0$ ) values was found to be decreased from -20.5 KJ/mole to -23.7 KJ/mole with the increase of temperature from 25°C to 45°C respectively. The increases of  $\Delta G^0$  values with the increases of solution temperature indicates an energetically favourable and spontaneous adsorption process. This may be due to increase of active sites and also due to increase of the mobility of the dye molecules with increasing temperature (Salleh et al. 2011). This may also due to increase in the pore size and activation of adsorbent surface. Further, a chemical adsorption is considered when the enthalpy change ( $\Delta H^0$ ) is greater than 40 kJ mol<sup>-1</sup> and From Table 6.1, the enthalpy change ( $\Delta H^0$ ) was calculated as 27.2 kJ mol<sup>-1</sup> therefore indicates a physical adsorption process controlled by Van der Waals interaction. The positive entropy value ( $\Delta S^0$ ) of 0.16 kJ/mol.K indicates that the adsorption process is entropy driven rather than enthalpy driven force (Tran et al. 2016). The increase in entropy is presumably due to gain of translational entropy by the dye molecules during adsorption process. The experimental data and detailed calculation on the adsorption capacity  $q_t$  (mg/g) and percentage dye removal are presented in Appendix C-4.

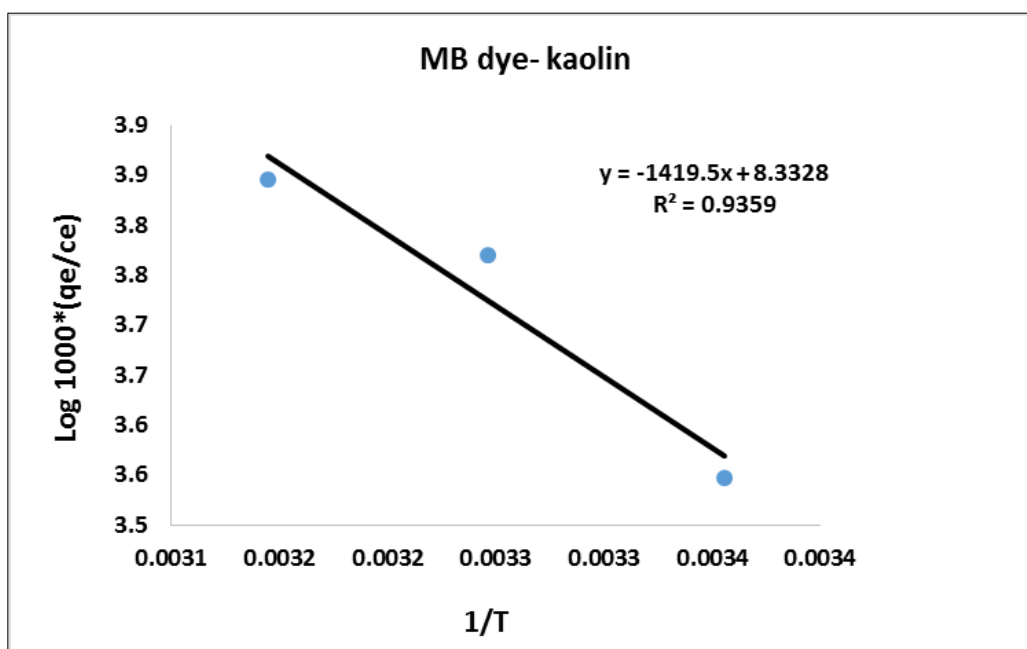


**Figure 6.5:** Plot of Van't Hoff equation for MB dye- kaolin adsorption.



**Table 6.1:** The thermodynamic properties of MB dye adsorption onto Kaolin clay.

Temp (K)	$\Delta G^\circ$ (kJ/mole)	$\Delta H^\circ$ (Kj /mole)	$\Delta S^\circ$ (Kj /mole.K)
298	-20.50	27.18	0.16
308	-22.10	27.18	0.16
318	-23.70	27.18	0.16

### 6.3 Adsorption kinetic and mechanism of adsorption

Batch adsorption kinetics have been studied under various physio-chemical process parameters such as adsorbent dose, initial adsorbate concentration, solution pH, temperature and contact time. The mechanism of adsorption, rate of control and the transient behaviour of dye adsorption process have been evaluated by Lagergren Pseudo-first-order, Pseudo-second-order and Intra particles diffusion kinetic models in order to determine the most suitable and practical model in term of high adsorption capacity and fast adsorption rate. The theory of these models are detailed in section 2.7 of chapter 2. The value of linear regression coefficient was used to determine the applicability of these kinetic models. Also, Chi-square is a statistic test used to evaluate the accuracy and the applicability of Pseudo-first-order and Pseudo-second-order kinetics models by determine the error between experimental ( $q_e$ ) and calculated ( $q_e$ ) and it is calculated from equation (2.4).

#### 6.3.1 Pseudo- first -order kinetic model

Analysing the batch adsorption kinetic experiments play a major role in the designing, optimisation and performance of industrial adsorption column. The nature of the adsorption process depends on physical and chemical characteristics of the adsorbent and on the system conditions. The applicability of pseudo-first-order model was tested by fitting the experimental data under various physico-chemical process parameters into equation (2.6). The calculated amount of dye adsorbed  $q_e$  (mg/g) values were obtained from the intercept of the linearized form of the plots  $\log (q_e - q_t)$  verses time ( $t$ ) as shown in Fig.6.6 and the fitted kinetic parameters were presented in Table 6.2.

From Table 6.2, it was observed that the adsorption capacity  $q_e$  (mg/g) increased with the increase in initial dye concentration, solution pH and temperature but decreased with the increase of amount of kaolin dose. The linear regression coefficient ( $R^2$ ) values were found in the range of 0.54 to 0.82 and the calculated adsorption capacity  $q_e$  (mg/g) values were significantly lower than the experimental equilibrium adsorption capacity  $q_e$  (mg/g) as shown in Table 6.2. Therefore, low linear regression coefficient ( $R^2$ ) values, lower calculated adsorption capacity  $q_{e(calculated)}$  in compare to experimental adsorption capacity  $q_{e(exp)}$  as well as the high error value obtained from Chi square test indicate the inaccuracy and inapplicability of Pseudo-first-order kinetic model.

**Table 6.2:** Fitted pseudo –first- order kinetic model parameters for MB dye adsorption by kaolin.

System Parameters	$q_e$ (mg/g), Experimental	$K_f$ ( $\text{min}^{-1}$ )	$q_e$ (mg/g), Calculated	Chi square	$R^2$
<b>Initial MB dye Concentration (mg/L)</b>					
10	19.76	0.04	2.40	125.85	0.731
20	35.09	0.05	3.26	310.85	0.717
30	47.79	0.06	5.12	355.32	0.646
50	64.15	0.05	5.32	650.13	0.822
70	73.43	0.05	6.21	727.36	0.798
<b>Solution pH</b>					
2.3	17.56	0.02	2.54	88.86	0.661
5.8	21.30	0.05	2.72	127.14	0.800
7	28.19	0.02	2.03	337.90	0.546
9.1	32.37	0.05	3.02	285.31	0.716
11.3	35.09	0.05	3.26	310.85	0.717
<b>Solution temperature</b>					
25 <sup>0</sup> C	29.27	0.05	3.21	211.34	0.708
35 <sup>0</sup> C	35.09	0.05	3.26	310.85	0.717
45 <sup>0</sup> C	36.86	0.05	3.33	337.41	0.709
<b>kaolin dosage (mg)</b>					
10	51.45	0.06	2.65	899.56	0.752
20	35.09	0.05	3.26	310.85	0.717
30	25.50	0.05	2.90	176.02	0.692
40	19.98	0.05	2.47	124.13	0.715
50	16.24	0.04	2.12	94.04	0.747

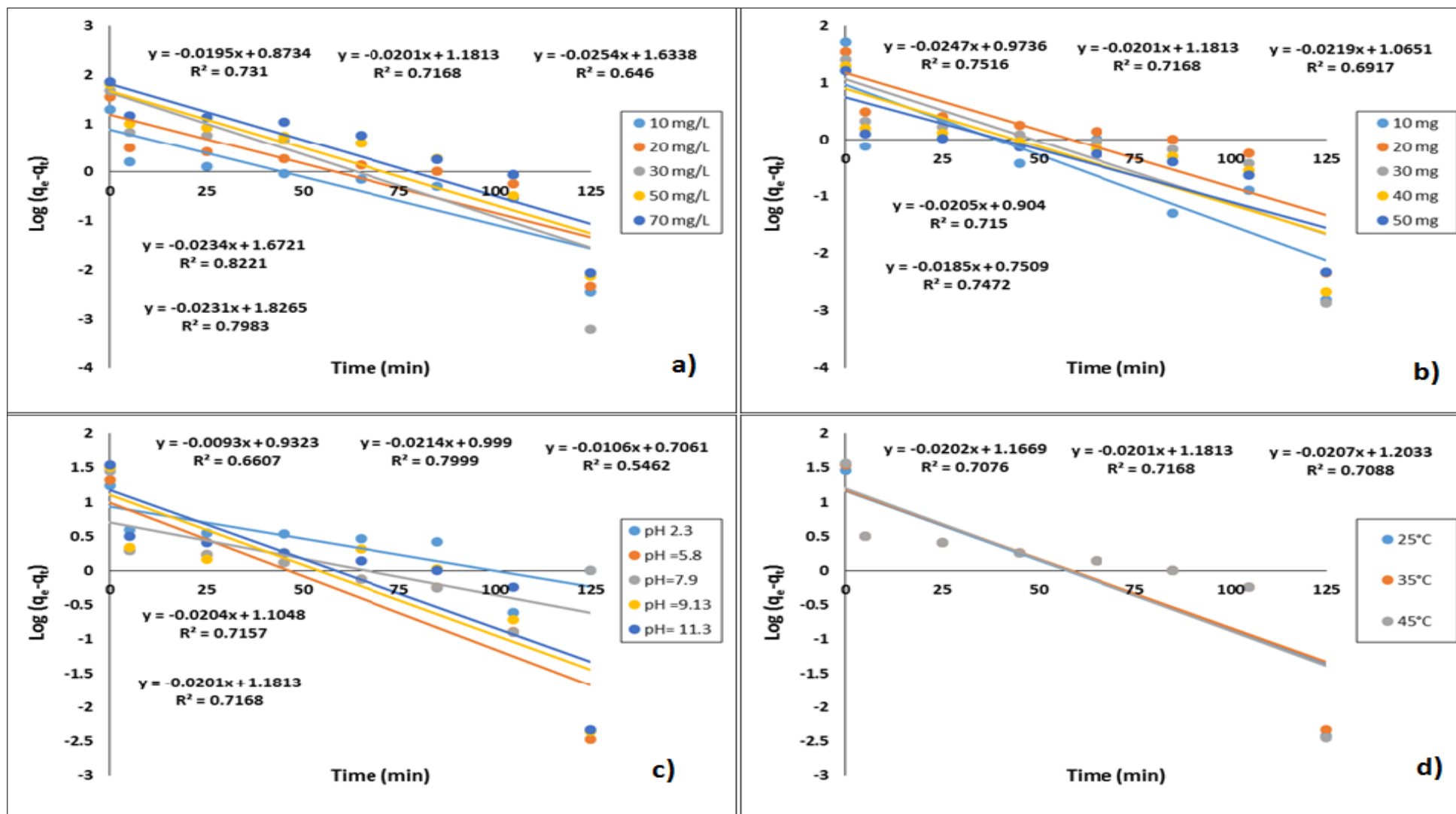


**Figure 6.6:** Fitted pseudo-first-order kinetic parameters for the adsorption of MB dye onto kaolin at various a) initial MB concentration, b) kaolin dosage, c) solution pH and d) solution temperature.

### 6.3.2 Pseudo-second -order kinetic model

Pseudo-second-order kinetic model was applied to investigate the applicability of MB dye adsorption on kaolin clay. Experimental data were applied into pseudo-second - order kinetic model as per equation (2.8) and the calculated amount of dye adsorbed  $q_e$  (mg/g) was obtained from the slope of the linearized form where  $(t/q_t)$  verses time ( $t$ ) as shown in Fig.6.7. All the kinetic parameters under various physio-chemical process parameters for second-order model were presented Table.6.3. High linear regression coefficients ( $R^2$ ) values were found in the range of 0.983 to 0.999 as shown in Table 6.3. Also, it was observed that the calculated amount of dye adsorbed ( $q_e$ ) values were almost identical to the experimental amount of dye adsorbed ( $q_e$ ). The adsorption capacity  $q_e$  (mg/g) of MB dye on kaolin clay were found to increase with the increase in initial dye concentration, solution pH and temperature and decrease with the increase of kaolin dosage.

Pseudo-second order rate constant  $K_s$  (g/mg.min) was found to decrease with the increases of initial MB dye concentration and increase with the increases of kaolin dose except for initial kaolin dose of 10 mg. This may be due to the lower competition for the sorption sites at lower adsorbate concentration. At higher dye concentrations, the competition for the surface-active sites will be high and hence lower adsorption rates are attained. The initial adsorption rate  $h$  (mg/g.min) was calculated as per equation (2.9) and it was found to increase with the increases of solution temperature and decrease with the increase of kaolin dosage. Chi square ( $\chi^2$ ) test values were found to be lower than 0.006 for various process parameters as shown in Table 6.3. Therefore, high linear regression coefficient ( $R^2$ ) values and low error values presented from Chi-square ( $\chi^2$ ) test indicate the accuracy and applicability pseudo-second-order model.

**Table 6.3:** Fitted pseudo-second-order kinetic model calculated parameters for MB dye adsorption onto kaolin.

<b>System Parameters</b>	<b>q<sub>e</sub> (mg/g), Experimental</b>	<b>K<sub>s</sub> (g/mg-min)</b>	<b>q<sub>e</sub> (mg/g), Calculated</b>	<b>Chi square</b>	<b>h (mg/g.min)</b>	<b>R<sup>2</sup></b>
<b>Initial MB dye Concentration (mg/L)</b>						
<b>10</b>	19.76	0.05	19.69	0.000	17.67	0.999
<b>20</b>	35.09	0.02	34.97	0.000	27.62	0.999
<b>30</b>	47.79	0.01	47.62	0.001	20.00	0.998
<b>50</b>	64.15	0.01	64.52	0.002	27.32	0.998
<b>70</b>	73.43	0.00	74.07	0.006	20.70	0.996
<b>Solution pH</b>						
<b>2.3</b>	17.56	0.01	17.33	0.003	3.33	0.983
<b>5.8</b>	21.30	0.03	21.32	0.000	14.77	0.999
<b>7</b>	28.19	0.03	28.25	0.000	26.39	0.999
<b>9.1</b>	32.37	0.02	32.26	0.000	24.81	0.999
<b>11.3</b>	35.09	0.02	34.97	0.000	27.62	0.999
<b>Solution temperature</b>						
<b>25<sup>0</sup>C</b>	29.3	0.02	29.2	0.000	18.94	0.999
<b>35<sup>0</sup>C</b>	35.1	0.02	35.0	0.000	27.62	0.999
<b>45<sup>0</sup>C</b>	36.9	0.02	36.8	0.000	30.58	0.999
<b>Kaolin dosage (mg)</b>						
<b>10</b>	51.45	0.04	51.55	0.000	108.70	0.999
<b>20</b>	35.09	0.02	34.97	0.000	27.62	0.999
<b>30</b>	25.50	0.03	25.38	0.001	22.03	0.999
<b>40</b>	19.98	0.05	19.92	0.000	18.05	0.999
<b>50</b>	16.24	0.06	16.18	0.000	14.92	0.999

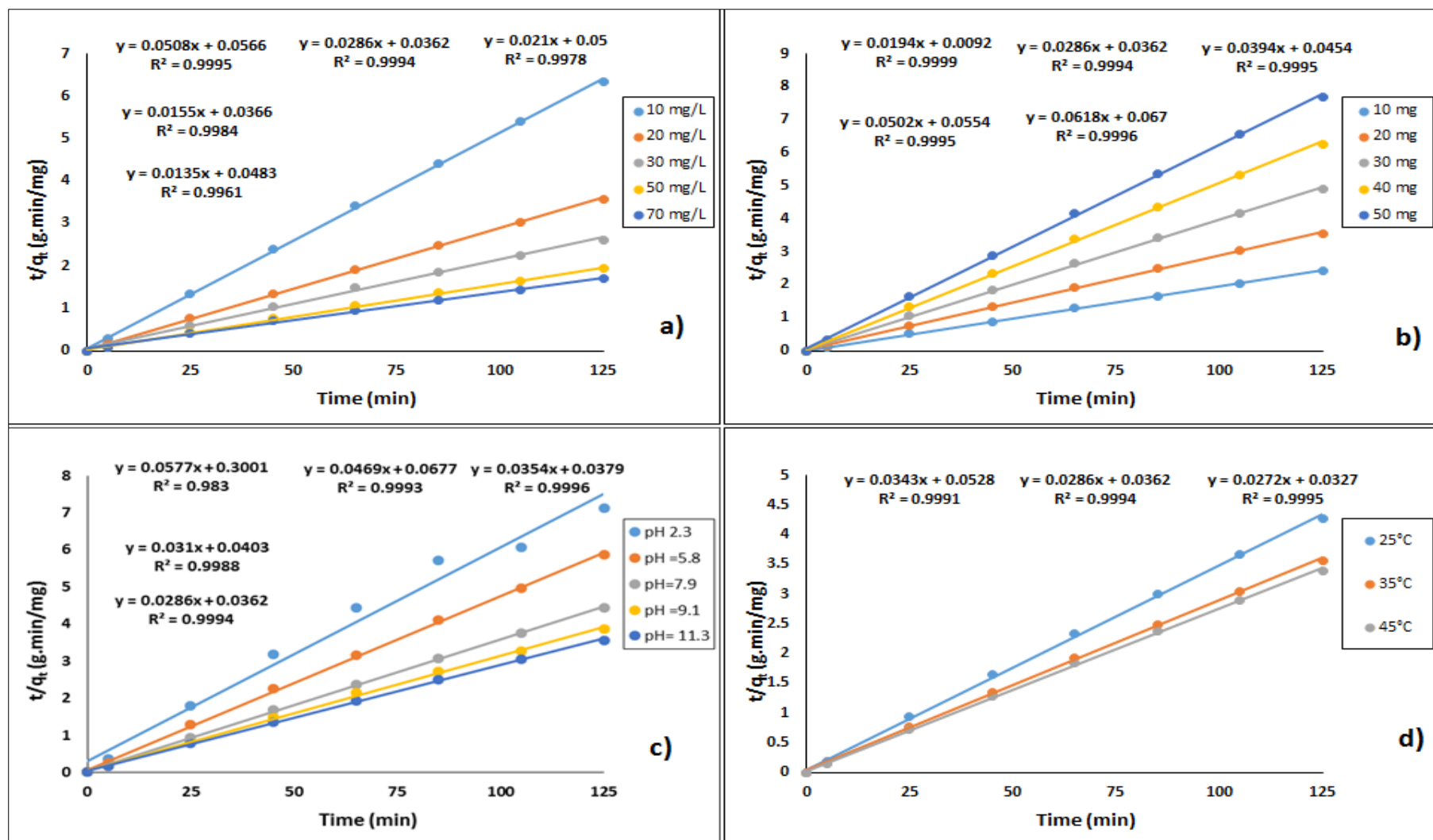


**Figure 6.7:** Pseudo-second-order kinetic model for the adsorption of MB dye onto kaolin at various a) initial MB concentration, b) kaolin dosage, c) solution pH and d) solution temperature.

### 6.3.3 Intra-particle-diffusion model

The adsorption mechanism and the dynamic behaviour of MB dye adsorption on kaolin clay have been evaluated by fitting the experimental data into Intra-particle-diffusion model as per equation (2.10). Intra-particle diffusion plots of the amount of dye adsorbed ( $q_t$ ) versus the square roots of contact ( $t$ )<sup>0.5</sup> for various process parameters such as initial dye concentration, solution pH, adsorbent dose and temperature are presented in Fig 6.8. The plots presented in Fig 6.8 were not linear over the entire contact time and can be separated into two regions which confirmed the multi stages of adsorption where migration of the dye molecules from the bulk solution to the surface of the sorbent take place, diffusion through the boundary layer to the surface of the sorbent, adsorption at sites and followed by intra-particle diffusion into the interior of the sorbent (Konicki et al. 2013).

Also, it was found that the removal of MB dye by kaolin adsorbent was rapid at the initial period of contact time and then became slow and almost constant with the increases in contact time. This trend indicates the multi-stages of adsorption where the MB dye molecules are adsorbed due to the external mass transfer followed by intra particle diffusion respectively. The initial linear stage of the plot indicates the boundary layer effect where the second stage indicates an intra-particle diffusion and the final stage is due to the chemical reaction. The intra-particle diffusion rate constant  $k_{id}$  (mg/g min<sup>0.5</sup>), boundary effect (C) and the linear regression coefficients ( $R^2$ ) values were calculated and presented in Table 6.4. The intercept (C) values described the boundary layer effect where higher C values are an indicative of higher boundary layer effect. C values were found in the range of 5.6 to 24.9 thus indicates the inapplicability of pore diffusion as the only rate-determining step in describing the dynamics of the adsorption process (Sewu et al. 2017). Moreover, the linear regression coefficient values ( $R^2$ ) presented in Table 6.4 were calculated lower than 0.78 which indicates the inaccuracy of intra-particle-diffusion model. However, the influence of this model cannot be totally neglected.

**Table 6.4:** Intra particle diffusion model parameters for MB dye adsorption on kaolin.

<b>System Parameters</b>	<b>q<sub>e</sub> (mg/g), Experimental</b>	<b>K<sub>id</sub> (mg/g min<sup>0.5</sup>)</b>	<b>C</b>	<b>R<sup>2</sup></b>
<b>Initial MB dye Concentration (mg/L)</b>				
<b>10</b>	19.76	1.25	8.41	0.532
<b>20</b>	35.09	2.23	14.71	0.542
<b>30</b>	47.79	3.11	18.40	0.595
<b>50</b>	64.15	4.30	24.07	0.622
<b>70</b>	73.43	5.08	24.92	0.679
<b>Solution pH</b>				
<b>2.3</b>	17.56	1.16	5.64	0.673
<b>5.8</b>	21.30	1.37	8.84	0.552
<b>7</b>	28.19	1.78	12.12	0.528
<b>9.1</b>	32.37	2.01	13.98	0.515
<b>11.3</b>	35.09	2.23	14.71	0.542
<b>Solution temperature</b>				
<b>25<sup>o</sup>C</b>	29.3	1.88	11.9	0.559
<b>35<sup>o</sup>C</b>	35.1	2.23	14.7	0.542
<b>45<sup>o</sup>C</b>	36.9	2.34	15.6	0.538
<b>Kaolin dosage (mg)</b>				
<b>10</b>	51.45	3.17	23.60	0.481
<b>20</b>	35.09	2.23	14.71	0.542
<b>30</b>	25.50	1.61	10.81	0.535
<b>40</b>	19.98	1.26	8.51	0.531
<b>50</b>	16.24	1.03	6.93	0.530



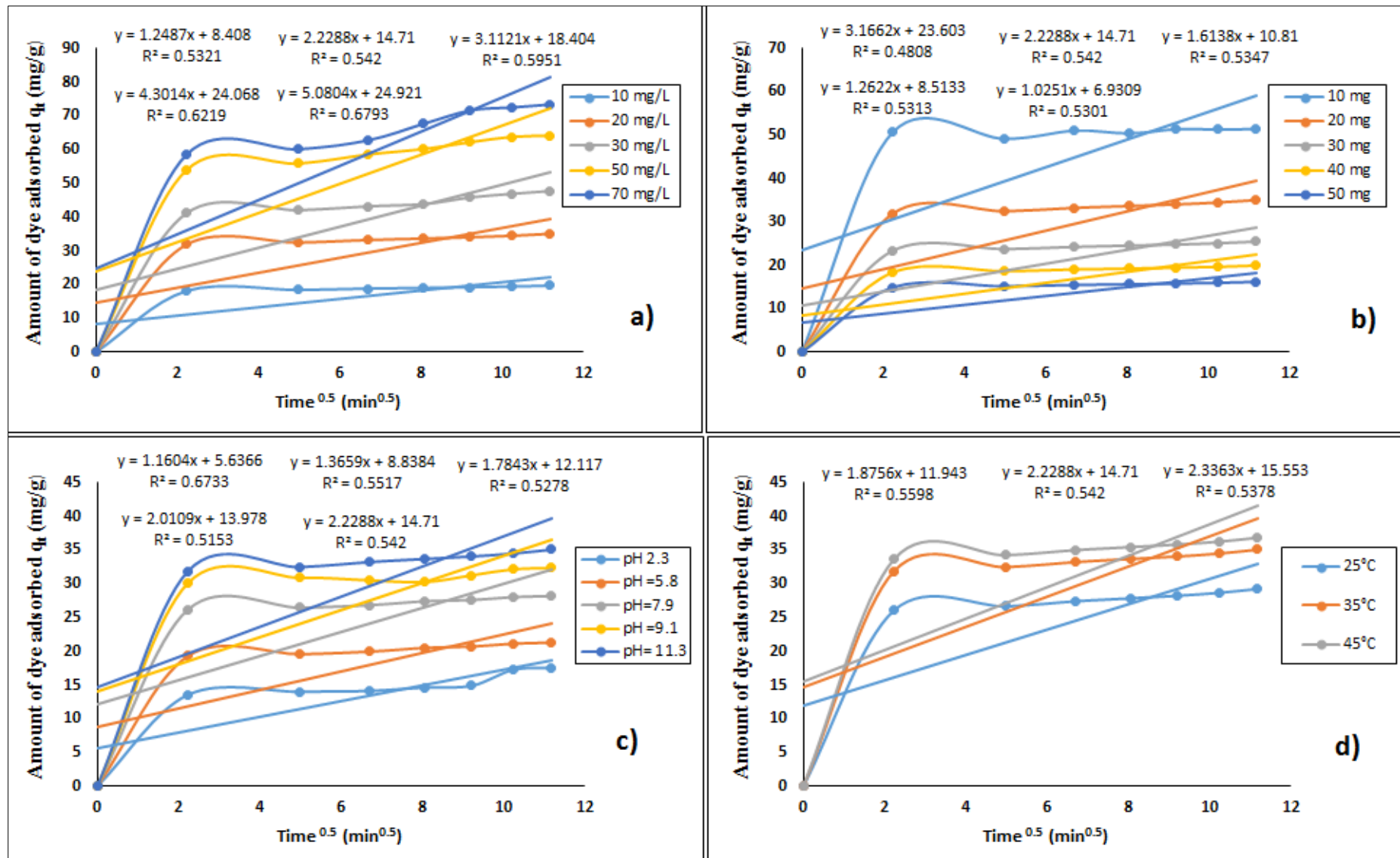


**Figure 6.8:** Intra particle diffusion model for the adsorption of MB dye onto kaolin at various a) initial MB dye concentration, b) adsorbent dosage, c) solution pH and d) solution temperature.

## 6.4 Adsorption Equilibrium Isotherm

The adsorption equilibrium isotherm explains the specific relationship between the adsorbate concentration and its degree of accumulation onto the adsorbent surface at constant temperature (Liu and Zhang 2015). Various isotherm models have been employed to fit the experimental data and evaluate the applicability of these models for MB dye adsorption. The isotherm experiment was carried out as per section 3.6 of chapter 3 and the theory of these models are detailed in section 2.8 of chapter 2. The experimental isotherm data were fitted into Freundlich and Langmuir (I) and (II) models as shown in Fig.6.9, Fig 6.10 (a) and (b) respectively.

Freundlich isotherm model is valid for multilayer adsorption and is derived by assuming a heterogeneous surface with interaction between adsorbed molecules with a non-uniform distribution of heat of sorption over the surface. The equilibrium experimental data were fitted into equation (2.12). The adsorption capacity of the system,  $K_f$  (L/g) and the heterogeneity factor  $1/n$  can be calculated from slope and intercept of the linear plot of  $\ln(q_e)$  versus  $\ln(Ce)$  as shown in Fig.6.9. The adsorption capacity of the system,  $K_f$  was calculated as 21.2 L/g and Freundlich constant  $n$  was calculated above the unity as 2.9 as shown in Table 6.5 and this indicates a favourable and a physical adsorption process (Tran et al. 2017). Also, linear regression coefficient ( $R^2$ ) for Freundlich model was calculated as 0.996.

Langmuir isotherm is valid for monolayer adsorption on the adsorbent surface containing a finite number of identical sites. The equilibrium experimental data were fitted into equations (2.13) for Langmuir (I) and (2.14) for Langmuir (II). It was found that Langmuir (I) isotherm gives a higher linear regression coefficient ( $R^2$ ) of 0.99 compared to 0.94 for Langmuir (II) isotherm as shown in Table 6.5. The maximum adsorption capacity,  $q_m$  (mg/g) and Langmuir constant  $K_L$  (L/mg) were calculated from the slope and intercept of equations (2.13) and (2.14) as shown in Fig.6.10 (a) and (b) respectively.

The maximum adsorption capacity,  $q_m$  and Langmuir constant  $K_L$  were calculated as 80.65 mg/g and 0.19 L/g for Langmuir (I) and 62.11 mg/g and 0.47 L/g for Langmuir (II) respectively. Also, the low separation factor ( $R_L$ ) values for various initial dye concentrations were calculated as per equation (2.15). The  $R_{(L-I)}$  for Langmuir (I) values were found to decrease from 0.34 to 0.07 and from 0.18 to 0.03 for Langmuir (II) with the increase of initial MB dye concentration from 10 mg/L to 100 mg/L respectively. Similar trend is observed for  $R_{(L-II)}$ . The dimensionless factor ( $R_L$ ) were found to be  $0 < R_L < 1$  thus indicates a feasible and physical adsorption process (Kaur et al. 2013).

From the results presented in Table 6.5, it can be concluded that the adsorption behaviour of MB dye onto kaolin clay follows both Freundlich and Langmuir (I) isotherm models. The adsorption capacity of MB dye onto kaolin clay has been compared with other non-conventional adsorbents under similar experimental conditions as presented in Table 6.6. Thus indicates the effectiveness and the applicability of kaolin clay as an adsorbent in the removal of MB dye.

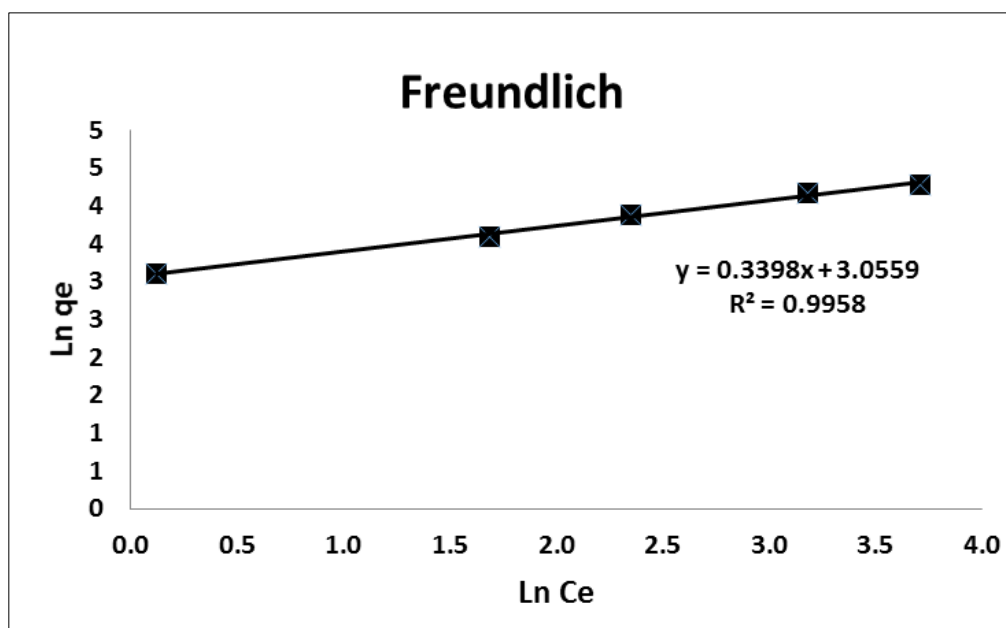


**Figure 6.9:** Freundlich isotherm model for MB dye onto kaolin, pH solution =11.3, Volume =50 ml, Initial dose=20mg, temperature =35 °C, Shaker Speed 130 rpm at time=150 min.

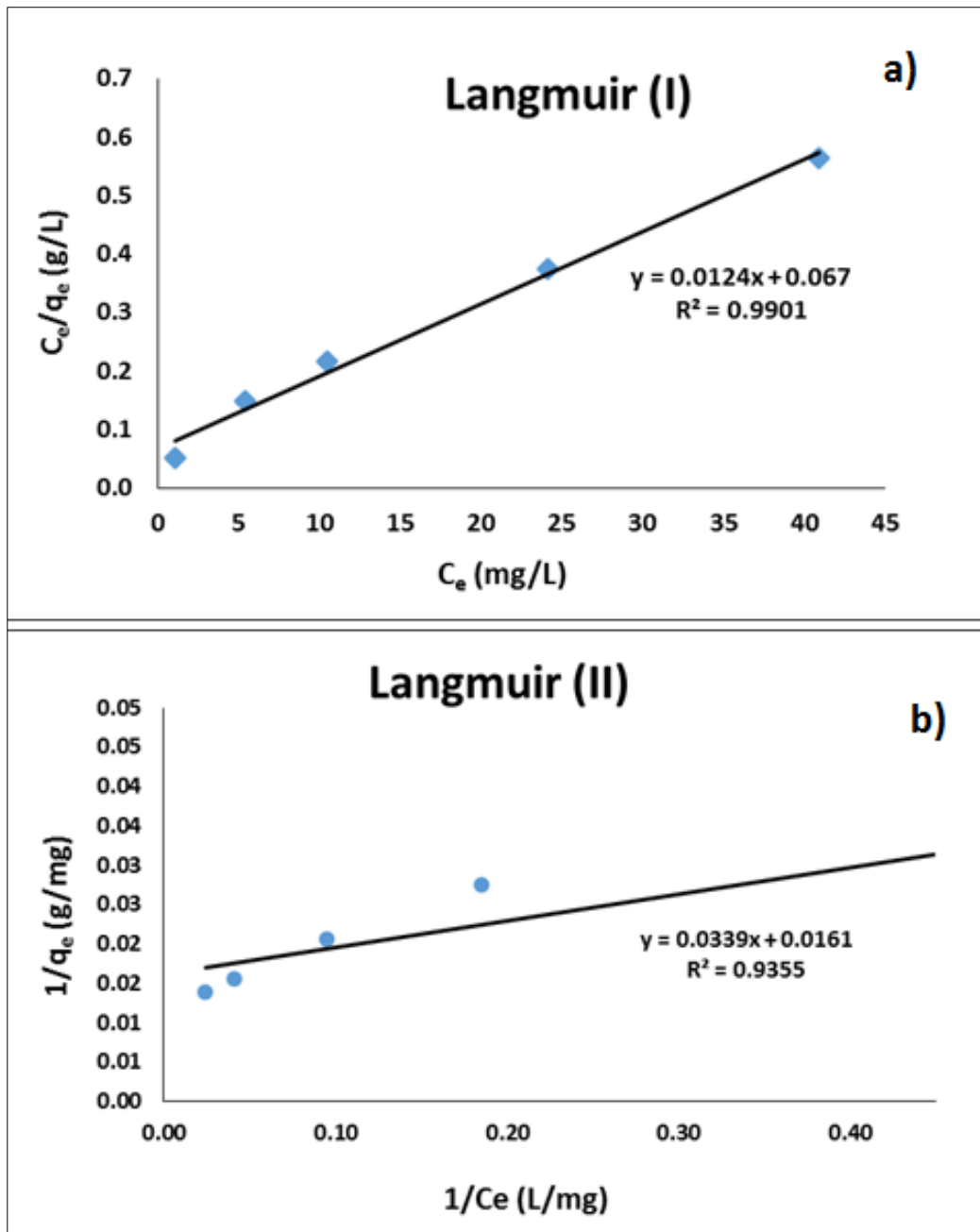


**Figure 6.10:** a) Langmuir (I) plot, b) Langmuir (II) plot, pH solution =11.3, Volume =50 ml, Initial dose=20mg, temperature =35 °C, Shaker Speed 130 rpm at time=150 min.

**Table 6.5:** Calculated values for Freundlich and Langmuir isotherm models.

<b>Freundlich</b>		
<b>K<sub>f</sub> (L/g)</b>	<b>n</b>	<b>R<sup>2</sup></b>
21.24	2.94	0.996
<b>Langmuir (I)</b>		
<b>q<sub>m</sub> (mg/g)</b>	<b>K<sub>L</sub> (L/g)</b>	<b>R<sup>2</sup></b>
80.65	0.19	0.990
<b>Langmuir (II)</b>		
<b>q<sub>m</sub> (mg/g)</b>	<b>K<sub>L</sub> (L/g)</b>	<b>R<sup>2</sup></b>
62.11	0.47	0.936

**Table 6.6:** Comparison of adsorption capacities of various adsorbents in the removal of MB dye.

<b>Adsorbents</b>	<b>q<sub>max</sub> (mg/g)</b>	<b>References</b>
Modified orange tree waste	78.7	(Azzaz et al. 2017)
Oxidized weed biochar	161.3	(Güzel et al. 2017)
Bentonite/zeolite composite	36.2	(Shaban et al. 2017)
Acid modified zeolite	2.1	(Hor et al. 2016)
Nut shell activated carbon	5.3	(Ragupathy et al. 2015)
Macoře fruit shell carbon	10.6	(Aboua et al. 2015)
Cashew shell activated carbon	4.8	(Ragupathy et al. 2015)
Palm tree activated carbon	128	(AlOthman et al. 2014)
kaolin	45.0	(Rida et al. 2013b)
Cold plasma kaolin	51.0	(Yavuz and Saka 2013)

Bio-char Ash	178	(Özbay et al. 2013)
Wheat straw bio-char	12.03	(Liu et al. 2012)
Kenaf fibre char	22.7	(Mahmoud et al. 2012)
Cotton stalk	147.1	(Deng et al. 2011)
Granular activated carbon	21.5	(Yener et al. 2008)
Kaolin	80.7	Present study

## 6.5 Single Stage Batch Adsorption Design

Adsorption isotherm data has been applied in this research study to design a single-stage batch adsorption system as per method developed by (Kumar et al. 2010). Due to the lack of extensive experimental data, empirical design procedures based on adsorption isotherm studies are the most common method to predict the adsorber size and performance. (Dawood et al. 2014, Sen et al. 2011). From isotherm experiment data, it was found that Freundlich isotherm model is well fitted with the experimental data with linear regression coefficients ( $R^2$ ) of 0.996. The design objective was to decrease the initial MB initial dye concentration from  $C_0$  to  $C_t$  (mg/L) for which total volume of dye solution is  $V$  (L). The amount of added adsorbent was  $m$  (g) and the solute loading changes from  $q_0$  (mg/g) to  $q_t$  (mg/g). The MB dye concentration on solid changes from  $q_0 = 0$  to  $q_t$  due to added adsorbent into the system. The mass balance for the MB dye in the single-stage operation under equilibrium is presented as per equation (6.2). Freundlich adsorption isotherm data has been utilised in this study to design a single-stage batch adsorption system as per method developed by (Kumar et al. 2010). Rearranging equations (2.12) and (6.2) thus can be written as per equation (6.3).

$$V (C_0 - C_e) = m (q_e - q_0) = m \cdot q_e \quad (6.2)$$

$$\frac{m}{V} = \frac{C_0 - C_e}{q_e} = \frac{C_0 - C_e}{K_f C_e^{\frac{1}{n}}} \quad (6.3)$$

Figure 6.11, shows series of plots derived from equation (6.3) to predict the amount of kaolin required (g) in the remove of initial MB dye concentrations of 100 (mg/L) for various dye removal assumptions of 50%, 60%, 70% , 80% and 90% vs. the volume of dye effluent (L) for a single-stage batch adsorption. For example, to obtain 90% MB dye removal, it is required 1.94, 3.88, 5.81, 7.75, 9.69, 11.63, 13.56, 15.50, 17.44 and 19.38 g of kaolin clay to remove 1-10 L of MB dye solution respectively.

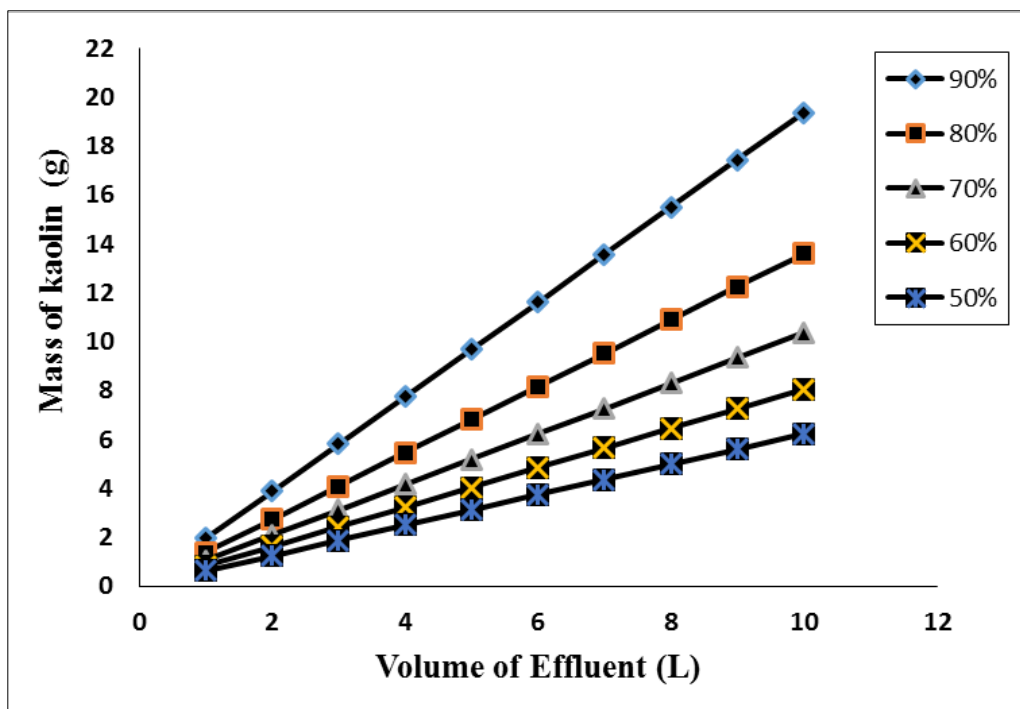


**Figure 6.11:** Design of single stage batch adsorber- Adsorbent mass (m) against volume of solution treated (L).

## 6.6 Conclusion

In this present research, raw kaolin clay was used as an adsorbent to investigate its effectiveness in the removal of cationic methylene Blue dye from its aqueous solution. Kaolin is a low cost natural clay with crystalline structure and it is available worldwide. The amount of dye adsorbed  $q_t$  (mg/g) and percentage of dye removal were determined under various process conditions such as initial dye concentration, solution pH, temperature and adsorbent dose. It was observed that the amount of dye adsorbed  $q_t$  (mg/g) was increased with the increase of initial dye concentration, solution pH and temperature but decreased with the increase of adsorbent dose. Furthermore, experimental data were fitted well with pseudo-second-order kinetic model compared to pseudo-first-order model and intra particle -diffusion kinetic models. Equilibrium data were best represented by both Freundlich and Langmuir (I) isotherm models with a maximum adsorption capacity ( $q_m$ ) of 80.65 (mg/g) which is very much comparative to other clay minerals. Thermodynamic parameters such as Entropy change ( $\Delta S^\circ$ ), Gibbs free energy change ( $\Delta G^\circ$ ) and Enthalpy change ( $\Delta H^\circ$ ) indicated that the adsorption process was an endothermic, spontaneous and physical in nature. These results indicate the feasibility of raw kaolin clay as an effective alternative cost effective sustainable adsorbent in the removal of cationic Methylene Blue dye from wastewater.



## 6.7 References

- Aboua, K.N., Yobouet, Y.A., Yao, K.B., Goné, D.L. and Trokourey, A. (2015) "Investigation of dye adsorption onto activated carbon from the shells of Macoré fruit". Journal of Environmental Management **156**, 10-14.
- AlOthman, Z.A., Habila, M.A., Ali, R., Abdel Ghafar, A. and El-din Hassouna, M.S. (2014) "Valorization of two waste streams into activated carbon and studying its adsorption kinetics, equilibrium isotherms and thermodynamics for methylene blue removal". Arabian Journal of Chemistry **7**(6), 1148-1158.
- Azzaz, A.A., Jellali, S., Akrouf, H., Assadi, A.A. and Bousselmi, L. (2017) "Optimization of a cationic dye removal by a chemically modified agriculture by-product using response surface methodology: biomasses characterization and adsorption properties". Environmental Science and Pollution Research **24**(11), 9831-9846.
- Dawood, S., Sen, T.K. and Phan, C. (2014) "Synthesis and characterisation of novel-activated carbon from waste biomass pine cone and its application in the removal of congo red dye from aqueous solution by adsorption". Water, Air, and Soil Pollution **225**(1).
- Deng, H., Lu, J., Li, G., Zhang, G. and Wang, X. (2011) "Adsorption of methylene blue on adsorbent materials produced from cotton stalk". Chemical Engineering Journal **172**(1), 326-334.
- Güzel, F., Saygılı, H., Akkaya Saygılı, G., Koyuncu, F. and Yılmaz, C. (2017) "Optimal oxidation with nitric acid of biochar derived from pyrolysis of weeds and its application in removal of hazardous dye methylene blue from aqueous solution". Journal of Cleaner Production **144**(Supplement C), 260-265.
- Hor, K.Y., Chee, J.M.C., Chong, M.N., Jin, B., Saint, C., Poh, P.E. and Aryal, R. (2016) "Evaluation of physicochemical methods in enhancing the adsorption performance of natural zeolite as low-cost adsorbent of methylene blue dye from wastewater". Journal of Cleaner Production **118**(Supplement C), 197-209.

Kaur, S., Rani, S. and Mahajan, R.K. (2013) " Adsorption Kinetics for the Removal of Hazardous Dye Congo Red by Biowaste Materials as Adsorbents". Journal of Chemistry **2013**, 12.

Konicki, W., Sibera, D., Mijowska, E., Lendzion-Bieluń, Z. and Narkiewicz, U. (2013) "Equilibrium and kinetic studies on acid dye Acid Red 88 adsorption by magnetic ZnFe<sub>2</sub>O<sub>4</sub> spinel ferrite nanoparticles". Journal of Colloid and Interface Science **398**, 152-160.

Kumar, P., Ramalingam, S., Senthamarai, C., Niranjanaa, M., Vijayalakshmi, P. and Sivanesan, S. (2010) "Adsorption of dye from aqueous solution by cashew nut shell: Studies on equilibrium isotherm, kinetics and thermodynamics of interactions". Desalination **261**(1–2), 52-60.

Leyh, R.G., Kofidis, T., Struber, M., Fischer, S., Knobloch, K., Wachsmann, B., Hagl, C., Simon, A.R. and Haverich, A. (2003) "Methylene blue: the drug of choice for catecholamine-refractory vasoplegia after cardiopulmonary bypass?". J Thorac Cardiovasc Surg **125**(6), 1426-1431.

Liu, X. and Zhang, L. (2015) "Removal of phosphate anions using the modified chitosan beads: Adsorption kinetic, isotherm and mechanism studies". Powder Technology **277**, 112-119.

Liu, Y., Zhao, X., Li, J., Ma, D. and Han, R. (2012) "Characterization of bio-char from pyrolysis of wheat straw and its evaluation on methylene blue adsorption". Desalination and Water Treatment **46**(1-3), 115-123.

Mahmoud, D.K., Salleh, M.A.M., Karim, W.A.W.A., Idris, A. and Abidin, Z.Z. (2012) "Batch adsorption of basic dye using acid treated kenaf fibre char: Equilibrium, kinetic and thermodynamic studies". Chemical Engineering Journal **181–182**(0), 449-457.

Mukherjee, K., Kedia, A., Jagajjani Rao, K., Dhir, S. and Paria, S. (2015) "Adsorption enhancement of methylene blue dye at kaolinite clay-water interface influenced by electrolyte solutions". RSC Advances **5**(39), 30654-30659.

Nandi, B.K., Goswami, A. and Purkait, M.K. (2009a) "Removal of cationic dyes from aqueous solutions by kaolin: Kinetic and equilibrium studies". Applied Clay Science **42**(3–4), 583-590.

Nandi, B.K., Goswami, A. and Purkait, M.K. (2009b) "Adsorption characteristics of brilliant green dye on kaolin". Journal of Hazardous Materials **161**(1), 387-395.

Özbay, İ., Özdemir, U., Özbay, B. and Veli, S. (2013) "Kinetic, thermodynamic, and equilibrium studies for adsorption of azo reactive dye onto a novel waste adsorbent: charcoal ash". Desalination and Water Treatment **51**(31-33), 6091-6100.

Ragupathy, S., Raghu, K. and Prabu, P. (2015) "Synthesis and characterization of TiO<sub>2</sub> loaded cashew nut shell activated carbon and photocatalytic activity on BG and MB dyes under sunlight radiation". Spectrochimica Acta Part A: Molecular and Biomolecular Spectroscopy **138**, 314-320.

Rida, K., Bouraoui, S. and Hadnine, S. (2013a) "Adsorption of methylene blue from aqueous solution by kaolin and zeolite". Applied Clay Science **83-84**, 99-105.

Rida, K., Bouraoui, S. and Hadnine, S. (2013b) "Adsorption of methylene blue from aqueous solution by kaolin and zeolite". Applied Clay Science **83-84**(Supplement C), 99-105.

Salleh, M.A.M., Mahmoud, D.K., Karim, W.A. and Idris, A. (2011) "Cationic and anionic dye adsorption by agricultural solid wastes: a comprehensive review". Desalination **280**(1-3), 1-13.

Sen, T.K., Afroze, S. and Ang, H.M. (2011) "Equilibrium, kinetics and mechanism of removal of methylene blue from aqueous solution by adsorption onto pine cone biomass of *Pinus radiata*". Water Air Soil Pollut **218**, 499-515.

Sewu, D.D., Boakye, P. and Woo, S.H. (2017) "Highly efficient adsorption of cationic dye by biochar produced with Korean cabbage waste". Bioresource Technology **224**, 206-213.

Shaban, M., Abukhadra, M.R., Shahien, M. and Ibrahim, S.S. (2017) "Novel bentonite/zeolite-NaP composite efficiently removes methylene blue and Congo red dyes". Environmental Chemistry Letters, 1-6.

Shakoor, S. and Nasar, A. (2016) "Removal of methylene blue dye from artificially contaminated water using citrus limetta peel waste as a very low cost adsorbent". Journal of the Taiwan Institute of Chemical Engineers **66**, 154-163.

Tran, H.N., You, S.-J. and Chao, H.-P. (2016) "Thermodynamic parameters of cadmium adsorption onto orange peel calculated from various methods: A comparison study". Journal of Environmental Chemical Engineering **4**(3), 2671-2682.

Tran, H.N., You, S.-J., Hosseini-Bandegharai, A. and Chao, H.-P. (2017) "Mistakes and inconsistencies regarding adsorption of contaminants from aqueous solutions: A critical review". Water Research **120**(Supplement C), 88-116.

Yagub, M.T., Sen, T.K., Afroze, S. and Ang, H.M. (2014) "Dye and its removal from aqueous solution by adsorption: A review". Advances in Colloid and Interface Science **209**(0), 172-184.

Yavuz, Ö. and Saka, C. (2013) "Surface modification with cold plasma application on kaolin and its effects on the adsorption of methylene blue". Applied Clay Science **85**, 96-102.

Yener, J., Kopac, T., Dogu, G. and Dogu, T. (2008) "Dynamic analysis of sorption of methylene blue dye on granular and powdered activated carbon". Chemical Engineering Journal **144**(3), 400-406.

*Every reasonable effort has been made to acknowledge the owners of copyright material.*

*I would be pleased to hear from any copyright owner who has been omitted or incorrectly acknowledged.*

# **CHAPTER 7**

**PERFORMANCE AND DYNAMIC  
MODELLING OF PINE CONE  
BIOCHAR AND KAOLIN PACKED  
BED ADSORPTION COLUMN IN  
THE REMOVAL OF METHYLENE  
BLUE DYE FROM ITS AQUEOUS  
PHASE.**

## ABSTRACT

This present study evaluates the adsorptive effectiveness of pine cone biochar and kaolin clay in removing methylene blue dye from its aqueous solution using a two layered packed-bed column adsorption experiment. A series of column experiments were performed to determine the breakthrough curves (BTCs) by varying bed height (3-7 cm), inlet feed flow rate (13- 17 ml/min) and initial MB dye concentration (50 -150 mg/L) and various characteristic parameters such as percentage dye removal, initial breakthrough time, used bed length and unused bed length, mass transfer zone (MTZ) and dye adsorption density  $q_{(total)}$  were determined. The MB dye adsorption was found to be most favourable under low inlet flow rate, high adsorbent bed height and high initial MB dye concentrations. Thomas, Yoon-Nelson, Clark and Bed Depth Service Time (BDST) column dynamic models were fitted against the experimental data to predict the column breakthrough curves (BTC) under various operational conditions. All models were found to be suitable in describing the dynamic behaviour of the column. The various adsorptive kinetic parameters such as rate constant, the adsorption capacity for Thomas model, the time for 50% breakthrough in Yoon-Nelson model, Clark constants, the service time for BDST model and unused bed are determined and critically analysed which are useful for designing of a large-scale fixed bed column operation. This continuous column study revealed the applicability of pine cone biochar and kaolin clay to remove organic methylene blue dye from aqueous solution in a fixed bed column system thus these adsorbents can be used as alternative sustainable adsorbents for dye-bearing wastewater treatment.

---

\* Dawood, S., Sen, T.K. and Phan, C. (2018) "Performance and dynamic modelling of biochar and kaolin packed bed adsorption column for aqueous phase methylene blue dye removal". Environmental Technology, 2018: p. 1-11.

## 7.1 Introduction

The aim of this chapter is to investigate the effectiveness of pine cone biochar and kaolin clay as adsorbents in the removal of organic methylene blue dye from aqueous solution through the dynamic fixed bed adsorption column performance. Understanding the adsorption dynamic and modelling are important in term of sorbent capacity and estimate the time required to reach the breakthrough curve. The results obtain from the batch adsorption studies such as the maximum adsorption capacity and adsorption mechanism are fundamental and need further conclusion whether the adsorption system is applicable in the industrial application (Afroze et al. 2016). Further, isotherm experimental data cannot apply directly to fixed bed column study because the continuous column study is not at equilibrium. Therefore. It is important to perform adsorption study using a fixed bed continuous column. The nature of the breakthrough curves (BTC) and the breakthrough time at which MB dye concentration reaches the threshold values were determined and studied at various operation parameters such as adsorbent bed height (3-7 cm), inlet flow rate (13-17 ml/min) and initial dye concentration (50-150 mg/L). Previous batch studies were carried out in chapter 5 and 6 to evaluate the effectiveness of the cost-effective pine cone biochar and kaolin clay adsorbents in the removal of methylene blue (MB) dye respectively. Thus to make the adsorption process more commercially feasible, two layers of pine cone based biochar and kaolin clay were used as packed bed adsorbents in a fixed bed column at a volume ratio of 1:1. The column experimental data were fitted into various dynamic models such as Thomas model, Yoon-Nelson model, Clark model and Bed Depth Service Time (BDST) model to gain a better understanding about the adsorption mechanism and its feasibility for actual industrial applications.

## 7.2 Results and Discussion

### 7.2.1 Effect of adsorbents bed height on BTC

The amount of packed bed adsorbent materials presented in a packed bed column strongly affect the adsorbate accumulation, the steepness of all BTCs and the column adsorption performance. The effect of packed bed height on the BTC and MB dye adsorption was studied by varying the bed height (3, 5 and 7 cm) while the initial MB dye concentration of 100 mg/L, solution pH of 6.9, solution temperature of  $25 \pm 1$  °C and inlet flow rate of 15 ml/min were kept constant. Two separate layers of pine cone bio-char and kaolin clay at a volume ratio of 1:1 were used as packed bed adsorbents in various bed height. The breakthrough curves of the plot of  $(C_t/C_o)$  versus  $t$  (min) for different bed height were obtained from the experimental data as shown in Figure 7.1. The breakthrough curve parameters were calculated and presented in Table 7.1. It was found from Fig.7.1 that an increase in the bed height from 3cm to 7 cm resulted in increased breakthrough time and the saturation time respectively. Upon the increases in the bed height, the breakthrough time was increased from 79 to 157 mins respectively as shown in Table 7.1.

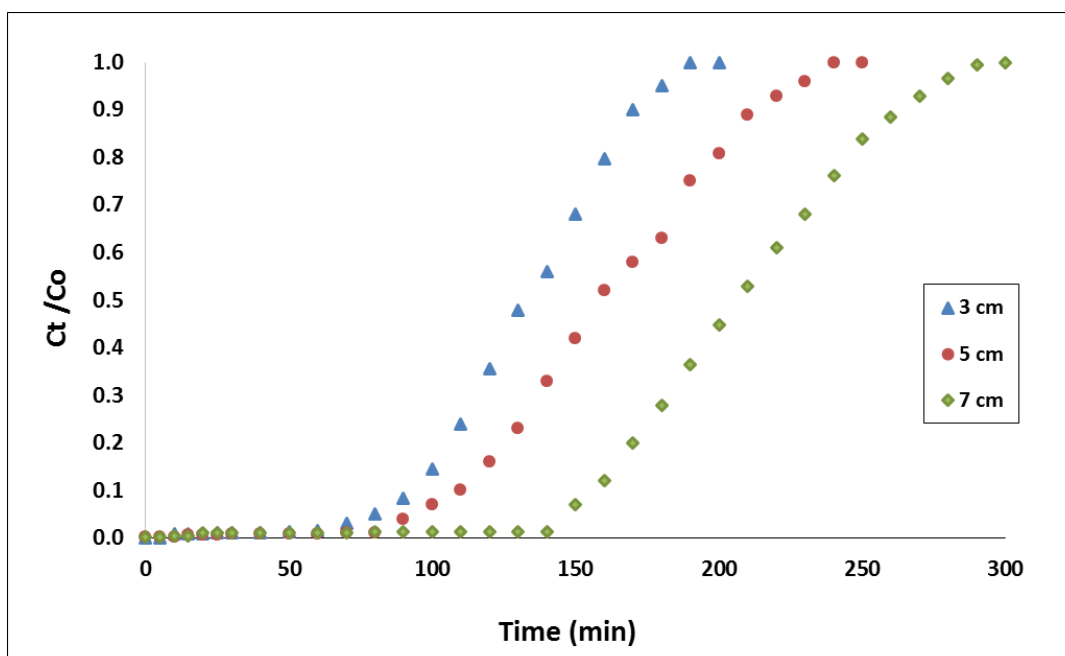


**Figure 7.1:** The breakthrough curves (BTC) for MB dye adsorption at various column bed heights where initial MB dye =100 mg/L, flow rate= 15 ml/min, solution pH 6.9, and solution temperature = $25 \pm 1$  °C.



The steepness of the breakthrough curve decreased with increasing bed height due to a higher mass transferring zone. Further, the total amount of MB dye adsorbed,  $q_{total}$  and percentage dye removal were increased from 197.5 mg to 310.1 mg and from 62.7 % to 68.9 % with the increases of bed height as shown in Table 7.1. With the increased of bed height, the amount of pine cone bio-char and kaolin clay adsorbents increased as well as the residence time of MB dye solution inside the packed bed column increased. This allows the dye molecules to diffuse deeper into the adsorbents particles therefore higher percentage dye removal and used bed height ( $H_B$ ) are observed as shown in Table 7.1. Further the total treated MB dye volume was increased from 3000 ml to 4500 ml with increases of bed height as shown in Table 7.1. This is due to the fact that increasing the amount of packed adsorbents inside the packed bed leads to increase the number of active available sites for MB dye interaction at the adsorbents surface. Higher breakthrough times indicates a better intra-particle diffusion phenomenon and higher adsorption capacity of the dye molecules which can be attributed to the decrease in the mass transfer and axial dispersion, resulting in enough time for the solute to remain in column and diffuse into adsorbent, making more volumes of effluent to be treated (Vilvanathan and Shanthakumar 2017). Therefore, increasing bed height results in an increases in the total adsorption bed capacity which is favourable for industrial scale column adsorption operation. Similar observation was also reported by various researcher (Afroze et al. 2016, Shak et al. 2017, Yagub et al. 2015). Detailed calculation is included in appendix D-1.

**Table 7.1:** Breakthrough curves (BTCs) parameters for various bed height containing pine cone biochar and kaolin adsorbents in the removal of MB dye in a fixed bed column.

<b>Bed Height (cm)</b>	<b><math>t_b</math> (min)</b>	<b><math>t_t</math> (min)</b>	<b><math>H_{UNB}</math> (cm)</b>	<b><math>H_B</math> (cm)</b>	<b><math>V_{eff}</math> (ml)</b>	<b><math>q_{(total)}</math> (mg)</b>	<b><math>m_{(total)}</math> (mg)</b>	<b>Removal %</b>
3	79	132	1.2	1.8	3000.0	197.5	315	62.7
5	99	160	1.9	3.1	3750.0	240.3	375	64.1
7	148	207	2.0	5.0	4500.0	310.1	450	68.9

### 7.2.2 Effect of initial MB dye concentration on BTC

The effect of initial MB dye concentration on the BTC and adsorption capacity was studied by varying the initial MB dye concentration (50 mg/L, 100 mg/L and 150 mg/L) while other process parameters were kept constant as shown in Fig 7.2. The breakthrough curves of the plot of  $(C_t/C_o)$  versus  $t$  (min) for various initial MB dye concentration were obtained from the experimental data as shown in Figure 7.2 and the breakthrough curve parameters were calculated and presented in Table 7.2. It was observed from Fig.7.2 that an increase in the initial dye concentration from 50 mg/L to 150 mg/L decreased the breakthrough time and the saturation time as the packed bed adsorbents get saturated rapidly. The breakthrough time was decreased from 138 to 69 mins with the increase of MB dye concentration as shown in Table 7.2.

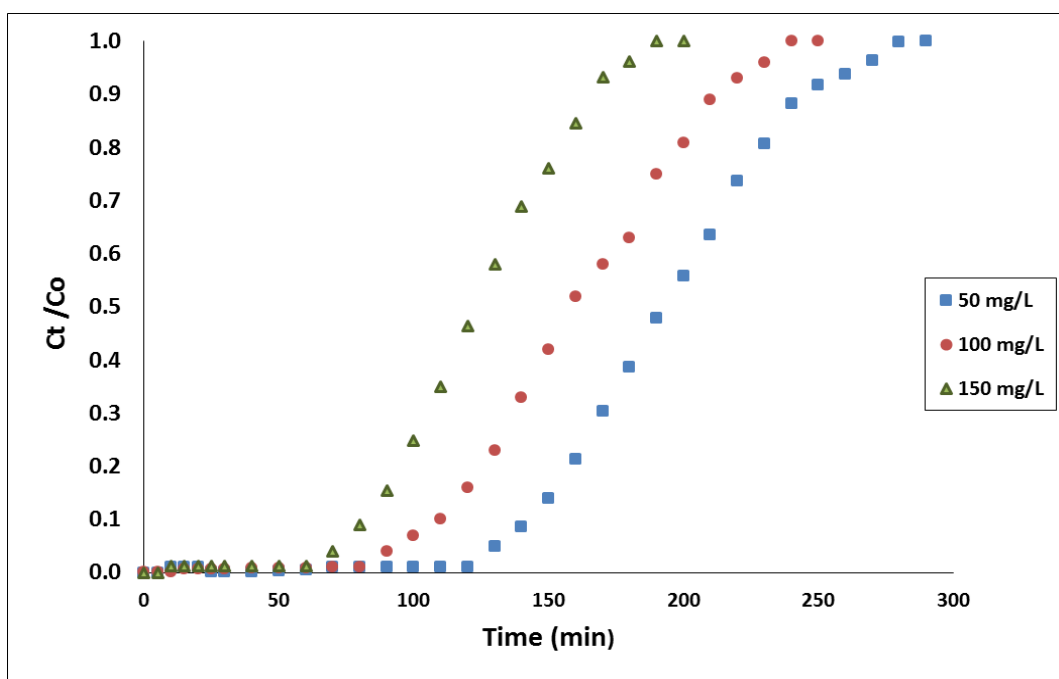


**Figure 7.2:** The breakthrough curves (BTC) for MB dye adsorption at various initial MB dye concentration where bed height= 5 cm, flow rate= 15 ml/min, solution pH 6.9, and solution temperature = $25 \pm 1$  °C.

From Fig.7.2, it shows that at lower MB dye concentration, the breakthrough time was flatter indicating a wide MTZ and film control process. At higher dye concentration, the breakthrough curve was sharp indicating a smaller MTZ and intra particle diffusion controlled process (Afroze et al. 2016) . At lower MB dye concentration, the packed bed adsorbents get saturated slowly thus the breakthrough time increased. Further, the total amount of MB dye adsorbed,  $q_{total}$  was increased from 144.9 mg to 277.2 mg while the percentage dye removal was decreased from 66.6 % to 61.6 % with the increases of initial dye concentration as shown in Table 7.2. This is due to the fact that packed bed adsorbents active binding sites were occupied and saturated quickly, causing an earlier breakthrough time. Also, higher initial adsorbate concentration provides a higher driving force for the transfer process to overcome the mass transfer resistance. Further, the total volume of MB dye effluents were decreased from 4350 ml to 3000 ml with the increase of initial dye concentration respectively as shown in Table 7.2. Similar observation in the removal of various dyes and metal ions on BTC were also observed by other researchers such as (Ahmad and Hameed 2010, Vilvanathan and Shanthakumar 2017). Detailed fixed bed column calculation is included in appendix D-2.

**Table 7.2:** Breakthrough curves (BTCs) parameters for various initial MB dye concentration in a fixed bed column.

$C_o$ Mg/ L	$t_b$ (min)	$t_t$ (min)	$H_{UNB}$ (cm)	$H_B$ (cm)	$V_{eff}$ (ml)	$q_{(total)}$ (mg)	$m_{(total)}$ (mg)	Removal %
<b>50</b>	138	193	1.4	3.6	4350.0	144.9	217.5	66.6
<b>100</b>	99	160	1.9	3.1	3750.0	240.3	375.0	64.1
<b>150</b>	69	123	2.2	2.8	3000.0	277.2	450.0	61.6

### 7.2.3 Effect of inlet MB dye flow rate

The flow rate affects the performance and efficiency of the adsorbents in a continuous column adsorption process. The effect of MB dye flow rate on the BTC and adsorption capacity was studied by varying flow rate while other process parameters such as initial MB dye concentration =100 mg/L, bed height of 5 cm, solution pH of 6.9 and solution temperature of  $25 \pm 1$  °C were kept constant. The breakthrough curves of the plot of  $(C_t/C_o)$  versus  $t$  (min) for different flow rate were obtained from the experimental data as shown in Figure 7.3 and the breakthrough curve parameters were calculated and presented in Table 7.3. It was observed from Fig.7.3 that an increase in MB dye flow rate from 13 ml/min to 17 ml/min decreased the breakthrough time and the saturation time respectively. The breakthrough time was decreased from 118 to 69 mins with the increase of MB flow rate as shown in Table 7.3

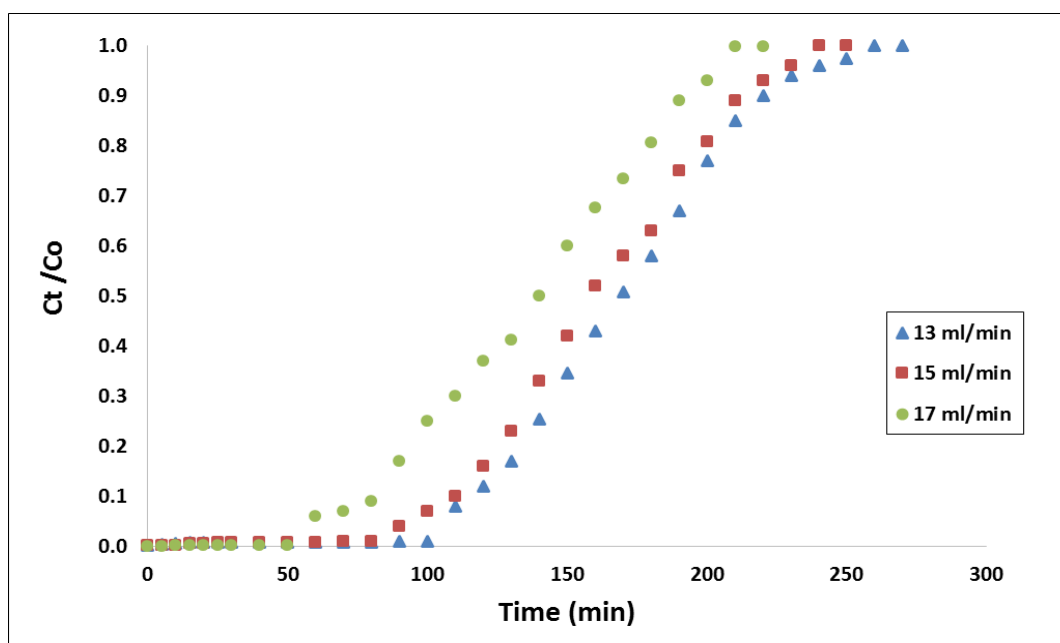


**Figure 7.3:** The breakthrough curves (BTC) for MB dye adsorption at various flow rate where initial MB dye =100 mg/L, bed height =5 cm, solution pH 6.9, and solution temperature = $25 \pm 1$  °C.

At higher flow rates, the volume of MB dye enters the column is higher thus more adsorbate molecule come in contact with the packed bed adsorbents and leading to a fast breakthrough time. Also at higher flow rate, the flow tends to be more turbulent therefore decreases the external bulk phase mass transfer resistance to the surface of solid adsorbents and hence the rate of movement of bulk phase MB dye molecules into adsorbent's surface will be high. From Fig.7.3, the breakthrough curve is shown to be steeper with increasing flow rate due to shorter contact time of MB molecules with the mixed-adsorbents bed, which resulted in lower adsorption capacity. From Table 7.3, the length of unused bed has increased from 1.5cm to 2.6 cm with the increases of MB flow rate from 13mL/min to 17mL/min respectively. This is further supported by the reduction in the percentage dye removal from 64.9 % to 62.2% for the same flow rate range. However, the total volume of MB dye entered in a fixed bed column was increased from 3510 ml to 3910 mL with increases of MB dye flow rate from 13mL/min to 17mL/min respectively, leading to more MB dye molecules binding with the adsorbent bed thus faster breakthrough time achieved. This result indicates that the lower flow rate yields higher percentage dye removal however it may not be practical for the treatment of large volume of dye bearing wastewater effluents due to long processing time. Similar trends were observed in the removal of dyes and metal ions by fixed bed column (Chowdhury et al. 2015, Cruz-Olivares et al. 2013, Mangaleshwaran et al. 2015, Shak et al. 2017) . Detailed calculation is included in appendix D-3.

**Table 7.3:** Breakthrough curves (BTCs) parameters for various inlet flow rate in a fixed bed column.

<b>Q (ml/min)</b>	<b>t<sub>b</sub> (min)</b>	<b>t<sub>t</sub> (min)</b>	<b>H<sub>UNB</sub> (cm)</b>	<b>H<sub>B</sub> (cm)</b>	<b>V<sub>eff</sub> (ml)</b>	<b>q<sub>(total)</sub> (mg)</b>	<b>m<sub>(total)</sub> (mg)</b>	<b>Removal %</b>
<b>13</b>	118	169	1.5	3.5	3510.0	219.2	338.0	64.9
<b>15</b>	99	160	1.9	3.1	3750.0	240.3	375.0	64.1
<b>17</b>	69	143	2.6	2.4	3910.0	243.1	391.0	62.2

## 7.2.4 Dynamic modelling of pine cone biochar and kaolin packed bed adsorption column

The dynamic behaviour and column performances of pine cone biochar and kaolin clay packed bed adsorbents in the removal of MB dye in a fixed bed column was evaluated using Thomas, Yoon-Nelson, Bed Depth Service Time and Clark kinetic models.

### 7.2.4.1 Application of Thomas dynamic model

Thomas model is simple model based on the equation for conservation of mass in a flow system. It assumes a plug flow behaviour in the bed and the rate driving force in adsorption follows the second-order reversible kinetics reaction and Langmuir isotherm model. Detailed theory is included in section 2.11.2.1 of chapter 2. The column experimental data from breakthrough curve were fitted against the Thomas model to calculate its maximum solid-phase concentration of MB,  $q_0$  (mg/g) and the Thomas kinetic rate constant,  $K_{Th}$  (ml/mg.min). The model parameters and linear correlation coefficient ( $R^2$ ) were determined from the plot  $\ln\left[\left(\frac{C_0}{C_t}\right) - 1\right]$  against  $t$  at a given flow rate as per equation (2.28).

The fitted linear plot of  $\ln\left[\left(\frac{C_0}{C_t}\right) - 1\right]$  against time ( $t$ ) under various bed heights (3,5 and 7cm), MB flow rates (13,15 and 17mL/min) and initial MB concentrations (50,100 and 150 mg/L) are shown in Fig.7.4 (a), (b) and (c) respectively. The values of  $K_{Th}$  and  $q_0$  are determined based on the slope and intercept of the plots respectively and are presented in Table 7.4. From Table 7.4, the  $K_{Th}$  values were decreased with the increases of adsorbents bed height and initial MB dye concentration respectively. For example,  $K_{Th}$  values was decreased from 0.868 mL/min-mg to 0.387 mL/min-mg with the increase of initial dye concentration respectively. The decrease in  $K_{Th}$  values is due to slower mass transfer. However, the  $K_{Th}$  value was almost constant with the increases of flow rate. Further, the  $q_0$  values were decreased from 24.8 mg/g to 15.7 mg/g with the increase of packed adsorbents bed height respectively.

Concurrently, the  $q_0$  values were increased from 9.2 mg/g to 17.2 mg/g and from 16.3 mg/g to 17.9 mg/g with the increases of initial MB dye concentration (50- 150mg/L) and inlet flow rate (13- 17ml/min) respectively. The concentration difference between the dye in the solution and the dye on the adsorbent's surface results in a high driving force thus a better column adsorption performance (Ehrampoush et al. 2010). Also, the calculated Thomas model  $q_0$  and the experimental maximum adsorption capacity  $q_0$  were very close with higher linear regression coefficient ( $R^2$ ) value for most of the process parameters as presented in Table 7.4. This results indicate the applicability of Thomas model and suggests an external mass transfer and negligible axial dispersion in the column adsorption. Hence, the fixed bed column performance was found better at higher MB initial concentration due to the higher adsorption driving force. According to Thomas model, higher adsorbent bed height, MB dye solution flow rate and MB dye initial concentration lead to a better performance of pine cone based bio-char and kaolin clay packed bed column in the removal of Methylene blue dye. Similar observation for Thomas constant for various systems were reported by Afroze et al. (Afroze et al. 2016) and Yagub et al. (Yagub et al. 2015).

**Table 7.4:** Kinetic parameters of Thomas Model under various experimental conditions.

Parameters	Bed Height (cm)			Flow Rate (mL/min)			Initial MB Concentration (mg/L)		
	3	5	7	13	15	17	50	100	150
$K_{Th}$ (mL/min·mg)	0.554	0.447	0.435	0.445	0.447	0.45	0.868	0.447	0.387
$q_0$ (mg/g)	24.8	16.9	15.7	16.3	16.9	17.9	9.2	16.9	17.2
$q_{o\ exp}$ (mg/g)	24.7	17.8	15.5	16.2	17.8	18.0	10.7	17.8	20.5
$R^2$	0.99	0.99	0.99	0.99	0.99	0.97	0.99	0.99	0.98

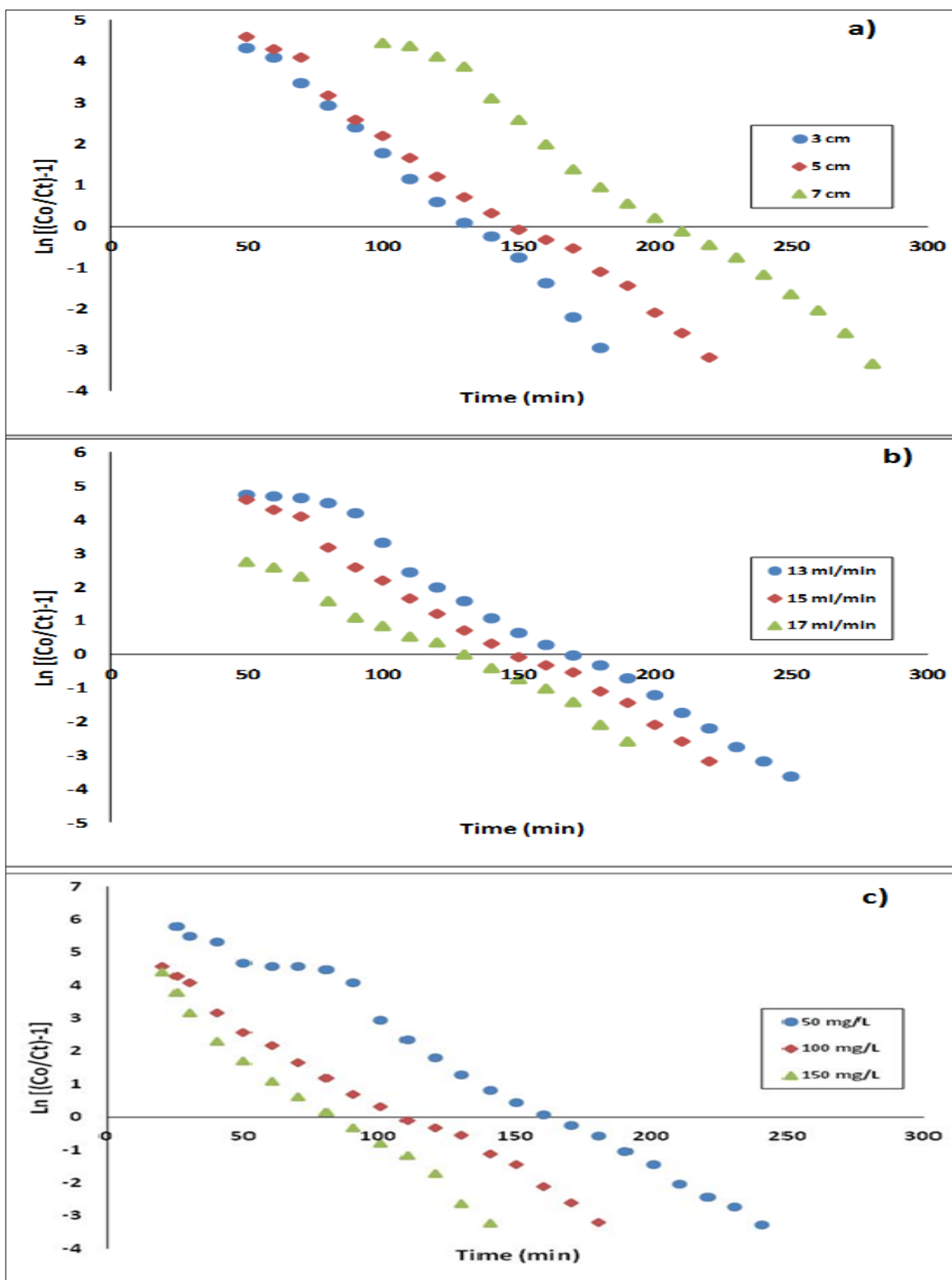


**Figure 7.4:** Thomas Kinetic Plots for Adsorption of MB dye under various effect (a) Effect of Bed Height, (b) Effect of Flow Rate ,(c) Effect of Initial MB Concentration, (Temperature  $25 \pm 1^\circ$  and solution pH =6.9.



#### 7.2.4.2 Application of Yoon-Nelson dynamic Model

The experimental data were also fitted into Yoon-Nelson dynamic model to study the breakthrough behaviour of MB dye on two separate layers of pine cone biochar and kaolin clay packed bed in a fixed bed column. Detailed theory is presented in section 2.11.2.2 of chapter 2. The parameters for Yoon-Nelson constant ( $K_{YN}$ ) and  $\tau$  (the time required for 50% sorbate breakthrough) were determined from linear equation (2.29). From equation (2.29), the plots of  $\ln[C_t/(C_o - C_t)]$  against time for various bed heights, inlet flow rates and initial MB concentrations are presented in Fig.7.5 (a), (b) and (c) respectively. The values of  $K_{YN}$  and  $\tau$  are calculated from the slope and intercept of the linear plots and results are presented in Table 7.5 with other calculated values.

Yoon-Nelson constant  $K_{YN}$  was found to increase with the increases of inlet flow rate and initial dye concentration and decreased with the increases of bed height respectively. For example,  $K_{YN}$  value increased from  $0.042 \text{ min}^{-1}$  to  $0.057 \text{ min}^{-1}$  with the increase of initial MB dye concentration. In fact, the increases in MB concentration causes adsorbate molecules to compete for available adsorption sites, leading to an increase in uptake rate (Hamdaoui 2006, Han et al. 2009). Also, it was found that the time required for 50% sorbate breakthrough  $\tau$  (min) were increased with the increases of column bed height and decreased with the increases of inlet flow rate and initial dye concentration respectively. From the experimental data, the time required for 50% sorbate breakthrough  $\tau_{exp}$  (min) were similar to the theoretical values which indicates the applicability of Yoon-Nelson model as shown in Table 7.5. Further, the high regression coefficients ( $R^2$ ) values obtained suggest the suitability of this model for this proposed system. Similar BTC trend was also reported in the removal of MB dye by (Shak et al. 2017) and food azo dyes (Vieira et al. 2014).

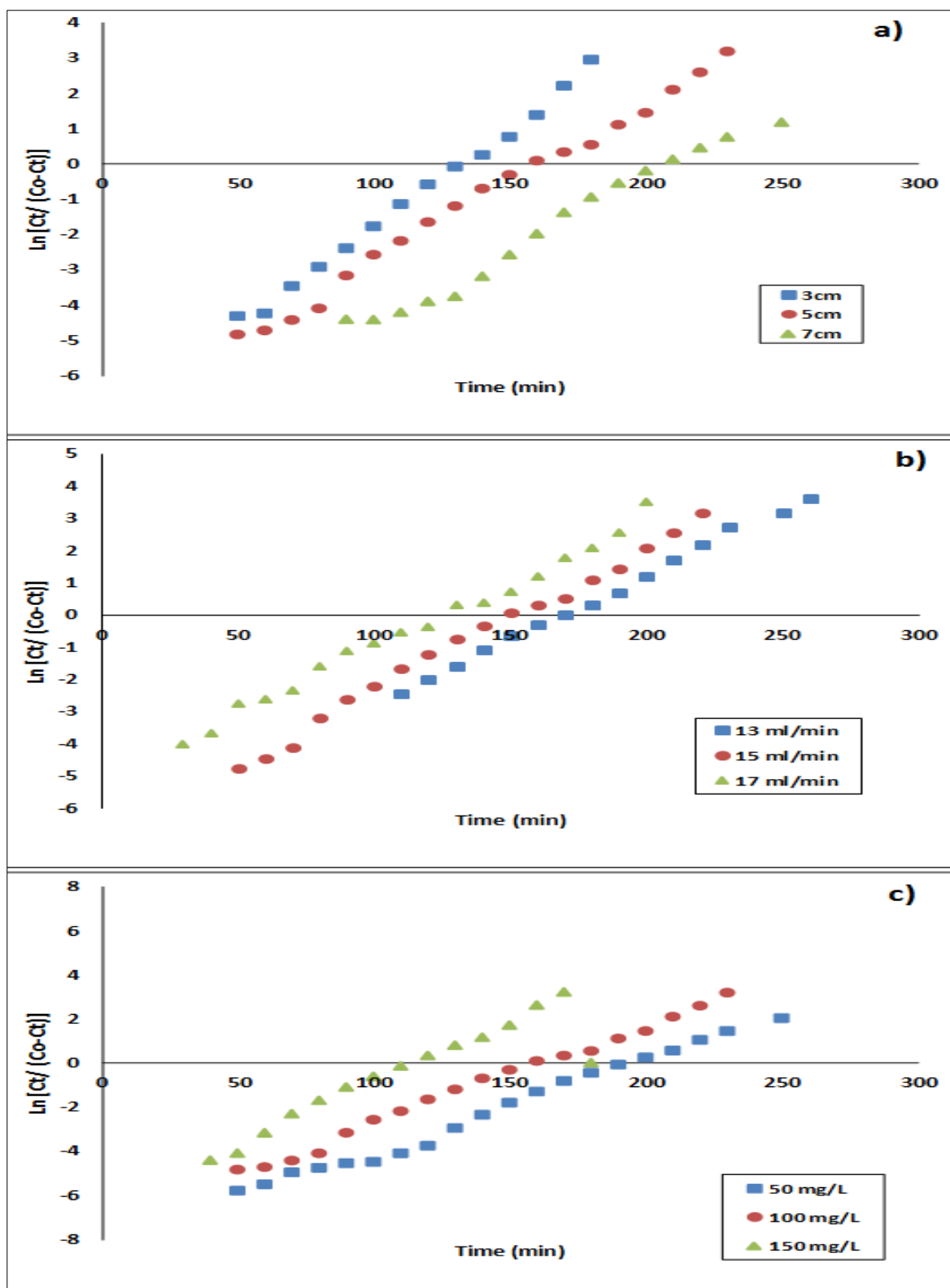


**Figure 7.5:** Yoon-Nelson kinetics plots for the adsorption of MB dye on pine cone biochar and kaolin clay under various effect (a) Effect of Bed Height, (b) Effect of Flow Rate, (c) Effect of Initial MB Concentration, (Temperature  $25 \pm 1^\circ$  and solution pH = 6.9).

**Table 7.5:** Yoon-Nelson calculated parameters under various experimental process conditions.

Process parameters	Bed Height (cm)			Flow Rate (mL/min)			Initial MB Concentration (mg/L)		
	3	5	7	13	15	17	50	100	150
$K_{YN} \times 10^2$ (min <sup>-1</sup> )	5.6	4.5	4.1	4.1	4.5	4.6	4.2	4.5	5.7
$\tau$ (min)	132	153	211	169	153	111	196	153	115
$\tau_{50\% \text{ exp}}$ (min)	127	148	195	157	148	125	184	148	108
$R^2$	0.99	0.99	0.98	0.99	0.99	0.98	0.99	0.99	0.99

#### 7.2.4.3 Application of Bed Depth Service Time (BDST) model

The experimental data obtained in the removal of MB dye by pine cone biochar and kaolin clay in a fixed bed column were fitted into BDST model to evaluate the effect of bed depth on the mode of the breakthrough curves. Detailed theory is presented in section 2.11.2.3 of chapter 2. BDST plot of service time against various bed height of 3, 5 and 7 cm respectively at a constant flow rate of 15 ml/min and initial dye concentration of 100 mg/L is presented in Fig 7.6. Column service time, also known as the exhaustion time is the time taken for all the active binding site of an adsorbent to become fully occupied by adsorbate molecules until regeneration is required. The values of sorption capacity of the bed per unit bed volume ( $N_o$ ) and rate constant ( $K_a$ ) were obtained from the slop and intercept of BDST plot assuming a constant initial concentration ( $C_o$ ) and linear velocity ( $v$ ) as per equation (2.31). The calculated model rate constant ( $K_a$ ) represents the rate of solute transfer from the fluid to the solid phase (Shak et al. 2017). The sorption capacity  $N_o$  and rate constant  $K_a$  were calculated as 7636 mg/L and 0.522 L/mg.min, respectively with a high linear regression coefficient ( $R^2$ ) value of 0.999. These results indicate the applicability of BDST model in the prediction of the adsorption performance for the adsorption of MB dye onto pine cone biochar and kaolin clay at various process operation conditions without further experimental runs.

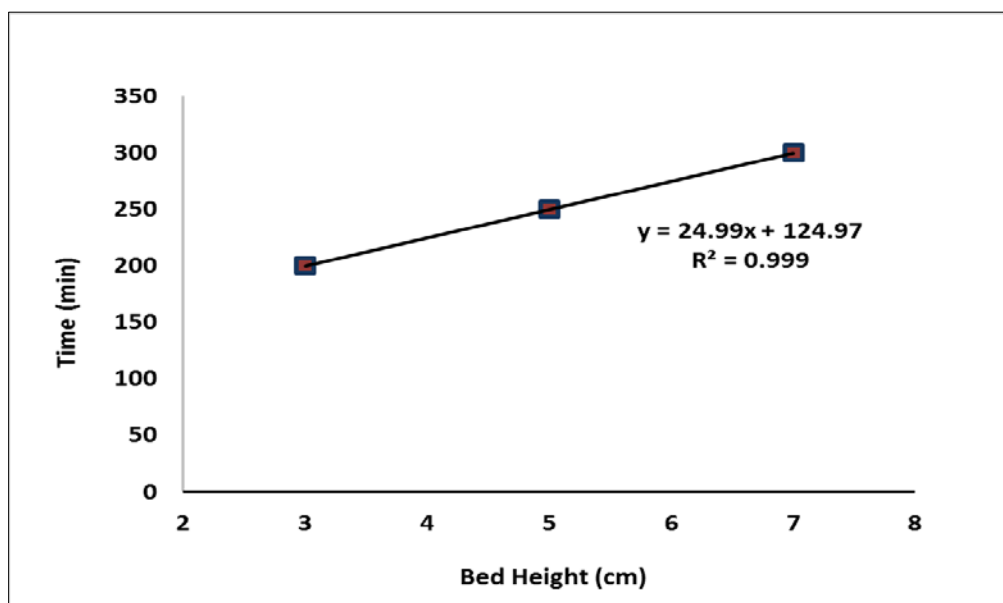


**Figure 7.6:** BDST kinetic plot for the adsorption of MB dye on pine cone biochar and kaolin at initial dye concentration of 100 mg/L and flow rate of 15 ml/min.

#### 7.2.4.4 Application of Clark model

The column experimental data from various breakthrough curves were fitted against the Clark model as shown in Fig 7.7 (a), (b) and (c). This model is based on the use of a mass-transfer concept in combination with the Freundlich isotherm constant. Theoretical details are presented in section 2.11.2.4 of chapter 2. Clark model uses Freundlich constant to simulate the modelling of the breakthrough curves in fixed bed adsorption as per equation (2.33). Batch adsorption and kinetics studies in the removal of MB dye by pine cone biochar (Dawood et al. 2017b) and kaolin (Dawood et al. 2017a) were used to calculate Freundlich constant ( $n$ ) and it was found to be above unity which indicates the applicability of the model. In this study, Freundlich constant ( $n$ ) was assumed to be 1.8. The calculated values of  $A$  and  $r$  ( $\text{min}^{-1}$ ) in the Clark model were determined from the intercept and slope of equation (2.33) respectively and presented in Table 7.6. It was found that  $r$  was decreasing slightly from  $0.051 \text{ min}^{-1}$  to  $0.041 \text{ min}^{-1}$  and from  $0.042 \text{ min}^{-1}$  to  $0.038 \text{ min}^{-1}$  with the increases of bed height and MB dye inlet flow rate respectively. However,  $r$  values were increased from  $0.041 \text{ min}^{-1}$  to  $0.053 \text{ min}^{-1}$  with the

increases of initial MB dye concentration. The constant  $A$  was found to increase from 121.5 to 487.8 with the increases of packed adsorbents bed height. However, the constant  $A$  was decreased from 561.2 to 81.5 and from 543.5 to 171.6 with the increases of inlet flow rate and initial dye concentration respectively. Furthermore, the linear regression coefficient ( $R^2$ ) were found to be above 0.99 under various operation parameters as shown in Table 7.6 which indicates the applicability of Clark model for the proposed adsorption system.

**Table 7.6:** Clark model parameters in the adsorption of MB dye on cone biochar and kaolin.

<b>Parameters</b>	<b>A</b>	<b>r (min<sup>-1</sup>)</b>	<b>R<sup>2</sup></b>
<b>3 cm</b>	121.5	0.051	0.99
<b>5 cm</b>	251.4	0.042	0.99
<b>7 cm</b>	487.8	0.041	0.99
<b>13 mL/min</b>	561.2	0.042	0.99
<b>15 mL/min</b>	251.4	0.041	0.99
<b>17 mL/min</b>	81.5	0.038	0.98
<b>50 mg/L</b>	543.5	0.041	0.99
<b>100 mg/L</b>	251.4	0.042	0.99
<b>150 mg/L</b>	171.6	0.053	0.99

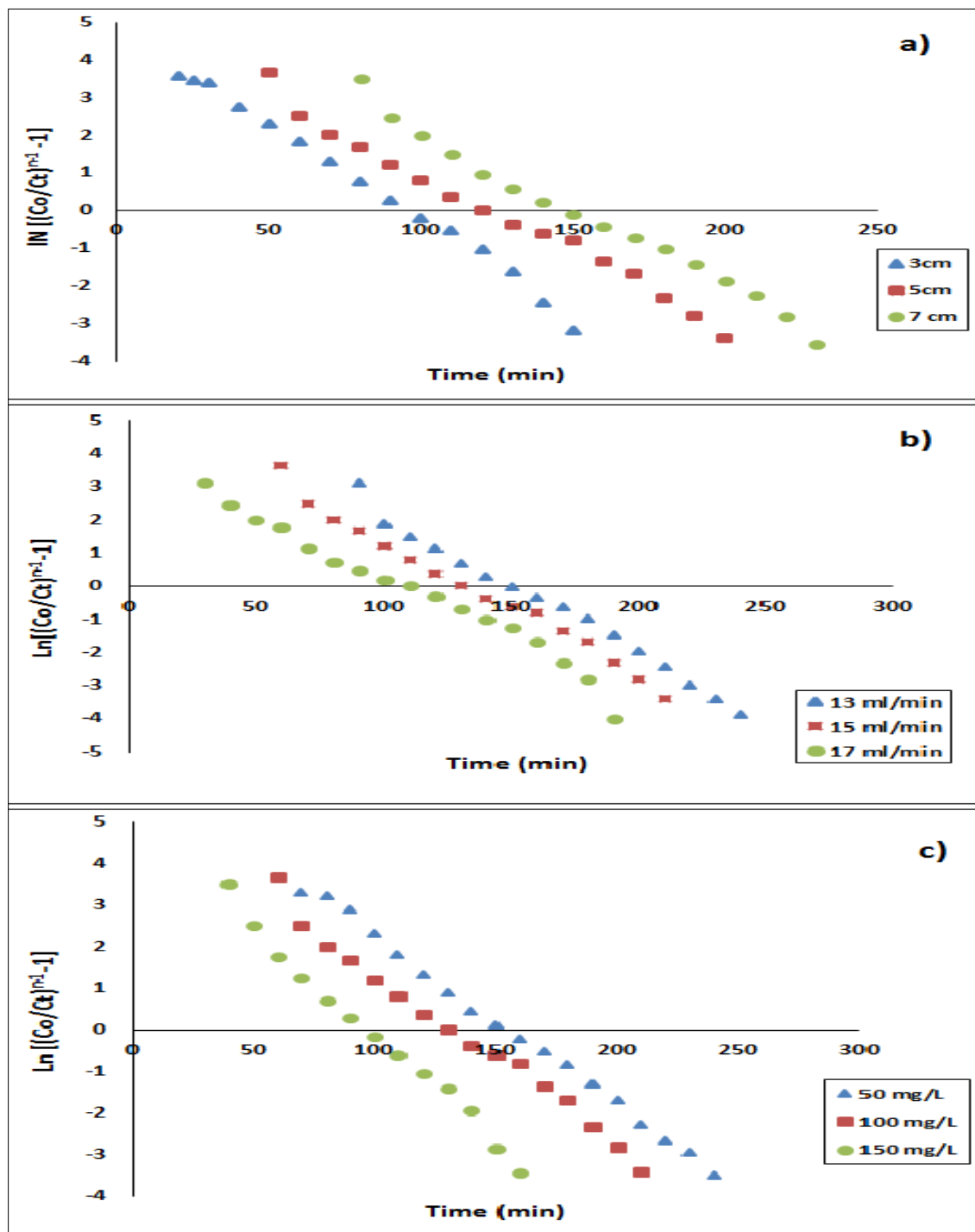


**Figure 7.7:** Clark plots for the adsorption of MB dye on pine cone biochar and kaolin clay under various effect (a) Effect of Bed Height, (b) Effect of Flow Rate ,(c) Effect of Initial MB Concentration, (Temperature  $25\pm 1^\circ$  and solution pH =6.9).

### 7.3 Conclusion

The effectiveness of two low-cost pine cone biochar and kaolin clay packed bed adsorbents in the removal of MB dye by a continuous packed bed column operation was investigated. The breakthrough curves (BTCs) obtained from the experimental data indicate the adsorption of MB dye was significantly depend on adsorbents packed bed height, inlet MB dye flow rate and initial MB dye concentration. The percentage MB dye removal was found to be increased from 63% to 69% with increases of adsorbents bed height respectively and decrease from 65% to 62% and from 67% to 62% with the increases of dye flow rate and initial dye concentration respectively. Further the breakthrough time  $t_b$  (min) was found to be increased with the increase of adsorbents bed height but decreased with the increase of dye flow rate and initial dye concentration respectively. Higher adsorbent bed height enables more intra-particle diffusion phenomena thus higher adsorption capacity was observed. At higher MB dye flow rate, the MB molecules have insufficient contact time with the adsorbent bed for intra-particle diffusion thus MB dye molecules leave the fixed bed column before attaining equilibrium.

The experimental data were then fitted against adsorption dynamic models such as Thomas, Yoon-Nelson, BDST and Clark to analyse the column performances in the removal of MB dye. Thomas model revealed that the value of maximum solid phase concentration ( $q_o$ ) increased with increasing flow rate and initial MB dye concentration and decreased with the increases of bed height. Also, Thomas rate constant ( $K_{Th}$ ) was found to be almost constant across various flow rates and decrease as the bed height and initial MB dye concentration increased. The application of Yoon-Nelson model showed that the time required for 50% adsorbate breakthrough ( $\tau$ ) were agreed with the experimental data ( $\tau_{50\% exp}$ ). Also, the value of Yoon-Nelson rate constant ( $K_{yn}$ ) was decreased as the bed height increased and increased with the increasing flow rate and initial MB dye concentration. The experimental data were fitted into BDST model at various adsorbents bed height and the bed sorption capacity ( $N_o$ ) was calculated as 7636 mg/L for MB dye adsorption by biochar and kaolin clay packed bed adsorbents. Clark model was applied and ( $r$ ) value was found to be decreased with the increase of bed height and flow rate and increased with the increase of initial MB dye concentration respectively. Further, the constant  $A$  was shown to increase with the increases of MB flow rate and decrease with the increases of initial dye concentration.

Higher linear regression coefficient ( $R^2$ ) for Thomas, Yoon-Nelson, BDST and Clark adsorption dynamic models under various operational parameters indicate the applicability of these models. Further, these results such the sorption capacity and the required time for an effective column operation indicate that an external mass transfer resistance significantly affects the mechanism of the adsorption process. In conclusion, these results indicate the suitability of pine cone biochar and kaolin clay packed bed adsorbents in the removal of MB dye from its aqueous solution in a fixed bed continuous column operation.



## 7.4 References

- Afroze, S., Sen, T.K. and Ang, H. (2016) "Adsorption performance of continuous fixed bed column for the removal of methylene blue (MB) dye using Eucalyptusheathiana bark biomass". Research on Chemical Intermediates **42**(3), 2343-2364.
- Ahmad, A.A. and Hameed, B.H. (2010) "Fixed-bed adsorption of reactive azo dye onto granular activated carbon prepared from waste". Journal of Hazardous Materials **175**(1), 298-303.
- Chowdhury, Z.Z., Abd Hamid, S.B. and Zain, S.M. (2015) "Evaluating design parameters for breakthrough curve analysis and kinetics of fixed bed columns for Cu(II) cations using lignocellulosic wastes". BioResources **10**(1), 732-749.
- Cruz-Olivares, J., Pérez-Alonso, C., Barrera-Díaz, C., Ureña-Nuñez, F., Chaparro-Mercado, M.C. and Bilyeu, B. (2013) "Modeling of lead (II) biosorption by residue of allspice in a fixed-bed column". Chemical Engineering Journal **228**(Supplement C), 21-27.
- Dawood, S., Gupta, T. and Sen, T.K. (2017a) "Adsorptive Removal of Methylene Blue (MB) Dye at Kaolin Clay-Water Interface: Kinetics, Isotherm Modelling and Process Design". Clay Minerals: Properties, Occurrence and Uses Sen, T.K. (ed), pp. 209-236, Nova Science Publisher Inc., New York, USA.
- Dawood, S., Sen, T.K. and Phan, C. (2017b) "Synthesis and characterization of slow pyrolysis pine cone bio-char in the removal of organic and inorganic pollutants from aqueous solution by adsorption: Kinetic, equilibrium, mechanism and thermodynamic". Bioresource Technology **246**, 76-81.
- Ehrampoush, M.H., Moussavi, G.R., Ghaneian, M.T., Rahimi, S. and Ahmadian, M. (2010) "Removal of Methylene Blue (MB) Dye from Textile Synthetic Wastewater Using TiO<sub>2</sub>/UV0C Photocatalytic Process". Australian Journal of Basic and Applied Sciences **4**(9), 4279-4285.
- Hamdaoui, O. (2006) "Dynamic sorption of methylene blue by cedar sawdust and crushed brick in fixed bed columns". Journal of Hazardous Materials **138**(2), 293-303.

Han, R., Wang, Y., Zhao, X., Wang, Y., Xie, F., Cheng, J. and Tang, M. (2009) "Adsorption of methylene blue by phoenix tree leaf powder in a fixed-bed column: experiments and prediction of breakthrough curves". Desalination **245**(1–3), 284-297.

Mangaleshwaran, L., Thirulogachandar, A., Rajasekar, V., Muthukumaran, C. and Rasappan, K. (2015) "Batch and fixed bed column studies on nickel (II) adsorption from aqueous solution by treated polyurethane foam". Journal of the Taiwan Institute of Chemical Engineers **55**, 112-118.

Shak, A., Dawood, S. and Sen, T.K. (2017) "Performance and dynamic modelling of mixed biomass-kaolin packed bed adsorption column for the removal of aqueous phase methylene blue (MB) dye". Desalination and Water Treatment **82**, 67-80.

Vieira, M.L.G., Esquerdo, V.M., Nobre, L.R., Dotto, G.L. and Pinto, L.A.A. (2014) "Glass beads coated with chitosan for the food azo dyes adsorption in a fixed bed column". Journal of Industrial and Engineering Chemistry **20**(5), 3387-3393.

Vilvanathan, S. and Shanthakumar, S. (2017) "Column adsorption studies on nickel and cobalt removal from aqueous solution using native and biochar form of *Tectona grandis*". Environmental Progress & Sustainable Energy.

Yagub, M.T., Sen, T.K., Afroze, S. and Ang, H.M. (2015) "Fixed-bed dynamic column adsorption study of methylene blue (MB) onto pine cone". Desalination and Water Treatment **55**(4), 1026-1039.

*Every reasonable effort has been made to acknowledge the owners of copyright material.*

*I would be pleased to hear from any copyright owner who has been omitted or incorrectly acknowledged.*

# **CHAPTER 8**

## **CONCLUSION AND RECOMMENDATIONS**

## 8.1 Conclusion

Wastewater effluents resulted from various industrial activities contains large volume of organic and inorganic pollutants. Their presence pose a serious risk to the ecosystem and human health and therefore their removal is essential. It has been estimated that the total amount of organic dye consumption in textile industry alone worldwide is more than 10,000 tonnes per year and approximately 2- 20 % of these dyes are discharged into water streams. Also, large amount of inorganic heavy metal ions are accumulated and presented in the wastewater due to anthropogenic activities such as fertilizer, mineral processing, textile, mining, smelting operations, industrial production, domestic and agricultural use of metals. Various physical, chemical and biological separation methods are used to treat these aqueous phase pollutants however adsorption process is widely used in the removal of organic dyes and inorganic heavy metal ions pollutants from wastewater due to its simple design, ease of operation, cost effective and insensitive to toxic substances. The effects of different physio-chemical process parameters such as initial adsorbate concentration, adsorbent dose, solution pH, solution temperature and contact time on adsorption process have been reviewed in chapter 2 of this research thesis. Also, chapter 2 highlights wide range of adsorbents used in the removal of these pollutants such as agricultural solid waste, modified biomass waste, biomass based bio-char, charcoal and activated carbon as well as inorganic clay mineral materials. Pine cone and eucalyptus bark solid wastes based biochar were synthesized through a slow pyrolysis process under various temperature profiles. Adsorbent characteristics were carried out to determine the most effective adsorbents. Biomasses based bio-char produced at a temperature of 500°C were chosen as adsorbents in this research study.

This thesis work investigates the feasibility of pine cone based biochar, EB based biochar and kaolin clay as an alternative cost-effective adsorbents in the removal of cationic methylene blue dye and Ni (II) ions from their aqueous solution through a batch and column adsorption study. Also, the removal of MB dye through a fixed bed column was studied under various operation parameters such as inlet flow rate, initial dye concentration and packed bed height. The results obtained in this research thesis were in agreement with other published research literature and thus confirm the feasibility and the applicability of this research study.

The significant findings are presented as follows:

- ❖ The textural and surface morphology of the synthesized adsorbents were analysed by various analytical instruments such as CHN-O analysis, Fourier-transform infrared spectroscopy (FTIR), Scanning Electron Microscope (SEM), Energy Dispersive X-ray Spectroscopy (EDS), X-Ray Diffraction spectrum (XRD) and BET surface area. Other adsorbents characteristics such as pore size, specific surface area, particle size, bulk density and Point of zero charge ( $\text{pH}_{\text{zpc}}$ ) were also determined as shown below:
  - The amount of carbon presented in the synthesized bio-char bio-char was determined by CHN-O analyser and were calculated as 60% for EB bio-char and 75.1 % for pine cone bio-char.
  - BET surface area was increased from 7.1  $\text{m}^2/\text{g}$  for EB biomass to 73  $\text{m}^2/\text{g}$  for EB bio-char while pine cone biomass surface area increased from 15.5  $\text{m}^2/\text{g}$  to 335  $\text{m}^2/\text{g}$  for pine cone bio-char. Kaolin clay surface area was found to be 30.5  $\text{m}^2/\text{g}$ .
  - The presence of different functional groups on bio-char surface by FT-IR analysis such as aromatic C=C stretching, C-H bending and O-H bend from carboxylic acid group indicate existence of acidic oxygen containing functional groups that increase the adsorption capacity of MB dye and Ni (II) ions. FTIR of kaolin clays suggests the presence of  $\nu$  (Si-O) planer stretching, O-H deformation and Si-O Stretching functional groups which are responsible for adsorption.
  - SEM and EDS analysis of EB biochar indicate the presence of carbon, oxygen and calcium while carbon, oxygen and a trace of sodium were presenting in pine cone biochar. Aluminium, silicon, oxygen and titanium were the main components presenting in kaolin clay.
  - The bulk density of EB biochar, pine cone biochar and kaolin were calculated as 0.42, 0.54 and 0.67  $\text{g}/\text{cm}^3$  respectively which indicates their suitability in an industrial operations.
  - The point of zero charge ( $\text{pH}_{\text{zpc}}$ ) for EB biochar, pine cone biochar and kaolin were calculated as 9.5, 8.5 and 6.5 respectively.

- ❖ The adsorptive removal of methylene blue (MB) dye from aqueous solution by bio-char prepared from eucalyptus bark EB under various physico-chemical process conditions was tested in chapter 4. It was found that the percentage dye removal increased with the increase in solution pH, solution temperature and adsorbent dose but decreased with the increase of initial dye concentration. The maximum dye removal was calculated as 87.9% at a solution temperature of 55°C with solution pH of 11.3, initial dye concentration of 20 mg/L and adsorbent dose of 0.02 g. The adsorption kinetic studies showed that the MB dye adsorption process followed pseudo-second –order model and it consists of multi -step processes: a rapid adsorption of dye onto the external surface followed by intra-particle- diffusion into the interior of adsorbent which has been confirmed by intra-particle-diffusion model. Langmuir maximum adsorption capacity  $q_m$  was calculated as 104.2 mg/g which is very comparative to other reported biomass based biochar as presented in Table 2.15 of chapter 2. Also, the dimensionless separation factor ( $R_L$ ) indicates the favourable adsorption process. Based on the thermodynamic analysis, it was observed that the adsorption system was an endothermic and spontaneous in nature
  
- ❖ The synthesis and adsorptive effectiveness of pine cone based bio-char in the removal of MB dye and Ni (II) ions from their aqueous solution were studied by batch adsorption process under various physico-chemical process conditions and presented in chapter 5. It was observed that the percentage adsorbates removal was increased with the increase of solution temperature, solution pH, and biochar dosage and contact time but decreased with the increase of initial adsorbate concentration. The kinetic studies showed that the adsorption process for both MB dye and Ni (II) ions followed pseudo-second order and the adsorption system was a multi-steps process: a rapid adsorption of dye onto the external surface followed by intra-particle- diffusion into the interior of adsorbent which has been confirmed by intra-particle-diffusion model. Langmuir maximum adsorption capacity  $q_m$  was calculated as 106.4 mg/g for MB dye and 117.7 mg/g for Ni (II) ions. These results are very much comparative with other reported biomass based biochar as presented in Table.2.15 of chapter 2. Also, the thermodynamic study indicates that the adsorption process was an endothermic, favourable and spontaneous in nature.

- ❖ Chapter 6 examined the effectiveness of raw kaolin clay in the removal of cationic methylene blue (MB) dye from its aqueous solution. The amount of dye adsorbed  $q_t$  (mg/g) and percentage of dye removal were determined under various physico-chemical conditions such as initial dye concentration, solution pH, temperature and adsorbent dose. It was observed that the amount of dye adsorbed  $q_t$  (mg/g) was increased with the increase of initial dye concentration, solution pH and temperature but decreased with the increase of adsorbent dose. Furthermore, experimental data were fitted well with pseudo-second-order kinetic model compared to pseudo-first-order model and intra particle -diffusion kinetic models. Also, equilibrium data were best represented by both Freundlich and Langmuir (I) isotherm models with a maximum adsorption capacity ( $q_m$ ) of 80.65 (mg/g) which is very much comparative to other clay minerals reported in Table 2.16 of chapter 2. Thermodynamic parameters such as Entropy change ( $\Delta S^\circ$ ), Gibbs free energy change ( $\Delta G^\circ$ ) and Enthalpy change ( $\Delta H^\circ$ ) indicated that the adsorption process was an endothermic, spontaneous and physical in nature. These results indicate the feasibility of raw kaolin clay as an effective alternative cost effective sustainable adsorbent in the removal of cationic Methylene Blue (MB) dye from wastewater.
  
- ❖ Chapter 7 presents the outcomes from the adsorption dynamic column study of a fixed bed column in the removal of MB dye contains two separate layer of pine cone based bio-char and kaolin clay at a volume ratio of 1:1 packed bed materials. A series of column experiments were performed to determine the breakthrough curves (BTCs) by varying bed height (3-7 cm), inlet flow rate (13- 17 ml/min) and initial MB dye concentration (50 -150 mg/L). Various characteristic parameters such as percentage dye removal, initial breakthrough time, used bed length and unused bed length, mass transfer zone (MTZ) and dye adsorption density  $q_{(total)}$  were determined. The percentage MB dye removal was found to be increased from 63% to 69% with increase of packed adsorbents bed height and decrease from 65% to 62% and from 67% to 62% with the increases of dye flow rate and initial dye concentration respectively. The various adsorptive column kinetic parameters such as rate constant, the adsorption capacity for Thomas model, the time for 50% breakthrough in Yoon-Nelson model, Clark constants, the service time for BDST model and unused bed are determined and critically analysed which are useful for designing of a large-scale fixed bed column operation. High linear regression coefficient ( $R^2$ ) values above 0.98 were obtained for all the four dynamic models under various operational parameters and thus indicate the applicability of these models. These results such the

sorption capacity and the required time for an effective column operation indicate that an external mass transfer resistance significantly affects the mechanism of the adsorption process. However, the effect of axial dispersion should not be neglected.

Finally, it can be concluded from this research study, that pine cone and eucalyptus bark (EB) biomasses are cost-effective and good precursors for the synthesis of cost-effective pine cone based biochar and EB based biochar. In fact, the utilization of these agricultural solid wastes help to provide low-cost and effective biochar adsorbents which are very comparative to available commercial activated carbon (CAC) as well as an implementation of an effective solid waste management. The results obtained from this research study demonstrated that the synthesized biochar and kaolin clay were effective and feasible adsorbents in the removal of cationic MB dye and inorganic Ni (II) ions from dye and metal ions bearing wastewater.

## **8.2 Recommendations and Future Research Direction**

The feasibility of the of kaolin clay and the synthesized pine cone and EB based biochar adsorbents in the removal of organic MB dye and inorganic Ni (II) ions were thoroughly examined in this research study. However, future study should be carried out to improve and examine other process conditions in order to evaluate the use of these adsorbents in real industrial applications. The list as shown below is not meant to be complete. It only indicates selected aspects and future research directions that currently considered to be important.

- ❖ The applicability of kaolin, pine cone and EB derived adsorbents should be extended in the removal of anionic and reactive dyes as well.
- ❖ Similar research study should be done on the production of biomass based biochar using other locally available biomass solid wastes such as pine cone leaves, pine cone bark, eucalyptus leaves, wheat straw etc. under similar operational conditions.



- ❖ Real industrial effluents contain wide range of organic and inorganic pollutants simultaneously therefore it is recommended to use real wastewater sample as adsorbates to evaluate the effectiveness of the biomass based biochar and kaolin adsorbents.
- ❖ Biomass derived adsorbent and kaolin clay should be used as packed bed adsorbents in the removal of inorganic heavy metal ions in a fixed bed column study.
- ❖ It is very important to produce effective and low-cost biochar adsorbents which can work effectively under natural conditions such as neutral pH, normal temperature with fast reaction time. Therefore, more experiments should be performed in this direction.
- ❖ Future research study is recommended in the productions of nano-magnetic, nanotubes, nano-wire and nano-dots biochar/carbon which have various industrial applications including their uses as adsorbents in the removal of organic and inorganic pollutants from wastewater.
- ❖ In the literature review, few efforts were made to relate the thermodynamic parameters. Therefore, more intensive study is required in this direction.
- ❖ In this research study, desorption study was carried out to evaluate the possibility of EB based biochar regeneration for reuse and recovery of the sorbed dye. Therefore, it is recommended to perform a full desorption study to evaluate the potential reuse of pine cone based biochar and kaolin in the recovery of the sorbed dye and heavy metal ions.
- ❖ Cost analysis study is recommended in the production of biomass based biochar to evaluate its feasibility in real industrial operations. The total cost must include the capital cost such site preparation, equipment and its installation costs and the operational costs such as energy and water usage, maintenance ,biomass collection and transportation costs.

# **APPENDIX A**

**Raw data for the removal of Methylene blue (MB) dye onto EB bio-char by adsorption process.**

## Appendix A-1

**Effect of initial pH solution on the adsorption of Methylene blue (MB) dye onto EB bio-char.**

### Experimental conditions

Adsorbent dose = 20 mg

Initial MB dye concentration = 20 mg/L

Solution Volume = 50 ml

Temperature = 35 °C

Rotating speed = 130 rpm

Initial pH solution = 11.3

Time, t (min)	C <sub>t</sub> (mg/L)	q <sub>t</sub> (mg/g)	% Adsorption
0	0.000	0.000	0.0
5	7.333	31.667	63.33
15	7.351	31.623	63.25
30	6.912	32.719	65.44
60	5.684	35.789	71.58
90	4.684	38.289	76.58
120	4.386	39.035	78.07
150	3.895	40.263	80.53

Initial pH solution = 10.1

Time, t (min)	C <sub>t</sub> (mg/L)	q <sub>t</sub> (mg/g)	% Adsorption
0	0.000	0.000	0.0
5	9.807	25.482	50.96
15	9.158	27.105	54.21
30	8.807	27.982	55.96
60	8.649	28.377	56.75
90	8.596	28.509	57.02
120	8.351	29.123	58.25
150	7.333	31.667	63.33

Initial pH solution= 9.1

<b>Time, t (min)</b>	<b>C<sub>t</sub> (mg/L)</b>	<b>q<sub>t</sub> (mg/g)</b>	<b>% Adsorption</b>
0	0.000	0.000	0.0
5	9.596	26.009	52.02
15	9.947	25.132	50.26
30	9.386	26.535	53.07
60	9.158	27.105	54.21
90	8.123	29.693	59.39
120	7.737	30.658	61.32
150	7.386	31.535	63.07

Initial pH solution= 7.4

<b>Time, t (min)</b>	<b>C<sub>t</sub> (mg/L)</b>	<b>q<sub>t</sub> (mg/g)</b>	<b>% Adsorption</b>
0	0.000	0.000	0.0
5	11.158	22.105	44.21
15	10.421	23.947	47.89
30	10.667	23.333	46.67
60	9.649	25.877	51.75
90	9.228	26.930	53.86
120	8.807	27.982	55.96
150	8.702	28.246	56.49

Initial pH solution= 6.3

<b>Time, t (min)</b>	<b>C<sub>t</sub> (mg/L)</b>	<b>q<sub>t</sub> (mg/g)</b>	<b>% Adsorption</b>
0	0.000	0.000	0.0
5	9.754	25.614	51.23
15	10.754	23.114	46.23
30	10.561	23.596	47.19
60	10.035	24.912	49.82
90	9.526	26.184	52.37
120	8.702	28.246	56.49
150	8.456	28.860	57.72

Initial pH solution= 4.8

<b>Time, t (min)</b>	<b>C<sub>t</sub> (mg/L)</b>	<b>q<sub>t</sub> (mg/g)</b>	<b>% Adsorption</b>
0	0.000	0.000	0.0
5	10.825	22.939	45.88
15	10.456	23.860	47.72
30	10.368	24.079	48.16
60	10.298	24.254	48.51
90	9.684	25.789	51.58
120	9.421	26.447	52.89
150	9.316	26.711	53.42

## Appendix A-2

### Effect of initial EB bio-char dosage on the adsorption of Methylene blue (MB) dye.

#### Experimental conditions

Initial pH solution =11.3

Initial MB dye concentration =20 mg/L

Solution Volume= 50 ml

Temperature= 35 °C

Rotating speed= 130 rpm

EB bio-char dose= 10 mg

Time, t (min)	C <sub>t</sub> (mg/L)	q <sub>t</sub> (mg/g)	% Adsorption
0	0.000	0.000	0.0
5	11.070	44.649	44.65
15	10.947	45.263	45.26
30	10.825	45.877	45.88
60	10.246	48.772	48.77
90	9.596	52.018	52.02
120	9.088	54.561	54.56
150	8.649	56.754	56.75

EB bio-char dose= 15 mg

Time, t (min)	C <sub>t</sub> (mg/L)	q <sub>t</sub> (mg/g)	% Adsorption
0	0.000	0.000	0.0
5	11.228	29.240	43.86
15	10.912	30.292	45.44
30	10.035	33.216	49.82
60	8.965	36.784	55.18
90	8.123	39.591	59.39
120	7.614	41.287	61.93
150	7.263	42.456	63.68

EB bio-char dose= 20 mg

<b>Time, t (min)</b>	<b>C<sub>t</sub> (mg/L)</b>	<b>q<sub>t</sub> (mg/g)</b>	<b>% Adsorption</b>
0	0.000	0.000	0.0
5	7.333	31.667	63.33
15	7.351	31.623	63.25
30	6.912	32.719	65.44
60	5.684	35.789	71.58
90	4.684	38.289	76.58
120	4.386	39.035	78.07
150	3.895	40.263	80.53

EB bio-char dose= 30 mg

<b>Time, t (min)</b>	<b>C<sub>t</sub> (mg/L)</b>	<b>q<sub>t</sub> (mg/g)</b>	<b>% Adsorption</b>
0	0.000	0.000	0.0
5	6.877	21.871	65.61
15	7.228	21.287	63.86
30	7.368	21.053	63.16
60	6.351	22.749	68.25
90	6.035	23.275	69.82
120	5.649	23.918	71.75
150	4.684	25.526	76.58

### Appendix A-3

#### Effect of initial Methylene blue (MB) dye concentration and contact time

##### Experimental conditions

Initial pH solution = 11.3

Solution Volume = 50 ml

Adsorbent dosage = 20 mg

Temperature = 35 °C

Rotating speed = 130 rpm

Initial MB dye concentration = 10 mg/L

Time, t (min)	C <sub>t</sub> (mg/L)	q <sub>t</sub> (mg/g)	% Adsorption
0	0.000	0.000	0
5	3.596	16.009	64.04
15	3.684	15.789	63.16
30	3.667	15.833	63.33
60	3.184	17.039	68.16
90	2.912	17.719	70.88
120	2.649	18.377	73.51
150	2.272	19.320	77.28

Initial MB dye concentration = 20 mg/L

Time, t (min)	C <sub>t</sub> (mg/L)	q <sub>t</sub> (mg/g)	% Adsorption
0	0.000	0.000	0
5	7.333	31.667	63.33
15	7.351	31.623	63.25
30	6.912	32.719	65.44
60	5.684	35.789	71.58
90	4.684	38.289	76.58
120	4.386	39.035	78.07
150	3.895	40.263	80.53



Initial MB dye concentration= 30 mg/L

<b>Time, t (min)</b>	<b>C<sub>t</sub> (mg/L)</b>	<b>q<sub>t</sub> (mg/g)</b>	<b>% Adsorption</b>
0	0.000	0.000	0
5	12.684	43.289	57.72
15	13.474	41.316	55.09
30	13.526	41.184	54.91
60	12.158	44.605	59.47
90	11.868	45.329	60.44
120	11.237	46.908	62.54
150	10.158	49.605	66.14

Initial MB dye concentration= 50 mg/L

<b>Time, t (min)</b>	<b>C<sub>t</sub> (mg/L)</b>	<b>q<sub>t</sub> (mg/g)</b>	<b>% Adsorption</b>
0	0.000	0.000	0
5	28.158	54.605	43.68
15	29.342	51.645	41.32
30	29.035	52.412	41.93
60	27.719	55.702	44.56
90	25.570	61.075	48.86
120	23.860	65.351	52.28
150	23.114	67.215	53.77

Initial MB dye concentration= 70 mg/L

<b>Time, t (min)</b>	<b>C<sub>t</sub> (mg/L)</b>	<b>q<sub>t</sub> (mg/g)</b>	<b>% Adsorption</b>
0	0.000	0.000	0
5	44.947	62.632	35.79
15	44.825	62.939	35.96
30	45.500	61.250	35.00
60	44.088	64.781	37.02
90	41.939	70.154	40.09
120	41.140	72.149	41.23
150	39.421	76.447	43.68

Initial MB dye concentration= 100 mg/L

<b>Time, t (min)</b>	<b>C<sub>t</sub> (mg/L)</b>	<b>q<sub>t</sub> (mg/g)</b>	<b>% Adsorption</b>
0	0.000	0.000	0
5	67.018	82.456	32.98
15	65.439	86.404	34.56
30	67.193	82.018	32.81
60	65.965	85.088	34.04
90	65.526	86.184	34.47
120	65.088	87.281	34.91
150	63.158	92.105	36.84

## Appendix A-4

### Effect of temperature profile on the adsorption process

#### Experimental conditions

Initial pH solution = 11.3

Solution Volume = 50 ml

Adsorbent dosage = 20 mg

Initial dye concentration = 20 mg/L

Rotating speed = 130 rpm

Temperature = 25 °C

Time, t (min)	C <sub>t</sub> (mg/L)	q <sub>t</sub> (mg/g)	% Adsorption
0	0.000	0.000	0
5	9.825	25.439	50.88
15	8.965	27.588	55.18
30	9.649	25.877	51.75
60	9.754	25.614	51.23
90	11.228	21.930	43.86
120	8.930	27.675	55.35
150	8.421	28.947	57.89

Temperature = 35 °C

Time, t (min)	C <sub>t</sub> (mg/L)	q <sub>t</sub> (mg/g)	% Adsorption
0	0.000	0.000	0
5	7.333	31.667	63.33
15	7.351	31.623	63.25
30	6.912	32.719	65.44
60	5.684	35.789	71.58
90	4.684	38.289	76.58
120	4.386	39.035	78.07
150	3.895	40.263	80.53

Temperature= 45 °C

<b>Time, t (min)</b>	<b>C<sub>t</sub> (mg/L)</b>	<b>q<sub>t</sub> (mg/g)</b>	<b>% Adsorption</b>
0	0.000	0.000	0
5	9.246	26.886	53.77
15	9.193	27.018	54.04
30	8.316	29.211	58.42
60	7.053	32.368	64.74
90	5.649	35.877	71.75
120	4.386	39.035	78.07
150	4.053	39.868	79.74

Temperature= 55 °C

<b>Time, t (min)</b>	<b>C<sub>t</sub> (mg/L)</b>	<b>q<sub>t</sub> (mg/g)</b>	<b>% Adsorption</b>
0	0.000	0.000	0
5	8.368	29.079	58.16
15	8.632	28.421	56.84
30	7.316	31.711	63.42
60	6.526	33.684	67.37
90	4.614	38.465	76.93
120	3.404	41.491	82.98
150	2.404	43.991	87.98

## Appendix A-5

### Effect of NaCl and CaCl<sub>2</sub> salt presence on the adsorption process

#### Experimental conditions

Initial pH solution = 11.3

Solution Volume = 50 ml

Initial dye concentration = 20 mg/L

Temperature = 25 °C

Adsorbent dosage = 20 mg and Rotating speed = 130 rpm

Initial Sodium chloride concentration = 150 mg/L

Time, t (min)	C <sub>t</sub> (mg/L)	q <sub>t</sub> (mg/g)	% Adsorption
0	0.000	0.000	0
5	8.263	29.342	58.68
15	8.158	29.605	59.21
30	7.912	30.219	60.44
60	7.719	30.702	61.40
90	7.368	31.579	63.16
120	7.158	32.105	64.21
150	6.544	33.640	67.28

Initial Sodium chloride concentration = 250 mg/L

Time, t (min)	C <sub>t</sub> (mg/L)	q <sub>t</sub> (mg/g)	% Adsorption
0	0.000	0.000	0
5	8.807	27.982	55.96
15	8.140	29.649	59.30
30	7.579	31.053	62.11
60	7.456	31.360	62.72
90	7.404	31.491	62.98
120	7.228	31.930	63.86
150	6.702	33.246	66.49

Initial Sodium chloride concentration= 400 mg/L

<b>Time, t (min)</b>	<b>C<sub>t</sub> (mg/L)</b>	<b>q<sub>t</sub> (mg/g)</b>	<b>% Adsorption</b>
0	0.000	0.000	0
5	8.544	28.640	57.28
15	8.561	28.596	57.19
30	8.456	28.860	57.72
60	8.333	29.167	58.33
90	7.649	30.877	61.75
120	7.123	32.193	64.39
150	6.947	32.632	65.26

Initial calcium chloride concentration= 150 mg/L

<b>Time, t (min)</b>	<b>C<sub>t</sub> (mg/L)</b>	<b>q<sub>t</sub> (mg/g)</b>	<b>% Adsorption</b>
0	0.000	0.000	0
5	9.421	26.447	52.89
15	9.333	26.667	53.33
30	9.000	27.500	55.00
60	8.351	29.123	58.25
90	7.930	30.175	60.35
120	7.649	30.877	61.75
150	7.632	30.921	61.84

Initial calcium chloride concentration= 250 mg/L

<b>Time, t (min)</b>	<b>C<sub>t</sub> (mg/L)</b>	<b>q<sub>t</sub> (mg/g)</b>	<b>% Adsorption</b>
0	0.000	0.000	0
5	10.228	24.430	48.86
15	10.211	24.474	48.95
30	9.667	25.833	51.67
60	9.561	26.096	52.19
90	9.035	27.412	54.82
120	8.175	29.561	59.12
150	7.912	30.219	60.44

Initial calcium chloride concentration= 400 mg/L

<b>Time, t (min)</b>	<b>C<sub>t</sub> (mg/L)</b>	<b>q<sub>t</sub> (mg/g)</b>	<b>% Adsorption</b>
0	0.000	0.000	0
5	10.035	24.912	49.82
15	10.000	25.000	50.00
30	9.281	26.798	53.60
60	8.316	29.211	58.42
90	8.105	29.737	59.47
120	7.930	30.175	60.35
150	8.088	29.781	59.56

# **APPENDIX B**

**Raw data for the removal of Methylene blue (MB) dye and Ni (II) ions onto pine cone bio-char by adsorption process.**



## Appendix B-1

### Effect of initial pH solution on the adsorption process

#### Experimental conditions

Adsorbent dose = 20 mg

Initial adsorbate concentration = 20 mg/L

Solution Volume = 50 ml

Temperature = 35 °C

Rotating speed = 130 rpm

Initial pH solution = 5.1

time (min)	MB dye			Ni (II) ions		
	Ct	qt (mg/g)	% Adsorption	Ct	qt (mg/g)	% Adsorption
0	0	0	0	0	0	0
5	12.95	17.63	35.26	18.05	4.87	9.74
15	12.58	18.55	37.11	17.98	5.06	10.11
30	12.49	18.77	37.54	17.97	5.07	10.15
45	12.42	18.95	37.89	17.97	5.07	10.15
60	11.81	20.48	40.96	17.94	5.14	10.28
90	11.54	21.14	42.28	17.93	5.18	10.36
120	11.44	21.40	42.81	17.90	5.24	10.49

Initial pH solution = 6.4

time (min)	MB dye			Ni (II) ions		
	Ct	qt (mg/g)	% Adsorption	Ct	qt (mg/g)	% Adsorption
0	0.000	0.000	0	0.000	0.000	0
5	10.842	22.895	45.79	17.416	6.461	12.92
15	10.298	24.254	48.51	17.303	6.742	13.48
30	10.193	24.518	49.04	16.929	7.678	15.36
45	9.368	26.579	53.16	16.592	8.521	17.04
60	9.088	27.281	54.56	16.517	8.708	17.42
90	8.579	28.553	57.11	16.255	9.363	18.73
120	8.193	29.518	59.04	16.142	9.644	19.29

Initial pH solution= 8.0

time (min)	MB dye			Ni (II) ions		
	Ct	qt (mg/g)	% Adsorption	Ct	qt (mg/g)	% Adsorption
0	0.000	0.000	0	0.000	0.000	0
5	10.772	23.070	46.14	11.536	21.161	42.32
15	10.860	22.851	45.70	10.566	23.586	47.17
30	10.982	22.544	45.09	10.307	24.232	48.46
45	8.614	28.465	56.93	9.528	26.180	52.36
60	7.930	30.175	60.35	9.105	27.238	54.48
90	7.404	31.491	62.98	8.502	28.745	57.49
120	7.228	31.930	63.86	8.240	29.401	58.80

Initial pH solution= 9.4

time (min)	MB dye			Ni (II) ions		
	Ct	qt (mg/g)	% Adsorption	Ct	qt (mg/g)	% Adsorption
0	0.000	0.000	0	0.000	0.000	0
5	9.035	27.412	54.82	6.828	32.931	65.86
15	8.053	29.868	59.74	6.116	34.710	69.42
30	7.614	30.965	61.93	6.079	34.803	69.61
45	7.228	31.930	63.86	5.978	35.056	70.11
60	6.561	33.596	67.19	5.446	36.386	72.77
90	5.702	35.746	71.49	5.011	37.472	74.94
120	5.175	37.061	74.12	4.993	37.519	75.04

Initial pH solution= 11.3

time (min)	MB dye			Ni (II) ions		
	Ct	qt (mg/g)	% Adsorption	Ct	qt (mg/g)	% Adsorption
0	0.000	0.000	0	0.000	0.000	0
5	6.982	32.544	65.09	12.921	17.697	35.39
15	6.667	33.333	66.67	12.210	19.476	38.95
30	6.298	34.254	68.51	12.172	19.569	39.14
45	5.000	37.500	75.00	12.071	19.822	39.64
60	4.421	38.947	77.89	11.914	20.215	40.43
90	4.281	39.298	78.60	11.723	20.693	41.39
120	3.544	41.140	82.28	11.610	20.974	41.95

## Appendix B-2

### Effect of initial pine cone bio-char dosage on the adsorption of Methylene blue (MB) dye and Ni (II) ions

#### Experimental conditions

Initial pH solution = (MB=11.3, Ni (II)=9.4)

Initial adsorbate concentration =20 mg/L

Solution Volume= 50 ml

Temperature= 35 °C

Rotating speed= 130 rpm

Pine cone bio-char dose= 10 mg

time (min)	MB dye			Ni (II) ions		
	Ct	qt (mg/g)	% Adsorption	Ct	qt (mg/g)	% Adsorption
0	0.00	0.000	0	0.00	0.00	0
5	8.79	56.053	56.05	10.35	48.26	48.26
15	9.00	55.000	55.00	9.64	51.82	51.82
30	9.46	52.719	52.72	9.60	52.00	52.00
45	8.81	55.965	55.96	9.50	52.51	52.51
60	8.07	59.649	59.65	9.30	53.48	53.48
90	7.44	62.807	62.81	8.87	55.66	55.66
120	6.68	66.579	66.58	8.85	55.75	55.75

Pine cone bio-char dose= 20 mg

time (min)	MB dye			Ni (II) ions		
	Ct	qt (mg/g)	% Adsorption	Ct	qt (mg/g)	% Adsorption
0	0.00	0.00	0.00	0.00	0.00	0.00
5	6.98	32.54	65.09	6.83	32.93	65.86
15	6.67	33.33	66.67	6.12	34.71	69.42
30	6.30	34.25	68.51	6.08	34.80	69.61
45	5.00	37.50	75.00	5.98	35.06	70.11
60	4.42	38.95	77.89	5.45	36.39	72.77
90	4.28	39.30	78.60	5.01	37.47	74.94
120	3.54	41.14	82.28	4.99	37.52	75.04

Pine cone bio-char dose= 30 mg

time (min)	MB dye			Ni (II) ions		
	Ct	qt (mg/g)	% Adsorption	Ct	qt (mg/g)	% Adsorption
0	0.00	0.00	0.00	0.00	0.00	0.00
5	6.38	22.70	68.09	6.00	23.33	69.98
15	6.07	23.22	69.67	5.29	24.51	73.54
30	5.70	23.84	71.51	5.25	24.58	73.73
45	4.40	26.00	78.00	5.15	24.74	74.23
60	3.89	26.84	80.53	5.00	25.01	75.02
90	3.75	27.08	81.23	4.56	25.73	77.19
120	3.02	28.30	84.91	4.54	25.76	77.28

Pine cone bio-char dose= 40 mg

time (min)	MB dye			Ni (II) ions		
	Ct	qt (mg/g)	% Adsorption	Ct	qt (mg/g)	% Adsorption
0	0.00	0.00	0.00	0.00	0.00	0.00
5	5.25	18.43	73.73	5.97	17.54	70.17
15	4.94	18.83	75.31	5.25	18.43	73.73
30	4.57	19.29	77.15	5.22	18.48	73.91
45	3.27	20.91	83.64	5.12	18.60	74.42
60	2.71	21.61	86.43	4.96	18.80	75.21
90	2.57	21.78	87.13	4.52	19.34	77.38
120	2.47	21.91	87.66	4.51	19.37	77.47

Pine cone bio-char dose= 50 mg

time (min)	MB dye			Ni (II) ions		
	Ct	qt (mg/g)	% Adsorption	Ct	qt (mg/g)	% Adsorption
0	0.00	0.00	0.00	0.00	0.00	0.00
5	5.61	14.39	71.97	6.31	13.69	68.46
15	5.29	14.71	73.55	5.60	14.40	72.02
30	4.92	15.08	75.39	5.56	14.44	72.21
45	3.62	16.38	81.89	5.46	14.54	72.72
60	3.06	16.94	84.68	5.30	14.70	73.50
90	2.92	17.08	85.38	4.87	15.13	75.67
120	2.82	17.18	85.90	4.85	15.15	75.77

### Appendix B-3

#### Effect of initial adsorbate concentration and contact time on the adsorption of Methylene blue (MB) dye and Ni (II) ions

##### Experimental conditions

Initial pH solution = (MB=11.3, Ni (II)=9.4)

Adsorbent dosage =20 mg

Solution Volume= 50 ml

Temperature= 35 °C

Rotating speed= 130 rpm

Initial adsorbate concentration =10 mg/L

time (min)	MB dye			Ni (II) ions		
	Ct	qt (mg/g)	% Adsorption	Ct	qt (mg/g)	% Adsorption
0	0.00	0.00	0.00	0.00	0.00	0.00
5	3.29	16.78	67.11	2.64	18.40	73.60
15	2.87	17.83	71.32	2.23	19.42	77.70
30	2.98	17.54	70.18	2.18	19.54	78.16
45	2.59	18.53	74.12	2.17	19.58	78.31
60	1.99	20.02	80.09	2.14	19.64	78.56
90	1.72	20.70	82.81	2.02	19.96	79.83
120	1.25	21.89	87.54	1.96	20.11	80.43

Initial adsorbate concentration =20 mg/L

time (min)	MB dye			Ni (II) ions		
	Ct	qt (mg/g)	% Adsorption	Ct	qt (mg/g)	% Adsorption
0	0.00	0.00	0.00	0.00	0.00	0.00
5	6.98	32.54	65.09	6.83	32.93	65.86
15	6.67	33.33	66.67	6.12	34.71	69.42
30	6.30	34.25	68.51	6.08	34.80	69.61
45	5.00	37.50	75.00	5.98	35.06	70.11
60	4.42	38.95	77.89	5.45	36.39	72.77
90	4.28	39.30	78.60	5.01	37.47	74.94
120	3.54	41.14	82.28	4.99	37.52	75.04

Initial adsorbate concentration =30 mg/L

time (min)	MB dye			Ni (II) ions		
	Ct	qt (mg/g)	% Adsorption	Ct	qt (mg/g)	% Adsorption
0	0.00	0.00	0.00	0.00	0.00	0.00
5	9.79	50.53	67.37	10.21	49.48	65.97
15	8.76	53.09	70.79	8.57	53.58	71.44
30	7.50	56.25	75.00	8.52	53.69	71.59
45	6.68	58.29	77.72	8.23	54.42	72.57
60	6.42	58.95	78.60	8.06	54.85	73.13
90	6.32	59.21	78.95	8.02	54.94	73.26
120	5.97	60.07	80.09	7.92	55.21	73.61

Initial adsorbate concentration =50 mg/L

time (min)	MB dye			Ni (II) ions		
	Ct	qt (mg/g)	% Adsorption	Ct	qt (mg/g)	% Adsorption
0	0.00	0.00	0.00	0.00	0.00	0.00
5	20.67	73.33	58.67	24.25	64.37	51.50
15	20.36	74.10	59.28	21.44	71.40	57.12
30	20.61	73.46	58.77	20.04	74.91	59.93
45	18.61	78.49	62.79	19.57	76.08	60.86
60	17.86	80.35	64.28	19.38	76.54	61.24
90	17.42	81.45	65.16	19.18	77.06	61.65
120	17.11	82.21	65.77	19.16	77.11	61.69

Initial adsorbate concentration =70 mg/L

time (min)	MB dye			Ni (II) ions		
	Ct	qt (mg/g)	% Adsorption	Ct	qt (mg/g)	% Adsorption
0	0.00	0.00	0.00	0.00	0.00	0.00
5	36.66	83.36	47.63	40.64	73.41	41.95
15	35.74	85.66	48.95	37.10	82.26	47.00
30	35.25	86.89	49.65	35.39	86.52	49.44
45	34.63	88.42	50.53	34.67	88.32	50.47
60	34.20	89.50	51.14	34.21	89.47	51.12
90	33.16	92.11	52.63	34.17	89.56	51.18
120	32.48	93.79	53.60	34.15	89.63	51.22

## Appendix B-4

### Effect of temperature profile on the adsorption process

#### Experimental conditions

Initial pH solution = (MB=11.3, Ni (II)=9.4)

Initial adsorbate concentration =20 mg/L

Adsorbent dosage =20 mg

Solution Volume= 50 ml

Rotating speed= 130 rpm

Temperature= 25 °C

time (min)	MB dye			Ni (II) ions		
	Ct	qt (mg/g)	% Adsorption	Ct	qt (mg/g)	% Adsorption
0	0.00	0.00	0.00	0.00	0.00	0.00
5	9.72	25.70	51.40	9.60	26.00	52.00
15	9.39	26.54	53.07	8.89	27.78	55.56
30	9.42	26.45	52.89	8.85	27.87	55.75
45	9.47	26.32	52.63	8.75	28.13	56.25
60	9.25	26.89	53.77	8.22	29.46	58.91
90	8.84	27.89	55.79	7.78	30.54	61.09
120	8.49	28.77	57.54	7.76	30.59	61.18

Temperature= 35 °C

time (min)	MB dye			Ni (II) ions		
	Ct	qt (mg/g)	% Adsorption	Ct	qt (mg/g)	% Adsorption
0	0.00	0.00	0.00	0.00	0.00	0.00
5	6.98	32.54	65.09	6.83	32.93	65.86
15	6.67	33.33	66.67	6.12	34.71	69.42
30	6.30	34.25	68.51	6.08	34.80	69.61
45	5.00	37.50	75.00	5.98	35.06	70.11
60	4.42	38.95	77.89	5.45	36.39	72.77
90	4.28	39.30	78.60	5.01	37.47	74.94
120	3.54	41.14	82.28	4.99	37.52	75.04

Temperature= 45 °C

time (min)	MB dye			Ni (II) ions		
	Ct	qt (mg/g)	% Adsorption	Ct	qt (mg/g)	% Adsorption
0	0.00	0.00	0.00	0.00	0.00	0.00
5	6.79	33.03	66.05	6.19	34.52	69.04
15	6.53	33.68	67.37	5.48	36.30	72.60
30	6.18	34.56	69.12	5.44	36.40	72.79
45	5.61	35.96	71.93	5.34	36.65	73.30
60	4.60	38.51	77.02	4.81	37.98	75.96
90	4.04	39.91	79.82	4.37	39.06	78.13
120	3.28	41.80	83.60	4.36	39.11	78.22



# APPENDIX C

**Raw data for the adsorptive removal of methylene blue (MB) dye onto kaolin clay.**

## Appendix C-1

**Effect of initial pH solution on the adsorption of Methylene blue (MB) dye onto Kaolin clay.**

### Experimental conditions

Adsorbent dose = 20 mg

Initial MB dye concentration = 20 mg/L

Solution Volume = 50 ml

Temperature = 35 °C

Rotating speed = 130 rpm

Initial pH solution = 11.3

<b>Time, t (min)</b>	<b>C<sub>t</sub> (mg/L)</b>	<b>q<sub>t</sub> (mg/g)</b>	<b>% Adsorption</b>
0	0.000	0.00	0
5	7.231	31.92	63.85
25	7.003	32.49	64.98
45	6.700	33.25	66.50
65	6.522	33.69	67.39
85	6.371	34.07	68.15
105	6.194	34.52	69.03
125	5.966	35.09	70.17

Initial pH solution= 9.1

<b>Time, t (min)</b>	<b>C<sub>t</sub> (mg/L)</b>	<b>q<sub>t</sub> (mg/g)</b>	<b>% Adsorption</b>
0	0.000	0	0
5	9.508	26.23	52.46
25	9.407	26.48	52.97
45	9.255	26.86	53.73
65	9.027	27.43	54.86
85	8.951	27.62	55.24
105	8.774	28.06	56.13
125	8.724	28.19	56.38

Initial pH solution= 7.9

<b>Time, t (min)</b>	<b>C<sub>t</sub> (mg/L)</b>	<b>q<sub>t</sub> (mg/g)</b>	<b>% Adsorption</b>
0	0.000	0.00	0
5	7.939	30.15	60.30
25	7.636	30.91	61.82
45	7.787	30.53	61.06
65	7.889	30.28	60.56
85	7.484	31.29	62.58
105	7.130	32.18	64.35
125	7.054	32.37	64.73

Initial pH solution= 5.8

<b>Time, t (min)</b>	<b>C<sub>t</sub> (mg/L)</b>	<b>q<sub>t</sub> (mg/g)</b>	<b>% Adsorption</b>
0	0.000	0.00	0
5	12.266	19.34	38.67
25	12.164	19.59	39.18
45	12.013	19.97	39.94
65	11.785	20.54	41.08
85	11.709	20.73	41.45
105	11.532	21.17	42.34
125	11.481	21.30	42.59

Initial pH solution= 2.3

<b>Time, t (min)</b>	<b>C<sub>t</sub> (mg/L)</b>	<b>q<sub>t</sub> (mg/g)</b>	<b>% Adsorption</b>
0	0.000	0.00	0
5	14.568	13.58	27.16
25	14.391	14.02	28.05
45	14.340	14.15	28.30
65	14.138	14.66	29.31
85	14.037	14.91	29.82
105	13.075	17.31	34.62
125	12.974	17.56	35.13

## Appendix C-2

Effect of initial Kaolin clay dosage on the adsorption of Methylene blue (MB) dye.

### Experimental conditions

Initial pH solution =11.3

Initial MB dye concentration =20 mg/L

Solution Volume= 50 ml

Temperature= 35 °C

Rotating speed= 130 rpm

Kaolin clay dose= 10 mg

Time, t (min)	C <sub>t</sub> (mg/L)	q <sub>t</sub> (mg/g)	% Adsorption
0	0.000	0.00	0
5	9.862	50.69	50.69
25	10.166	49.17	49.17
45	9.786	51.07	51.07
65	9.913	50.44	50.44
85	9.634	51.83	51.83
105	9.736	51.32	51.32
125	9.710	51.45	51.45

Kaolin clay dose=20mg

Time, t (min)	C <sub>t</sub> (mg/L)	q <sub>t</sub> (mg/g)	% Adsorption
0	0.000	0.00	0
5	7.231	31.92	63.85
25	7.003	32.49	64.98
45	6.700	33.25	66.50
65	6.522	33.69	67.39
85	6.371	34.07	68.15
105	6.194	34.52	69.03
125	5.966	35.09	70.17

Kaolin clay dose= 30 mg

<b>Time, t (min)</b>	<b>C<sub>t</sub> (mg/L)</b>	<b>q<sub>t</sub> (mg/g)</b>	<b>% Adsorption</b>
0	0.000	0.00	0
5	5.966	23.39	70.17
25	5.738	23.77	71.31
45	5.435	24.28	72.83
65	5.257	24.57	73.71
85	5.106	24.82	74.47
105	4.929	25.12	75.36
125	4.701	25.50	76.50

Kaolin clay dose= 40 mg

<b>Time, t (min)</b>	<b>C<sub>t</sub> (mg/L)</b>	<b>q<sub>t</sub> (mg/g)</b>	<b>% Adsorption</b>
0	0.000	0.00	0
5	5.283	18.40	73.59
25	5.055	18.68	74.72
45	4.751	19.06	76.24
65	4.574	19.28	77.13
85	4.423	19.47	77.89
105	4.245	19.69	78.77
125	4.018	19.98	79.91

Kaolin clay dose= 50 mg

<b>Time, t (min)</b>	<b>C<sub>t</sub> (mg/L)</b>	<b>q<sub>t</sub> (mg/g)</b>	<b>% Adsorption</b>
0	0.000	0.00	0
5	5.030	14.97	74.85
25	4.802	15.20	75.99
45	4.498	15.50	77.51
65	4.321	15.68	78.39
85	4.170	15.83	79.15
105	3.992	16.01	80.04
125	3.765	16.24	81.18

### Appendix C-3

#### Effect of initial Methylene blue (MB) dye concentration and contact time

##### Experimental conditions

Initial pH solution = 11.3

Solution Volume = 50 ml

Adsorbent dosage = 20 mg

Temperature = 35 °C

Rotating speed = 130 rpm

Initial MB dye concentration = 10 mg/L

Time, t (min)	C <sub>t</sub> (mg/L)	q <sub>t</sub> (mg/g)	% Adsorption
0	0.000	0.00	0
5	2.730	18.18	72.70
25	2.616	18.46	73.84
45	2.464	18.84	75.36
65	2.376	19.06	76.24
85	2.300	19.25	77.00
105	2.211	19.47	77.89
125	2.097	19.76	79.03

Initial MB dye concentration = 20 mg/L

Time, t (min)	C <sub>t</sub> (mg/L)	q <sub>t</sub> (mg/g)	% Adsorption
0	0.000	0.00	0
5	7.231	31.92	63.85
25	7.003	32.49	64.98
45	6.700	33.25	66.50
65	6.522	33.69	67.39
85	6.371	34.07	68.15
105	6.194	34.52	69.03
125	5.966	35.09	70.17



Initial MB dye concentration= 30 mg/L

<b>Time, t (min)</b>	<b>C<sub>t</sub> (mg/L)</b>	<b>q<sub>t</sub> (mg/g)</b>	<b>% Adsorption</b>
0	0.000	0.00	0
5	13.503	41.24	54.99
25	13.161	42.10	56.13
45	12.706	43.24	57.65
65	12.440	43.90	58.53
85	11.643	45.89	61.19
105	11.226	46.94	62.58
125	10.884	47.79	63.72

Initial MB dye concentration= 50 mg/L

<b>Time, t (min)</b>	<b>C<sub>t</sub> (mg/L)</b>	<b>q<sub>t</sub> (mg/g)</b>	<b>% Adsorption</b>
0	0.000	0.00	0
5	28.387	54.03	43.23
25	27.628	55.93	44.74
45	26.553	58.62	46.89
65	25.920	60.20	48.16
85	25.098	62.25	49.80
105	24.466	63.84	51.07
125	24.339	64.15	51.32

Initial MB dye concentration= 70 mg/L

<b>Time, t (min)</b>	<b>C<sub>t</sub> (mg/L)</b>	<b>q<sub>t</sub> (mg/g)</b>	<b>% Adsorption</b>
0	0.000	0.00	0
5	46.560	58.60	33.49
25	45.941	60.15	34.37
45	44.878	62.81	35.89
65	42.930	67.68	38.67
85	41.336	71.66	40.95
105	40.982	72.55	41.45
125	40.627	73.43	41.96

## Appendix C-4

### Effect of temperature profile on the adsorption process

#### Experimental conditions

Initial pH solution = 11.3

Solution Volume = 50 ml

Adsorbent dosage = 20 mg

Initial dye concentration = 20 mg/L

Rotating speed = 130 rpm

Temperature = 25 °C

<b>Time, t (min)</b>	<b>C<sub>t</sub> (mg/L)</b>	<b>q<sub>t</sub> (mg/g)</b>	<b>% Adsorption</b>
0	0.000	0.00	0
5	9.559	26.10	52.21
25	9.331	26.67	53.35
45	9.027	27.43	54.86
65	8.850	27.87	55.75
85	8.698	28.25	56.51
105	8.521	28.70	57.39
125	8.293	29.27	58.53

Temperature= 35 °C

<b>Time, t (min)</b>	<b>C<sub>t</sub> (mg/L)</b>	<b>q<sub>t</sub> (mg/g)</b>	<b>% Adsorption</b>
0	0.000	0.00	0
5	7.231	31.92	63.85
25	7.003	32.49	64.98
45	6.700	33.25	66.50
65	6.522	33.69	67.39
85	6.371	34.07	68.15
105	6.194	34.52	69.03
125	5.966	35.09	70.17

Temperature= 45 °C

<b>Time, t (min)</b>	<b>C<sub>t</sub> (mg/L)</b>	<b>q<sub>t</sub> (mg/g)</b>	<b>% Adsorption</b>
0	0.000	0.00	0
5	6.522	33.69	67.39
25	6.295	34.26	68.53
45	5.991	35.02	70.04
65	5.814	35.46	70.93
85	5.662	35.84	71.69
105	5.485	36.29	72.57
125	5.257	36.86	73.71

# **APPENDIX D**

**Raw data for fixed bed column in the removal of MB dye by pine cone bio-char and kaolin adsorbents.**

## Appendix D-1

### Effect of column bed heights

#### Experimental conditions

MB dye flow rate = 15 ml/min

Initial MB dye concentration = 100 mg/L

Temperature = 25 °C

Solution pH = 6.9

Bed Height = 3 cm

Time (min)	C <sub>t</sub> (mg/L)	C <sub>t</sub> /C <sub>0</sub>
0	0.00	0.00
5	0.00	0.00
10	0.85	0.01
15	0.88	0.01
20	0.93	0.01
25	0.95	0.01
30	1.00	0.01
40	1.10	0.01
50	1.30	0.01
60	1.40	0.01
70	2.99	0.03
80	5.05	0.05
90	8.28	0.08
100	14.43	0.14
110	24.00	0.24
120	35.55	0.36
130	47.80	0.48
140	56.00	0.56
150	68.00	0.68
160	79.82	0.80
170	90.04	0.90
180	95.00	0.95
190	99.85	1.00
200	100.00	1.00

Bed Height =5 cm

<b>Time (min)</b>	<b>C<sub>t</sub> (mg/L)</b>	<b>C<sub>t</sub>/C<sub>o</sub></b>
0	0.10	0.00
5	0.10	0.00
10	0.10	0.00
15	0.60	0.01
20	0.65	0.01
25	0.70	0.01
30	0.73	0.01
40	0.85	0.01
50	0.85	0.01
60	0.87	0.01
70	0.99	0.01
80	0.99	0.01
90	4.00	0.04
100	7.00	0.07
110	10.00	0.10
120	15.93	0.16
130	23.00	0.23
140	32.92	0.33
150	42.00	0.42
160	52.00	0.52
170	58.00	0.58
180	63.00	0.63
190	75.00	0.75
200	80.79	0.81
210	89.00	0.89
220	93.00	0.93
230	96.00	0.96
240	100.00	1.00
250	100.00	1.00

Bed Height =7 cm

Time (min)	C <sub>t</sub> (mg/L)	C <sub>t</sub> /C <sub>o</sub>
0	0.10	0.00
5	0.10	0.00
10	0.30	0.00
15	0.40	0.00
20	1.00	0.01
25	1.05	0.01
30	1.13	0.01
40	1.14	0.01
50	1.14	0.01
60	1.15	0.01
70	1.16	0.01
80	1.17	0.01
90	1.18	0.01
100	1.18	0.01
110	1.18	0.01
120	1.19	0.01
130	1.19	0.01
140	1.20	0.01
150	7.00	0.07
160	12.00	0.12
170	20.00	0.20
180	27.84	0.28
190	36.49	0.36
200	44.86	0.45
210	53.00	0.53
220	61.00	0.61
230	68.00	0.68
240	76.31	0.76
250	83.81	0.84
260	88.44	0.88
270	93.00	0.93
280	96.55	0.97
290	99.50	1.00
300	100.00	1.00



## Appendix D-2

### Effect of initial MB dye concentration

#### Experimental conditions

MB dye flow rate = 15 ml/min

Temperature= 25 °C, Solution pH =6.9 and Bed Height =5 cm

Initial MB dye concentration =50 mg/L

Time (min)	$C_t$ (mg/L)	$C_t/C_o$
0	0.000	0.000
5	0.000	0.000
10	0.495	0.010
15	0.498	0.010
20	0.499	0.010
25	0.050	0.001
30	0.053	0.001
40	0.080	0.002
50	0.150	0.003
60	0.200	0.004
70	0.500	0.010
80	0.515	0.010
90	0.520	0.010
100	0.520	0.010
110	0.521	0.010
120	0.520	0.010
130	2.454	0.049
140	4.304	0.086
150	6.994	0.140
160	10.620	0.212
170	15.188	0.304
180	19.332	0.387
190	23.914	0.478
200	27.908	0.558
210	31.741	0.635
220	36.882	0.738
230	40.376	0.808
240	44.153	0.883
250	45.870	0.917
260	46.870	0.937
270	48.133	0.963
280	49.950	0.999

Initial MB dye concentration =100 mg/L

<b>Time (min)</b>	<b>C<sub>t</sub> (mg/L)</b>	<b>C<sub>t</sub>/C<sub>0</sub></b>
0	0.100	0.001
5	0.100	0.001
10	0.100	0.001
15	0.600	0.006
20	0.650	0.007
25	0.700	0.007
30	0.730	0.007
40	0.848	0.008
50	0.848	0.008
60	0.870	0.009
70	0.994	0.010
80	0.994	0.010
90	4.000	0.040
100	7.000	0.070
110	10.000	0.100
120	15.935	0.159
130	23.000	0.230
140	32.922	0.329
150	42.000	0.420
160	52.000	0.520
170	58.000	0.580
180	63.000	0.630
190	75.000	0.750
200	80.795	0.808
210	89.000	0.890
220	93.000	0.930
230	96.000	0.960
240	100.000	1.000
250	100.000	1.000

Initial MB dye concentration =150 mg/L

<b>Time (min)</b>	<b>C<sub>t</sub> (mg/L)</b>	<b>C<sub>t</sub>/C<sub>0</sub></b>
0	0.000	0.000
5	0.000	0.000
10	1.695	0.011
15	1.710	0.011
20	1.725	0.012
25	1.740	0.012
30	1.755	0.012
40	1.767	0.012
50	1.778	0.012
60	1.791	0.012
70	6.000	0.040
80	13.500	0.090
90	23.013	0.153
100	37.305	0.249
110	52.500	0.350
120	69.441	0.463
130	87.000	0.580
140	103.315	0.689
150	114.000	0.760
160	126.923	0.846
170	139.794	0.932
180	144.197	0.961
190	150.000	1.000
200	150.000	1.000

## Appendix D-3

### Effect of inlet flow rate

#### Experimental conditions

Initial MB dye concentration =100 mg/L

Bed Height =5 cm, Temperature= 25 °C and Solution pH =6.9

MB dye flow rate = 13 ml/min

Time (min)	C <sub>t</sub> (mg/L)	C <sub>t</sub> /C <sub>o</sub>
0	0.200	0.002
5	0.400	0.004
10	0.500	0.005
15	0.853	0.009
20	0.854	0.009
25	0.856	0.009
30	0.857	0.009
40	0.859	0.009
50	0.860	0.009
60	0.862	0.009
70	0.864	0.009
80	0.869	0.009
90	0.910	0.009
100	0.990	0.010
110	8.000	0.080
120	12.000	0.120
130	17.000	0.170
140	25.421	0.254
150	34.482	0.345
160	42.954	0.430
170	50.721	0.507
180	58.000	0.580
190	67.000	0.670
200	77.000	0.770
210	85.000	0.850
220	90.000	0.900
230	94.000	0.940
240	96.000	0.960
250	97.412	0.974
260	100.000	1.000
270	100.000	1.000

MB dye flow rate = 15 ml/min

<b>Time (min)</b>	<b>C<sub>t</sub> (mg/L)</b>	<b>C<sub>t</sub>/C<sub>o</sub></b>
0	0.100	0.001
5	0.100	0.001
10	0.100	0.001
15	0.600	0.006
20	0.650	0.007
25	0.700	0.007
30	0.730	0.007
40	0.848	0.008
50	0.848	0.008
60	0.870	0.009
70	0.994	0.010
80	0.994	0.010
90	4.000	0.040
100	7.000	0.070
110	10.000	0.100
120	15.935	0.159
130	23.000	0.230
140	32.922	0.329
150	42.000	0.420
160	52.000	0.520
170	58.000	0.580
180	63.000	0.630
190	75.000	0.750
200	80.795	0.808
210	89.000	0.890
220	93.000	0.930
230	96.000	0.960
240	100.000	1.000
250	100.000	1.000

MB dye flow rate = 17 ml/min

Time (min)	$C_t$ (mg/L)	$C_t/C_o$
0	0.000	0.000
5	0.000	0.000
10	0.085	0.001
15	0.120	0.001
20	0.117	0.001
25	0.182	0.002
30	0.188	0.002
40	0.196	0.002
50	0.199	0.002
60	6.000	0.060
70	7.000	0.070
80	9.000	0.090
90	17.000	0.170
100	25.000	0.250
110	30.000	0.300
120	37.000	0.370
130	41.211	0.412
140	50.000	0.500
150	60.000	0.600
160	67.562	0.676
170	73.412	0.734
180	80.455	0.805
190	89.000	0.890
200	93.000	0.930
210	99.708	0.997
220	99.708	0.997